UNIVERSITY OF CALIFORNIA,
IRVINE

Effect of Chirality and Chimeras on Amyloid Aggregation

THESIS

submitted in partial satisfaction of the requirements
for the degree of

MASTER OF SCIENCE

in Chemistry

by

Kim Virginia Le

Thesis Committee:
Professor James S. Nowick, Chair
Professor David L. Van Vranken
Professor Vy M. Dong

2014

DEDICATION

In loving memory

of

Nancy Salmeron (1968 - 2003)

Hiep Ngoc Le (1965 - 2012)

and

Ryan Ly (1982 – 2014)

Who taught me to pledge my loyalty to the struggle. Your love is a midsummer's evening breeze that wraps my skin and reminds me you are always by my side.

TABLE OF CONTENTS

LIST OF FIGURES

LIST OF TABLES

ACKNOWLEDGMENTS

I would like to express my deepest gratitude to Dr. John Greaves. His eagerness to teach mass spectrometry and solve problems made Irvine a warm place to learn and work and nourished my own passion for mass spectrometry. John added richness and beauty to the details in my mass spectrometric work as a graduate student and helped me appreciate the valuable in mass spectrometry. John's influence has permanently cemented my adoration for analytical chemistry.

I would also like to extend my warmest thanks to Professor David L. Van Vranken. His commitment to teaching and open door policy has deeply influenced my understanding of chemistry and career path. An asset to the Irvine faculty, his worldly perspective on the biological and chemical sciences made my learning experience fulfilling and fascinating. David's Socratic method of teaching and his problem sets built my intuition and confidence as a chemist. I am forever grateful for his presence as a mentor and committee member.

I would also like to thank Dr. Michael Lampson at the University of Pennsylvania. His willingness to train me in microscopy fostered my passion in molecular biology and commitment to collecting publication quality data. I am thankful for the level of commitment and responsibility granted upon me during my experience in his lab.

I would like to thank the Department of Education for graciously funding my graduate career and the esteemed honor of being selected as a GAANN fellow for two consecutive years.

I would also like to thank Professor Vy M. Dong, for sitting on my committee and insightful questions during advancement.

I would like to thank my advisor, Professor James S. Nowick, for his mentorship and guidance as an experimental chemist and as a writer. His unrelenting pursuit for a complete

global picture and critical eye led me into pushing the envelope of my learning limits. James has molded me into the scientist I am today, demanding my best work and strongest efforts. I am truly grateful for the priceless hours of one-on-one mentoring and writing, his teachings of consistency and clarity, and for passing on his love of NMR spectroscopy and nurturing it within me. I couldn't accomplish my breadth of work without the high expectations James instilled upon me.

I would like to thank my friends and family for their love and support throughout my graduate career. I am deeply indebted to Mary Huynh, Ryan Ly, Vincent Ly, Cedric Ulad, Christopher Ulad, John Chan, Gau Ly, Nguyen Ho, Shannon Stevens and Niko Le for their tender hearts, strong shoulders and open ears, and a love that overcomes distances and adversity.

I would like to thank my parents, Nancy Salmeron and Hiep Ngoc Le, for teaching me the satisfaction in hard work and giving me the opportunity to pursue my dreams and goals.

ABSTRACT OF THE THESIS

Effect of Chirality and Chimeras on Amyloid Aggregation Kinetics

By

Kim Virginia Le

Master of Science in Chemistry

University of California, Irvine, 2014

Professor James S. Nowick, Chair

This thesis reports the activity of macrocyclic β-sheets and their activity against amyloid aggregation. Macrocyclic D-amino acid β-sheets delay or suppress amyloid aggregation at substoichiometric concentrations and show increased activity compared to their L-enantiomers. Fluorescence assays highlight differences between enantiomers and transmission electron microscopy shows the absence of amyloid fibrils in the presence of D-amino acid macrocycles. The diastereomers of the D-amino acid macrocycles are less effective in halting amyloid aggregation. Macrocyclic β-sheet chimeras can suppress or delay amyloid aggregation at stoichiometric amounts. Fluorescence assays show macrocycles containing Aβ-tau hybrid sequences interact with amyloids and delay fibrillization. These studies indicate amyloidogenic peptides are sensitive to chirality and can participate in interactions with chimera peptides.

CHAPTER 1

Effect of Chirality on $A\beta_{40}$ Aggregation

PREFACE

Chapter 1 aims to study the effects of macrocyclic β–sheet stereochemistry on $A\beta_{40}$ aggregation. These D-amino acid macrocyclic β-sheets show increased delay or suppression relative to their L-enantiomers. The differences in D- versus L-macrocycles are apparent by fluorescence and transmission electron microscopy (TEM). This project on macrocycle chirality was my most successful project and allowed me to explore NMR, fluorescence assays and microscopy.

Chapter 1 builds and expands on prior work showing L-amino acid macrocyclic β-sheet **1.2a** stalls $A\beta_{40}$ aggregation. While **1.2a** stalls aggregation, its D-enantiomer **1.2b** effectively suppresses $A\beta_{40}$ aggregation at substoichiometric concentrations. Prior work focuses on building D-amino acid inhibitors to combat amyloid aggregation without probing how structure or stereochemistry influences inhibitor activity. This chapter shows **1.1a** and **1.1b** are well-folded β-sheets while their diastereomers **1.1c** and **1.1d** are poorly folded using NMR spectroscopy. Similarly, NMR spectroscopic studies show **1.2a** and **1.2b** adopt well-folded β-sheet structures while their diastereomers **1.2c** and **1.2d** are partially folded β-sheets. Preorganization of **1.1b** and **1.2b** into a β-sheet shows peptide structure influences its activity against $A\beta_{40}$ aggregation and the increased interaction of **1.2b** with $A\beta_{40}$ suggests the growing $A\beta_{40}$ aggregates are β-sheet in nature. D-Peptide **1.1b** is less effective than D-peptide **1.2b** presumably because of its smaller surface area as a pentapeptide, while **1.2b** offers a larger surface are of interaction as a heptapeptide.

This project also represents my first effort at a single author publication and project. Chapter 1 is also my first opportunity to work alongside with Professor Nowick and experience publication level scientific writing. I am thankful for our writing meetings and discussions to bring my efforts at the bench into organized fruition on paper. In this study I am grateful to Dr. Phil Dennison and Dr. Jian-Guo Zheng for their extensive training on NMR and microscopy. The training I received helped bolster my case for enantiomeric macrocyclic β-sheets.

INTRODUCTION

Chirality is a central feature in peptides and proteins. Enantiomeric protein-protein interactions can lead to improved X-ray crystallographic resolution, such as Kent's racemic crystal structure of plectasin.[1] Heterochiral protein-peptide interactions have expanded substrate scope; D-peptides are attractive ligands to protein targets because of their proteolytic stability and ability to interact with native L-proteins.[2] There is an increased interest in enantiomeric peptide-peptide interactions, as D-NFGAILS peptides can halt L-amylin aggregation[3] while enantiomeric D-polyQ peptides can seed L-polyQ peptides and induce aggregation and cytotoxicity associated with Huntington's disease.[4] Studying chiral interactions in amyloidogenic peptides increases understanding of the pathway to aggregation.

We have previously studied the effects of macrocyclic β-sheet peptides containing fragments of amyloid beta-40 ($A\beta_{40}$) upon the aggregation of $A\beta_{40}$.[5] The peptide models **1** and **2** allow studies into the role chirality plays on aggregation prone peptides, focusing on the N-terminus $A\beta_{40}$. The $A\beta_{40}$ N-terminus is constrained into a macrocyclic β-sheet, with the ornithine turns linking β-strands in close proximity to promote interstrand hydrogen bonding. The unnatural amino acid Hao promotes rigidity of the β-sheet and prevents hydrogen bonding on the lower strand of the macrocycle. We found that macrocyclic β-sheet **1.1a**, which contains a pentapeptide strand from $A\beta_{17\text{-}21}$, is a weak inhibitor of Aβ aggregation and macrocyclic β-sheet **1.2a**, which contains a heptapeptide strand from $A\beta_{16\text{-}22}$, is a better inhibitor of $A\beta_{40}$ aggregation. Addition of 2 equivalents of **1.1a** to $A\beta_{40}$ delays aggregation by 30% and the addition of 0.5 equivalents of **1.2a** to a solution of $A\beta_{40}$ delays aggregation by 430%. To test the effect of chirality on inhibition, we prepared and synthesized the enantiomeric pentapeptide **1.1b** and heptapeptide **1.2b**.

In the current study we investigate the effects of chirality of macrocyclic β-sheets on $A\beta_{40}$ aggregation. We compared the effect of enantiomeric peptides **1.1b** and **1.2b** on $A\beta_{40}$ aggregation to that of L-enantiomers **1.1a** and **1.2a** (Figure 1.1). We further investigated the effects of diastereomeric peptides **1.1c** and **1.1d** and **1.2c** and **2d** on amyloid aggregation. **1.1c** contains L-amino acids linked with D-ornithine turns and **1.1d** contains D-amino acids linked with L-ornithine turns (Figure 1.2).

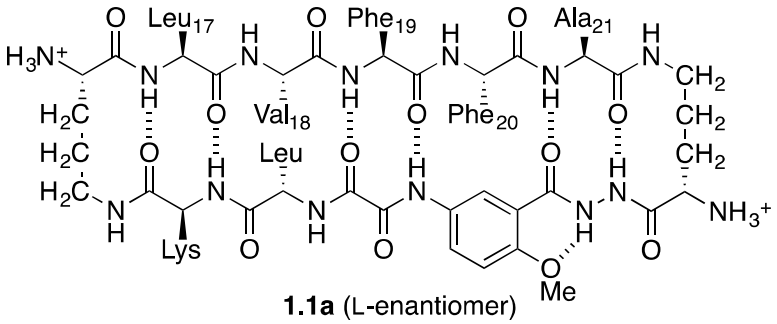

1.1a (L-enantiomer)

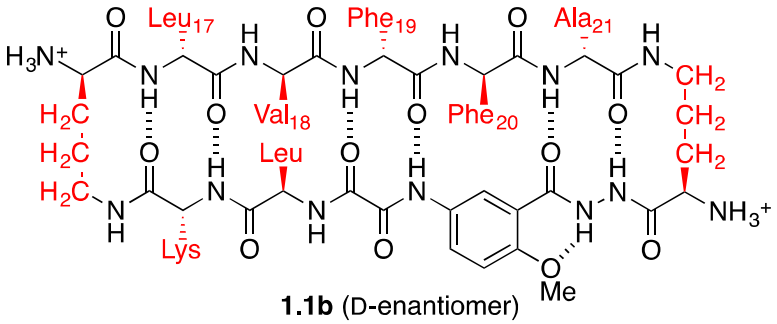

1.1b (D-enantiomer)

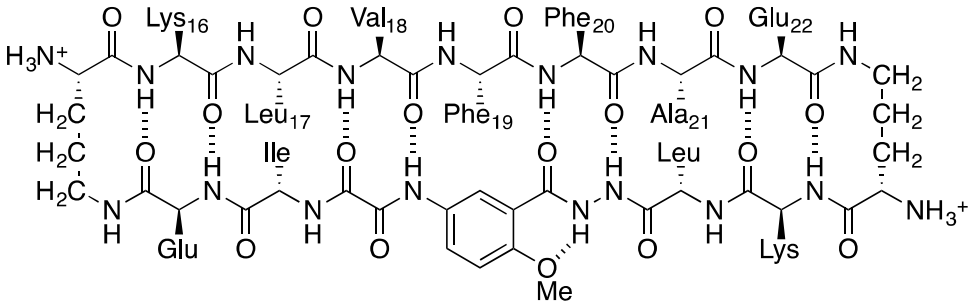

1.2a (L-enantiomer)

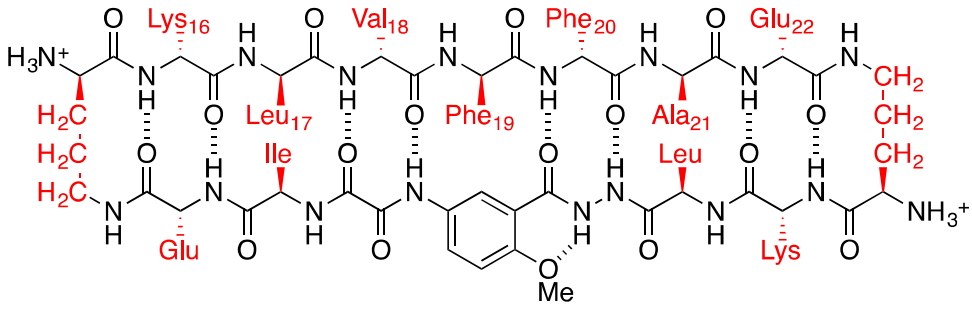

1.2b (D-enantiomer)

Figure 1.1. Macrocyclic L-enantiomer β-sheets **1.1a** and **1.2a** and their D-enantiomers **1.1b** and **1.2b**, respectively. D-Amino acids are highlighted in red.

RESULTS AND DISCUSSION

1. NMR studies of 1.1a, 1.1b, 1.2a and 1.2b. NMR spectroscopic studies show that enantiomers **1.1a** and **1.1b** and enantiomeric peptides **1.2a** and **1.2b** fold to adopt β-sheet

structures. Well-folded macrocyclic β-sheets are characterized by transannular nuclear Overhauser effect crosspeaks (NOEs) between alpha amino acid protons or alpha amino acid-Hao_6 protons of adjacent antiparallel strands (Tables 1.1 and 1.2). Downfield Hα chemical shifts also provide evidence of β-sheet folding (Figure 1.3). Since the only difference between **1.1a** and **1.1b** and **1.2a** and **1.2b** is chirality, the NMR spectra of enantiomeric pairs should be identical in chemical splitting resonances. Both pairs **1.1a** and **1.1b** and **1.2a** and **1.2b** possess overlapping chemical shifts and interstrand NOEs, confirming the β-sheet conformation (Tables, 1.1 and 1.2, Figures 1.3 and 1.4) and enantiomeric relationship between each pair.[6] The Hao_6-$F_{20}\alpha$ crosspeak in **1.1a** further supports the folding of **1.1a**.

2. NMR studies of 1.1c and 1.1d. Macrocyclic β-sheets **1.1c** and **1.1d** are enantiomers of each other and are diastereomers of **1.1a** and **1.1b**. In a similar fashion, macrocyclic β-sheets **1.2c** and **1.2d** are enantiomers of each other and are diastereomers of **1.2a** and **1.2b. 1.1c** and **1.1d** are identical by ^{1}H NMR, and possess differing chemical shifts compared to **1.1b**. The Hα chemical shifts of amino acids in a random coil peptide are more upfield than in a β-sheet structured peptide.[7] The Hα chemical shifts of **1.1a** are more downfield than previously published values of Hα chemical shifts in a random coil peptide, suggesting **1.1a** retains a β-sheet conformation (Figure 1.3). Inclusion of the D-ornithine turns causes the δHαs of **1.1d** to shift upfield and loss of the interstrand V_{18}-L and Hao-$Phe_{20}\alpha$ NOEs (Figure 1.3). These results suggest **1.1c** and **1.1d** are less structured than **1.1a** or **1.1b**.

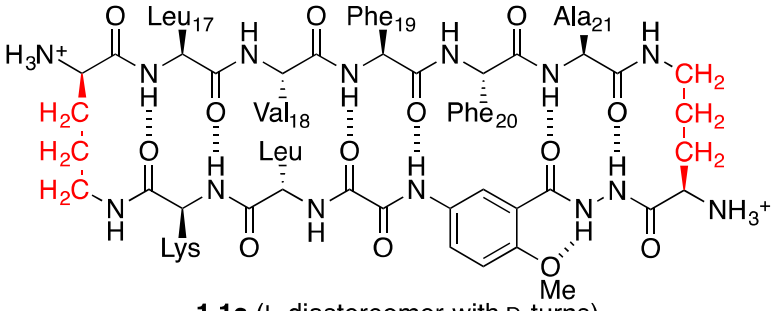

1.1c (L-diastereomer with D-turns)

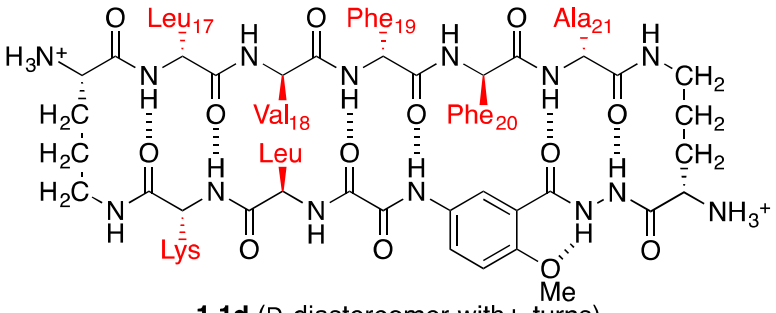

1.1d (D-diastereomer with L-turns)

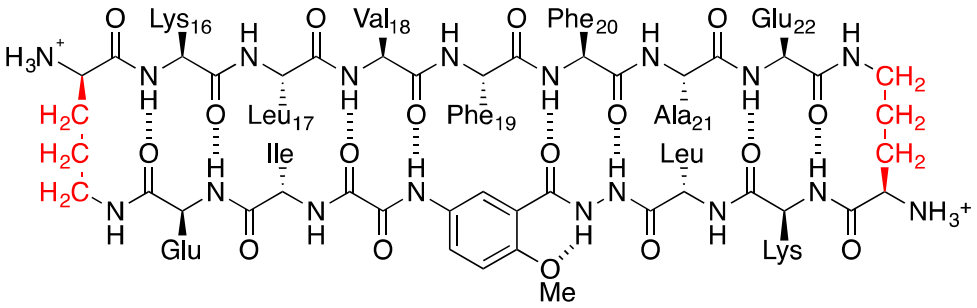

diastereomer **1.2c** with D-turns

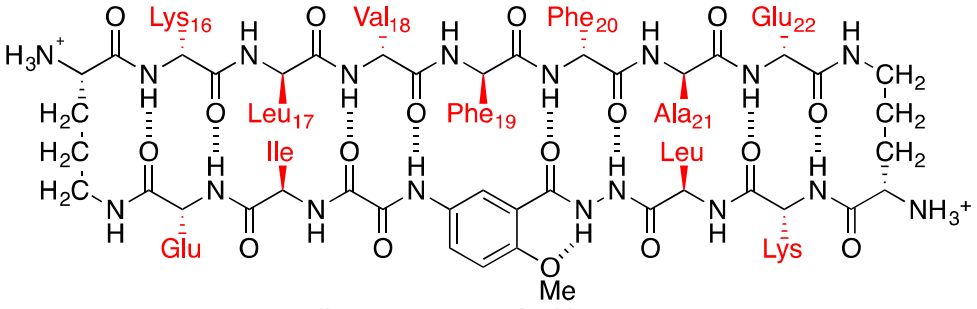

diastereomer **1.2d** with L-turns

Figure 1.2. Macrocyclic β-sheet pentapeptide diastereomers **1.1c** and **1.1d** and heptapeptide diastereomers **1.2c** and **1.2d.**

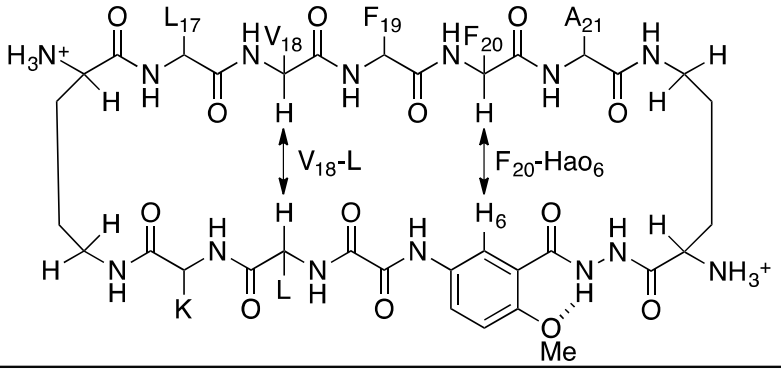

entry	sequence	V_{18}-L	F_{20}-Hao$_6$
1.1a	Orn-LVFFA-Orn-Hao-LK	Y	Y
1.1b	Orn-LVFFA-Orn-Hao-LK	Y	Y
1.1c	Orn-LVFFA-Orn-Hao-LK	N	N
1.1d	Orn-LVFFA-Orn-Hao-LK	N	N

Table 1.1. Observed NOEs of pentapeptide macrocyclic β-sheets **1.1**. The residues in red indicate D-amino acids. Y indicates observation of the NOE crosspeak and N indicates no NOE crosspeak was observed.

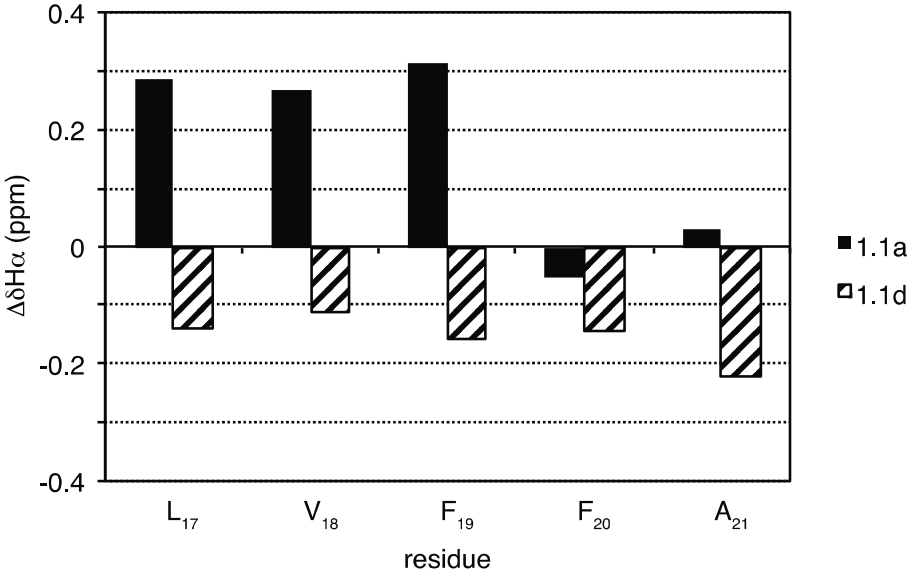

Figure 1.3. Hα chemical shift differences of **1.1a** and **1.1d.** Chemical shift differences of random coil H□ and calculated H□ in **1a** (black) and **1d** (striped).

3. NMR studies of 1.2c and 1.2d. The L-ornithine turns in **1.2a** were mutated to D-ornithine turns and the D-ornithine turns in **1.2b** were mutated to L-ornithine turns to create diastereomers **1.2c** and **1.2d,** respectively, to further probe the significance of chirality on inhibitor function of the heptapeptide macrocycles. The NMR spectra of **1.2c** and **1.2d** are identical, as they are enantiomeric pairs, and their chemical shifts differ in contrast to **1.2b**, their

diastereomeric counterpart. The Hα chemical shifts of **1.2a** are downfield compared to random coil values of Hα, and a strong NOE crosspeak between Hao_6-F_{19}α is observed in the **1.2a** ROESY spectrum, indicating **1.2a** is a well-folded β-sheet (Table 1.2). Substitution of D-ornithine turns into **1.2d** slightly perturbs folding; the flanking residues K_{16}, L_{17}, F_{19}, and A_{21} possess downfield δHαs (Figure 1.4). The F_{19} residue possesses the largest downfield Hα chemical shift difference, suggesting **1.2d** is in a partial β-sheet conformation. Retention of partial β-sheet structure in the core of **1.2d** is further evidenced by the Hao_6-Phe_{19}α interstrand NOE in **1.2d**. These data suggest diastereomers **1.2c** and **1.2d** are partially folded macrocycles, maintaining a β-sheet structure in the F_{19}-Hao core.

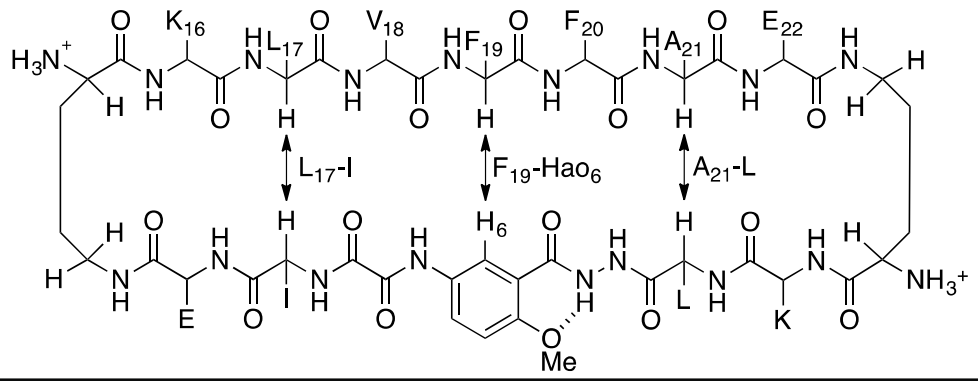

entry	sequence	L_{17}-I	F_{19}-Hao_6	A_{21}-L
1.2a	Orn-KLVFFAE-Orn-EI-Hao-LK	-*	Y	Y
1.2b	Orn-KLVFFAE-Orn-EI-Hao-LK	-*	Y	Y
1.2c	Orn-KLVFFAE-Orn-EI-Hao-LK	-*	Y	N
1.2d	Orn-KLVFFAE-Orn-EI-Hao-LK	-*	Y	N

-* NOE not observed due to overlap between resonances.

Table 1.2. Observed NOEs of pentapeptide macrocyclic β-sheets **1.1**. D-Amino acids are in red. Y indicates observation of the NOE crosspeak and N indicates no NOE crosspeak was observed.

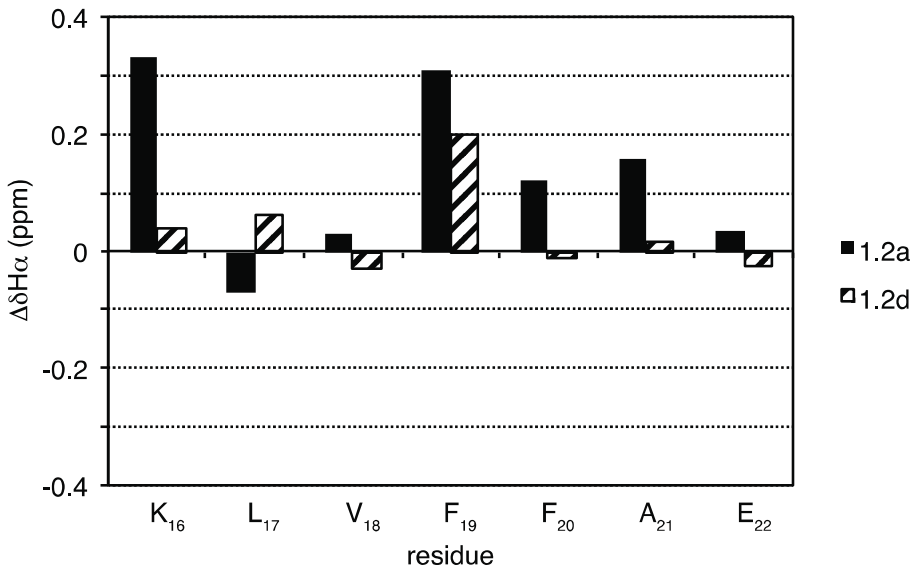

Figure 1.4. Hα chemical shift differences of **1.2a** and **1.2d.** Chemical shift differences of random coil Hα and calculated Hα in **1.2c**.

4. 1.1b delays $A\beta_{40}$ aggregation more effectively than 1.1a. Thioflavin T (ThT) fluorescence assays show **1.1a** only modestly inhibits $A\beta_{40}$ aggregation while **1.1b** perturbs aggregation with greater efficacy (Figure 1.5). **1.1a** has very modest effects on $A\beta_{40}$ kinetics at substoichiometric amounts; at 0.1 equivalents, lag time is increased by 118% while **1.1b** increases lag time by 607%. A dose dependent response is observed at higher amounts; $A\beta_{40}$ lag time is increased to 374% under 0.3 equivalents of **1.1a** and when $A\beta_{40}$ is mixed with 0.3 equivalents of **1.1b**, lag time is increased by 1206%. Building from our prior work, it is possible **1.1a** can target the growing intermediates, while **1.1b** is more effective at interfering with $A\beta_{40}$ at lower concentrations with a small sequence.

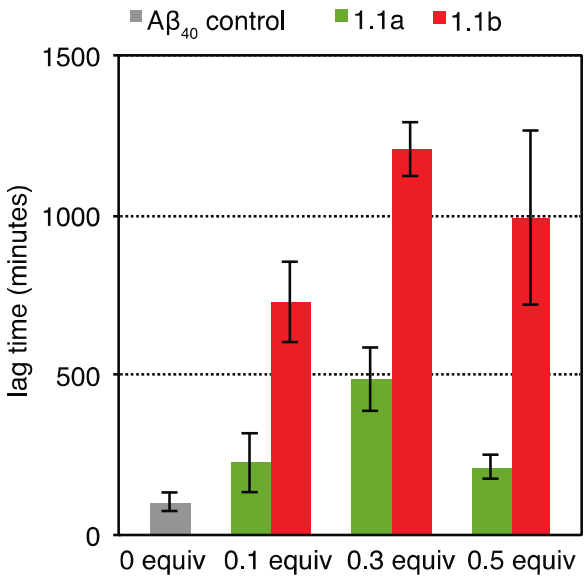

Figure 1.5. Effect of **1.1a** or **1.1b** on $A\beta_{40}$ aggregation. **1.1a** slightly delays aggregation and **1.1b** delays aggregation by more than twofold at similar concentrations.

5. $A\beta_{40}$ aggregation delay by 1.2a and suppression by 1.2b. ThT fluorescence assays show that peptides **1.2** are better inhibitors of $A\beta_{40}$ aggregation and **1.2b** can suppress $A\beta_{40}$ aggregation over time. To assess and compare macrocycle efficacy, fluorescence assays were executed in substoichiometric concentrations of either **1.2a** or **1.2b** (Figure 1.6). Fluorescence assays highlight a difference in $A\beta_{40}$ aggregation kinetics in the presence of **1.2a** or **1.2b** even at low concentrations; at 0.1 equivalents of **1.2a**, $A\beta_{40}$ fibrillization is delayed 186%, while at 0.1 equivalents of **1.2b** $A\beta_{40}$ lag time is increased by 380% (Figure 1.6). Differences between **1.2a** and **1.2b** are become more prominent at higher concentrations; 0.3 equivalents **1.2a** delays $A\beta_{40}$ accumulation by 308% while at 0.3 equivalents of **1.2b** $A\beta_{40}$ aggregation is halted by 3800%. Our work suggests the growing $A\beta_{40}$ nucleus is preferentially perturbed by enantiomeric β-sheets and intercalating interactions between L-$A\beta_{40}$ with D-macrocycles provides more stabilizing interactions than homochiral interactions.

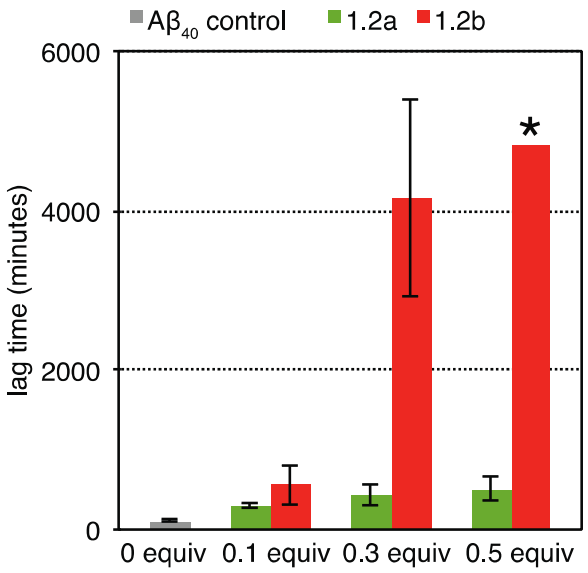

Figure 1.6. Effect of **1.2a** (green) or **1.2b** (red) on $A\beta_{40}$ aggregation. The asterisk above **1.2b** indicates indicates $A\beta_{40}$ fibrillization suppression throughout the course of the assay.

6. Diastereomers 1.1c and 1.1d are less effective at delaying $A\beta_{40}$ aggregation than 1.1b. To further test the effects of chirality on macrocyclic β-sheet function, each diastereomer **1.1c** and **1.1d** was tested against $A\beta_{40}$ fibrillization. Both **1.1c** and **1.1d** did not show greater lag times relative to **1.1b.** At 0.1 equivalents, **1.1c** slightly delays aggregation by 178% while **1.1d** delays aggregation by 126%, compared to **1.1b**'s aggregation delay by 607%. At 0.3 equivalents, inhibition is improved; **1.1c** delays aggregation by 360%, and **1.1d** delays aggregation by 450%, yet **1.1c** and **1.1d** are less effective than **1.1b** at 0.3 equivalents, delaying aggregation by 1077% (Figures 1.7 and 1.8). Even at elevated concentrations, **1.1b** outperforms **1.1c** and **1.1d**; **1.1b** delays aggregation by 868%, while **1.1c** delays aggregation by 40% and **1.1d** delays aggregation by 543%. This suggests chirality affects macrocycle affinity to $A\beta_{40}$. Diastereomer **1.1d** was more effective than **1.1c**, presumably because macrocycles have a greater affinity for $A\beta_{40}$ when D-amino acids are incorporated into the recognition strand.

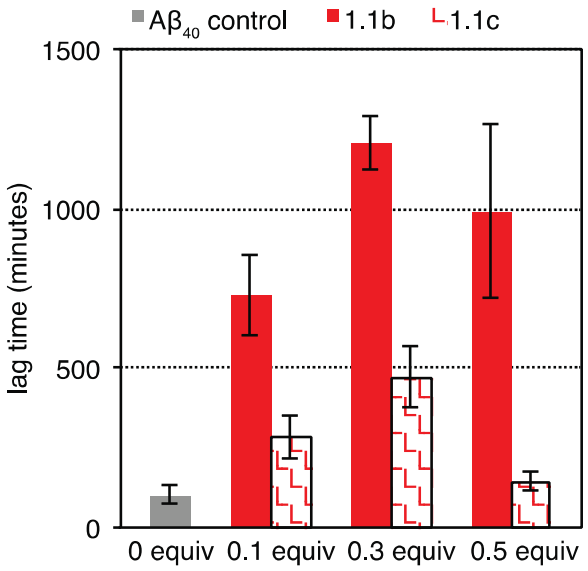

Figure 1.7. Effect of **1.1b** or **1.1c** on $A\beta_{40}$ aggregation. $A\beta_{40}$ lag times in the presence of **1.1b** or diastereomer **1.1c**.

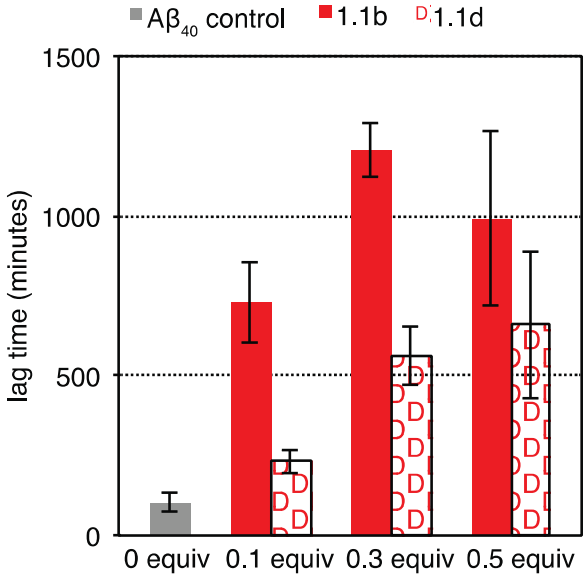

Figure 1.8. Effect of **1.1b** or **1.1d** on $A\beta_{40}$ aggregation. **1.1b** and diastereomer **1.1d** in the presence of $A\beta_{40}$.

7. Diastereomers 1.2c and 1.2d do not suppress $A\beta_{40}$ aggregation. Inhibition is hampered as 0.1 equivalents of **1.2b** stalls aggregation by 418% whereas 0.1 equivalents of **1.2c** stalls aggregation by 105% and **1.2d** stalls aggregation by 202%. Larger differences between **1.2b** versus **1.2c** and **1.2d** are observed at increased concentrations; at 0.3 equivalents, **1.2b** disrupts $A\beta_{40}$ accumulation by 3812% while **1.2c** slightly disrupts $A\beta_{40}$ accumulation by 52%

and **1.2d** disrupts aggregation by 1329% (Figures 1.9 and 1.10). At 0.5 equivalents, **1.2b** suppresses $A\beta_{40}$ aggregation for the duration of the assay (over 80 hours), trumping its diastereomers **1.2c,** which modestly delays aggregation by 229%, and **1.2d,** which delays aggregation by 1881%. These results suggest enantiomeric β-sheets preferentially interact with $A\beta_{40}$ intermediates. In reference to the nucleation dependent polymerization model, preorganization into a β-strand can preferentially accesses the growing oligomer nucleus.[8,9] The intercalating heterochiral interactions provided by **1.2b** are more easily accessed when initially constrained into a β-sheet orientation.

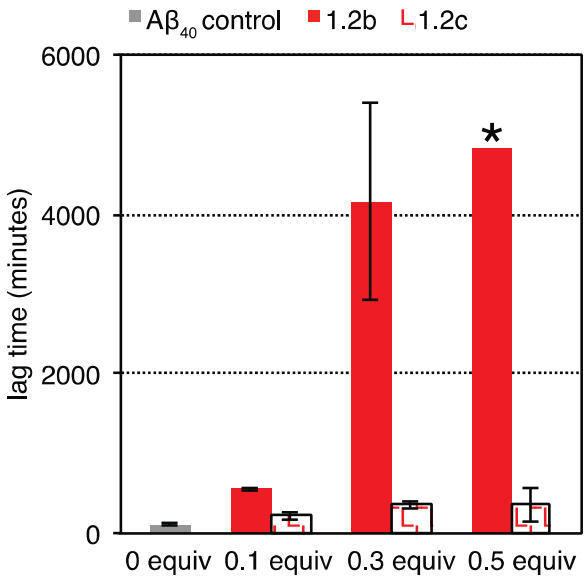

Figure 1.9. Effect of **1.2b** or **1.2c** on $A\beta_{40}$ aggregation. Diastereomer **1.2c** is much less effective at inhibiting $A\beta_{40}$ aggregation than **1.2b.**

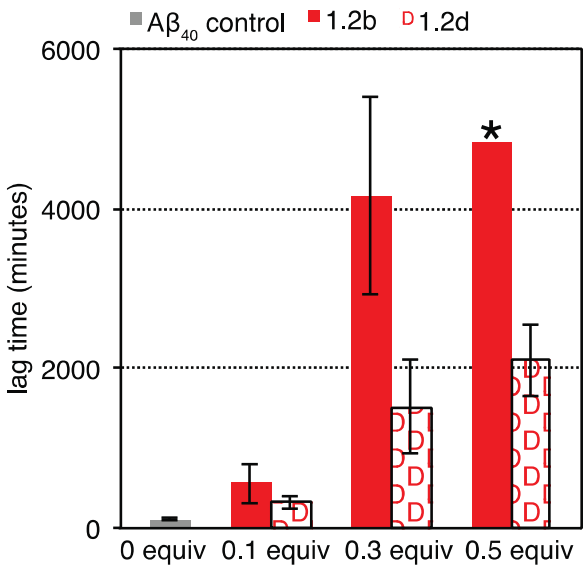

Figure 1.10. Effect of **1.2b** or **1.2d** on $A\beta_{40}$ aggregation. **1.2b** is more effective against $A\beta_{40}$ aggregation compared to its diastereomer **1.2d**. The asterisk above **1.2b** denotes suppression of ThT fluorescence during the entire assay.

8. TEM supports improved $A\beta_{40}$ suppression of 1.1b over 1.1a. Transmission electron microscopy (TEM) studies corroborate prior findings of aggregation suppression. In these studies 0.3 equivalents of macrocycle was incubated with $A\beta_{40}$ with shaking for 12 hours, and aliquots were spotted onto grids for examination. After 12 hours fibrils and their fragments were observed in the $A\beta_{40}$ control conditions (Figure 1.11, left) and in the presence of **1.1a** (Figure 1.1, middle), yet absent in the presence of **1.1b** (Figure 1.11, right), supporting the notion enantiopeptide **1.1b** preferentially interferes with $A\beta_{40}$ accumulation. The fibril shards observed in the $A\beta_{40}$ control are due to mechanical stress caused by shaking of the plate during the course of the assay, inducing long fibers to fragment.

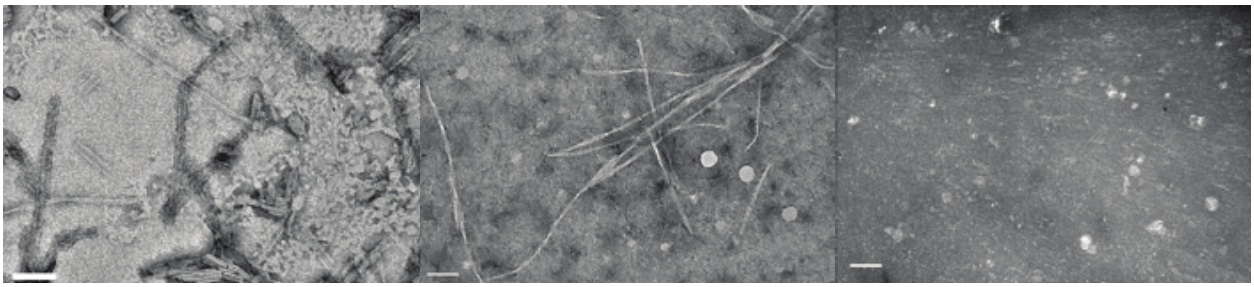

Figure 1.11. TEM images of **1.1a** and **1.1b** on $A\beta_{40}$ aggregation. $A\beta_{40}$ fibrillization in the absence (left) or presence of **1.1a** (middle) or **1.1b** (right) at 0.3 equivalents after 12 hours. The scale bars indicate 100 nm.

9. TEM shows $A\beta_{40}$ suppression by 1.2b. $A\beta_{40}$ incubation in the presence of **1.2a** or **1.2b** produced similar results. After 12 hours, fibrils appeared with $A\beta_{40}$ incubated with **1.2a** (Figure 1.12, middle), while fibrils were absent when $A\beta_{40}$ was incubated with **1.2b** (Figure 1.12, right). Images of $A\beta_{40}$ incubated with **1.2b** show small, round, artifacts, indicating **1.2b** is inducing $A\beta_{40}$ to create globular products. These images suggest $A\beta_{40}$ interacts with **1.2b** for a longer period of time compared to **1.2a**, and the interaction results in a spherical morphology.

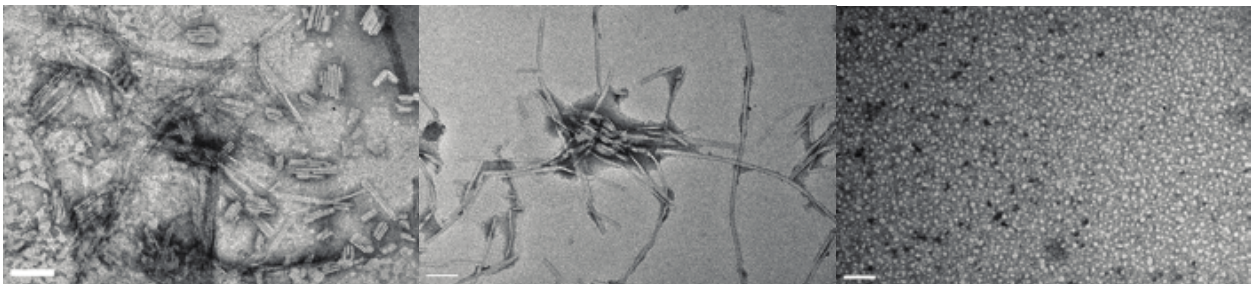

Figure 1.12. TEM images of **1.2a** and **1.2b** on $A\beta_{40}$ aggregation. $A\beta_{40}$ fibrillization in the absence (left) or presence of 0.3 equivalents **1.2a** (center) or **1.2b** (right) after 12 hours. The scale bars indicate 100 nm.

CONCLUSION

In conclusion, D-macrocyclic peptides show increased delay or suppression of fibrillization compared to previously published models. In both the 42- and 54-membered rings, the D-enantiomers of macrocyclic β-sheets inhibit the aggregation of $A\beta_{40}$ more strongly than the L-enantiomers. This finding is surprising, as the opportunity for eclipsing hydrophobic contacts is unavailable between heterochiral peptides. Peptide constraint into a β-sheet conformation

influences interactions between $A\beta_{40}$ and macrocycle and implies increased affinity of interactions between heterochiral peptides. The **c** and **d** diastereomers in each class of peptides are less folded than their **a** or **b** counterparts and perform less efficiently than **1.1b** or **1.2b.** It is possible to utilize **1.1b** and **1.2b** as kinetic tools to probe stabilized *in vitro* intermediates when coupled with analytical techniques.[10,11]

References and Notes

[1] Mandal, K.; Pentelute; B. L.; Tereshko, V.; Thammavongsa, V.; Scheewind, O.; Kossiakoff, A. A.; Kent, S. B. H. *Protein Sci.* **2009,** *18,* 1146-1154.

[2] Schumacher, T. N. M.; Mayr, L. M.; Minor Jr., D. L.; Milhollen, M. A.; Burgess, M. W.; Kim, P. S. *Science* **1996,** *271,* 1854-1857.

[3] Wang, L.; Li, Y.; Wang, L.; Li, F. *FEBS Lett.* **2014,** *588,* 884-891.

[4] Kar, K.; Arduini, I.; Drombowsky, K. W.; van der Wel, P. C. A.; Wetzel, R. *J. Mol. Biol.* **2014,** *426,* 816-829.

[5] Cheng, P.-N.; Liu, C.; Zhao, M.; Eisenberg, D.; Nowick, J. S. *Nat. Chem.* **2012,** *4,* 927-933.

[6] Woods. R. J.; Brower, J. O.; Castellanos, E.; Hashemzadeh, M.; Khakshoor, O.; Russu, W. R.; Nowick, J. S. *J. Am. Chem. Soc.* **2007,** *129,* 2548-2558.

[7] Wishart, D. S.; Case, D. A. *Methods Enzymol.* **2001,** *338,* 3-34.

[8] Harper, J. D.; Lansbury Jr., P. T. *Annu. Rev. Biochem.* **1997,** *66,* 385-407.

[9] Gillam, J. E.; MacPhee, C. E. *J. Phys. Condens. Matter* **2013,** *25,* 1-20.

[10] Bernstein, S. L.; Dupuis, N. F.; Lazo, N. D.; Wyttenbach, T.; Condron, M. M.; Bitan, G.; Teplow, D. B.; Shea, J.-E.; Ruotolo, B. T.; Robinson, C. V.; Bowers. M. T. *Nat. Chem.* **2009,** *1, 326-331.*

[11] Bleiholder, C.; Dupuis, N. F.; Wyttenbach, T.; Bowers, M. T. *Nat. Chem.* **2011,** *3,* 172-177.

Experimental Section for Chapter 1

Peptide synthesis. Peptides were as previously described[1], with the following modifications: 1) Fmoc-Hao-OH was used in substitution of Fmoc*-Hao-OH, 2) the linear protected peptide was cleaved from the 2-chlorotrityl chloride resin with a cocktail of 4:1 DCM:HFIP for one hour and concentrated by rotary evaporation to a clear film[2], and 3) HOBt and HBTU (6 equivalents each) were used in substitution of HCTU.

NMR spectroscopic studies. *Studies in D_2O.* Peptides **1.1a-d** were gravimetrically measured and dissolved in "100%" D_2O (Cambridge Isotope Laboratories, DLM-4) to a final concentration of 2 mM. Peptides **1.2a-d** were dissolved in D_2O to a final concentration of 1 mM. Molecular weights were calculated with the free amines as a TFA salt. 1D ^{1}H, 2D ROESY and TOCSY NMR spectra were conducted on a Bruker 500 MHz NMR spectrometer equipped with a cryoprobe at 298 K. ^{1}H NMR spectra were collected for 64 scans. 2D TOCSY spectra were collected with 150 ms spin-lock mixing time. 2D ROESY spectra were collected with 300 ms spin-lock mixing time. 2D TOCSY and ROESY spectra were executed with 2048 points in the *f*2 domain and 512 points in the *f*1 domain and processed to a 1024 x 1024 matrix using the QSINE processing parameters. NMR spectra were processed using Bruker XWinNMR software.

Studies in 9:1 H_2O:D_2O. Peptides **1.1** were dissolved in 9:1 H_2O:D_2O to a final concentration of 2 mM and peptides **1.2** were dissolved in 9:1 H_2O:D_2O to a final concentration of 1.5 mM. Molecular weights were calculated with the free amines as a TFA salt. 1D ^{1}H, 2D TOCSY and ROESY spectra were collected on a Bruker AVANCE600 NMR spectrometer fitted with a triple resonance broad band (TBI) probe at 278 K. 2D COSY spectra with solvent suppression were collected on a Bruker 500 mHz spectrometer equipped with a cryoprobe. ^{1}H NMR spectra with solvent suppression were collected for 32 scans. 2D TOCSY with solvent suppression using perfect echo watergate were collected with 200 ms spin-lock mixing time. 2D ROESY with

solvent suppression using perfect echo watergate were collected 100 ms spin-lock mixing time. 2D COSY spectra were collected for 16 scans. 2D TOCSY, ROESY and COSY spectra were collected with 2048 points in the *f2* dimension and 512 points in the *f*1 dimension and processed to a 1024 x 1024 matrix using QSINE processing parameters. Spectra were processed using Bruker XWinNMR software.

Thioflavin T (ThT) fluorescence assays. ThT fluorescence assays were carried out in Corning 96-well black clear bottom plates with shaking on a Gemini XPS fluorescence plate reader (Molecular Devices). Readings were collected at 37 °C every 10 minutes for 41 hours at excitation 442 nm, emission 482 nm, with 5 seconds shaking before the first reading and 575 seconds shaking in between readings.

Preparation of ThT stock solution. Thioflavin T stock was freshly prepared before each assay. 2.5 mg of ThT (Sigma-Aldrich, T3516-5G) was gravimetrically measured and dissolved in 10 mLs 18 MΩ H_2O and filtered through 0.2 μM nylon filters. The Thioflavin T solution was diluted to 1/25 and was measured at 412 nm with a JASCO-V-530 UV-Vis spectrophotometer (ε_{ThT} = 36,000 $M^{-1}\cdot cm^{-1}$). The Thioflavin T solution was further diluted with 0.2 μM filtered 10x PBS with 0.02% NaN_3, pH 7.4 to create a working stock of 100 μM ThT in 5x PBS, pH 7.4.

Preparation of inhibitor solutions. Peptides were measured gravimetrically to create a 1 mM solution in 18 MΩ H_2O. An aliquot was diluted by 1/25 for spectrophotometric measurements using a JACSO-V-530-UV-Vis spectrophotometer (ε_{Hao} = 9850 $M^{-1}\cdot cm^{-1}$ at 280 nm). The 1 mM solution was further diluted with 18 MΩ H_2O to create a 200 μM working stock. The inhibitor was plated into the wells at the appropriate concentrations, followed by addition of 18 MΩ water and 100 μM ThT stock.

Preparation of $A\beta_{40}$ solution. Prior to the start of the experiment, three Nanosep 100 kDa centrifuge filters (Pall, OD100C34) were washed prior to the experiment with 500 μL of 18 MΩ water three times for 5 minutes at 10,000 rpm. Synthetic $A\beta_{40}$ was purchased from GL Biochem Shanghai. 1.5 mg $A\beta_{40}$ was measured gravimetrically in a 1.5 mL eppendorf tube and dissolved in 146 μL 100 mM NaOH (analytical grade, Fisher SS266-1) to create a 2 mM solution.[3] The $A\beta_{40}$ solution was sonicated for 30 seconds in a water bath and further diluted with 1315 μL of 18 MΩ water to create a working stock solution of 200 μM. The $A\beta_{40}$ solution was sonicated again for 30 seconds, and 500 μL aliquots were filtered through three washed Nanosep 100 kDa centrifuge filters for 5 minutes at 10,000 rpm. $A\beta_{40}$ was added lastly to the wells in 20 μL aliquots for a final total reaction volume of 200 μL. The plate was sealed with sealing film, inserted into the plate reader, and the experiment was initiated. Experiments were run in octuplicate, with the six most representative traces displayed and the two least representative traces omitted.

Table S1.1. Representative Volumes of 96-Well Reaction Plate.

Wells	ThT solution (μL)	inhibitor solution (μL)	water (μL)	$A\beta_{40}$ solution (μL)
ThT control	40	0	160	0
$A\beta_{40}$ control	40	0	140	20
$A\beta_{40}$ + 0.1 equiv inhibitor	40	2	138	20
$A\beta_{40}$ + 0.3 equiv inhibitor	40	6	134	20
$A\beta_{40}$ + 0.5 equiv inhibitor	40	10	130	20

Tht assays of **1.1a**

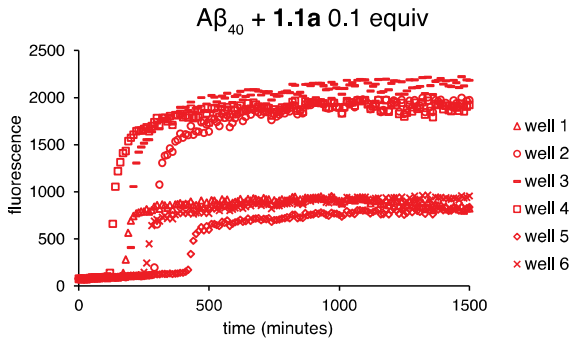

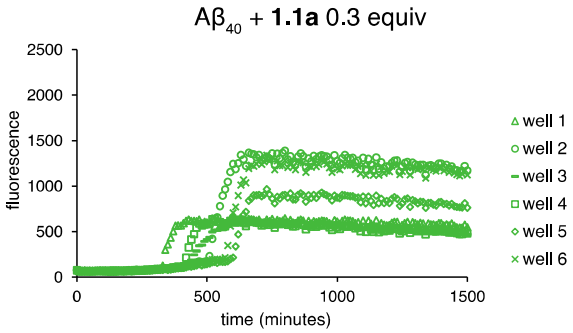

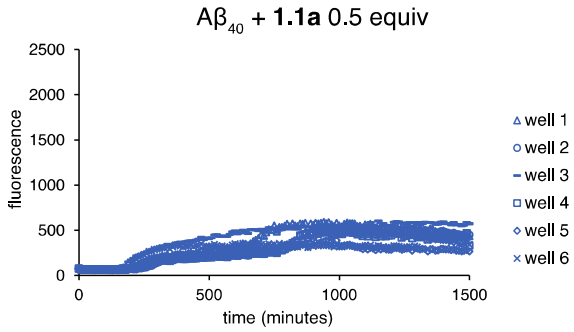

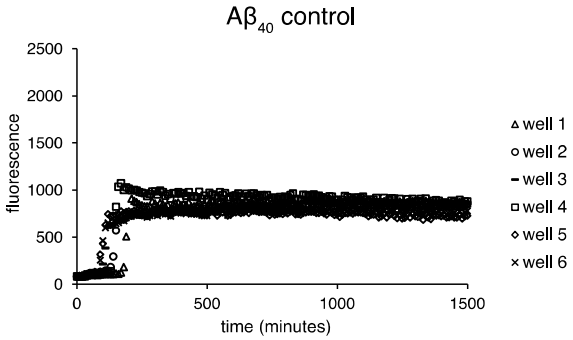

Tht assays of **1.1b**

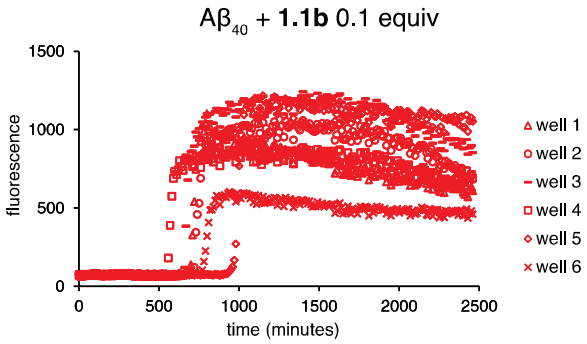

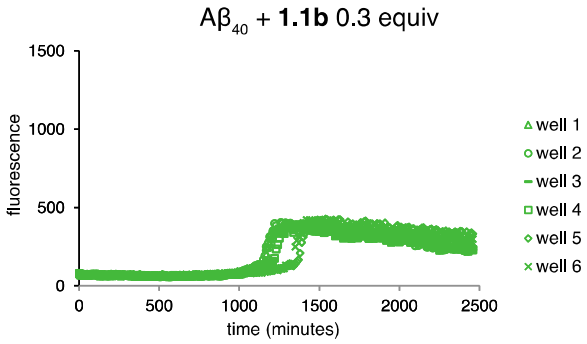

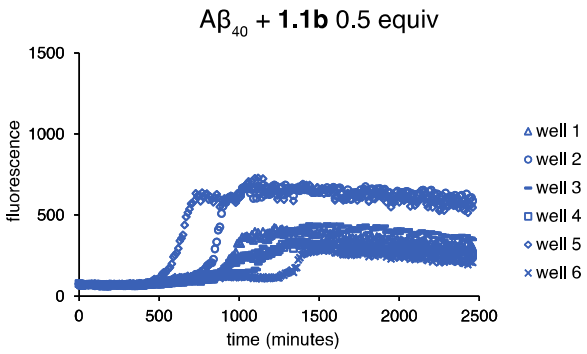

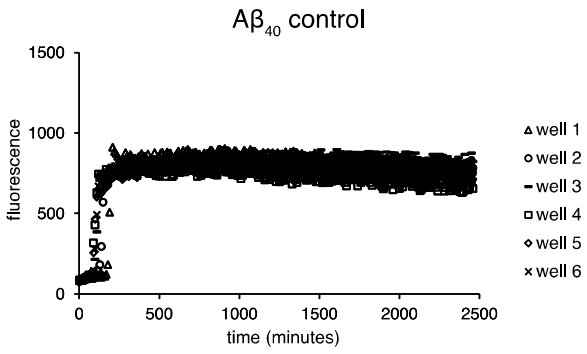

Tht assays of **1.1c**

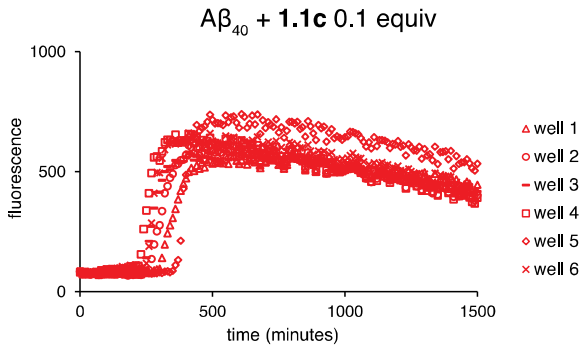

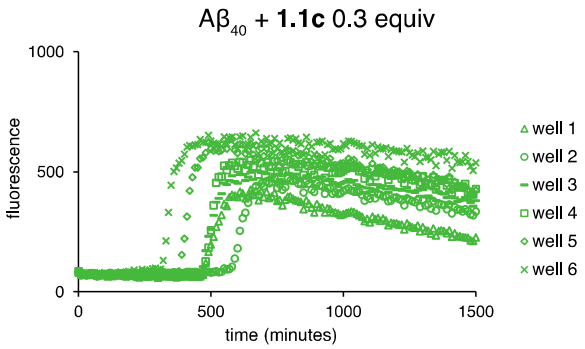

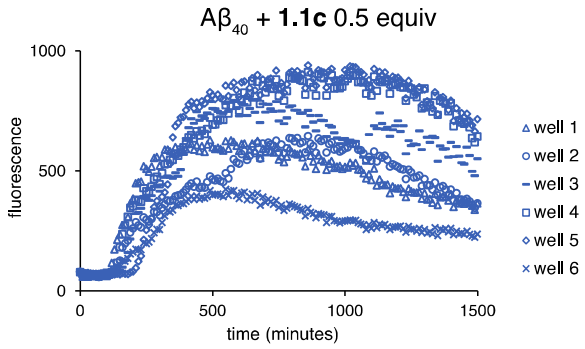

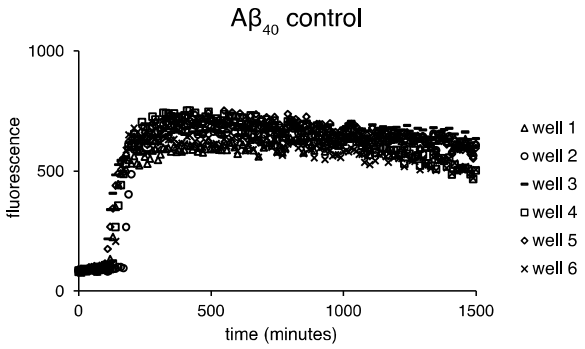

Tht assays of **1.1d**

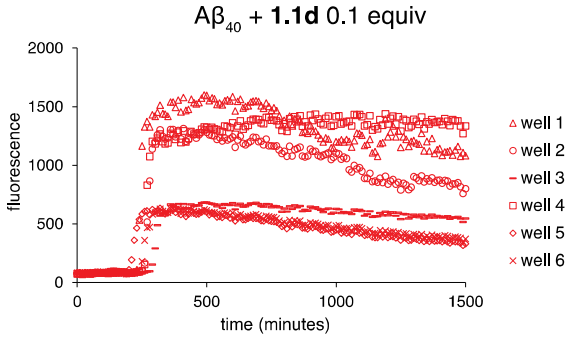

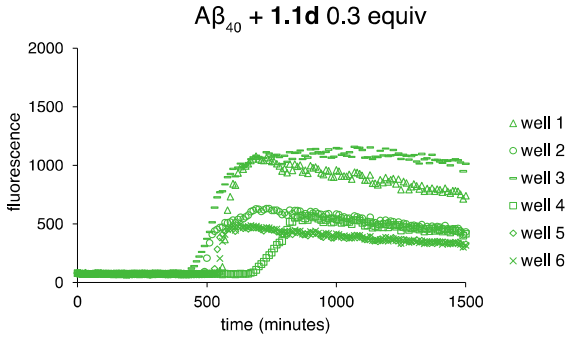

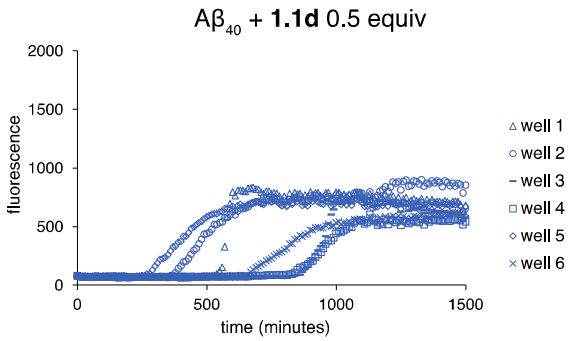

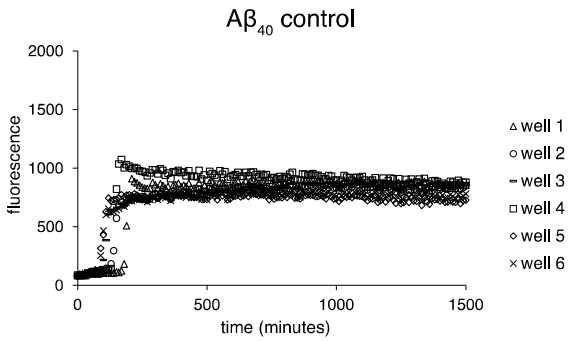

Tht assays of **1.2a**

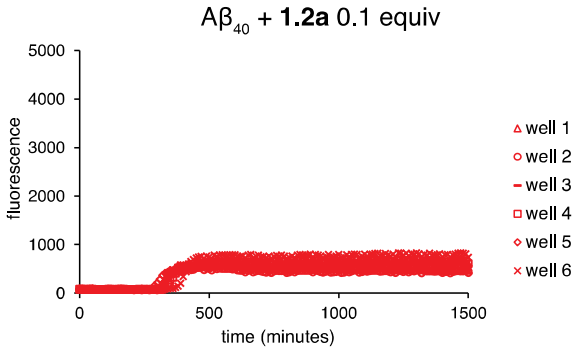

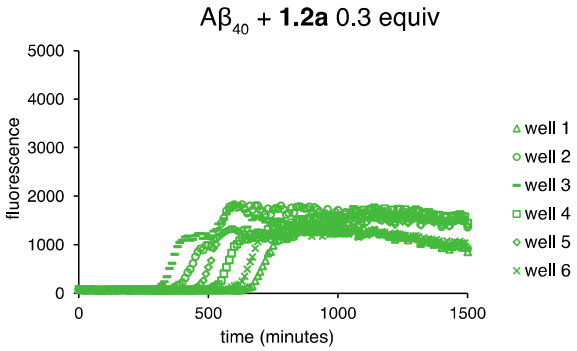

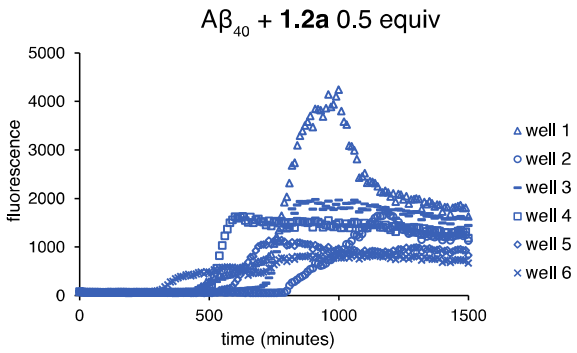

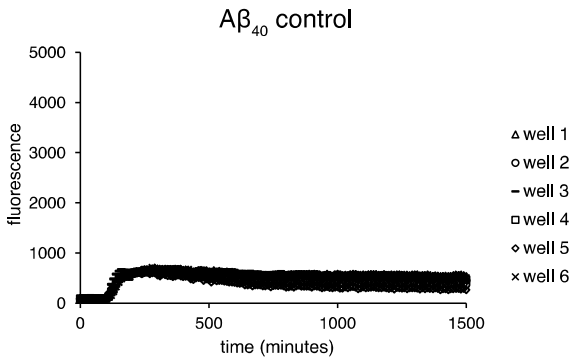

Tht assays of **1.2b**

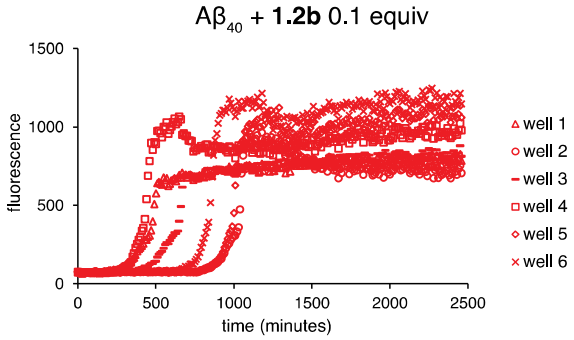

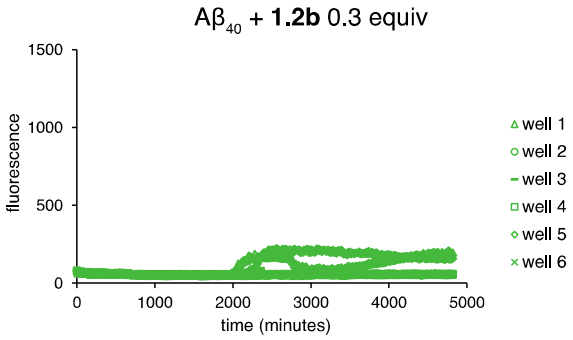

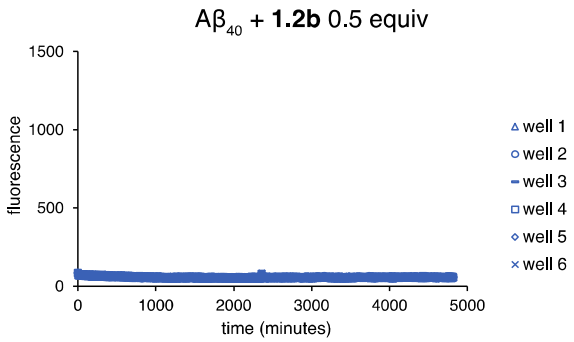

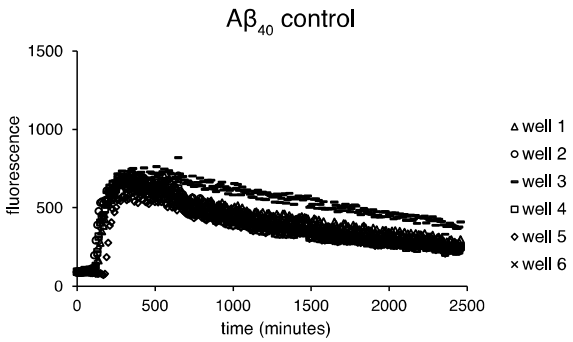

Tht assays of **1.2c**

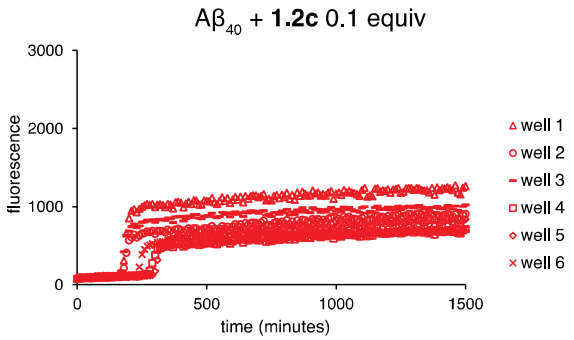

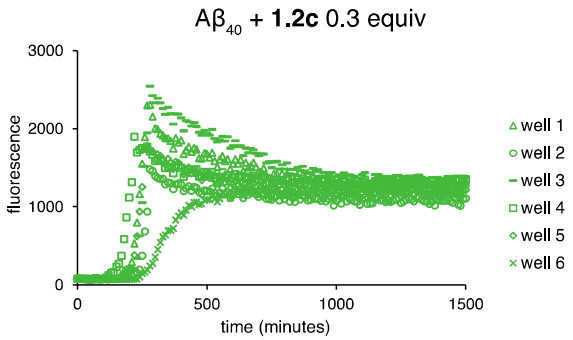

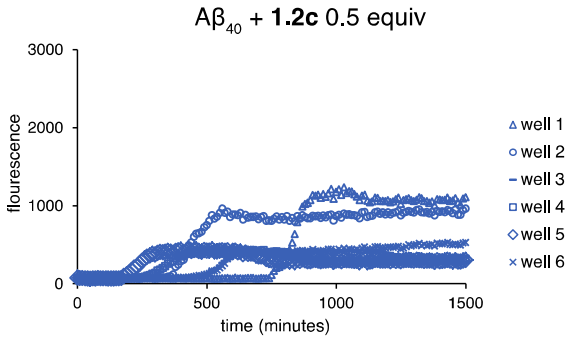

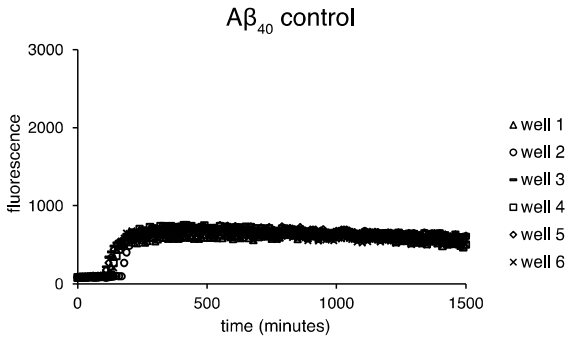

Tht assays of **1.2d**

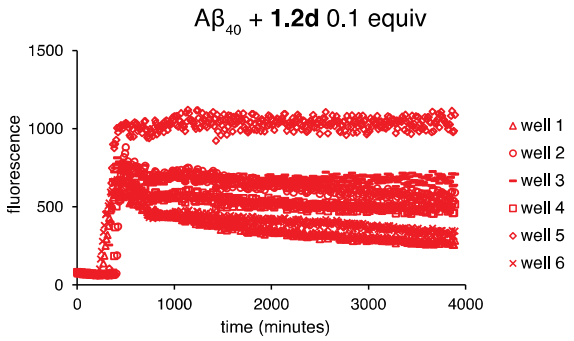

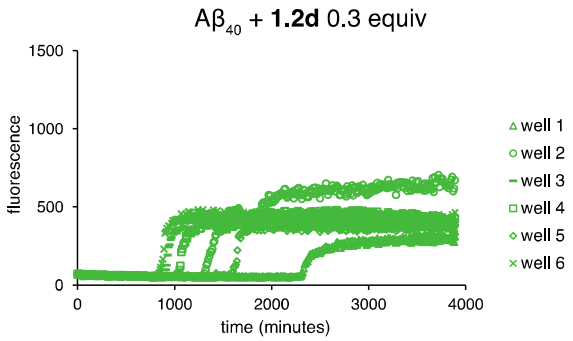

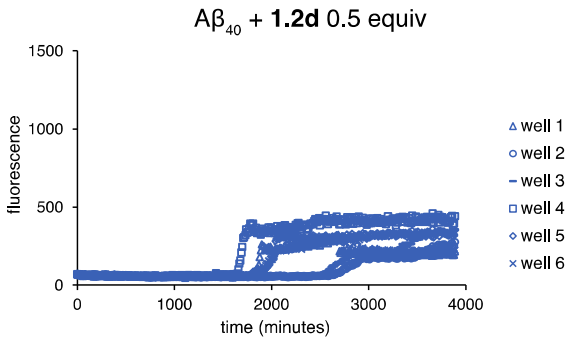

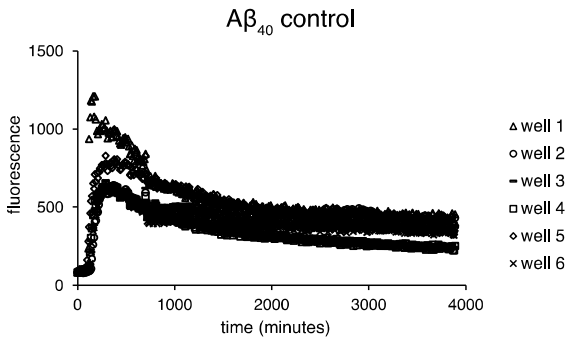

Transmission electron microscopy (TEM) sample preparation and imaging. Samples for TEM images were collected from the previously described ThT assays above. Aliquots were collected after 12 hours of incubation and shaking. 10 μL aliquots were collected and spotted onto carbon-formvar coated copper grids (Ted Pella, 400 mesh, 01754-F) and allowed to sit for one minute, and the excess liquid was wicked with filter paper. The samples were washed with 10 μL of double distilled water, allowed to sit for one minute, and the excess liquid was wicked with filter paper. The samples were stained with 10 μL of a 2% w/v uranyl acetate solution, allowed to sit for one minute, and the excess stain was wicked with filter paper. Samples were imaged on a Philips CM-20 electron microscope with an operating voltage of 80 kV connected to a Gatan Microdigital CCD camera.

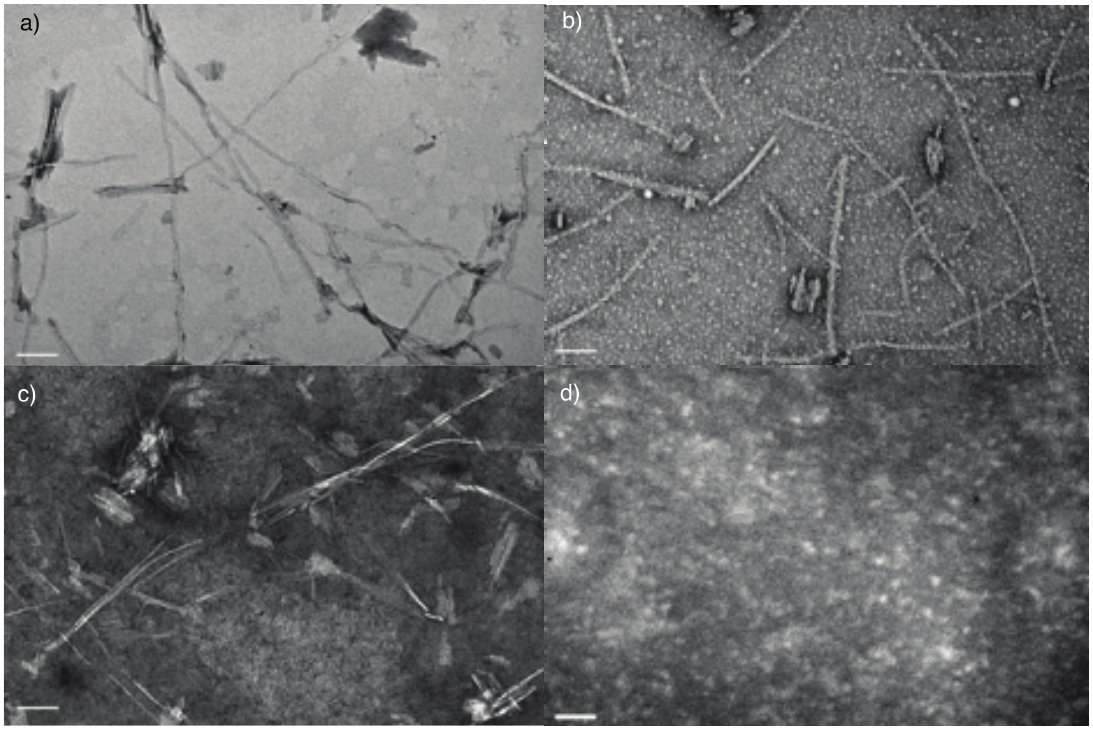

Figure S1.1. TEM images of $A\beta_{40}$ incubated with **1.1c** (top left, a), **1.1d** (top right, b), **1.2c** (bottom left, c) or **1.2d** (bottom right, d) for 12 hours. The scale bar indicates 100 nm.

HPLC trace of **1.1a**

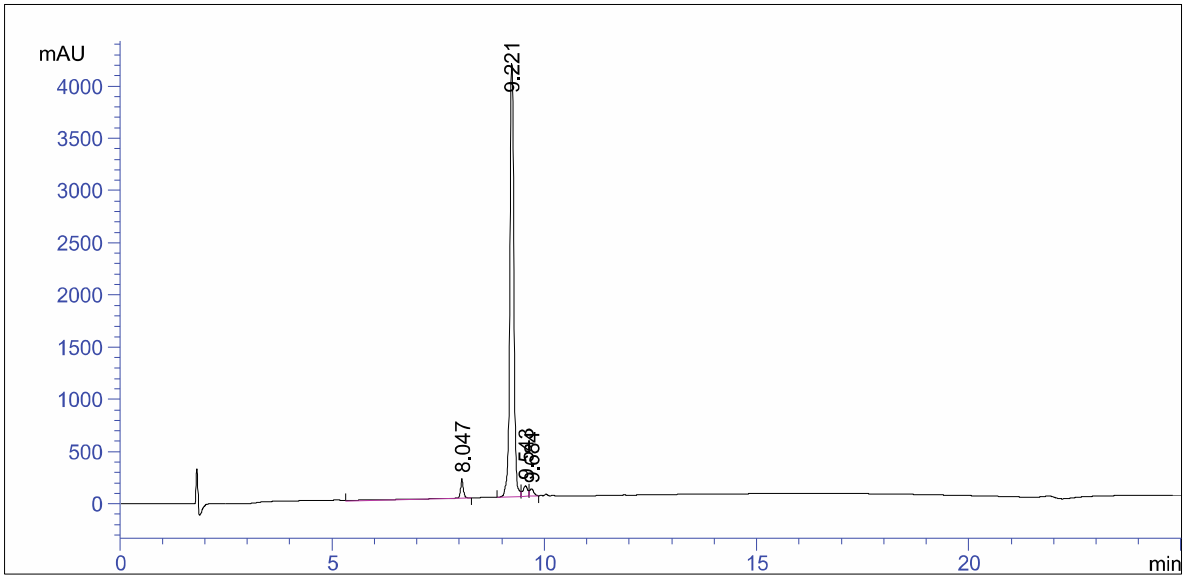


```
=====================================================================
                       Area Percent Report
=====================================================================
Signal 1: VWD1 A, Wavelength=214 nm

Peak RetTime Type  Width     Area      Height     Area
  #   [min]        [min]  mAU   *s   [mAU   ]       %
----|-------|----|-------|----------|----------|--------|
   1   8.047 VB    0.1003 1352.58594  187.33238   4.5195
   2   9.221 BV    0.1031 2.73758e4  4151.62305  91.4731
   3   9.543 VV    0.1087  730.39606   98.10030   2.4405
   4   9.684 VB    0.1033  468.92010   68.34472   1.5668

Totals :                  2.99277e4  4505.40044

=====================================================================
                       *** End of Report ***
```

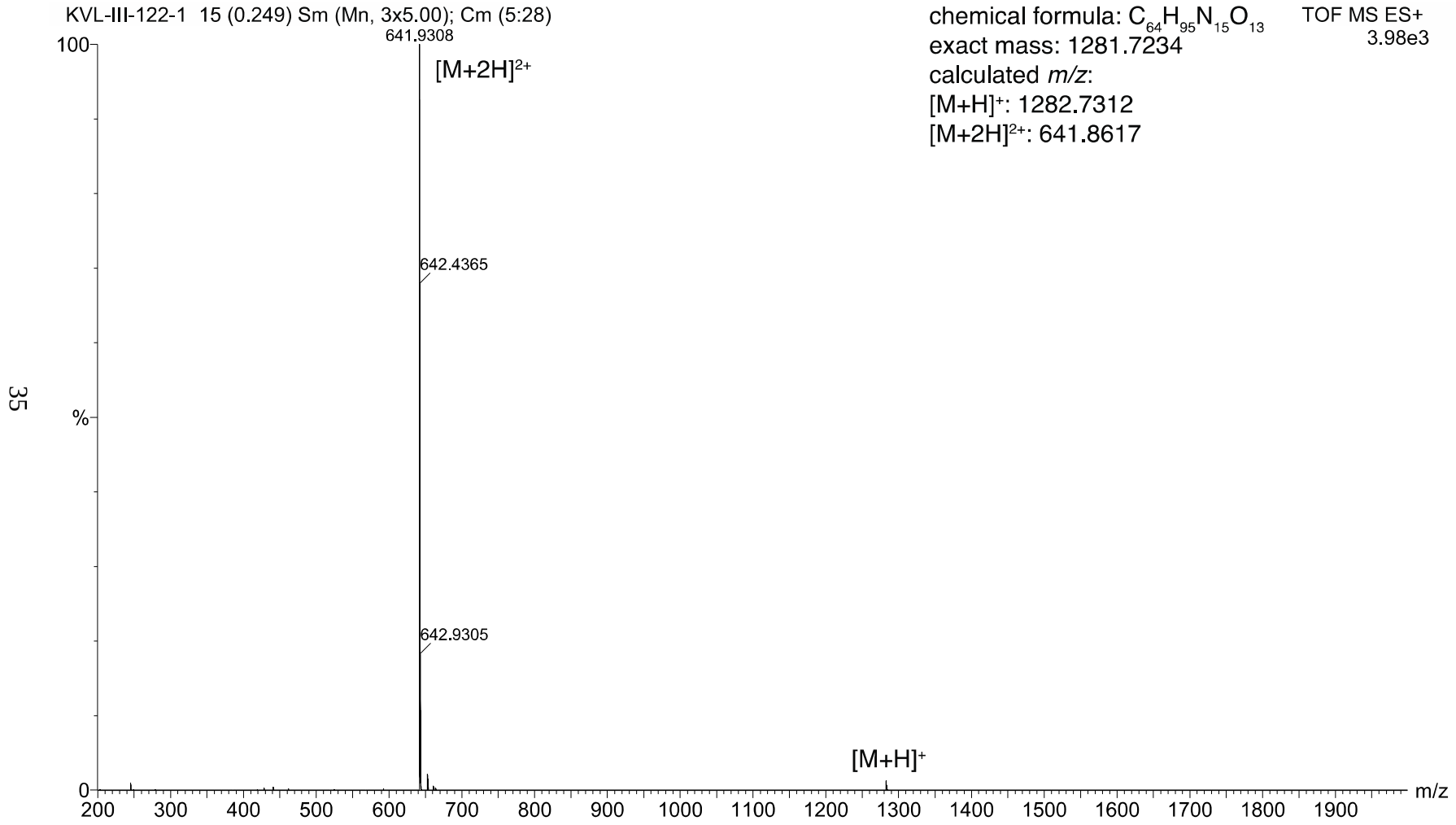

ESI-MS of **1.1a**
chemical formula: $C_{64}H_{95}N_{15}O_{13}$
exact mass: 1281.7234
calculated *m/z*:
$[M+H]^+$: 1282.7312
$[M+2H]^{2+}$: 641.8617

TOF MS ES+
3.98e3

1D ^{1}H NMR spectrum of **1.1a**, 500 mHz, 2 mM in D_2O, 298 K

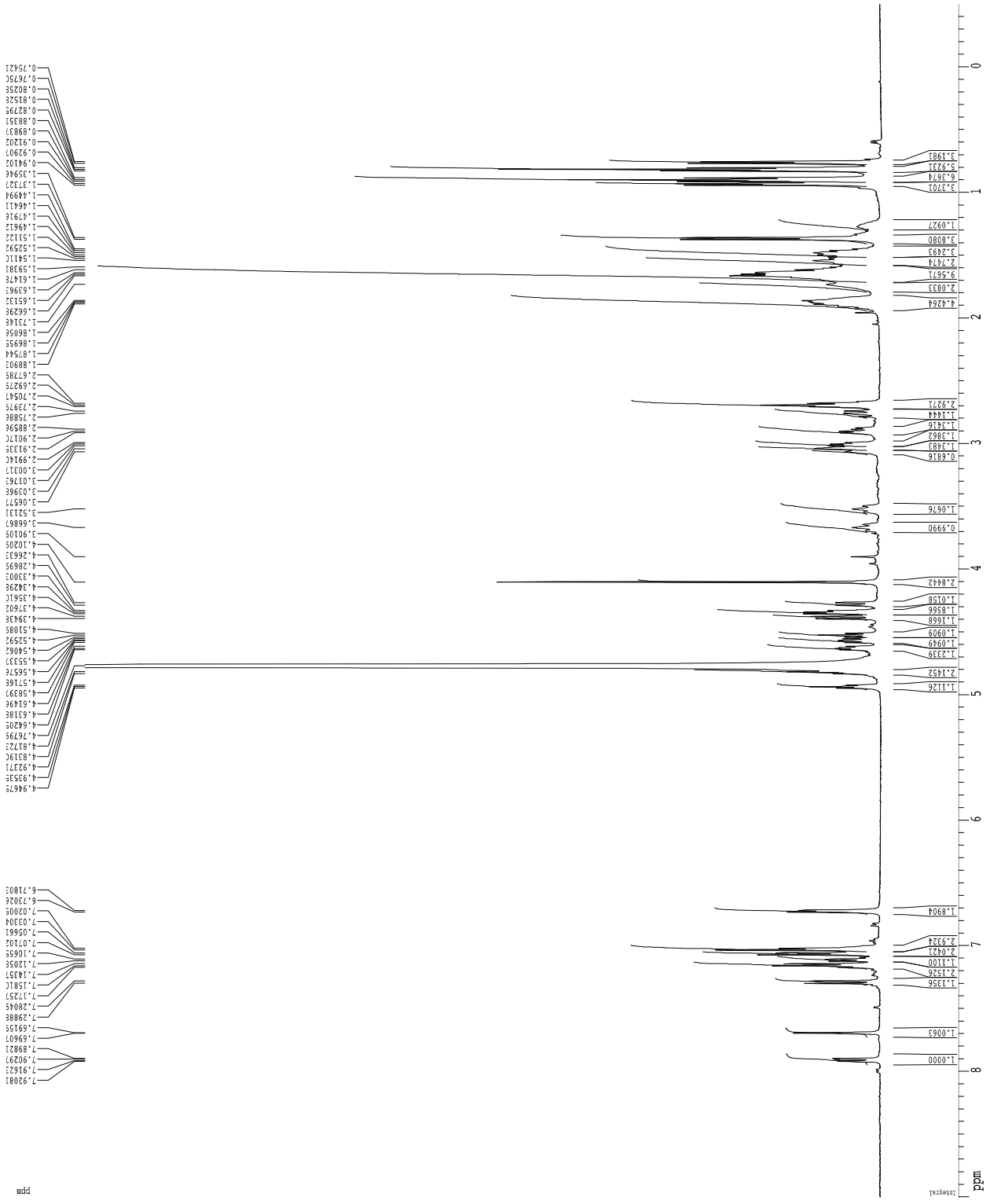

2D TOCSY spectrum of **1.1a**, 500 mHz, 2 mM in D_2O, 298 K, 150 ms spin-lock mixing time

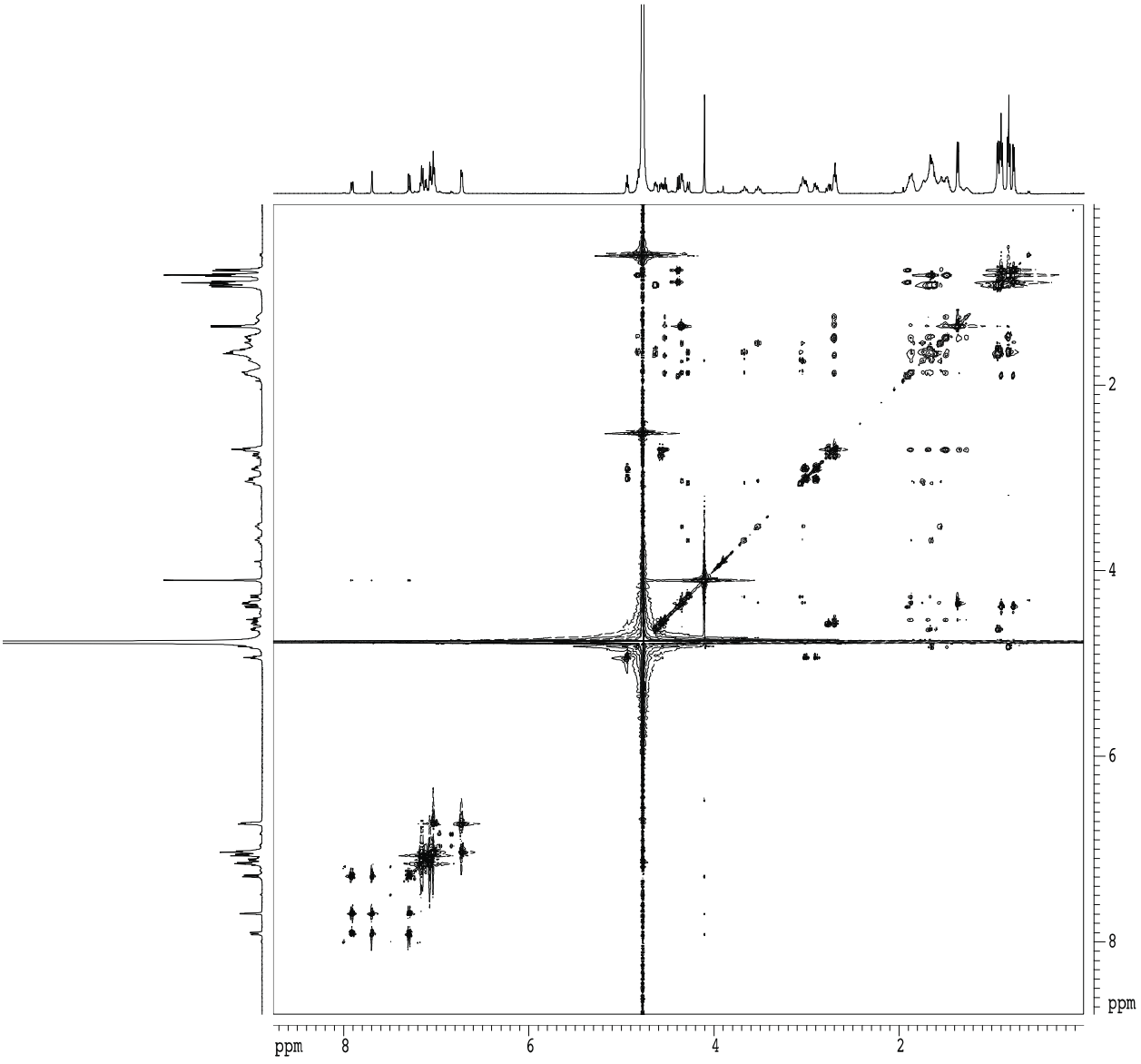

2D ROESY spectrum of **1.1a**, 500 mHz, 2 mM in D_2O, 298 K, 300 ms spin-lock time

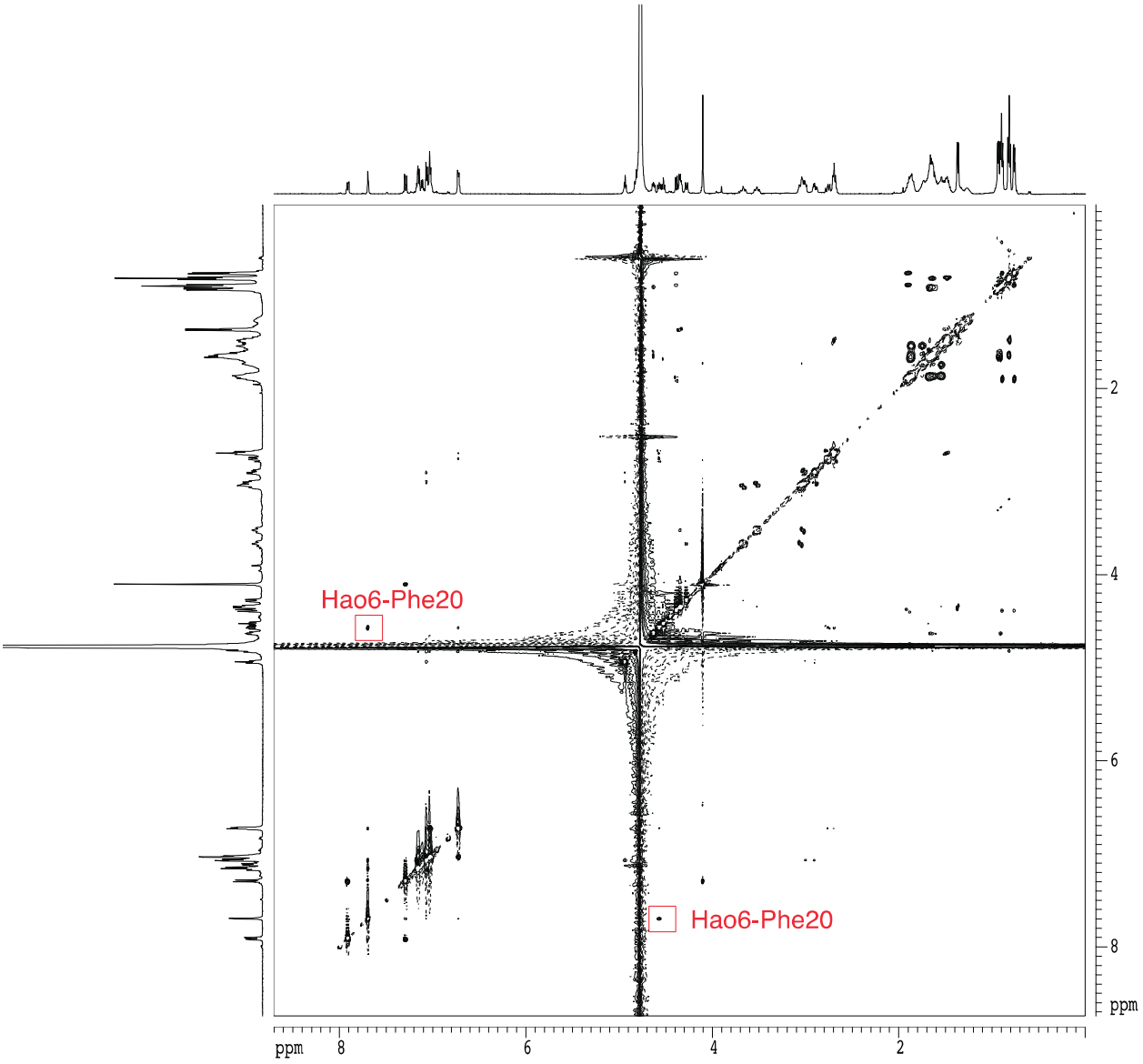

1D ^{1}H NMR spectrum of **1.1a** with solvent suppression, 600 mHz, 2 mM in 9:1 H_2O:D_2O, 278 K, 32 scans

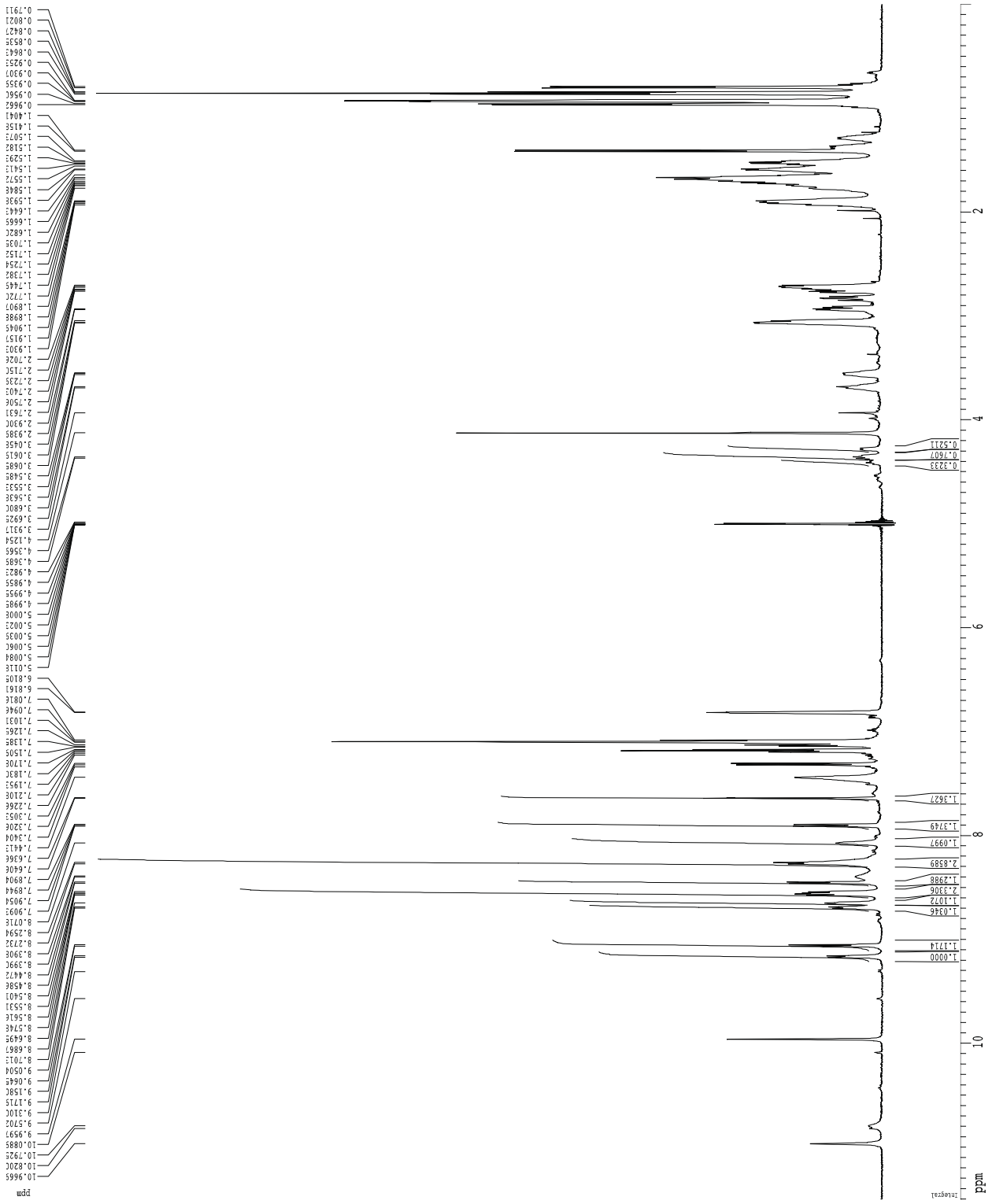

2D TOCSY spectrum of **1.1a** with solvent suppression, 600 mHz, 2 mM in 9:1 H_2O:D_2O, 278 K, 200 ms spin-lock mixing time

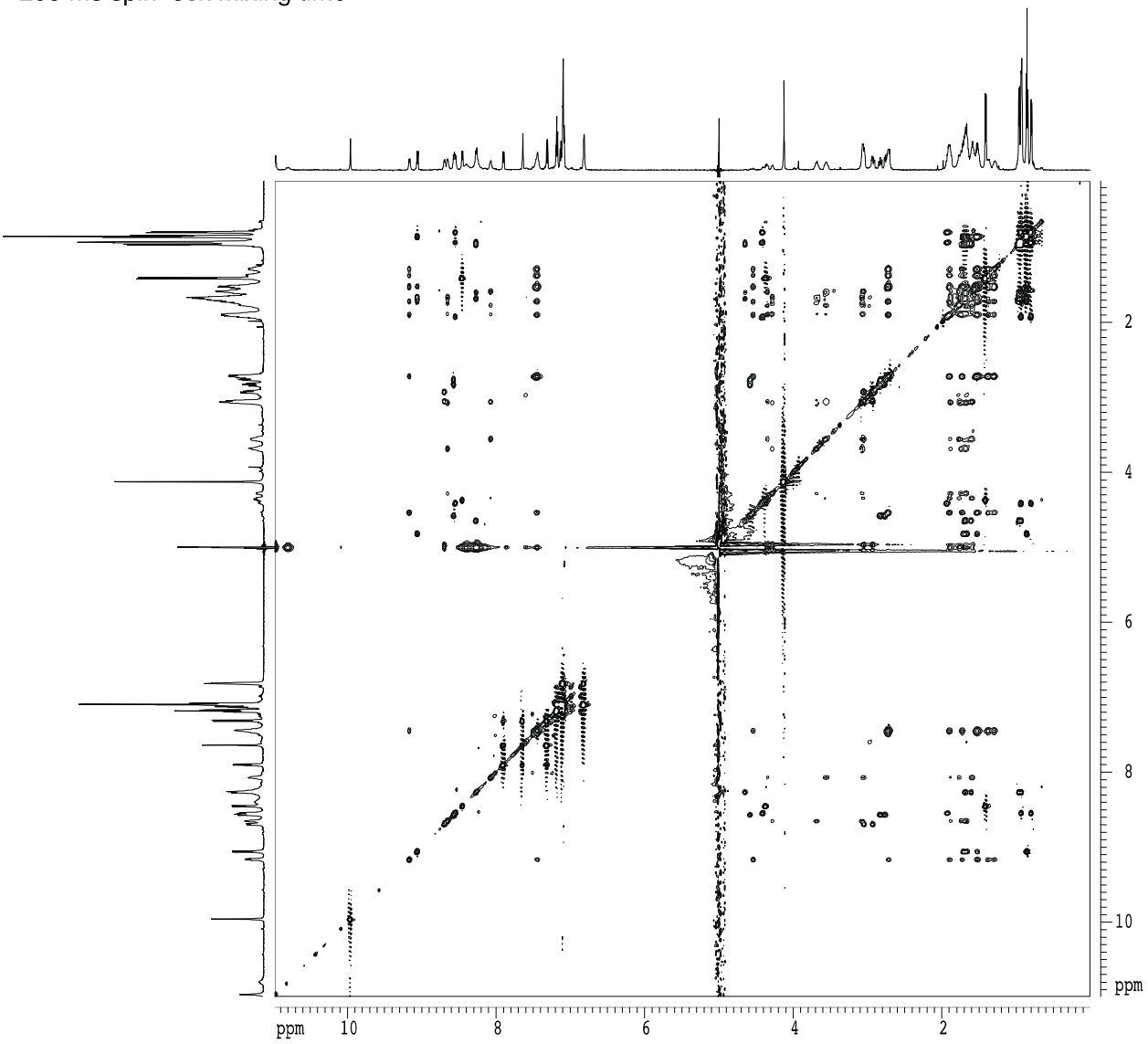

2D TOCSY spectrum of **1.1a** with solvent suppression, 600 mHz, 2 mM in 9:1 H_2O:D_2O, 278 K, 200 ms spin-lock mixing time

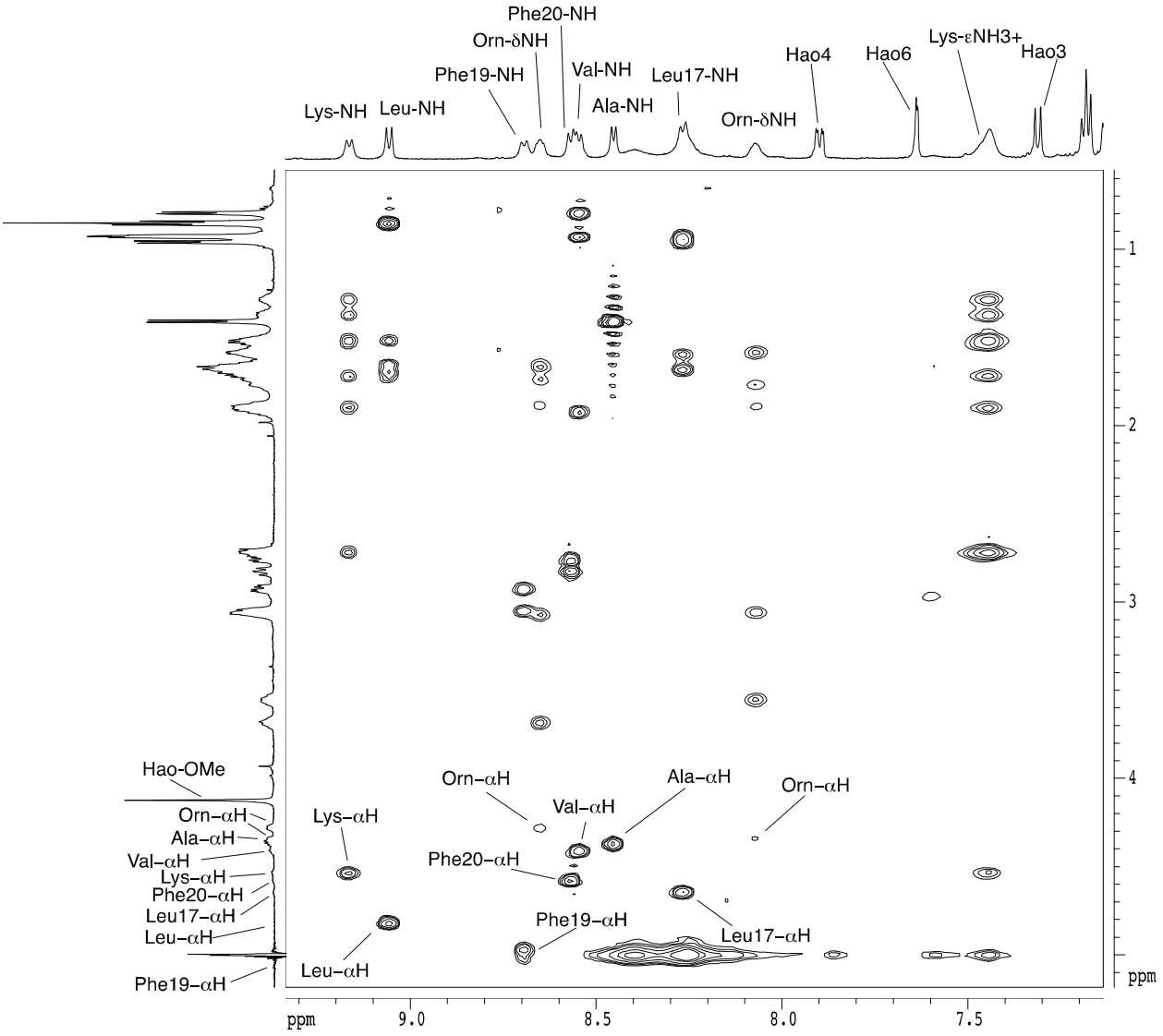

2D ROESY spectrum of **1.1a** with solvent suppression, 600 mHz, 2 mM in 9:1 H_2O:D_2O, 278 K, 100 ms spin-lock mixing time

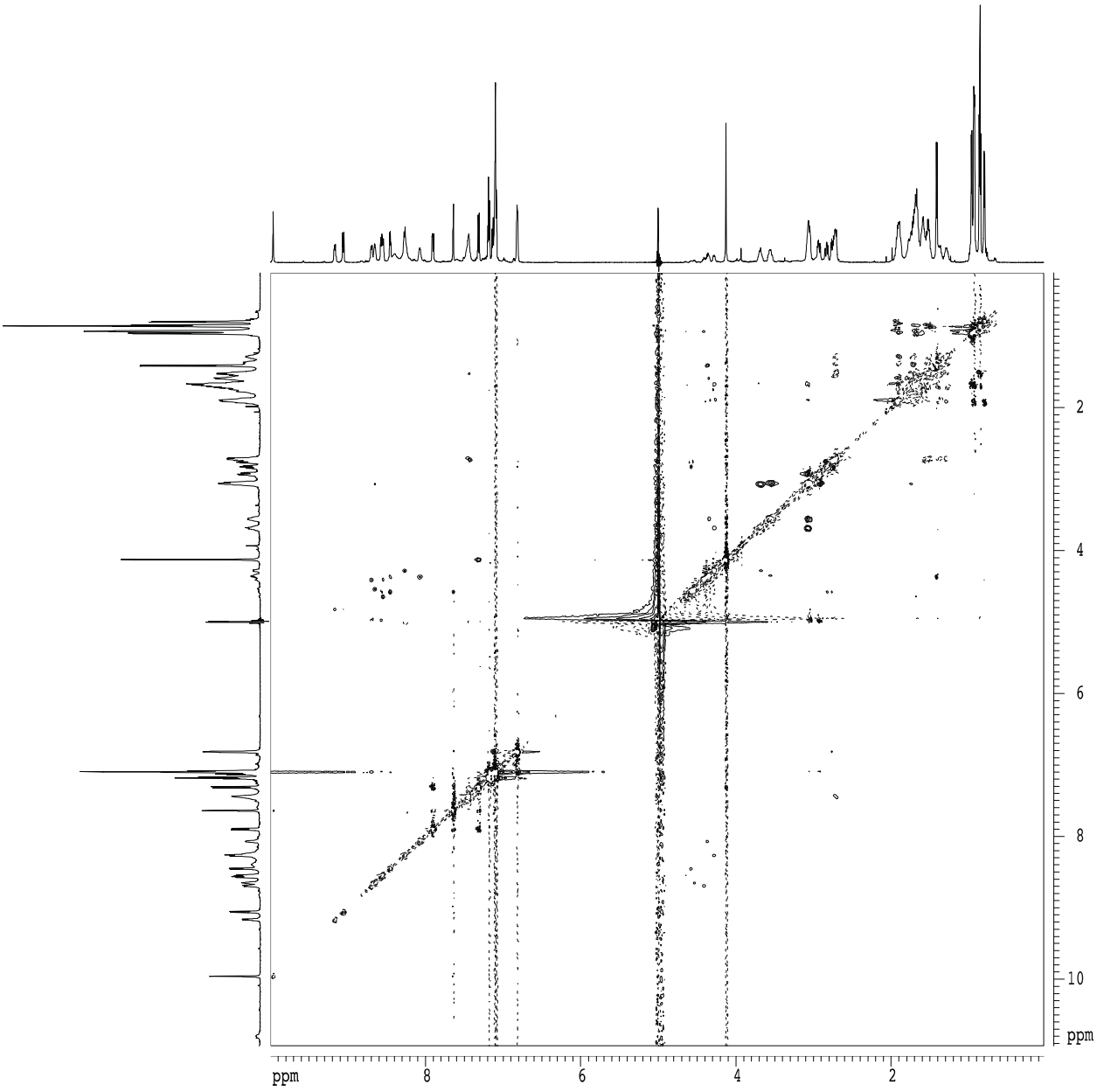

2D ROESY spectrum of **1.1a** with solvent suppression, 600 mHz, 2 mM in 9:1 H_2O:D_2O, 278 K, 100 ms spin-lock mixing time

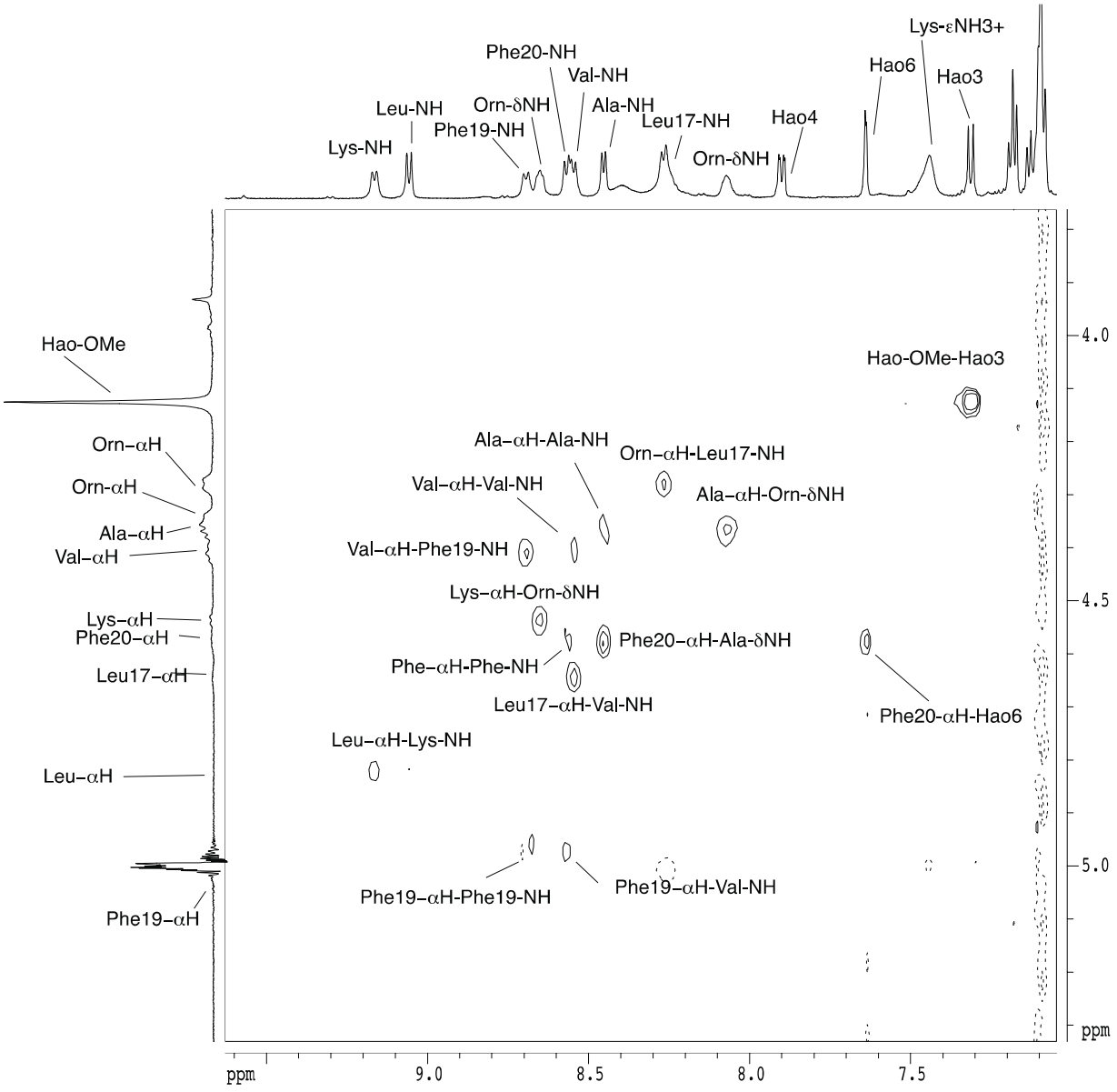

HPLC trace of **1.1b**

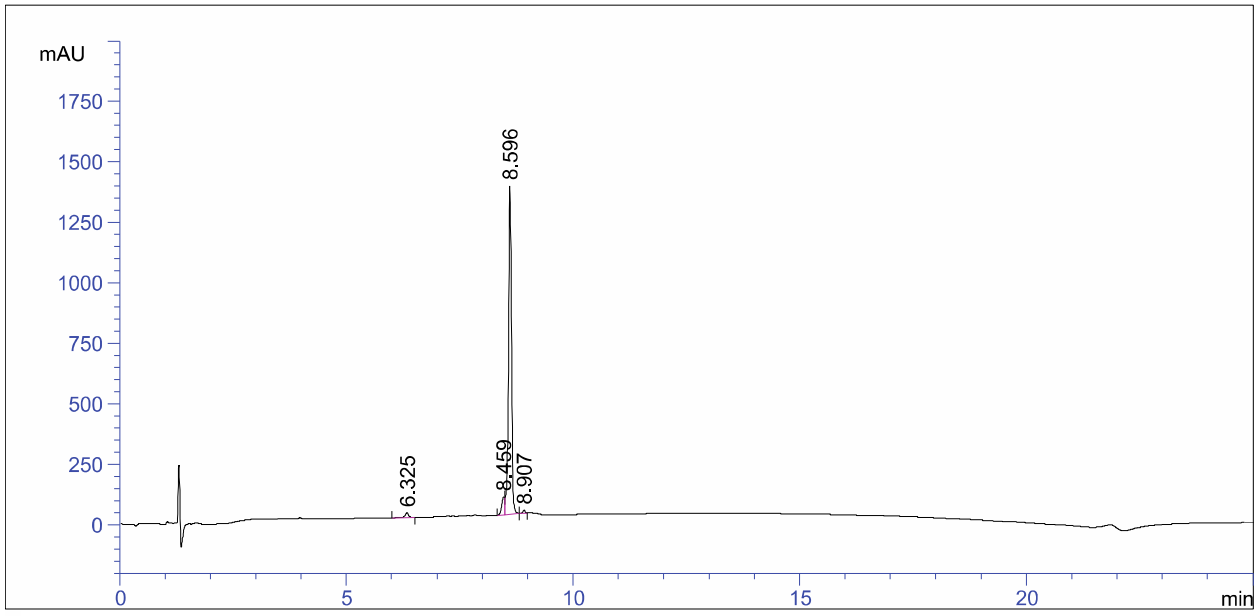


```
=====================================================================
                        Area Percent Report
=====================================================================


Signal 1: VWD1 A, Wavelength=214 nm

Peak RetTime Type  Width     Area      Height     Area
  #   [min]        [min]  mAU   *s    [mAU   ]      %
----|-------|----|-------|----------|----------|--------|
   1   6.325 BB    0.0742   93.02305   18.64573   1.4076
   2   8.459 BV    0.0645  317.34662   74.07159   4.8021
   3   8.596 VB    0.0688 6141.26611 1357.35608  92.9293
   4   8.907 BV    0.0573   56.90108   15.01045   0.8610

Totals :                  6608.53686 1465.08384


=====================================================================

                        *** End of Report ***
```

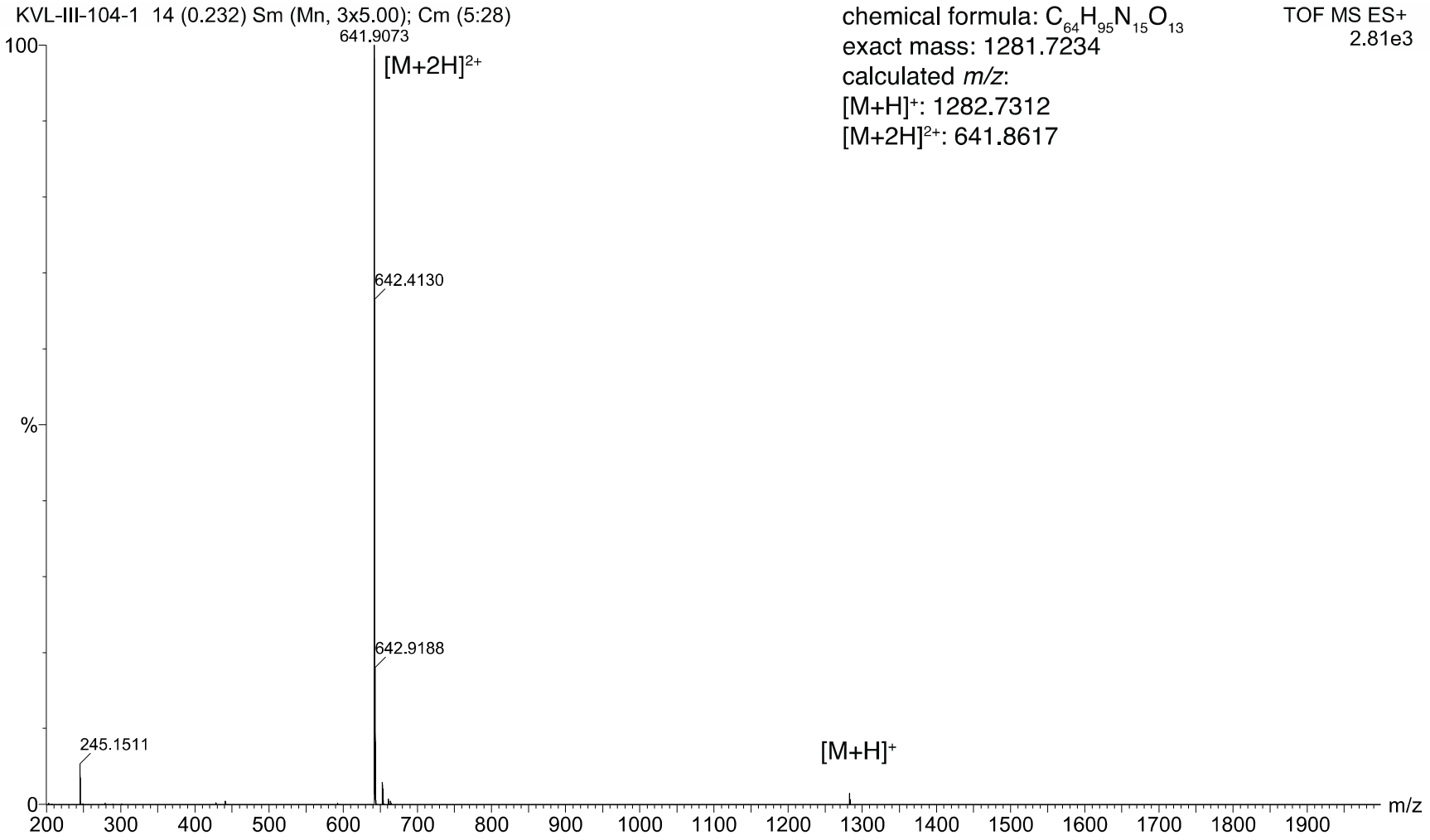

ESI-MS of **1.1b**
chemical formula: $C_{64}H_{95}N_{15}O_{13}$
exact mass: 1281.7234
calculated *m/z*:
$[M+H]^+$: 1282.7312
$[M+2H]^{2+}$: 641.8617

TOF MS ES+
2.81e3

1D ^{1}H NMR spectrum of **1.1b**, 500 mHz, 2 mM in D_2O, 298 K

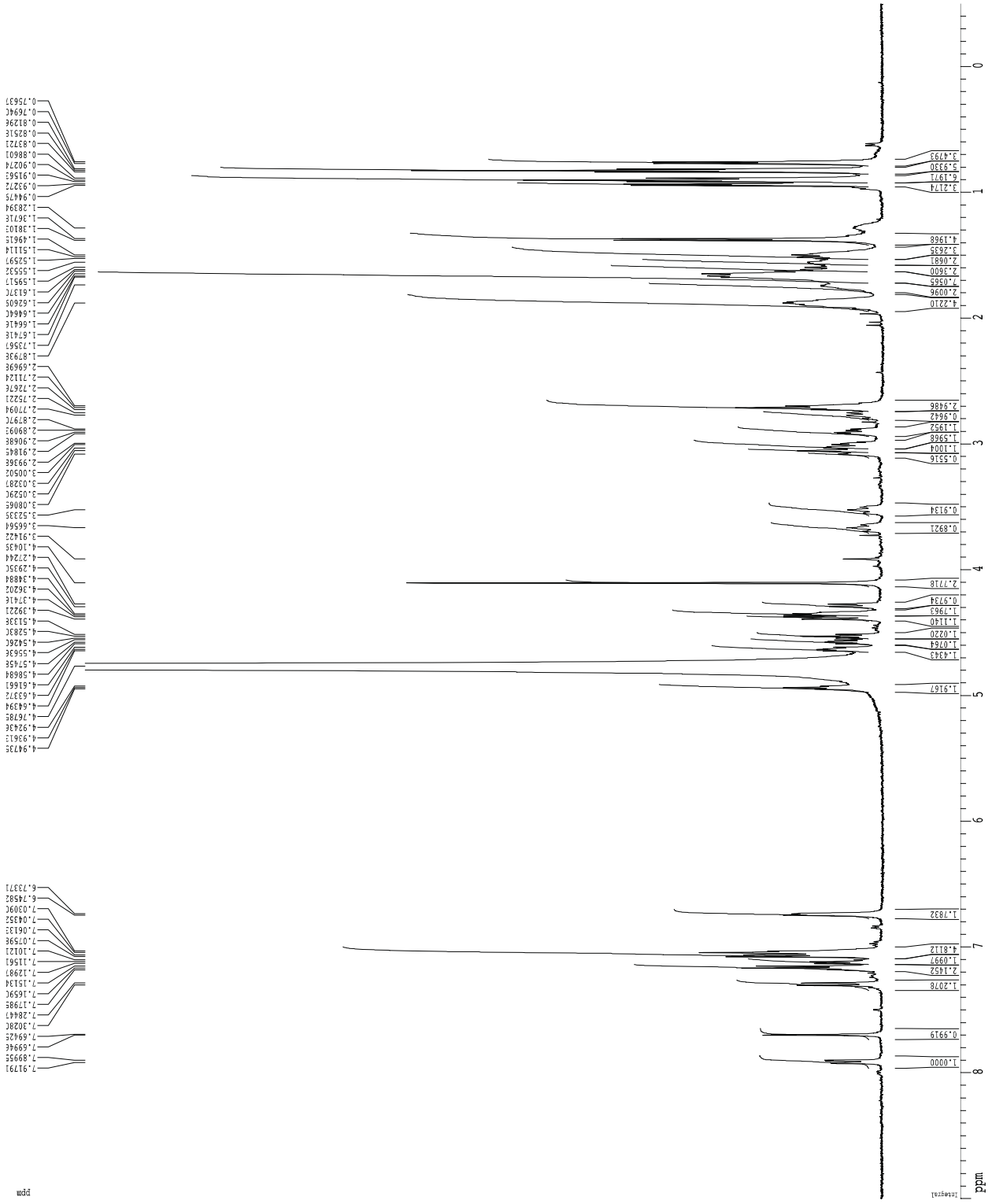

2D TOCSY spectrum of **1.1b**, 500 mHz, 2 mM in D_2O, 298 K, 150 ms spin-lock mixing time

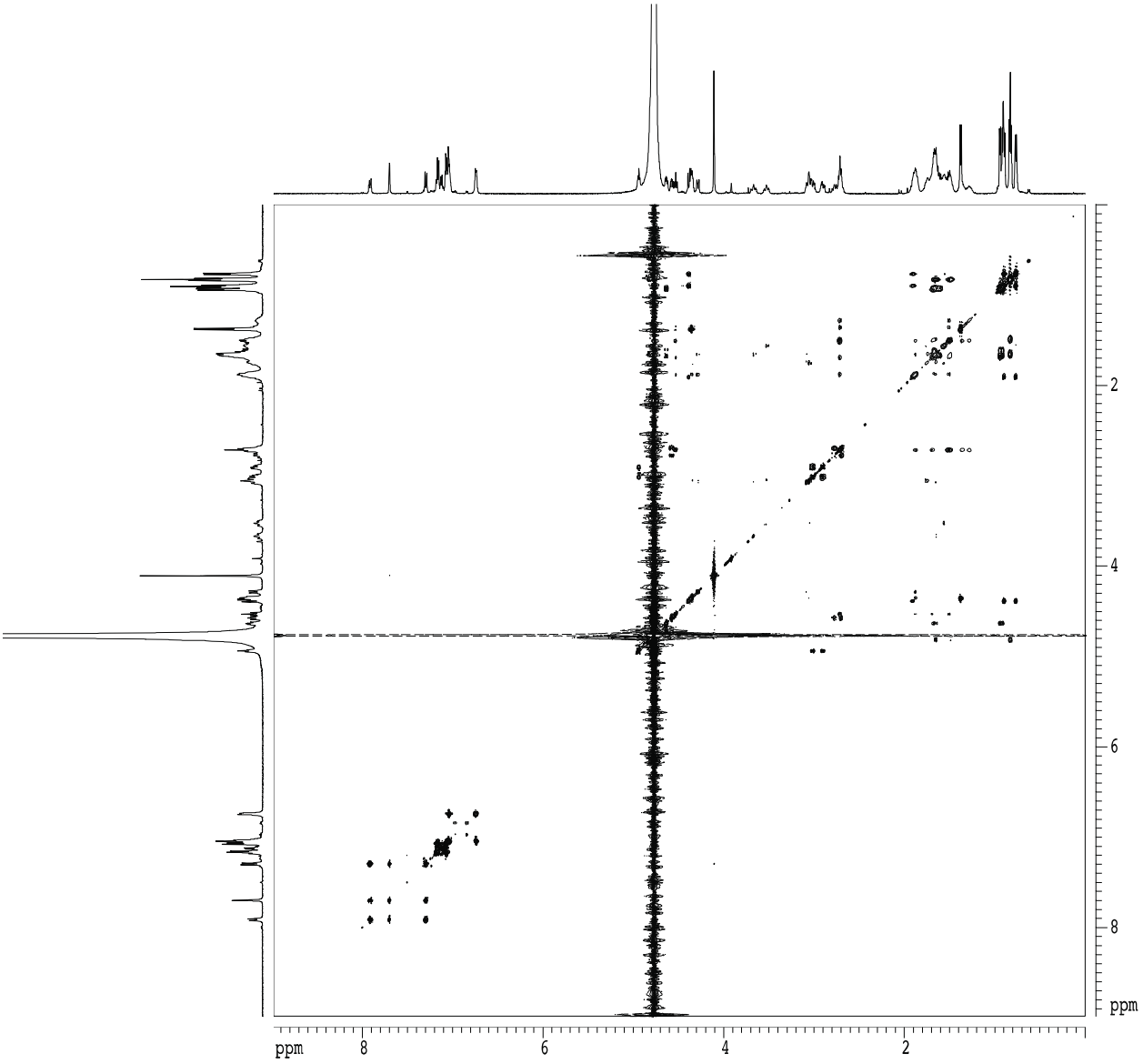

2D ROESY spectrum of **1.1b**, 500 mHz, 2 mM in D_2O, 298 K, 300 ms spin-lock mixing time

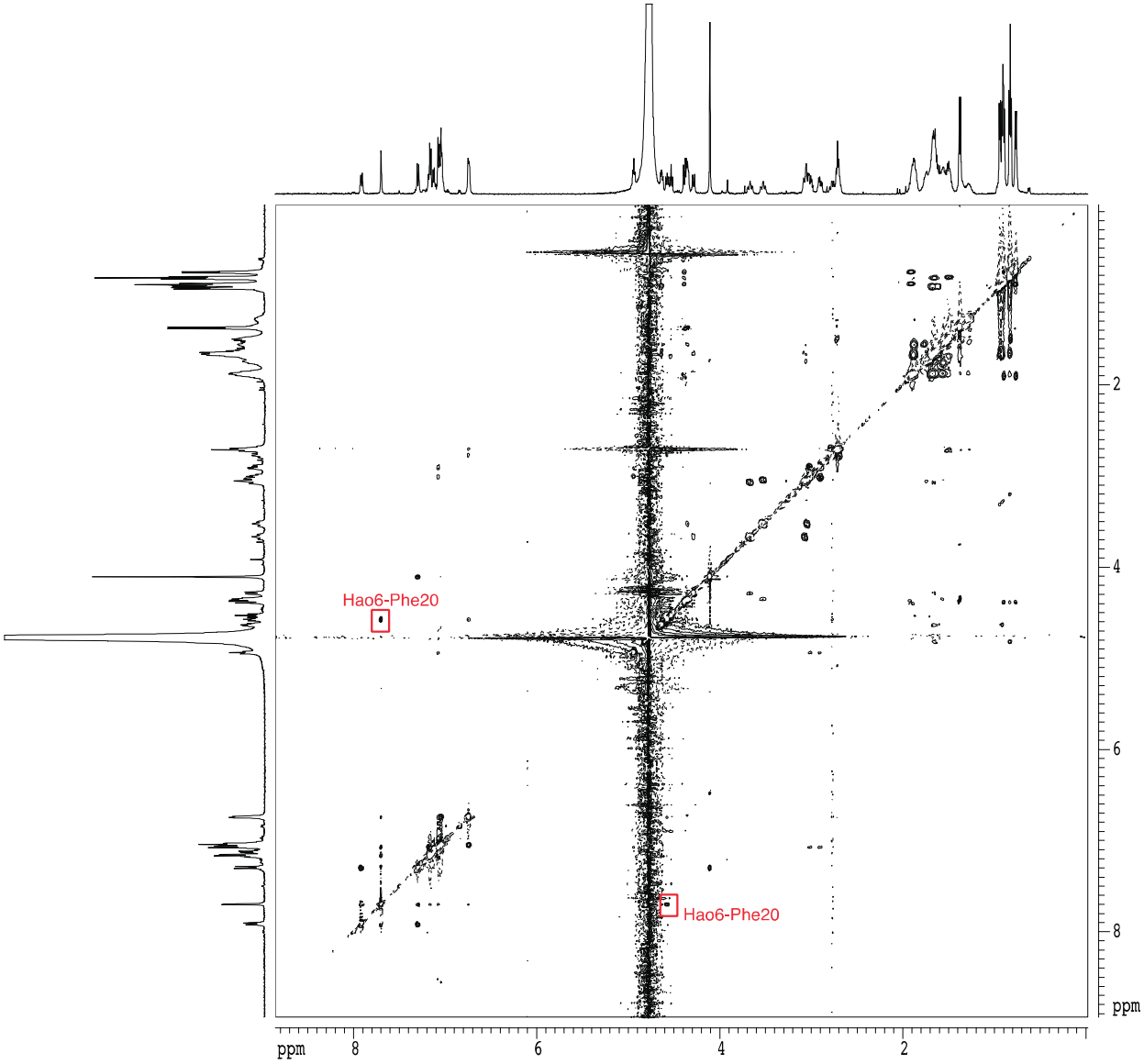

HPLC trace of **1.1c**

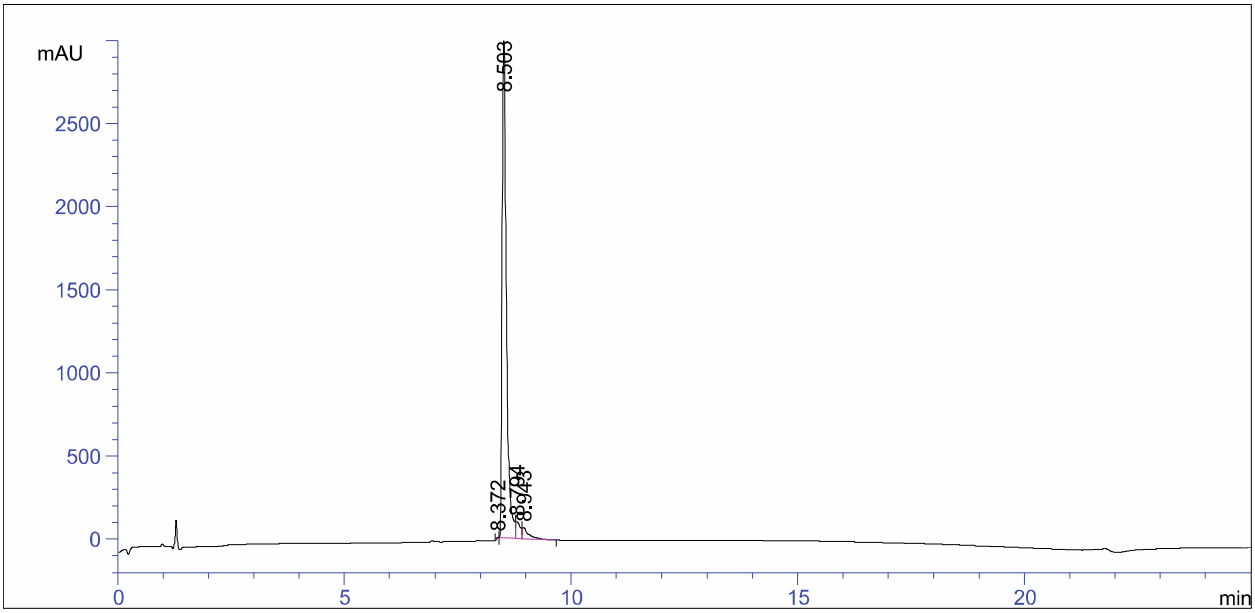


```
=====================================================================
                        Area Percent Report
=====================================================================

Signal 1: VWD1 A, Wavelength=214 nm

Peak RetTime Type  Width     Area      Height     Area
  #   [min]        [min]  mAU   *s    [mAU   ]      %
----|-------|----|-------|----------|----------|--------|
   1   8.372 BB    0.0486   26.40786    9.03954   0.1233
   2   8.503 BV    0.0972 1.99814e4  3093.74927  93.2979
   3   8.794 VV    0.0962  703.43842  102.36295   3.2845
   4   8.943 VB    0.1413  705.52911   68.09892   3.2943

Totals :                  2.14167e4  3273.25068

=====================================================================

                        *** End of Report ***
```

ESI-MS of **1.1c**
chemical formula: $C_{64}H_{95}N_{15}O_{13}$
exact mass: 1281.7234
calculated *m/z*:
$[M+H]^+$: 1282.7312
$[M+2H]^{2+}$: 641.8617
$[M+2H+K]^{3+}$: 440.9078

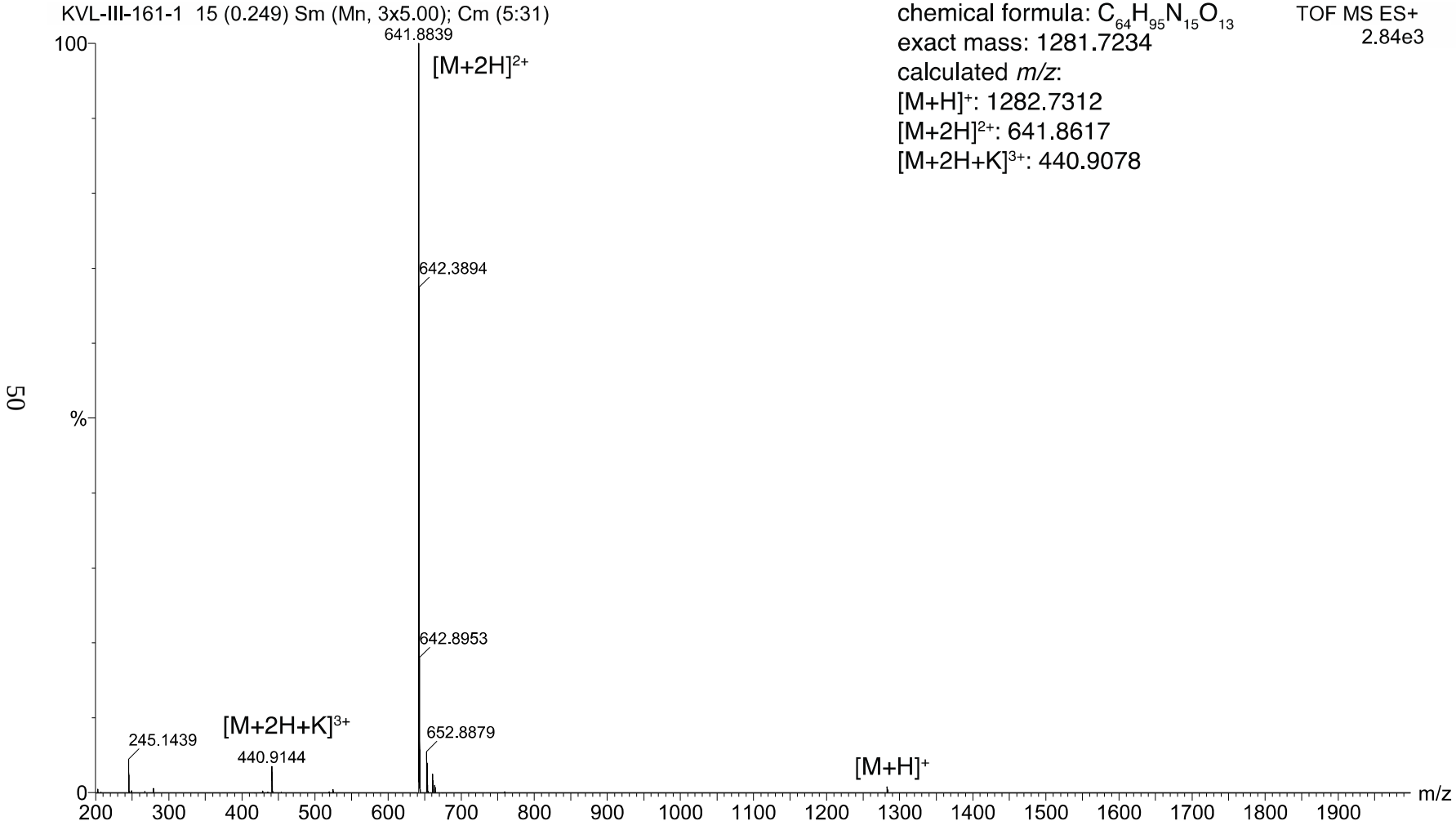

1D ^{1}H NMR spectrum of **1.1c**, 500 mHz, 2 mM in D_2O, 298 K

2D TOCSY spectrum of **1.1c**, 500 mHz, 2 mM in D_2O, 298 K, 150 ms spin-lock mixing time

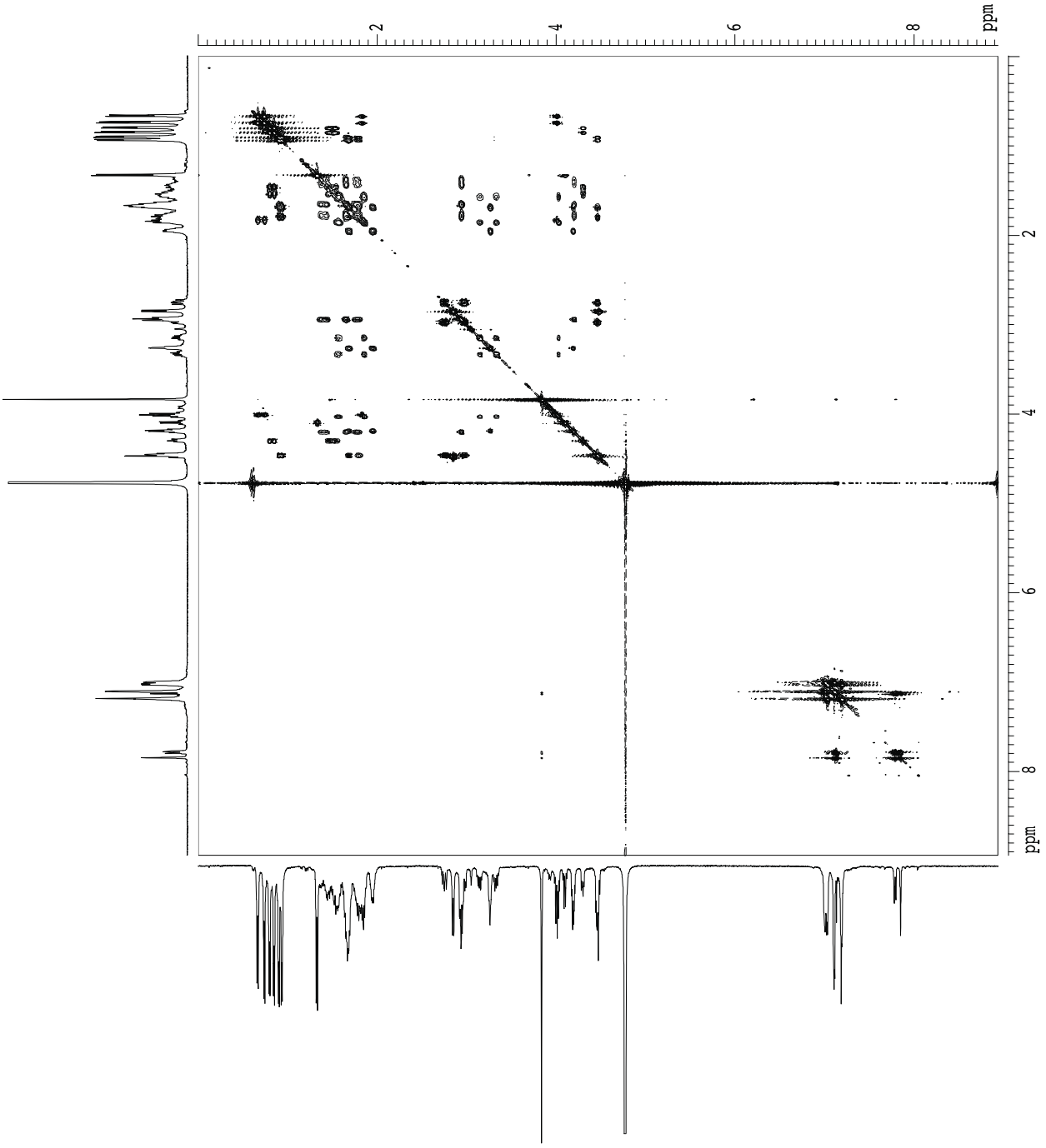

2D ROESY spectrum of **1.1c**, 500 mHz, 2 mM in D_2O, 298 K, 300 ms spin-lock mixing time

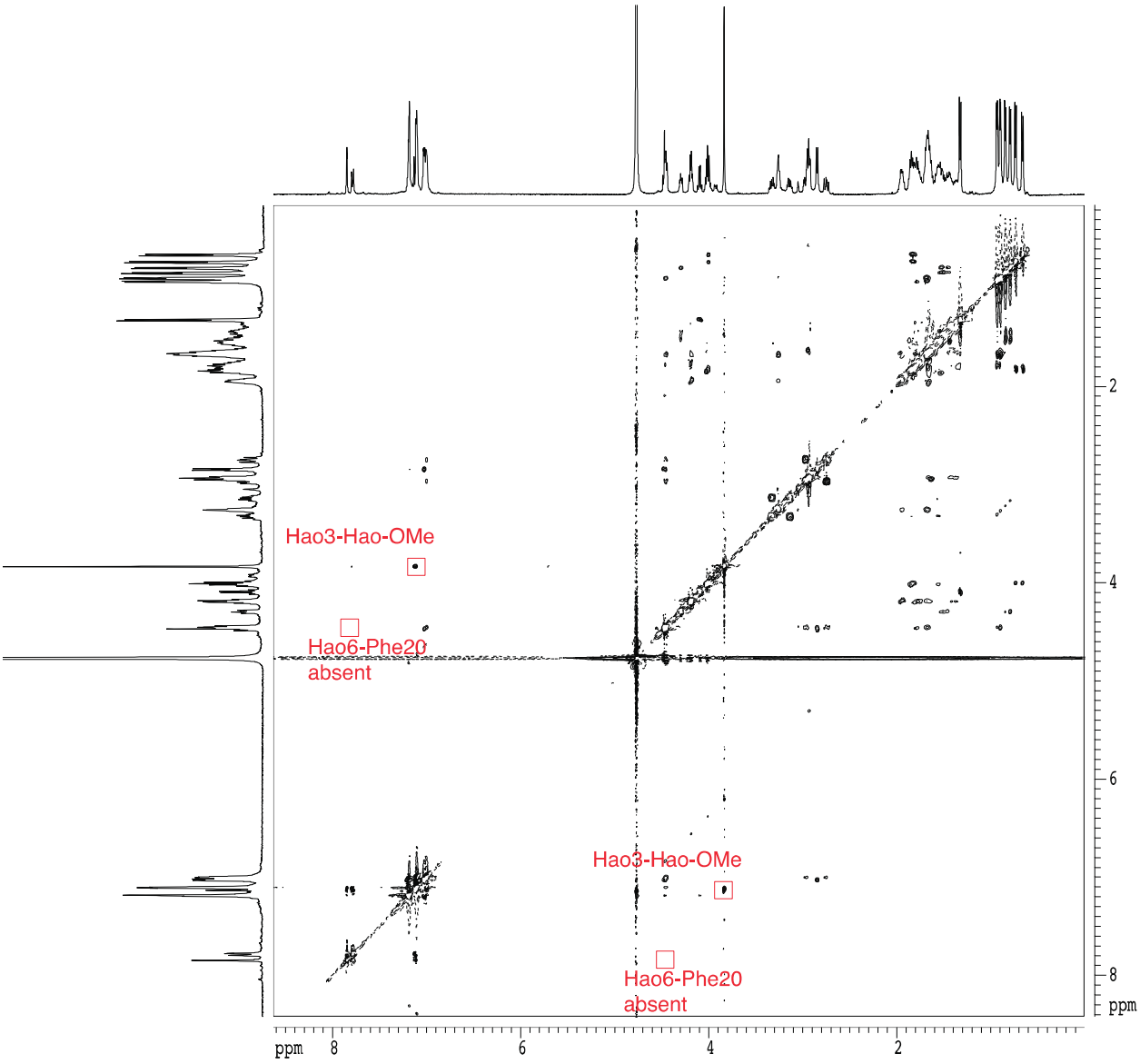

HPLC trace of **1.1d**

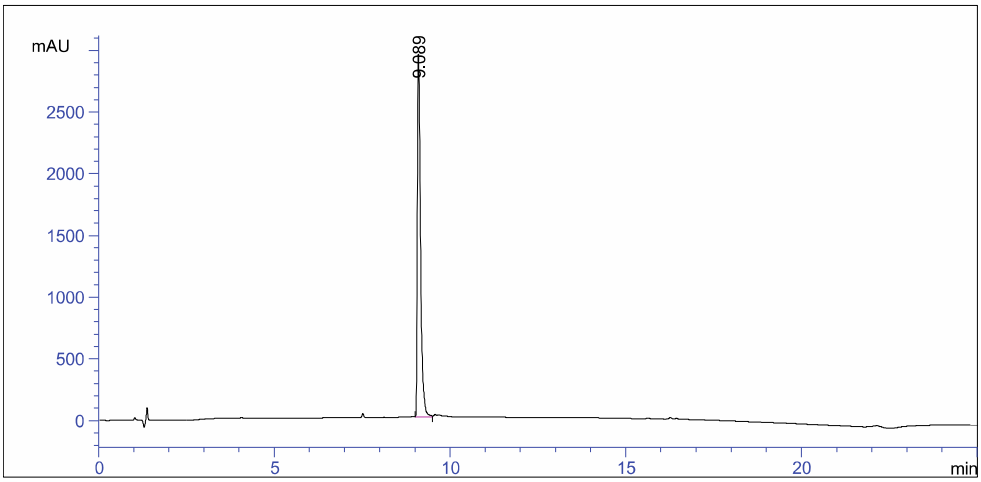


```
=====================================================================
                        Area Percent Report
=====================================================================

Signal 1: VWD1 A, Wavelength=214 nm

Peak RetTime Type  Width     Area      Height     Area
  #   [min]        [min]  mAU   *s    [mAU   ]      %
----|-------|----|-------|----------|----------|--------|
   1   9.089 BV    0.0926 1.82171e4  2941.87524 100.0000

Totals :                  1.82171e4  2941.87524

=====================================================================
                        *** End of Report ***
```

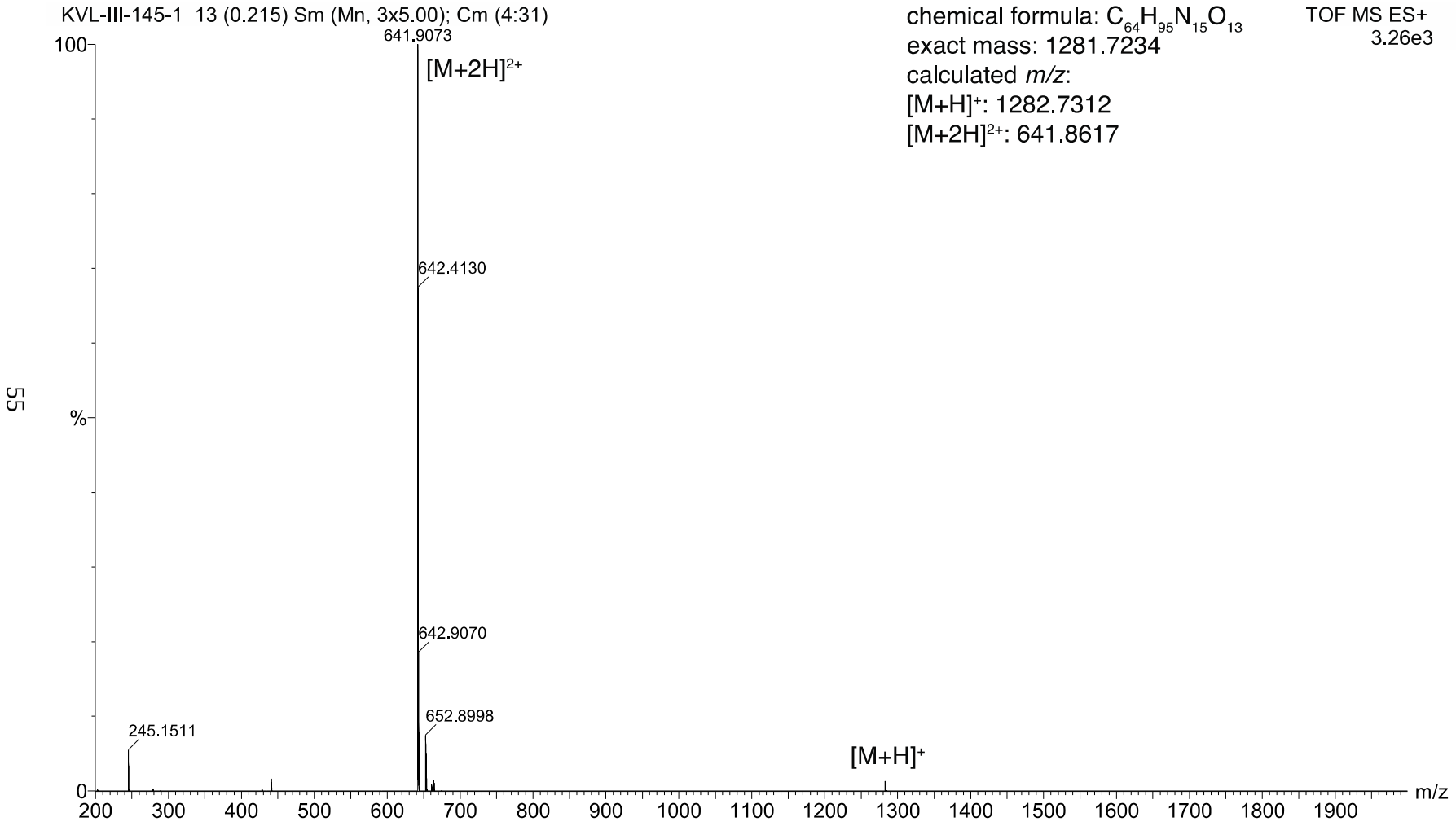
KVL-III-145-1 13 (0.215) Sm (Mn, 3x5.00); Cm (4:31)
ESI-MS of **1.1d**
chemical formula: $C_{64}H_{95}N_{15}O_{13}$
exact mass: 1281.7234
calculated *m/z*:
$[M+H]^+$: 1282.7312
$[M+2H]^{2+}$: 641.8617
TOF MS ES+
3.26e3
641.9073
$[M+2H]^{2+}$
642.4130
642.9070
652.8998
245.1511
$[M+H]^+$
100
%
0
55
200 300 400 500 600 700 800 900 1000 1100 1200 1300 1400 1500 1600 1700 1800 1900
m/z

1D ^{1}H NMR spectrum of **1.1d**, 500 mHz, 2 mM in D_2O, 298 K

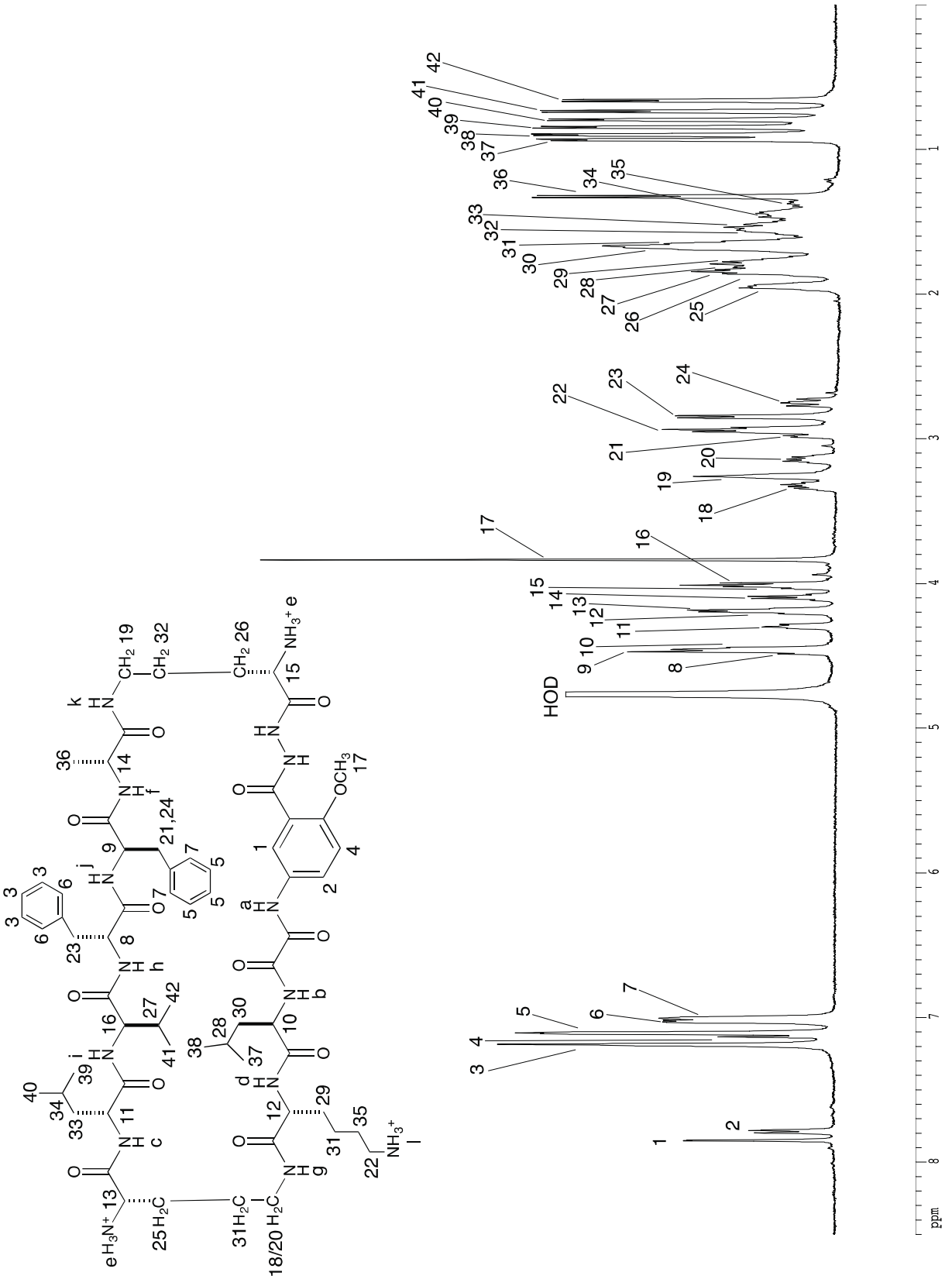

2D TOCSY spectrum of **1.1d**, 500 mHz, 2 mM in D_2O, 298 K, 150 ms spin-lock mixing time

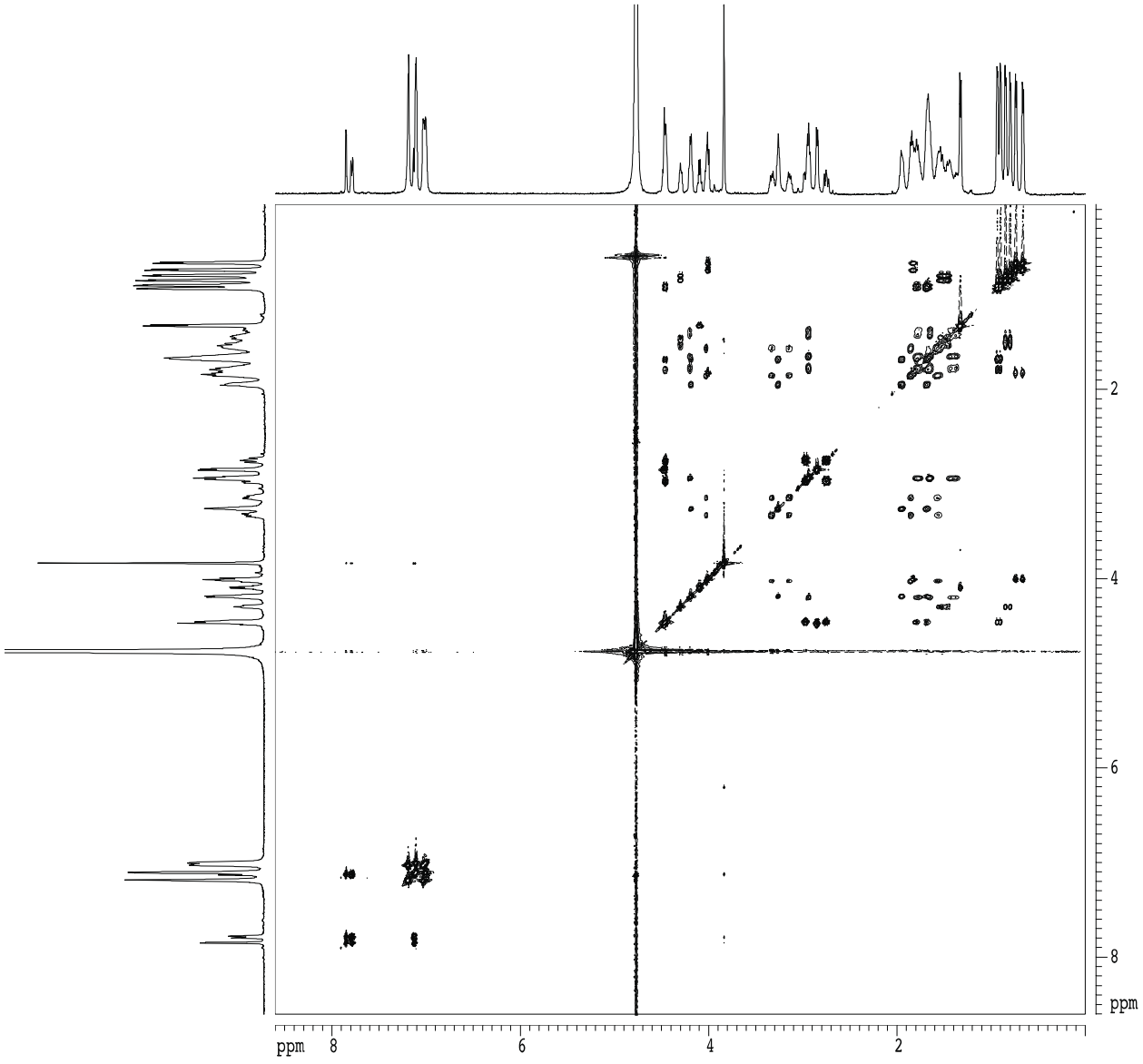

2D ROESY spectrum of **1.1d**, 500 mHz, 2 mM in D_2O, 298 K, 300 ms spin-lock mixing time

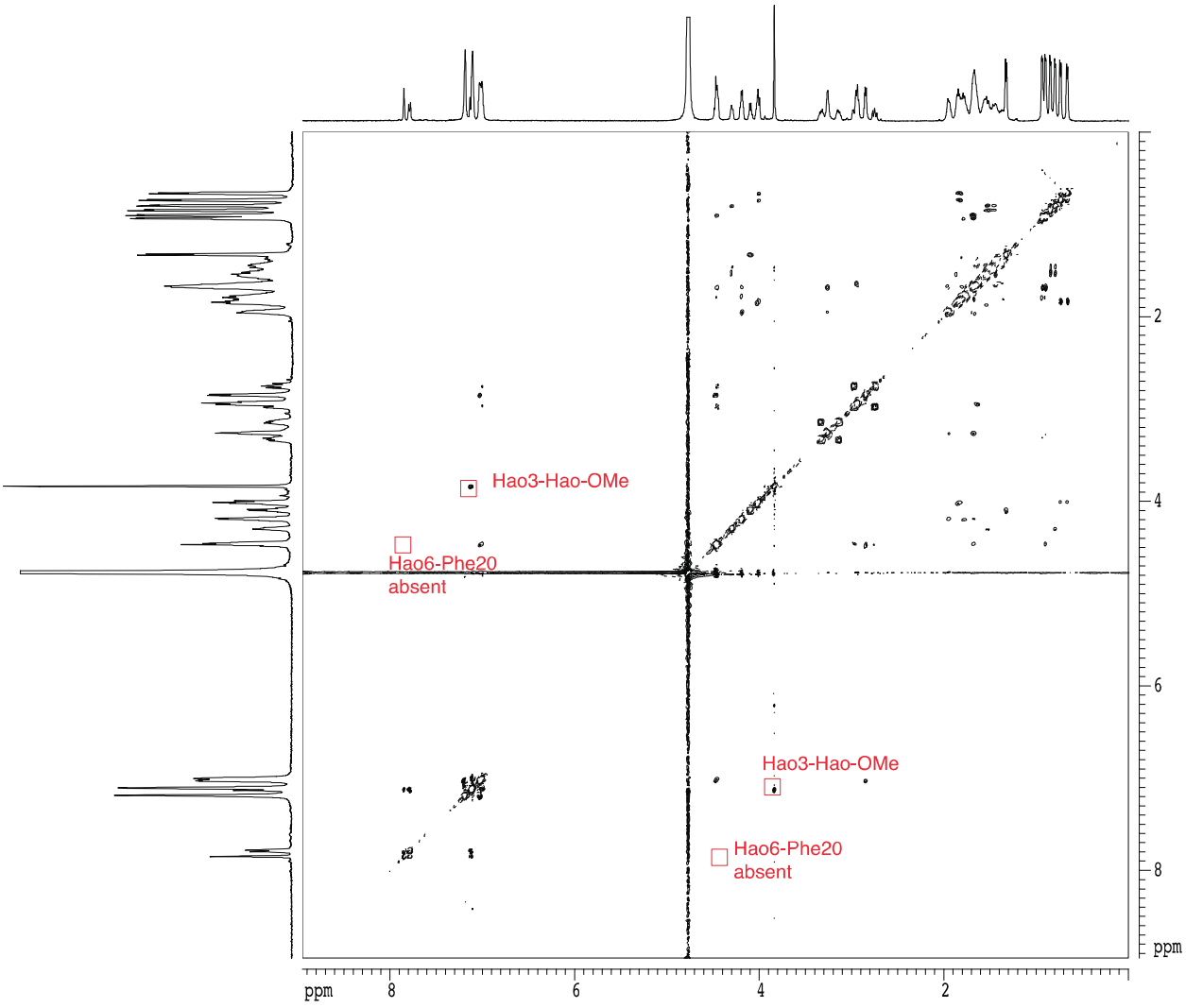

1D ^{1}H NMR spectrum of **1.1d** with solvent suppression, 600 mHz, 2 mM in 9:1 D_2O:H_2O, 278 K
32 scans

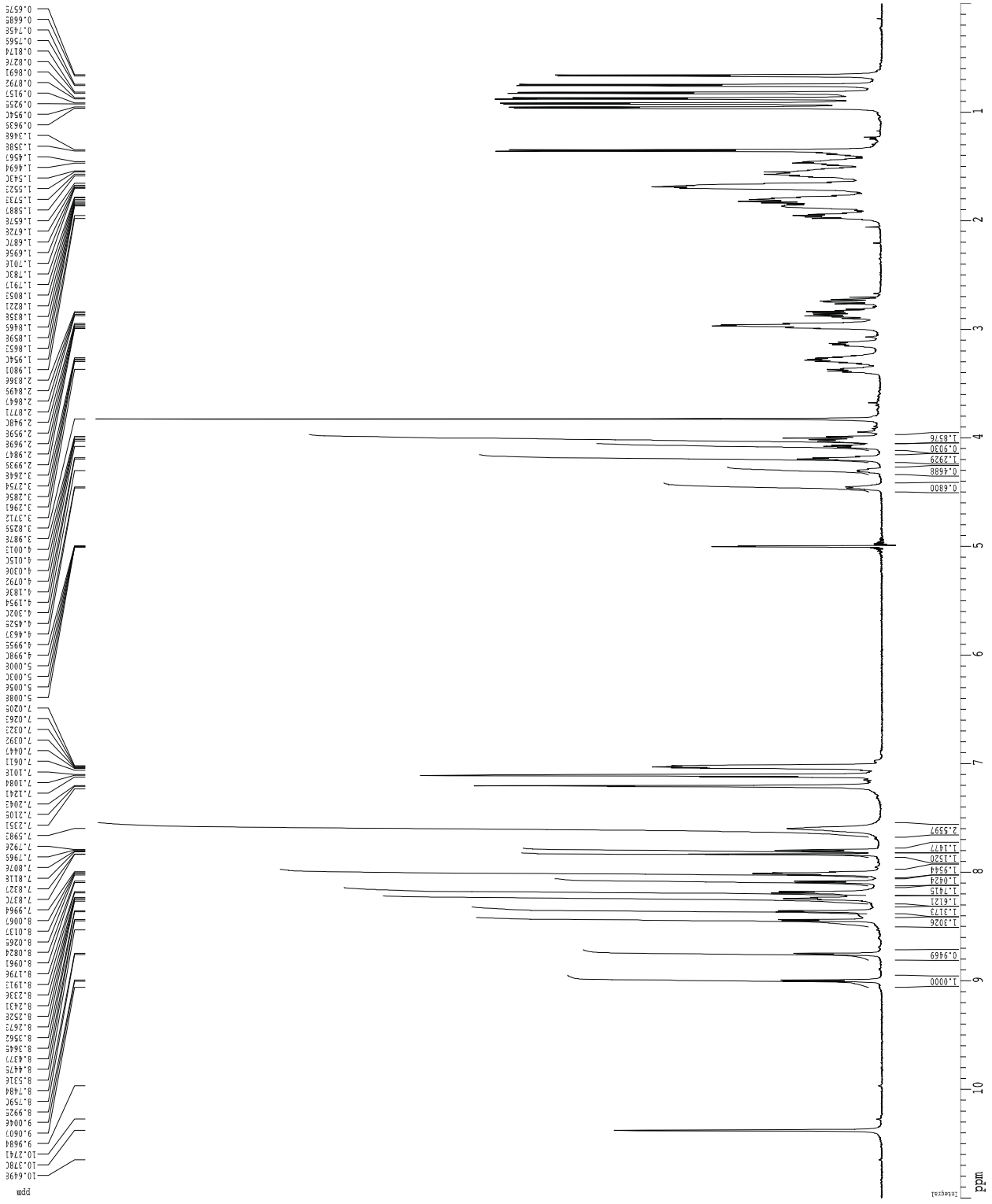

1D ^{1}H NMR spectrum of **1.1d** with solvent suppression, 600 mHz, 1.5 mM in 9:1 H_2O:D_2O, 278 K, 32 scans

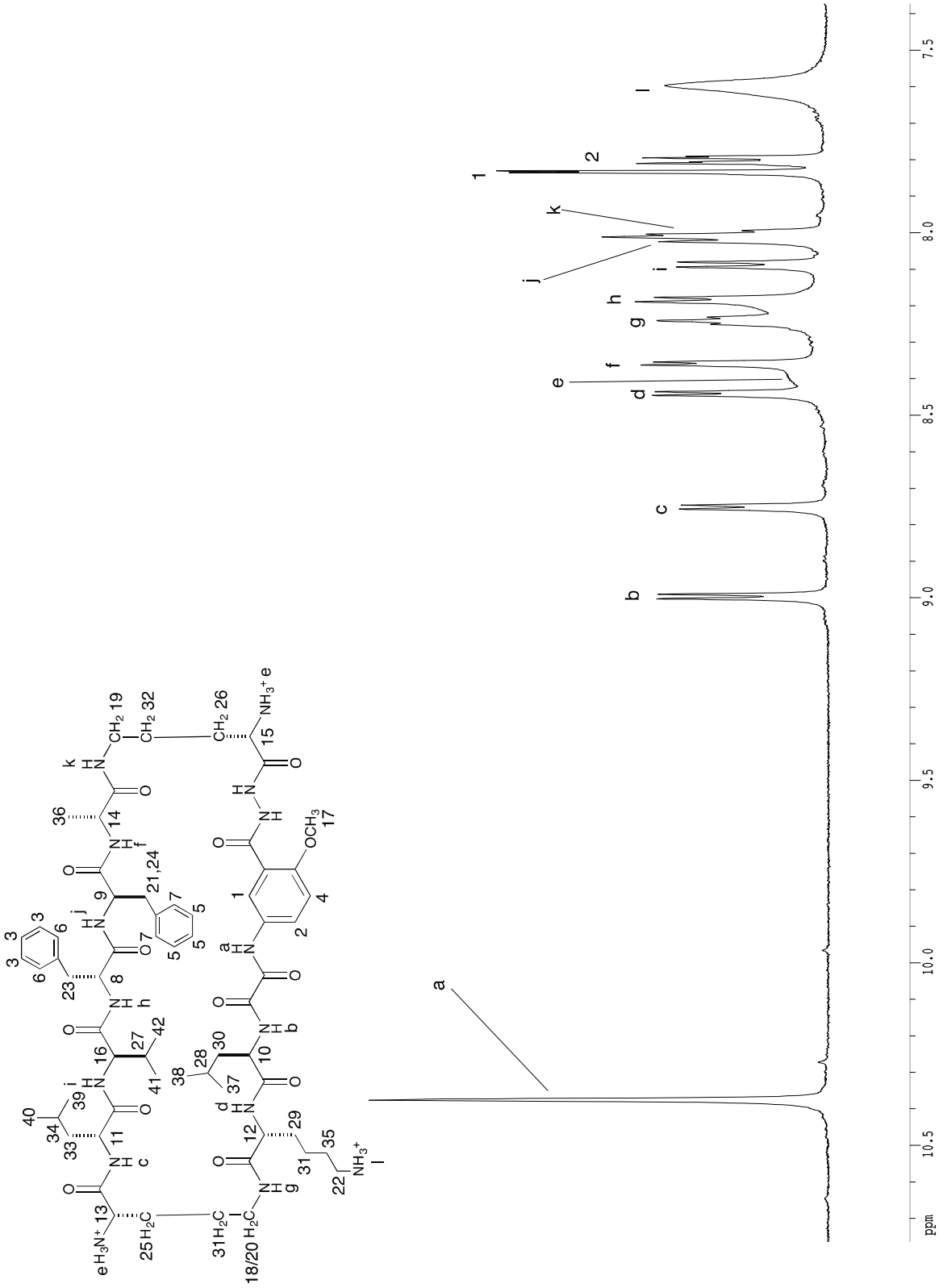

2D TOCSY spectrum of **1.1d** with solvent suppression, 600 mHz, 2 mM in 9:1 H_2O:D_2O, 278 K, 200 ms spin-lock mixing time

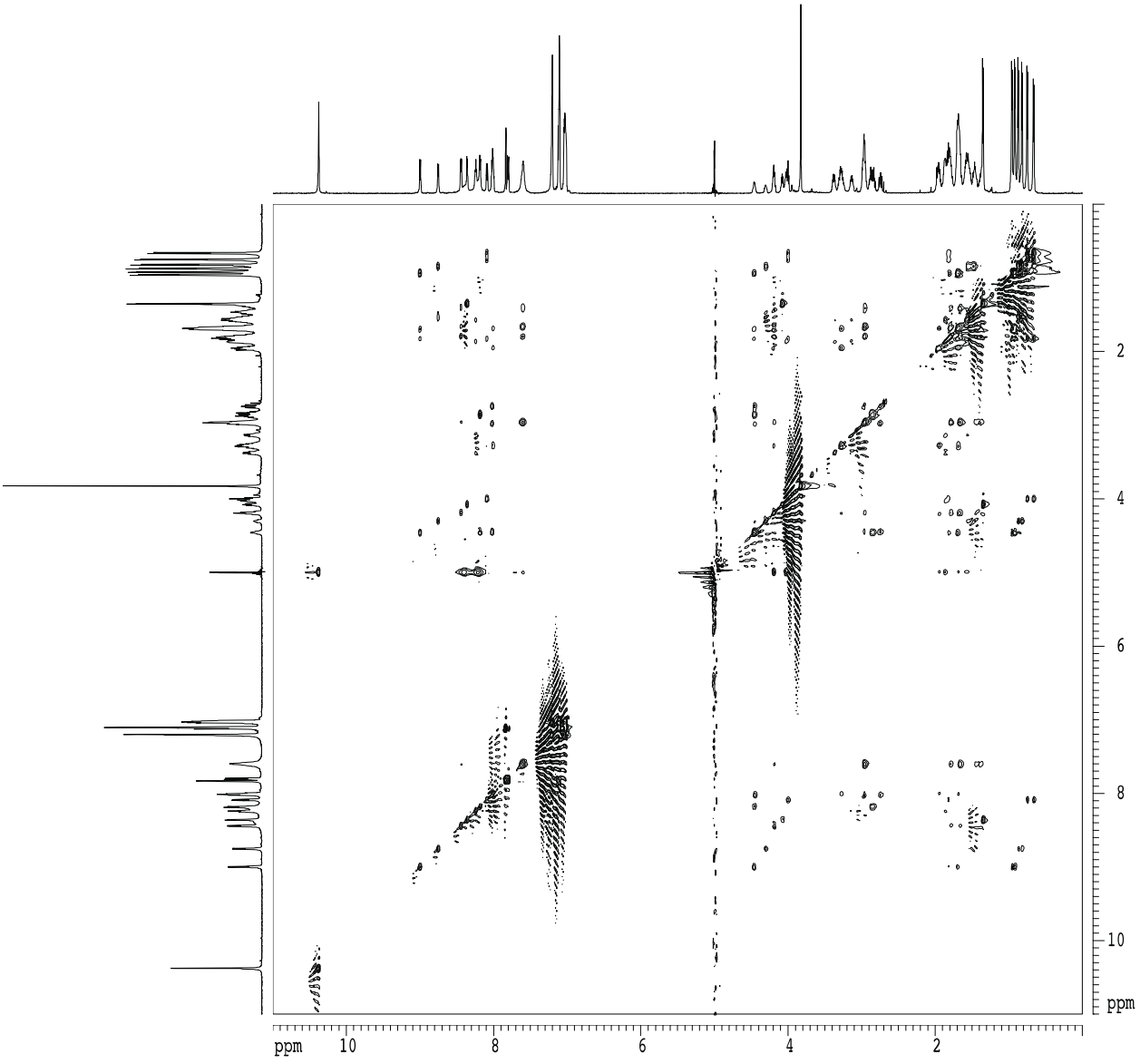

2D TOCSY spectrum of **1.1d** with solvent suppression, 600 mHz, 2 mM in 9:1 H_2O:D_2O, 278 K, 200 ms spin-lock mixing time

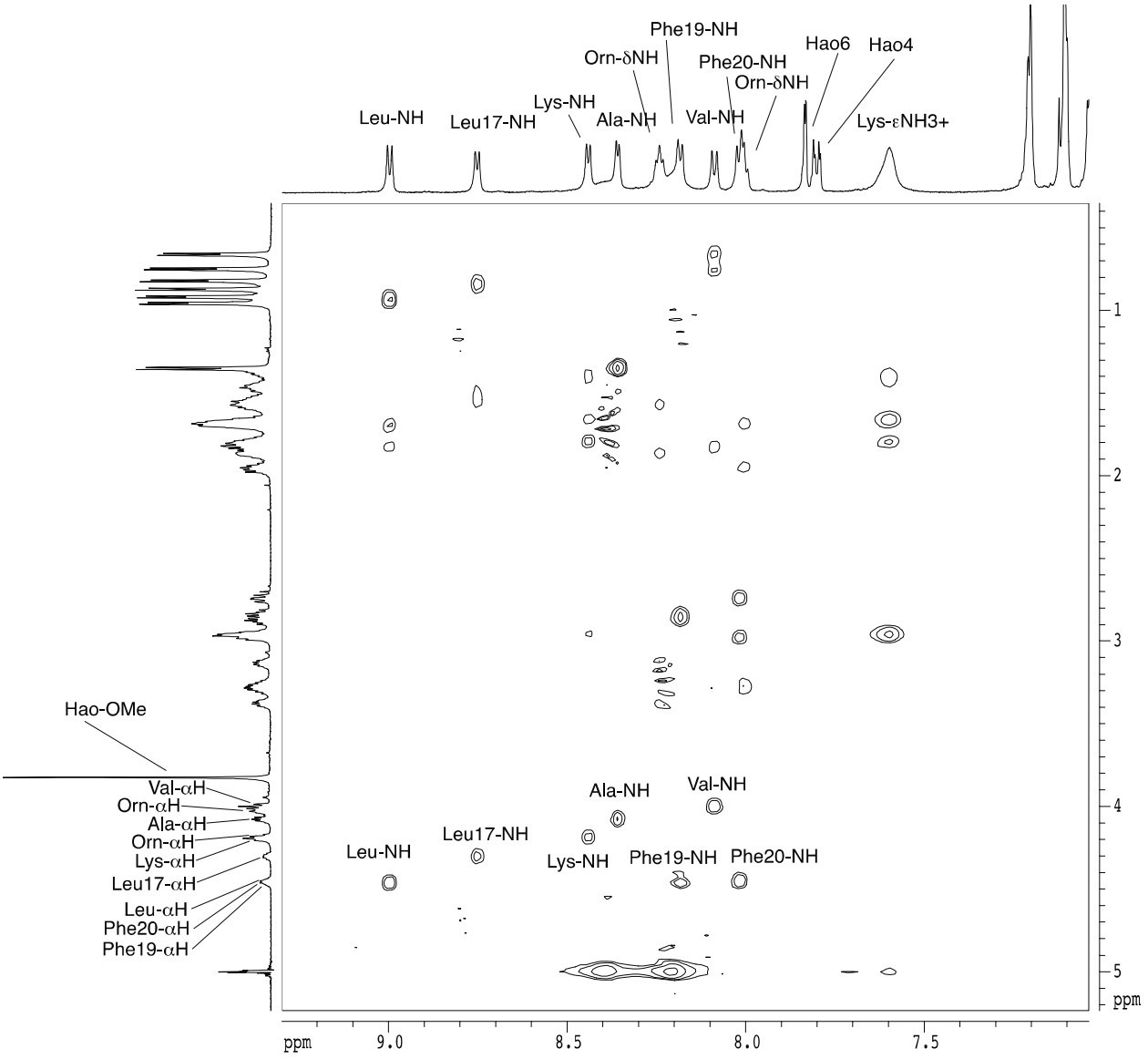

2D ROESY spectrum of **1.1d** with solvent suppression, 600 mHz, 2 mM in 9:1 D_2O:H_2O, 278 K, 100 ms spin-lock mixing time

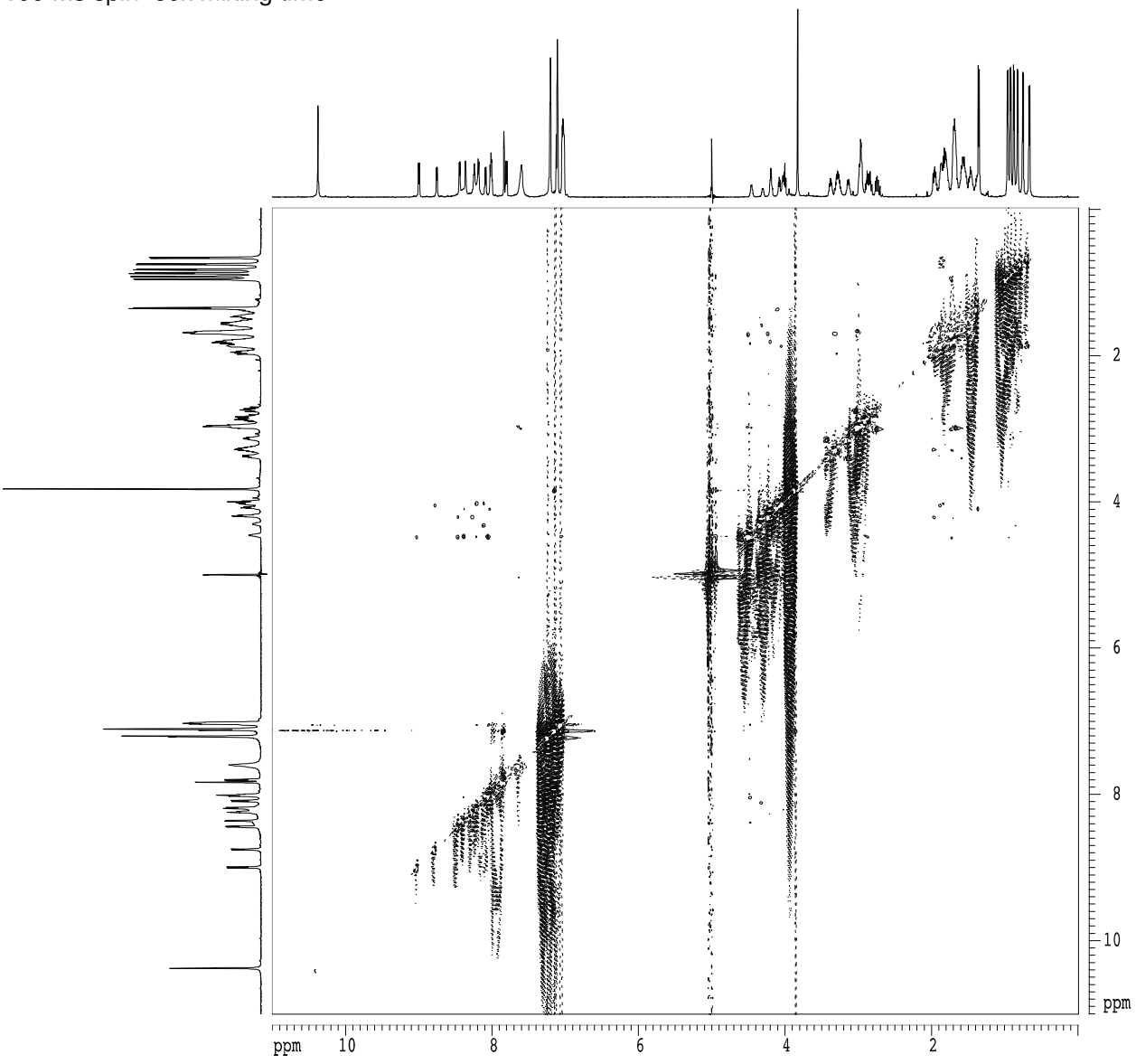

2D ROESY spectrum of **1.1d** with solvent suppression, 600 mHz, 2 mM in 9:1 H_2O:D_2O, 278 K, 100 ms spin-lock mixing time

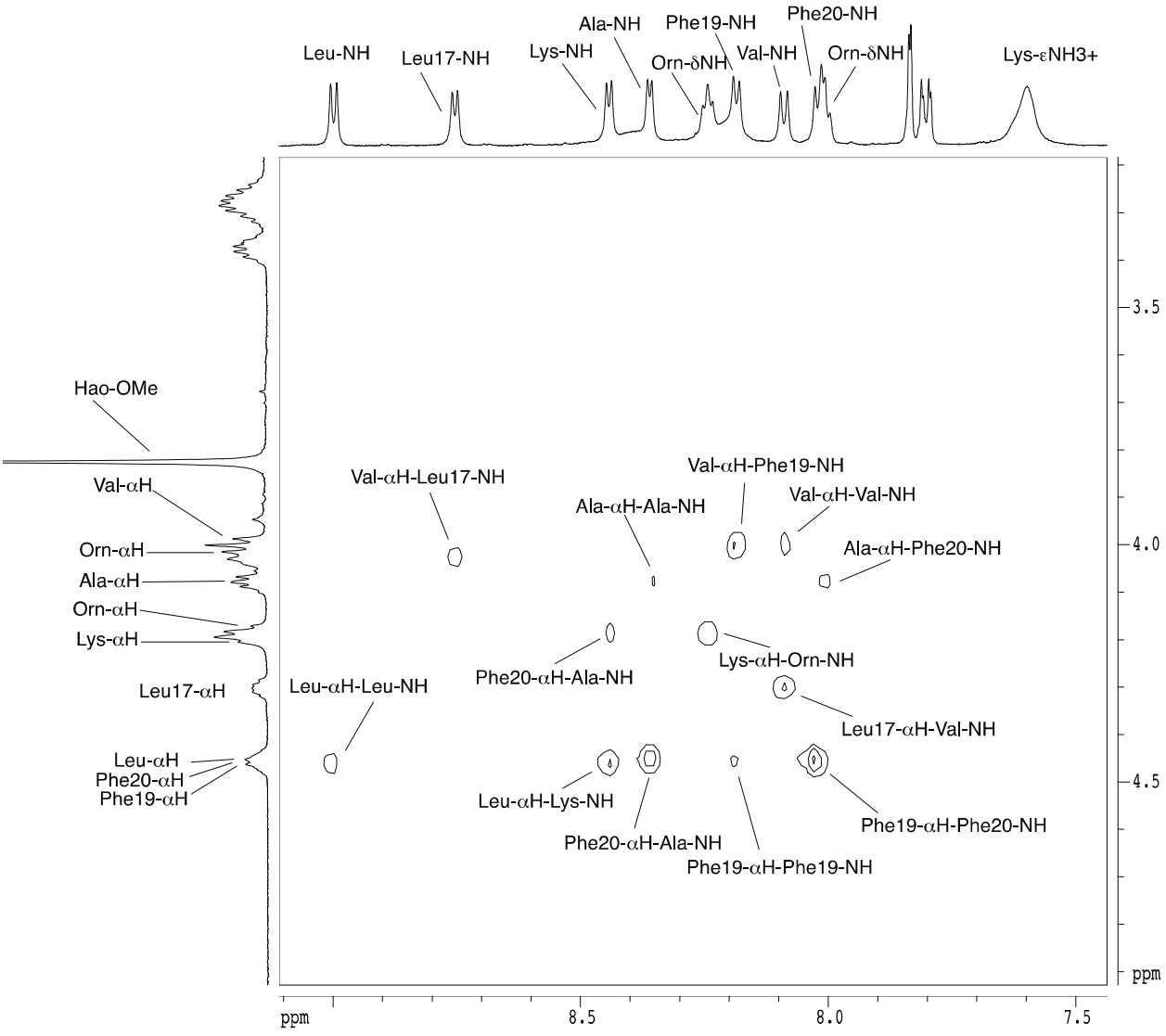

HPLC trace of **1.2a**

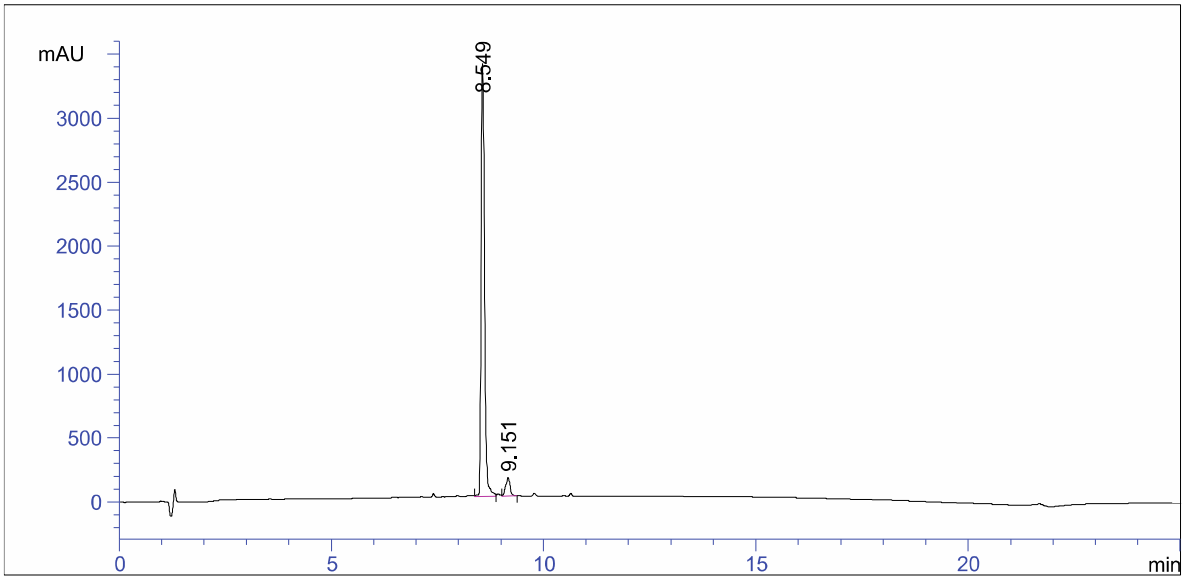


```
=====================================================================
                        Area Percent Report
=====================================================================

Signal 1: VWD1 A, Wavelength=214 nm

Peak RetTime Type  Width     Area      Height     Area
  #   [min]        [min]  mAU   *s    [mAU   ]      %
----|-------|----|-------|----------|----------|--------|
   1   8.549 VV    0.0866 1.88159e4  3389.87231  94.8980
   2   9.151 VB    0.1049 1011.59991  142.11832   5.1020

Totals :                  1.98275e4  3531.99063

=====================================================================
                        *** End of Report ***
```

ESI-MS of **1.2a**

chemical formula: $C_{86}H_{132}N_{20}O_{20}$

exact mass: 1780.9876

calculated *m/z*:

$[M+2H]^{2+}$: 891.4938

$[M+3H]^{3+}$: 594.6625

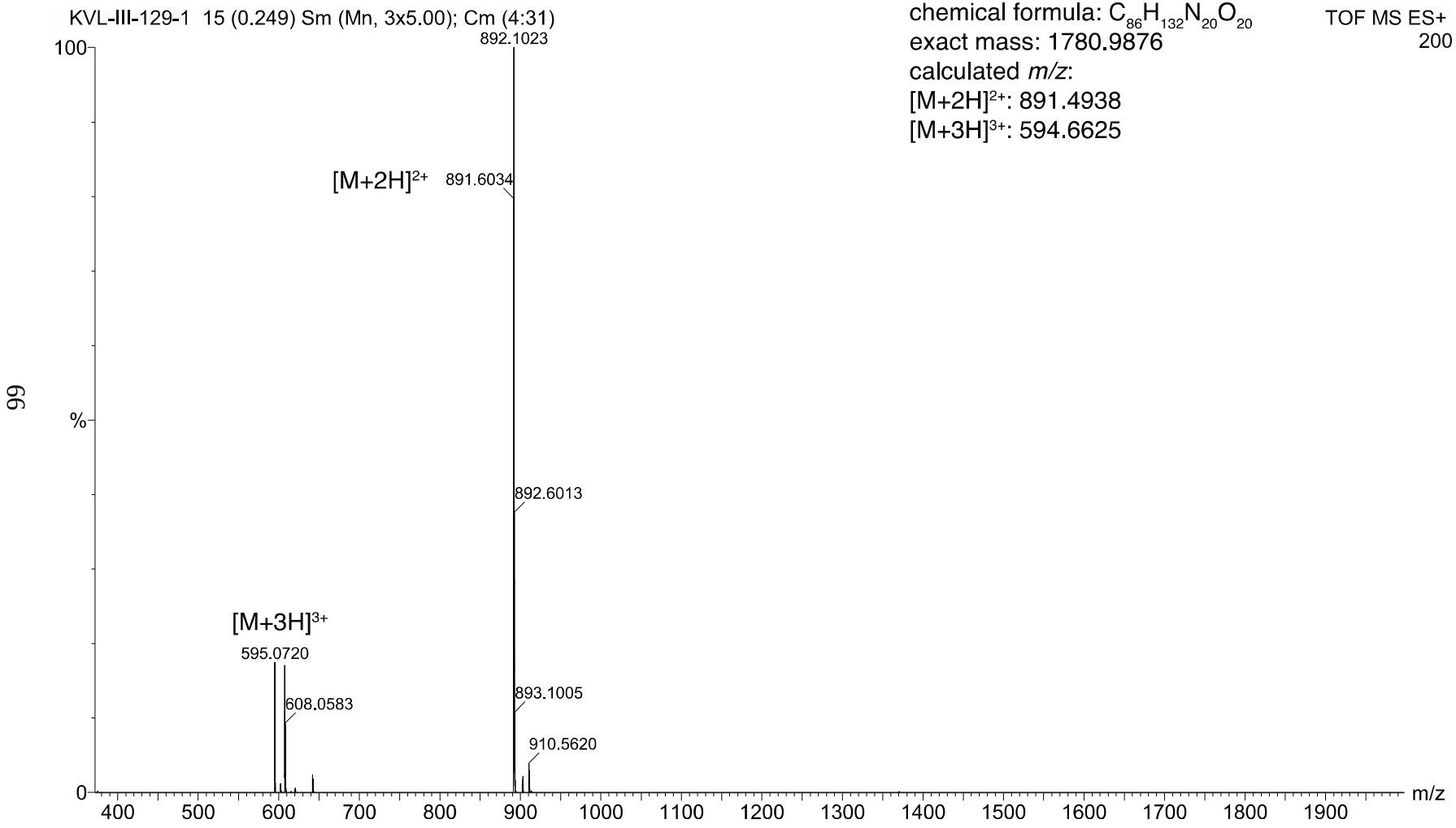

1D ^{1}H NMR spectrum of **1.2a**, 500 mHz, 1 mM in D_2O, 298 K

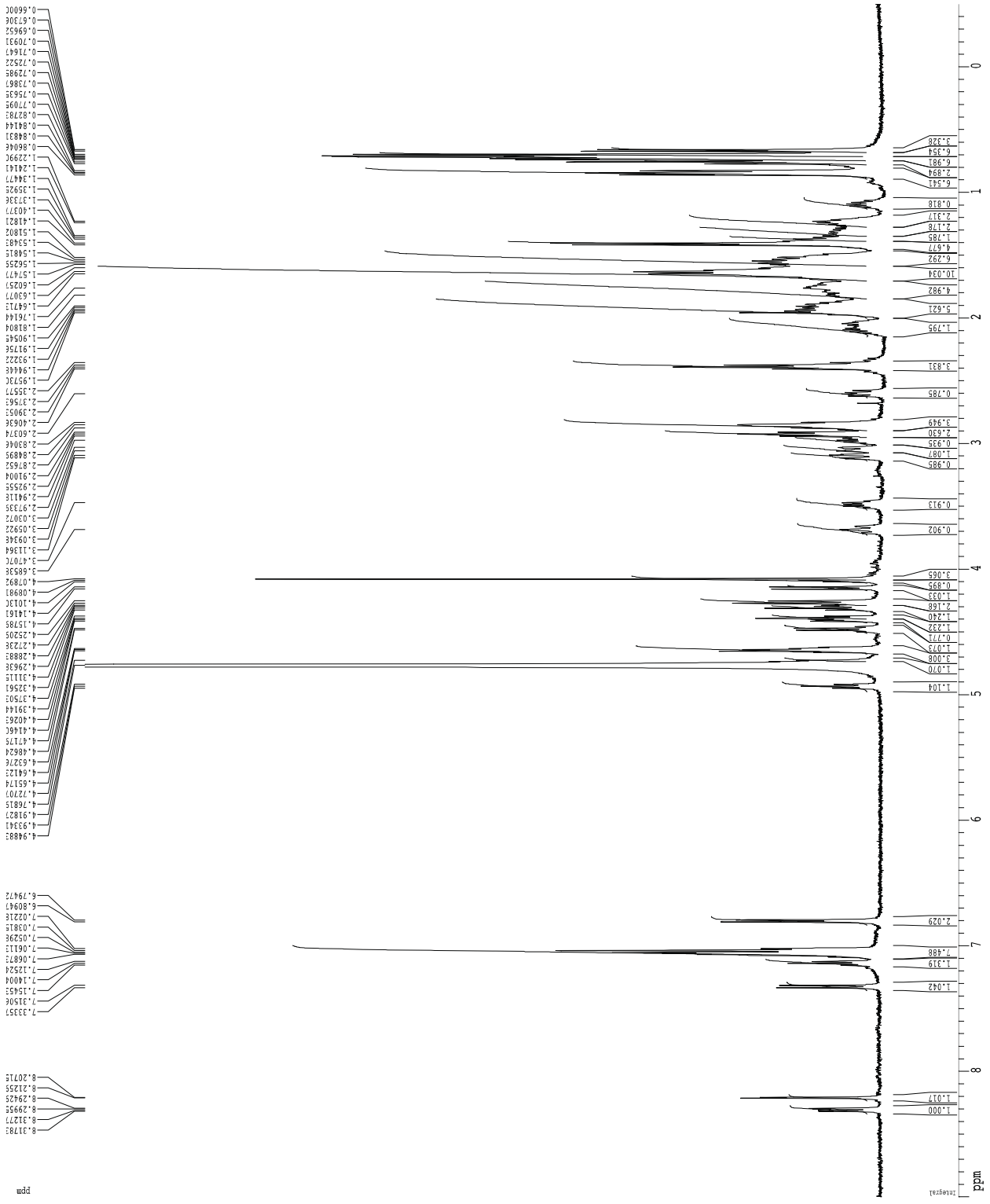

2D TOCSY spectrum of **1.2a**, 500 mHz, 1 mM in D_2O, 298 K, 150 ms spin-lock mixing time

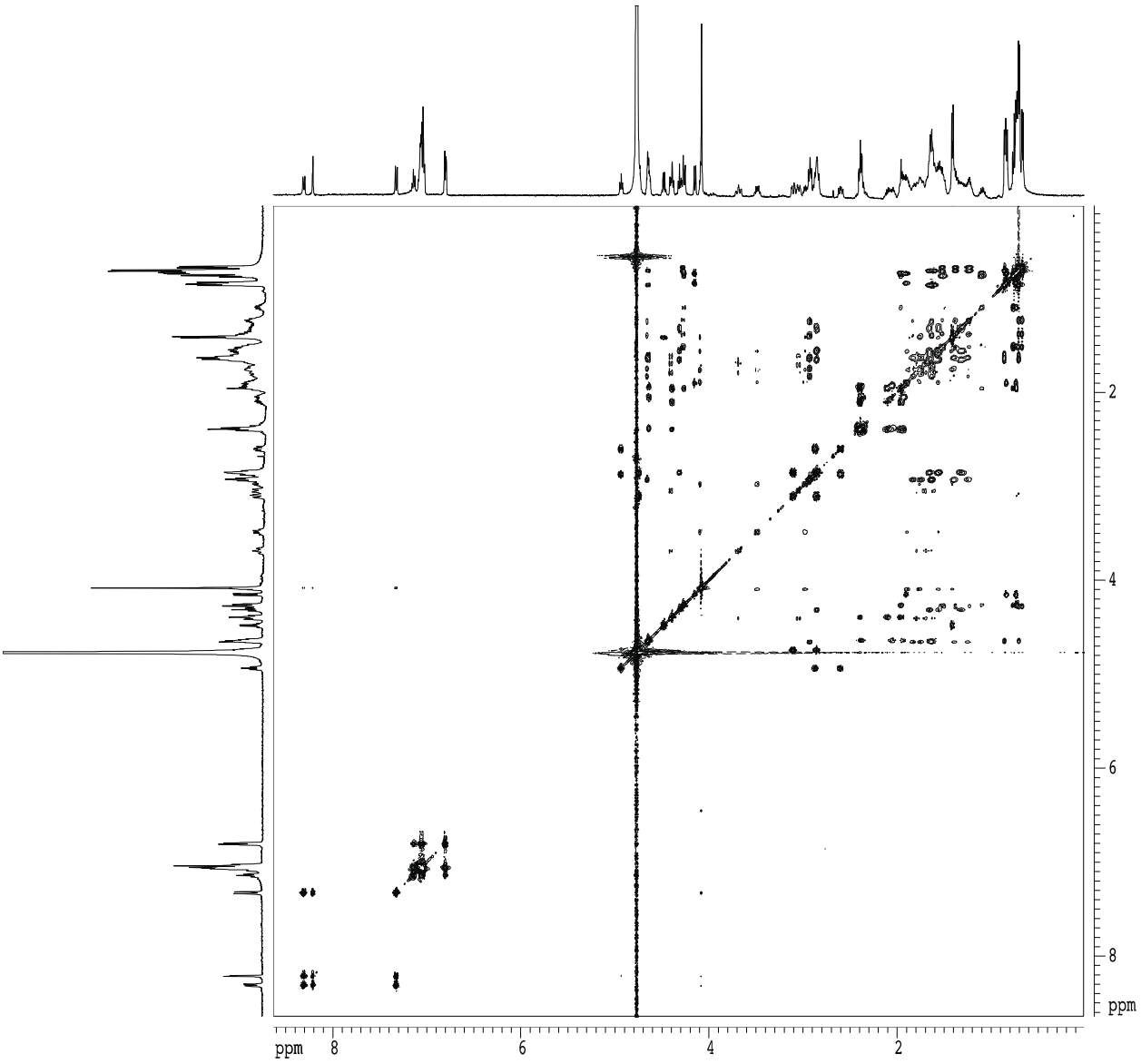

2D TOCSY spectrum of **1.2a**, 500 mHz, 1 mM in D_2O, 298 K, 150 ms spin-lock mixing time

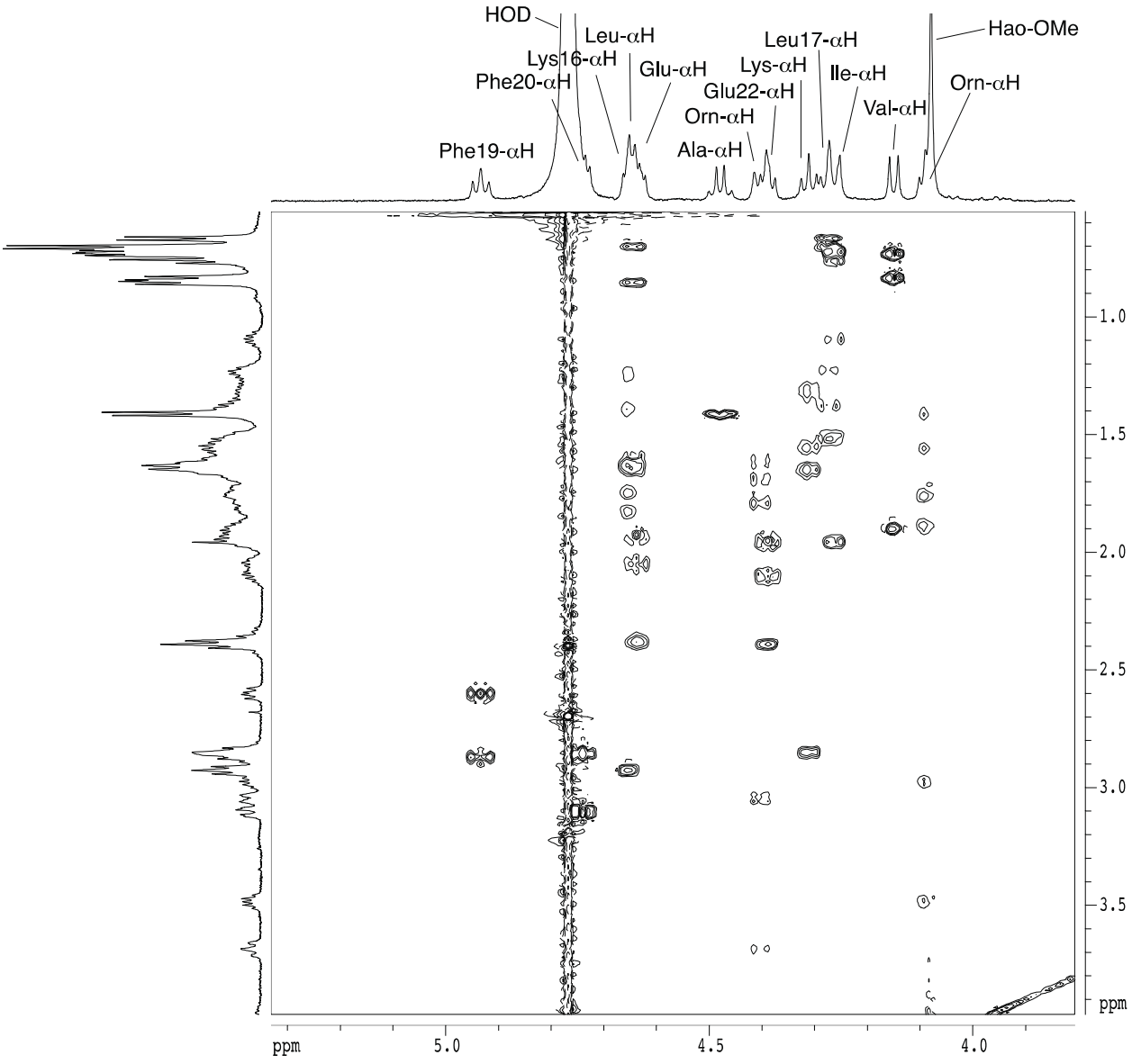

2D ROESY spectrum of **1.2a**, 500 mHz, 1 mM in D_2O, 298 K, 300 ms spin-lock mixing time

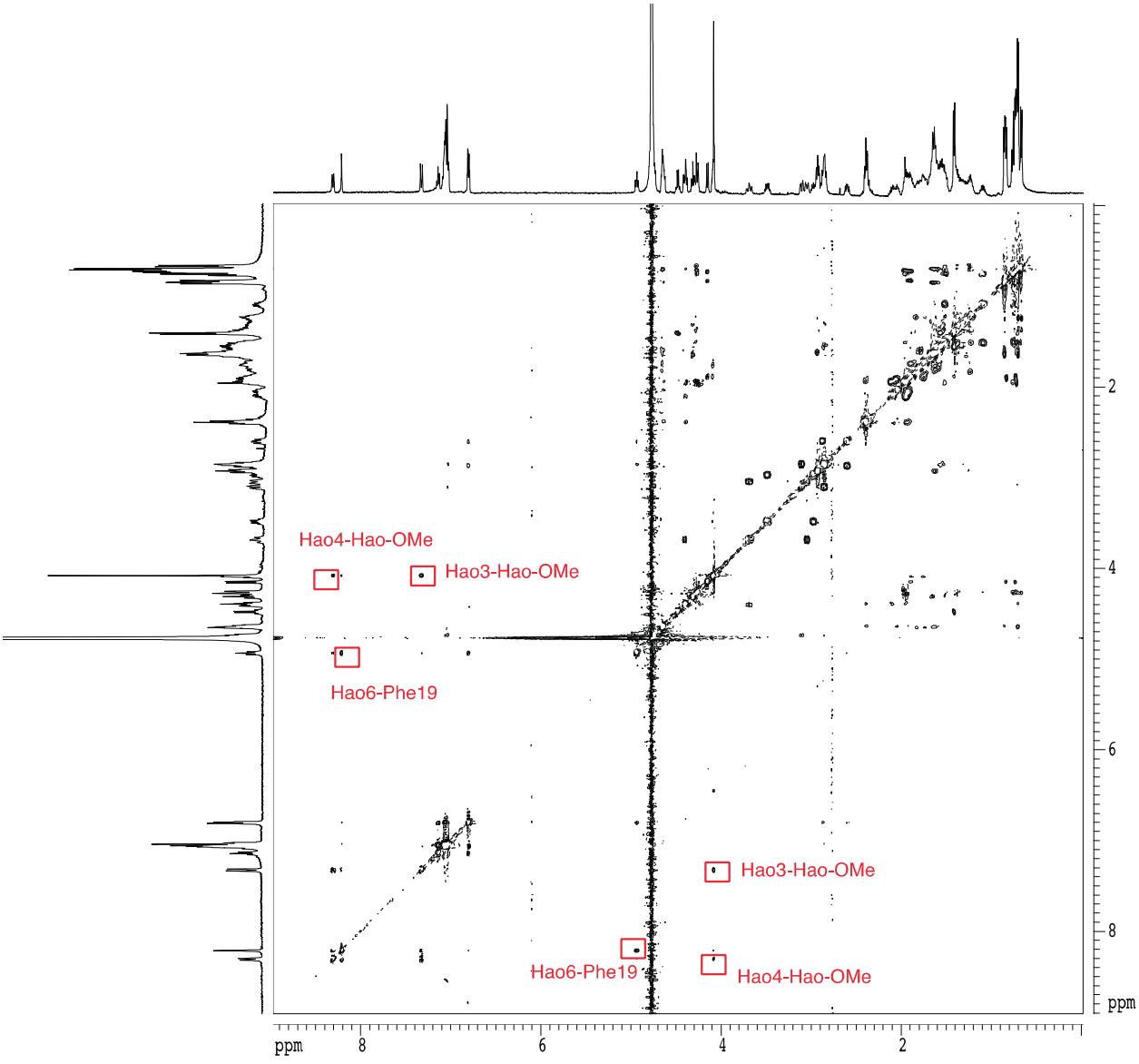

2D ROESY spectrum of **1.2a**, 500 mHz, 1 mM in D_2O, 298 K, 300 ms spin-lock mixing time

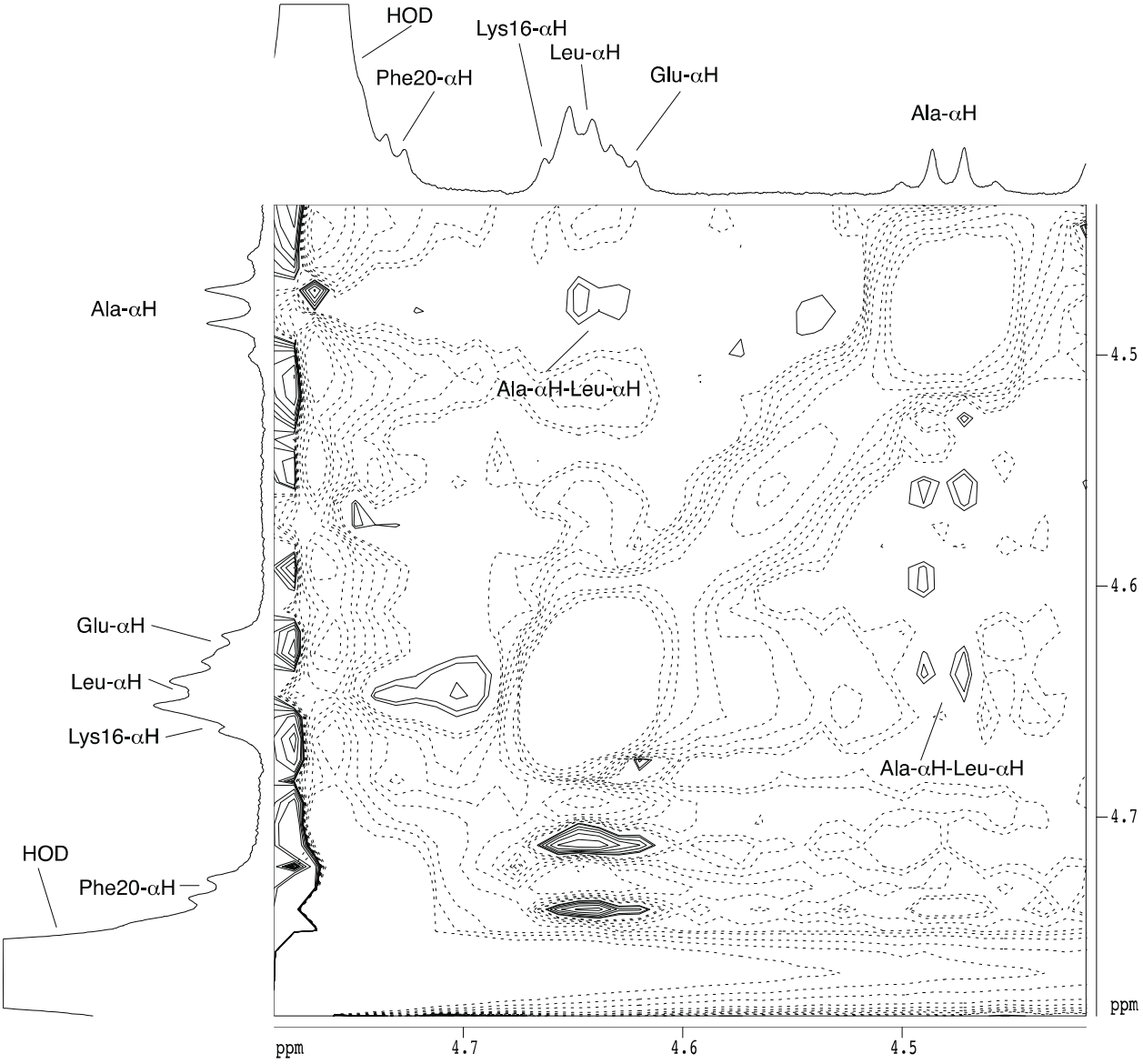

1D ^{1}H NMR spectrum of **1.2a** with solvent suppression, 600 mHz, 1.5 mM in 9:1 H_2O:D_2O, 278 K, 32 scans

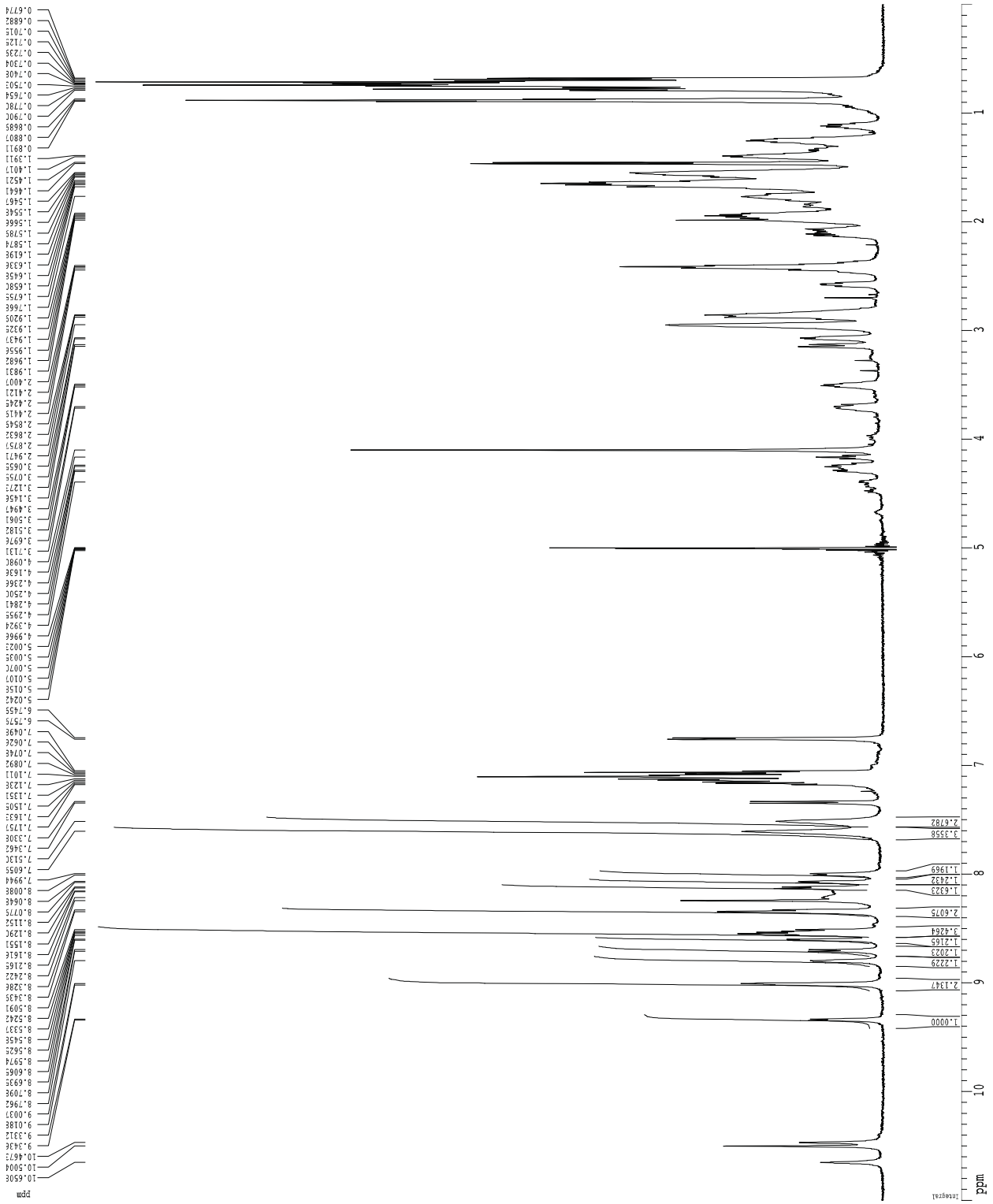

2D TOCSY spectrum of **1.2a** with solvent suppression, 500 mHz, 1.5 mM in 9:1 H_2O:D_2O, 278 K, 100 ms spin-lock mixing time

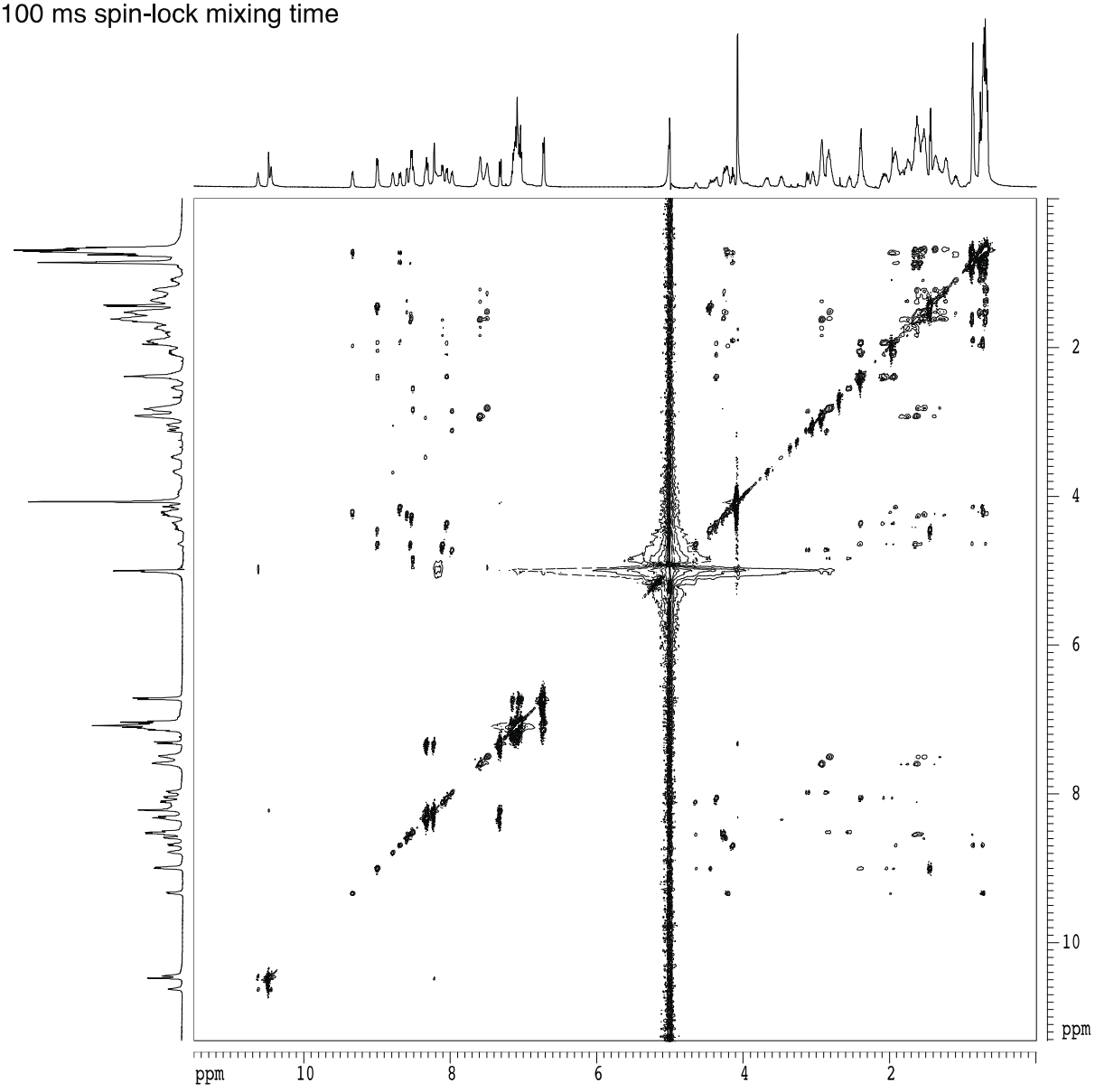

2D TOCSY spectrum of **1.2a** with solvent suppression, 500 mHz, 1.5 mM in 9:1 H_2O:D_2O, 278 K, 100 ms spin-lock mixing time

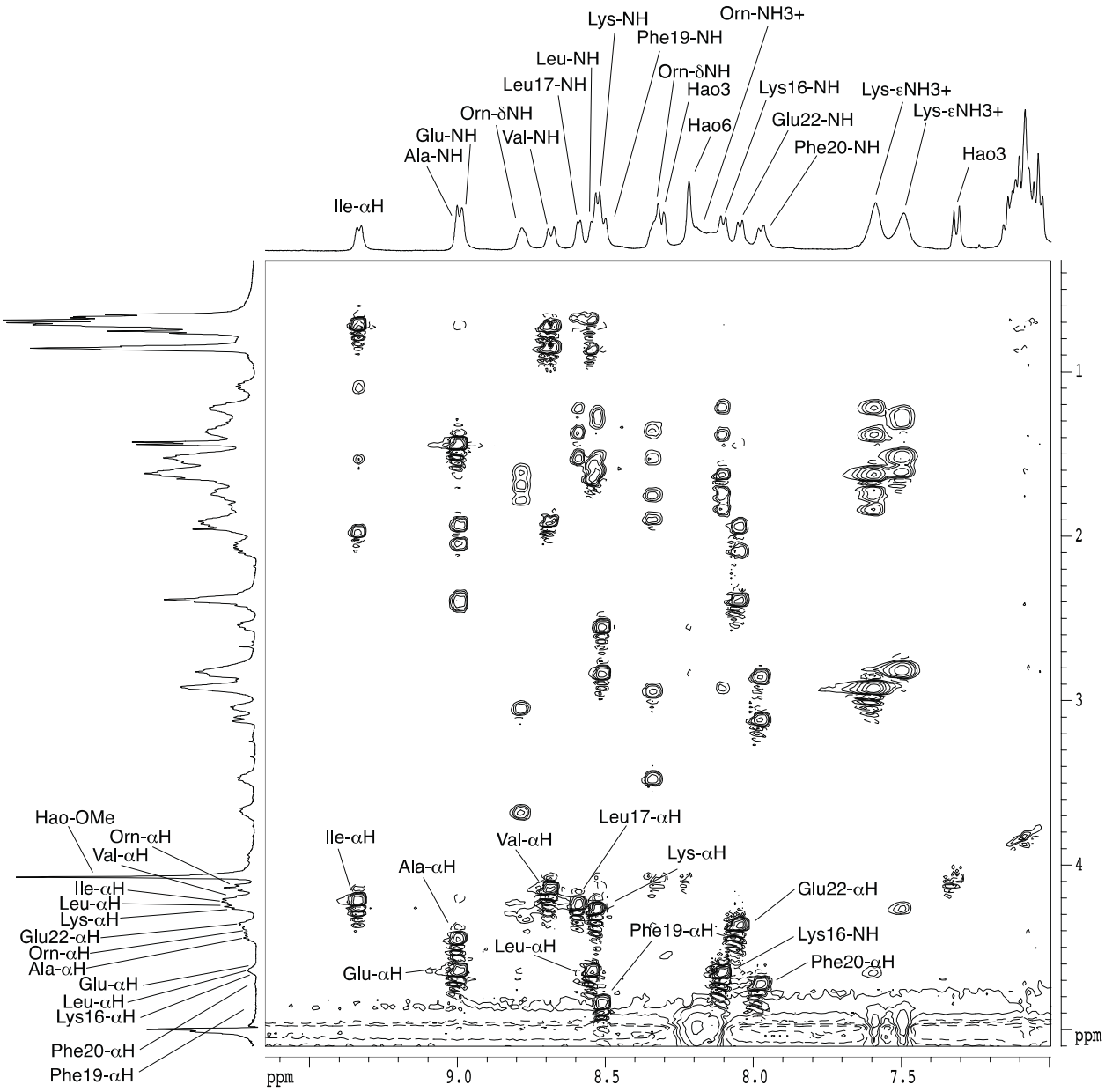

2D TOCSY spectrum of **1.2a** with solvent suppression, 600 mHz, 1.5 mM in 9:1 H_2O:D_2O, 278 K, 200 ms spin-lock mixing time

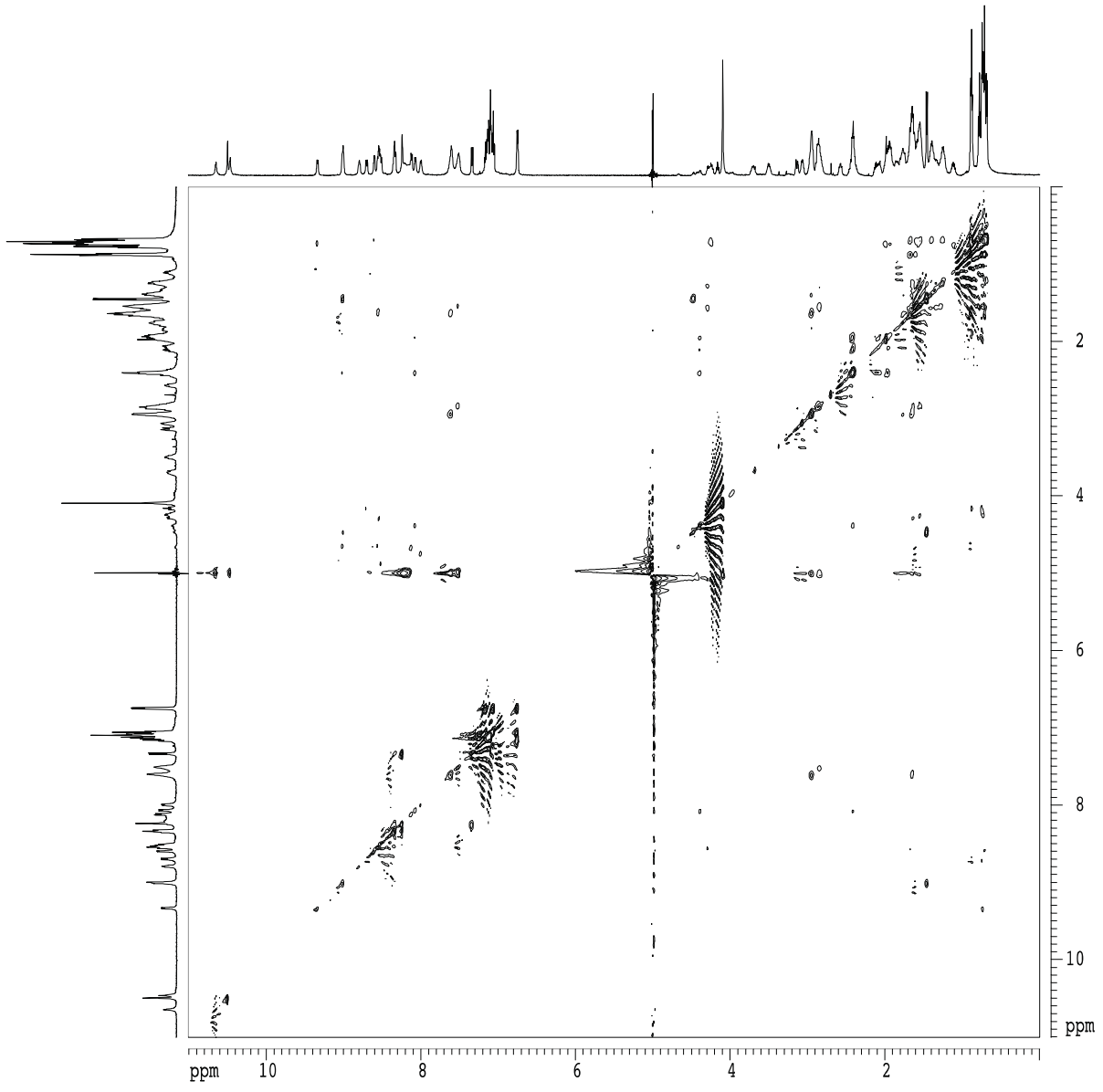

2D TOCSY spectrum of **1.2a** with solvent suppression, 600 mHz, 1.5 mM in 9:1 H_2O:D_2O, 278 K, 200 ms spin-lock mixing time

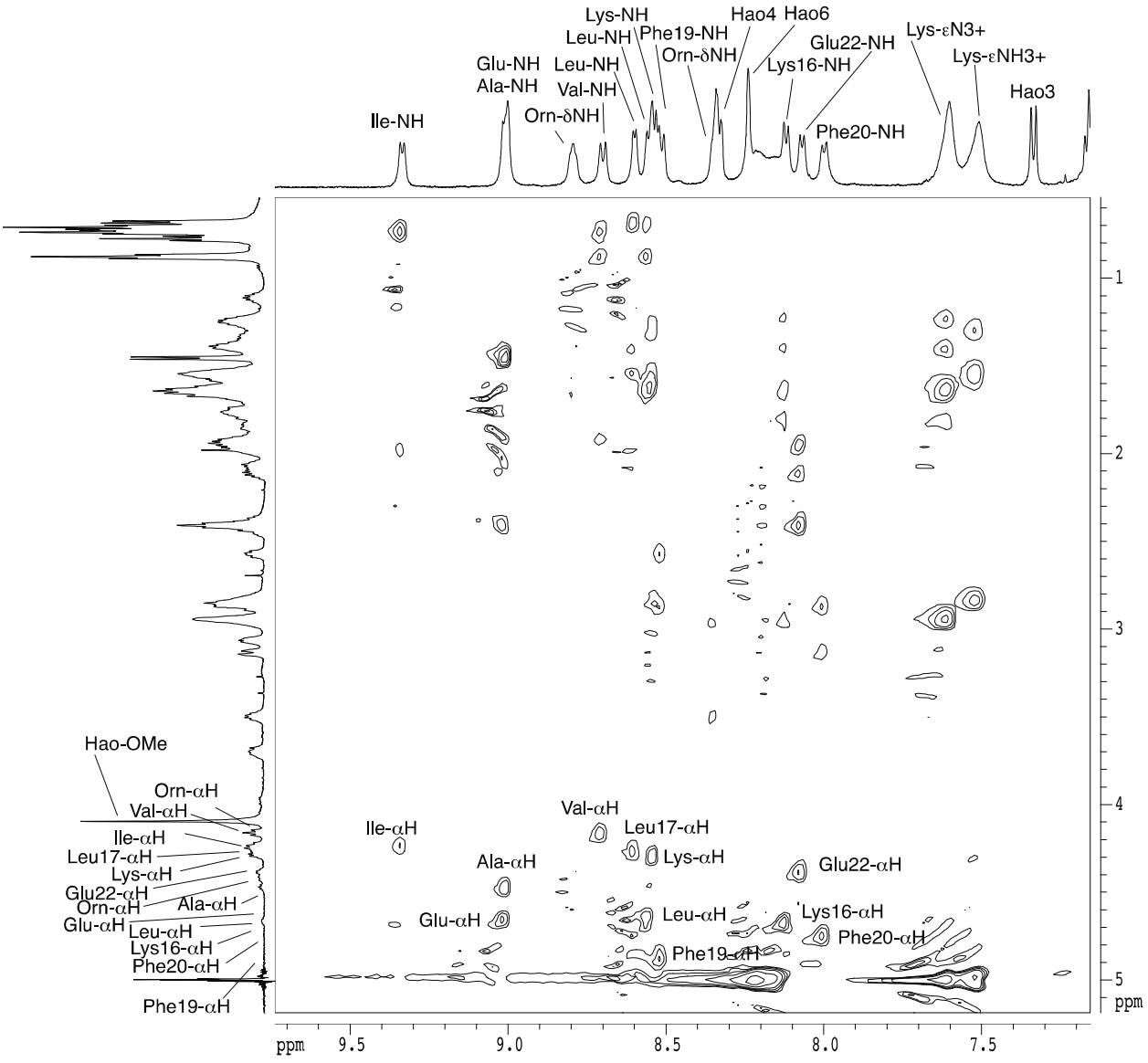

2D ROESY spectrum of **1.2a** with solvent suppression, 600 mHz, 1.5 mM in 9:1 H_2O:D_2O, 278 K, 100 ms spin-lock mixing time

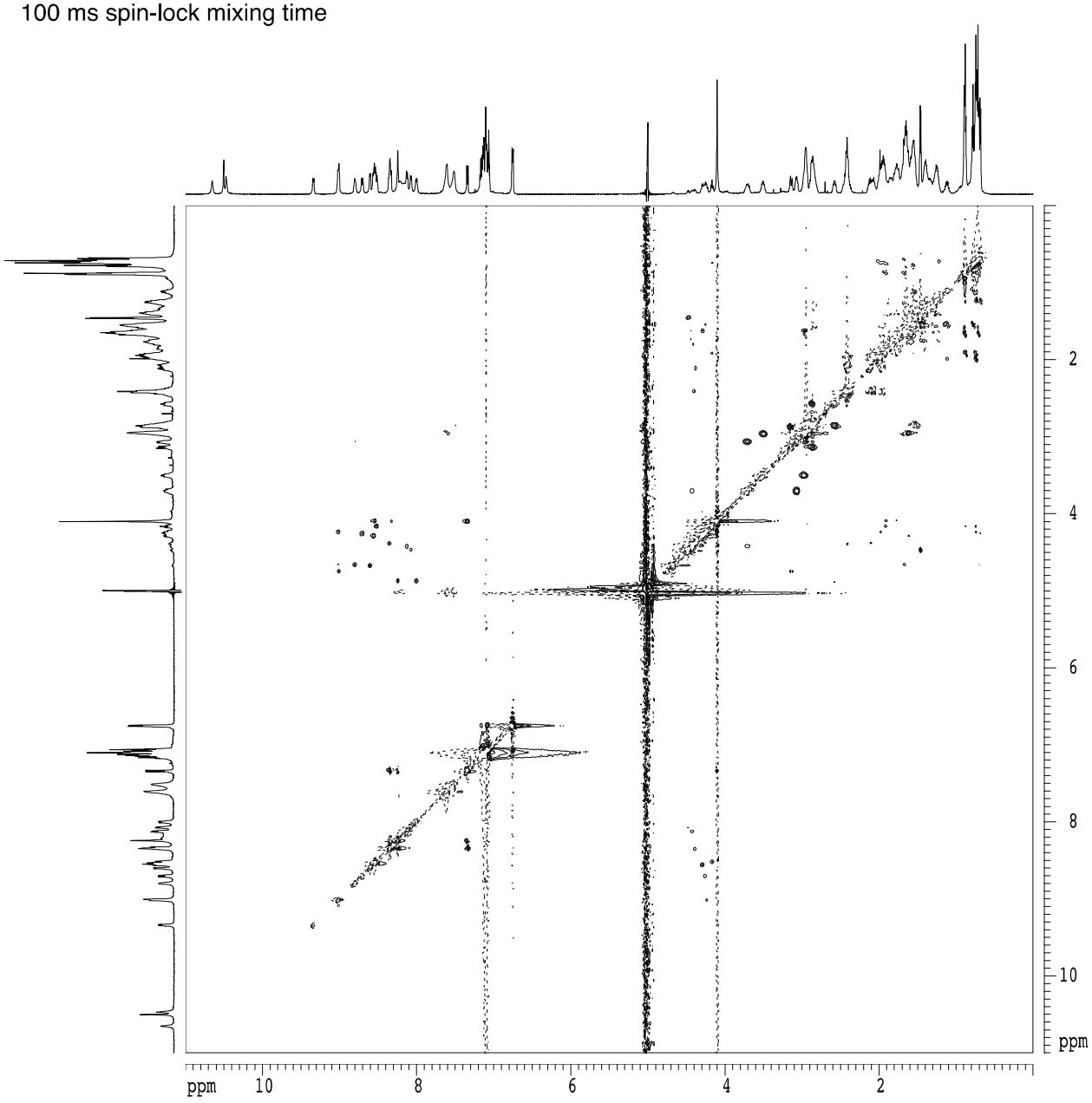

2D ROESY spectrum of **1.2a** with solvent suppression, 600 mHz, 1.5 mM in 9:1 H_2O:D_2O, 278 K, 100 ms spin-lock mixing time

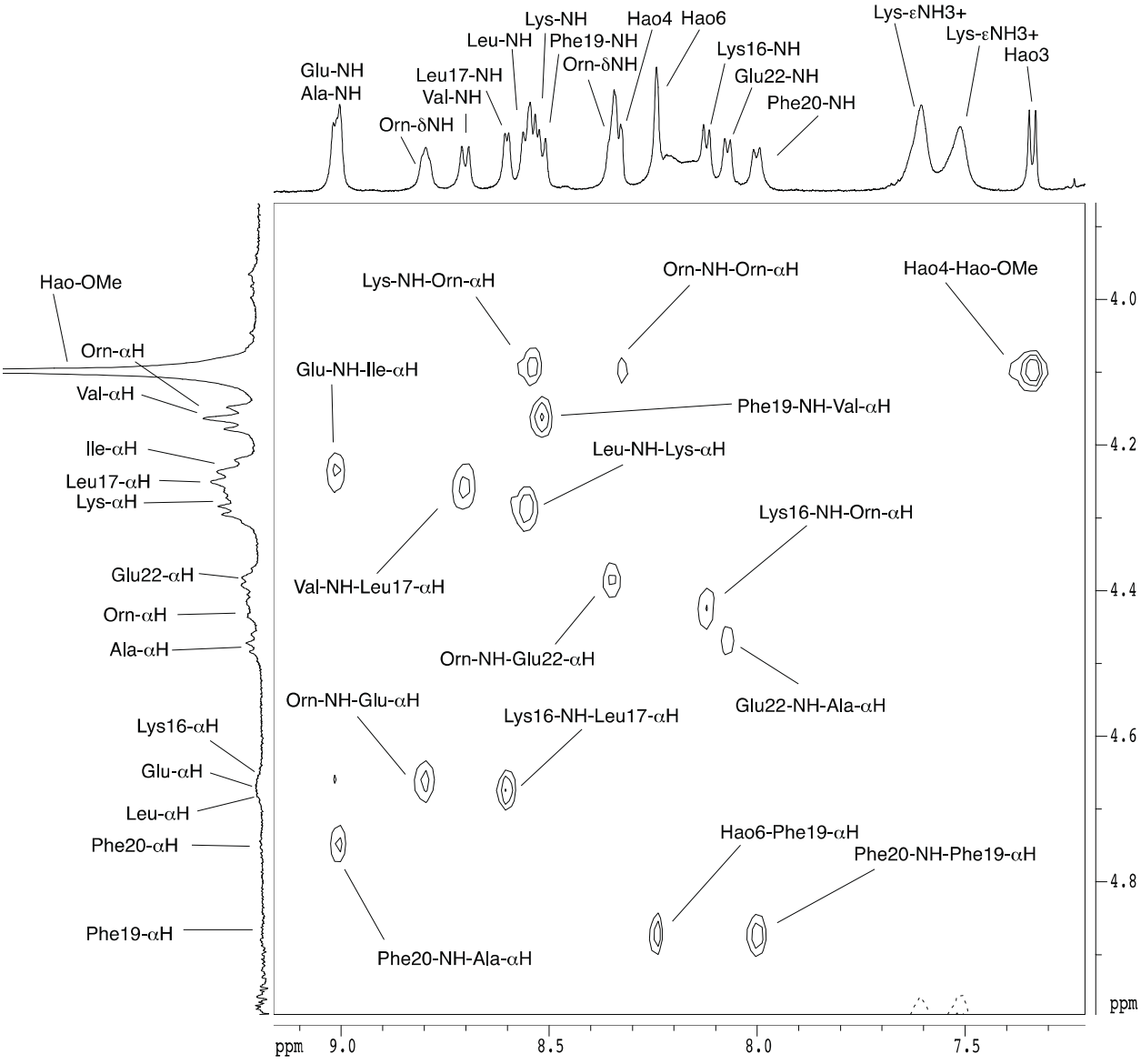

HPLC trace of **1.2b**

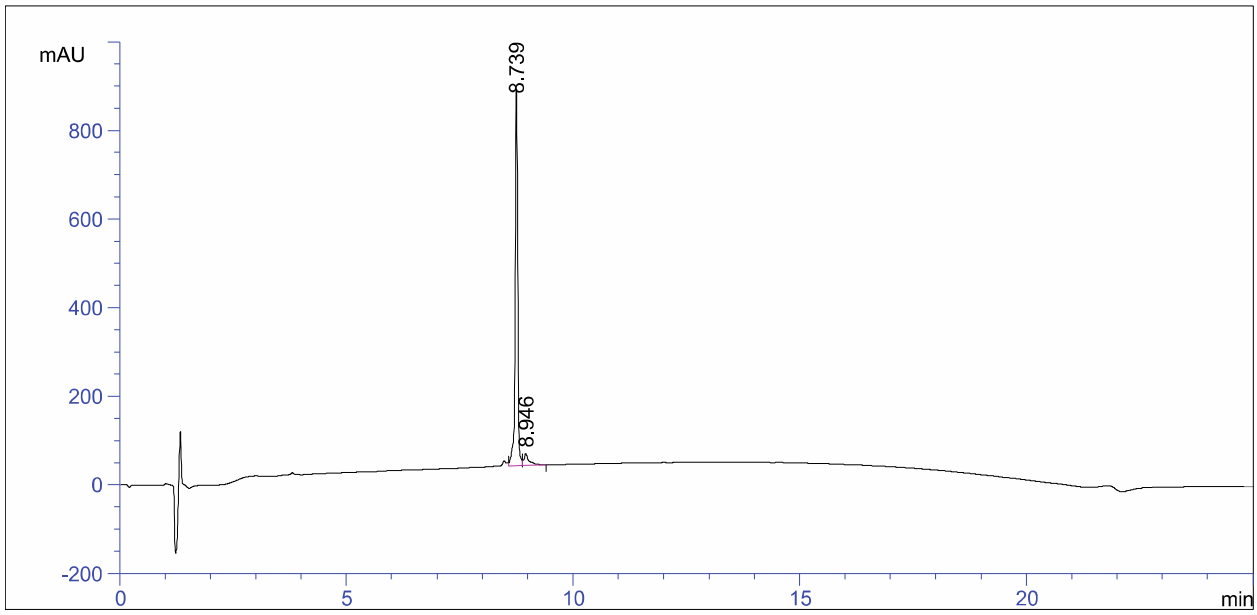


```
=====================================================================
                        Area Percent Report
=====================================================================

Signal 1: VWD1 A, Wavelength=214 nm

Peak RetTime Type  Width     Area      Height     Area
  #   [min]        [min]  mAU   *s    [mAU   ]       %
----|-------|----|-------|----------|----------|--------|
   1   8.739 VV    0.0601 3329.69800  853.64288  94.0092
   2   8.946 VB    0.1090  212.18593   27.05408   5.9908

Totals :                  3541.88393  880.69697

=====================================================================
                        *** End of Report ***
```

ESI-MS of **1.2b**
chemical formula: $C_{86}H_{132}N_{20}O_{20}$
exact mass: 1780.9876
calculated *m/z*:
$[M+2H]^{2+}$: 891.4938
$[M+3H]^{3+}$: 594.6625

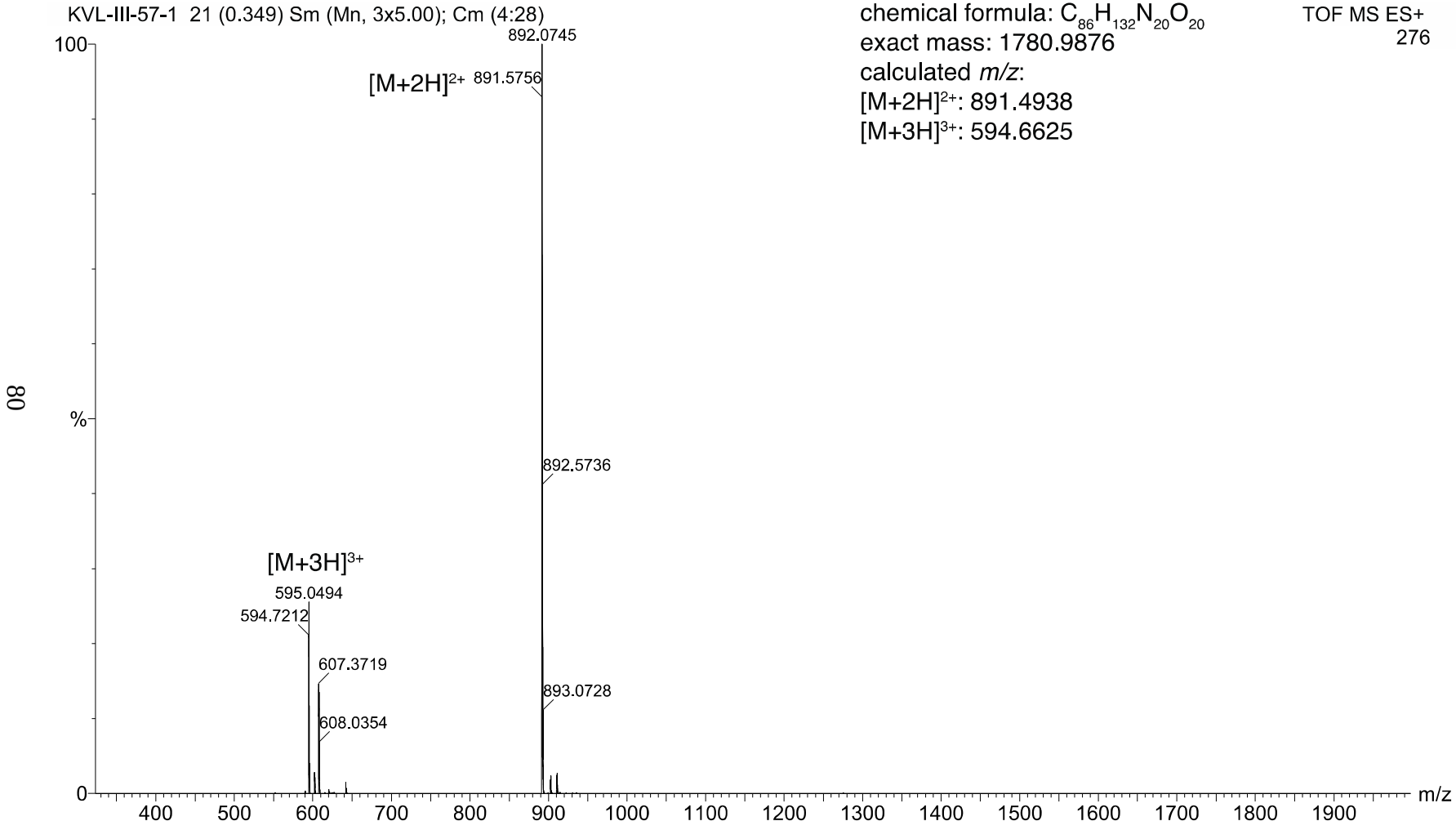

1D ^{1}H NMR spectrum of **1.2b**, 500 mHz, 1 mM in D_2O, 298 K

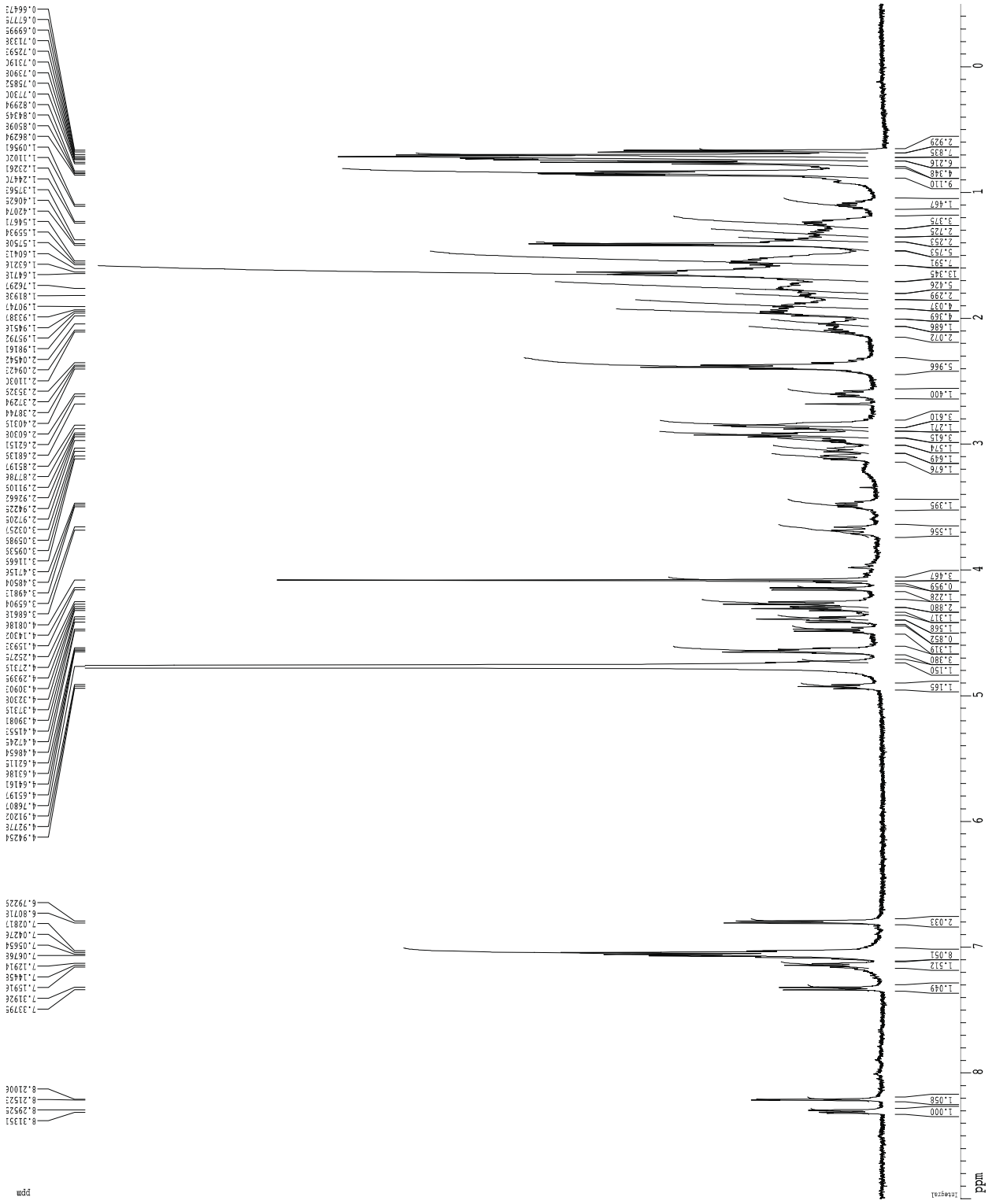

2D TOCSY spectrum of **1.2b**, 500 mHz, 1 mM in D_2O, 298 K, 150 ms spin-lock mixing time

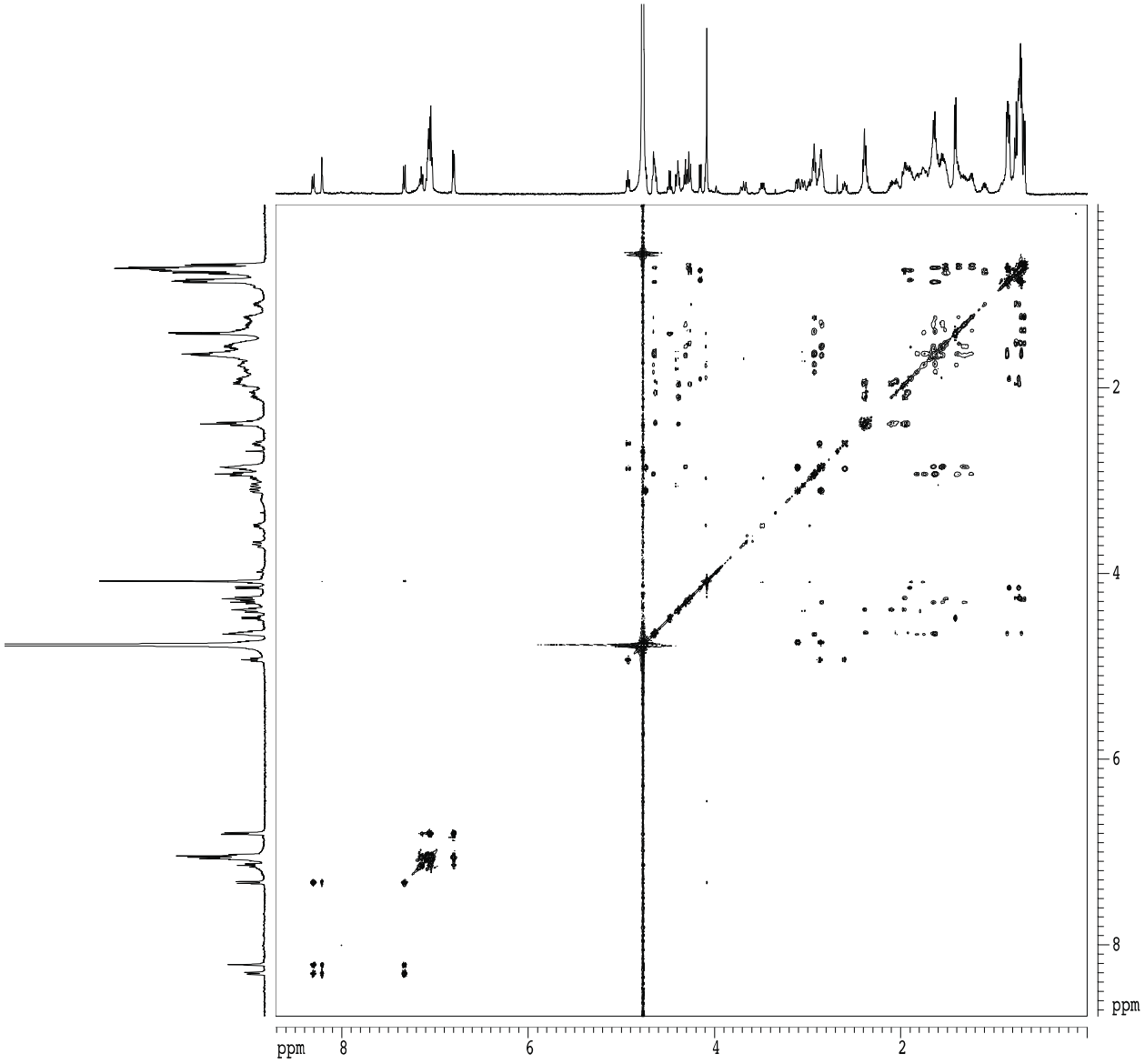

2D ROESY spectrum of **1.2b**, 500 mHz, 1 mM in D_2O, 298 K, 300 ms spin-lock mixing time

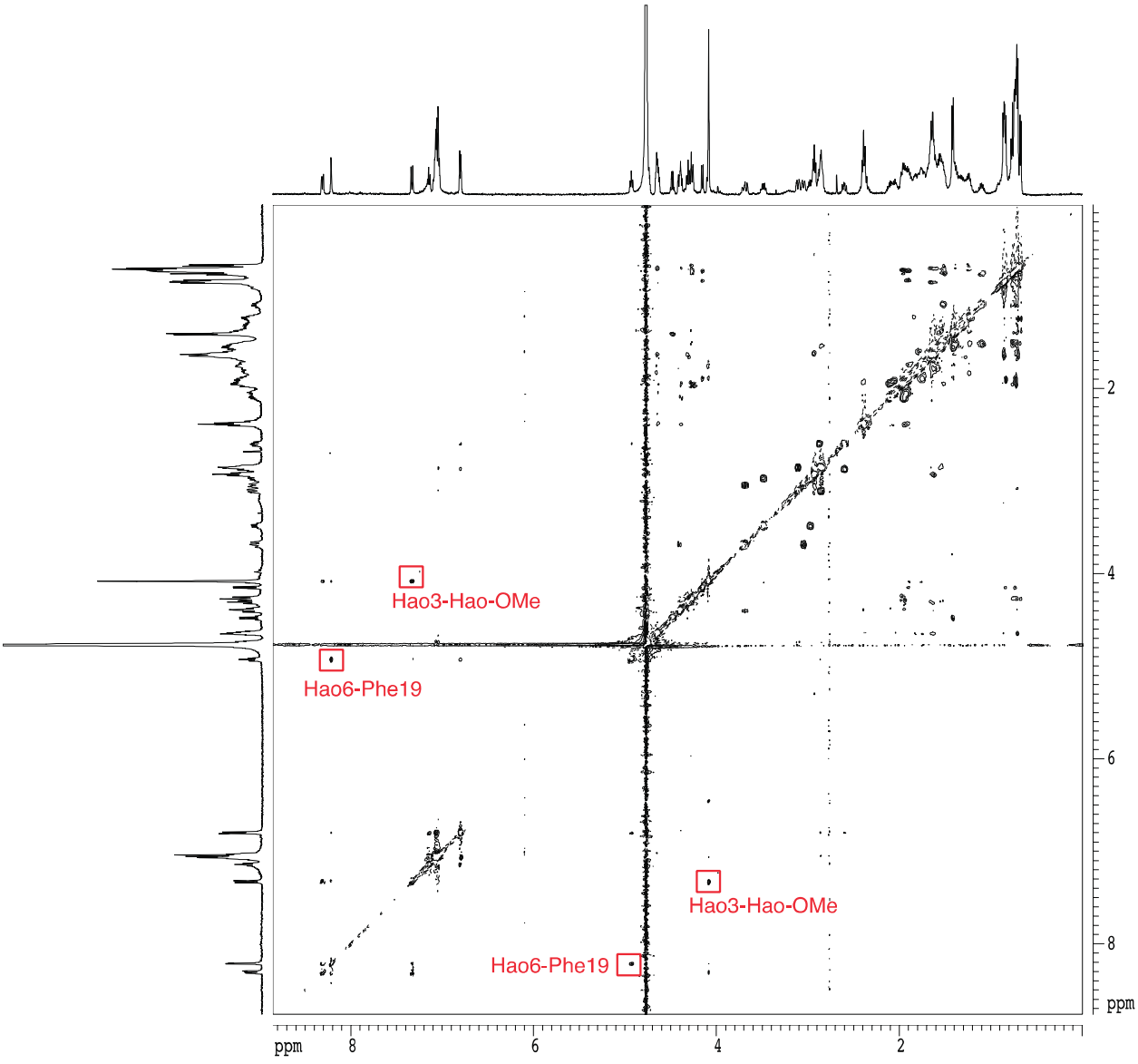

HPLC trace of **1.2c**

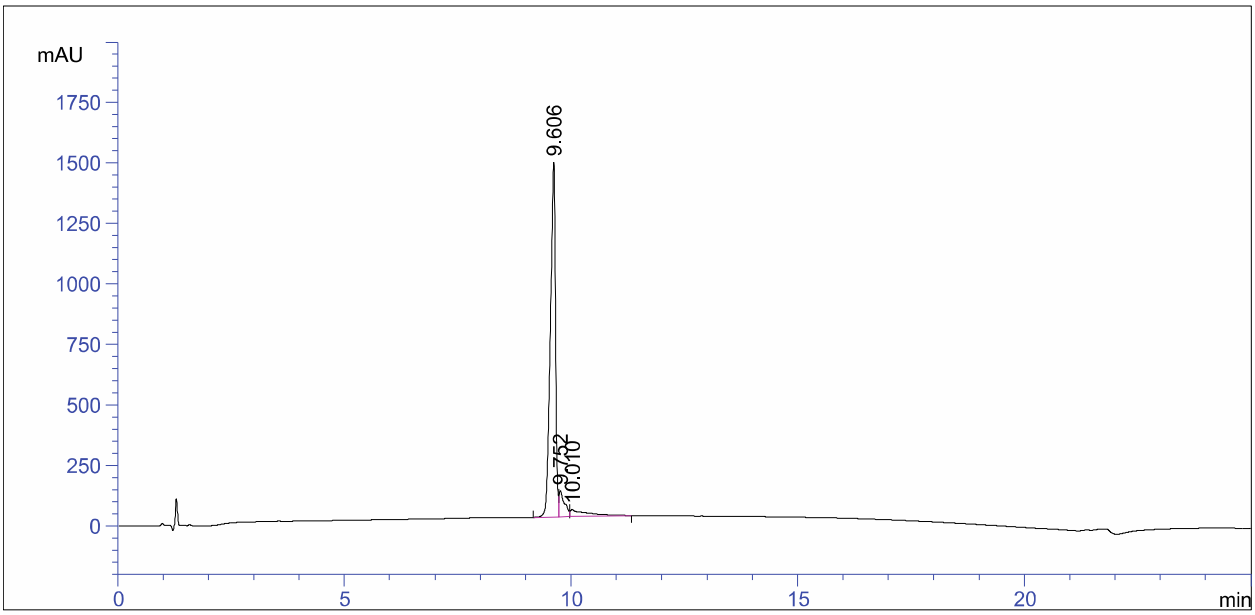


```
=====================================================================
                        Area Percent Report
=====================================================================

Signal 1: VWD1 A, Wavelength=214 nm

Peak RetTime Type  Width     Area      Height     Area
  #   [min]        [min]  mAU   *s    [mAU   ]      %
----|-------|----|-------|----------|----------|--------|
   1   9.606 BV    0.1183 1.15856e4  1467.66724  87.1553
   2   9.752 VV    0.1181  929.23199  107.75773   6.9904
   3  10.010 VB    0.3260  778.20648   29.29314   5.8543

Totals :                  1.32930e4  1604.71810

=====================================================================
                        *** End of Report ***
```

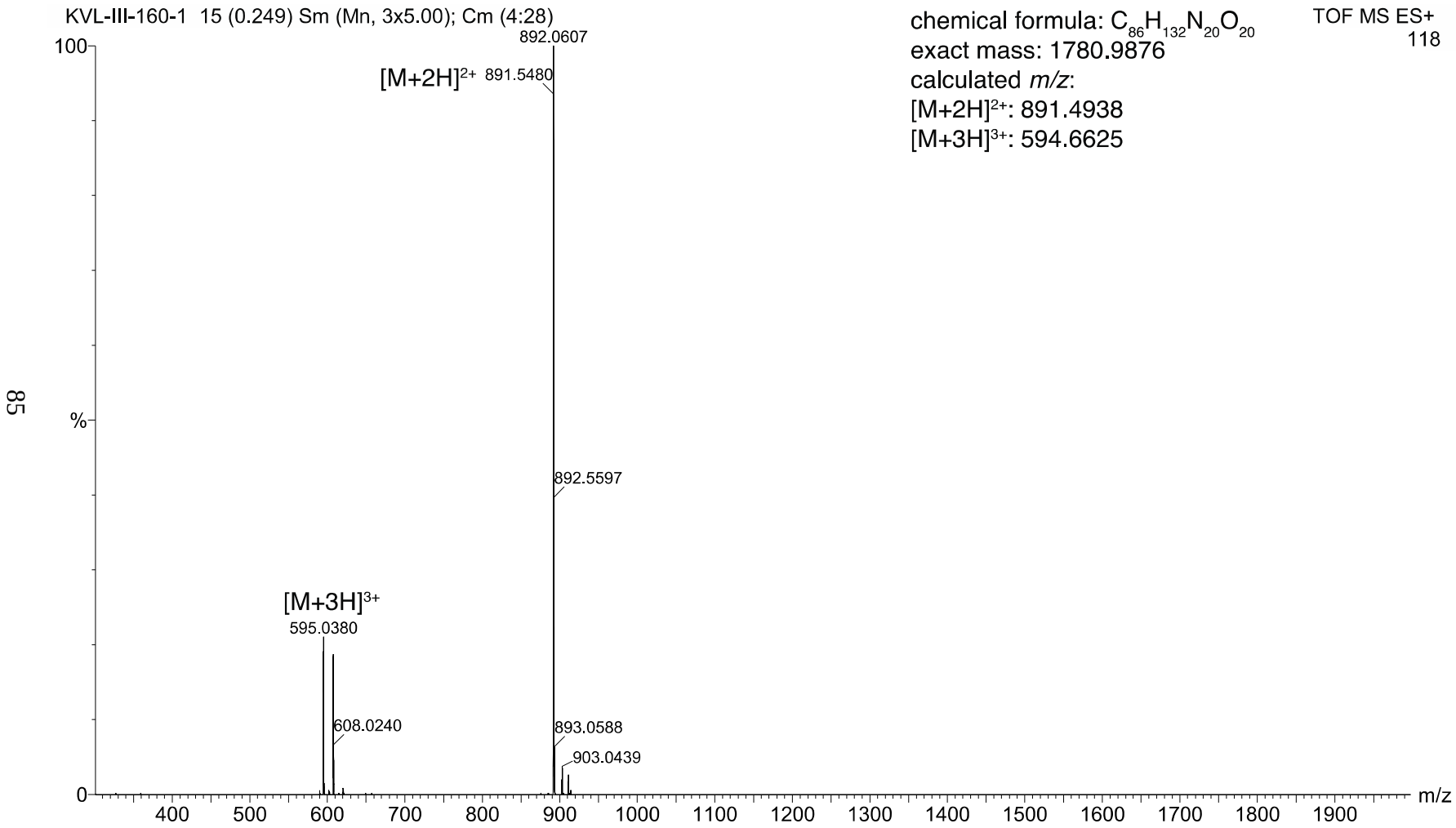
KVL-III-160-1 15 (0.249) Sm (Mn, 3x5.00); Cm (4:28)
TOF MS ES+
118
ESI-MS of 1.2c
chemical formula: C86H132N20O20
exact mass: 1780.9876
calculated m/z:
[M+2H]2+: 891.4938
[M+3H]3+: 594.6625
100
%
0
85
892.0607
[M+2H]2+ 891.5480
892.5597
[M+3H]3+
595.0380
608.0240
893.0588
903.0439
400
500
600
700
800
900
1000
1100
1200
1300
1400
1500
1600
1700
1800
1900
m/z

1D ^{1}H NMR spectrum of **1.2c**, 500 mHz, 1 mM in D_2O, 298 K

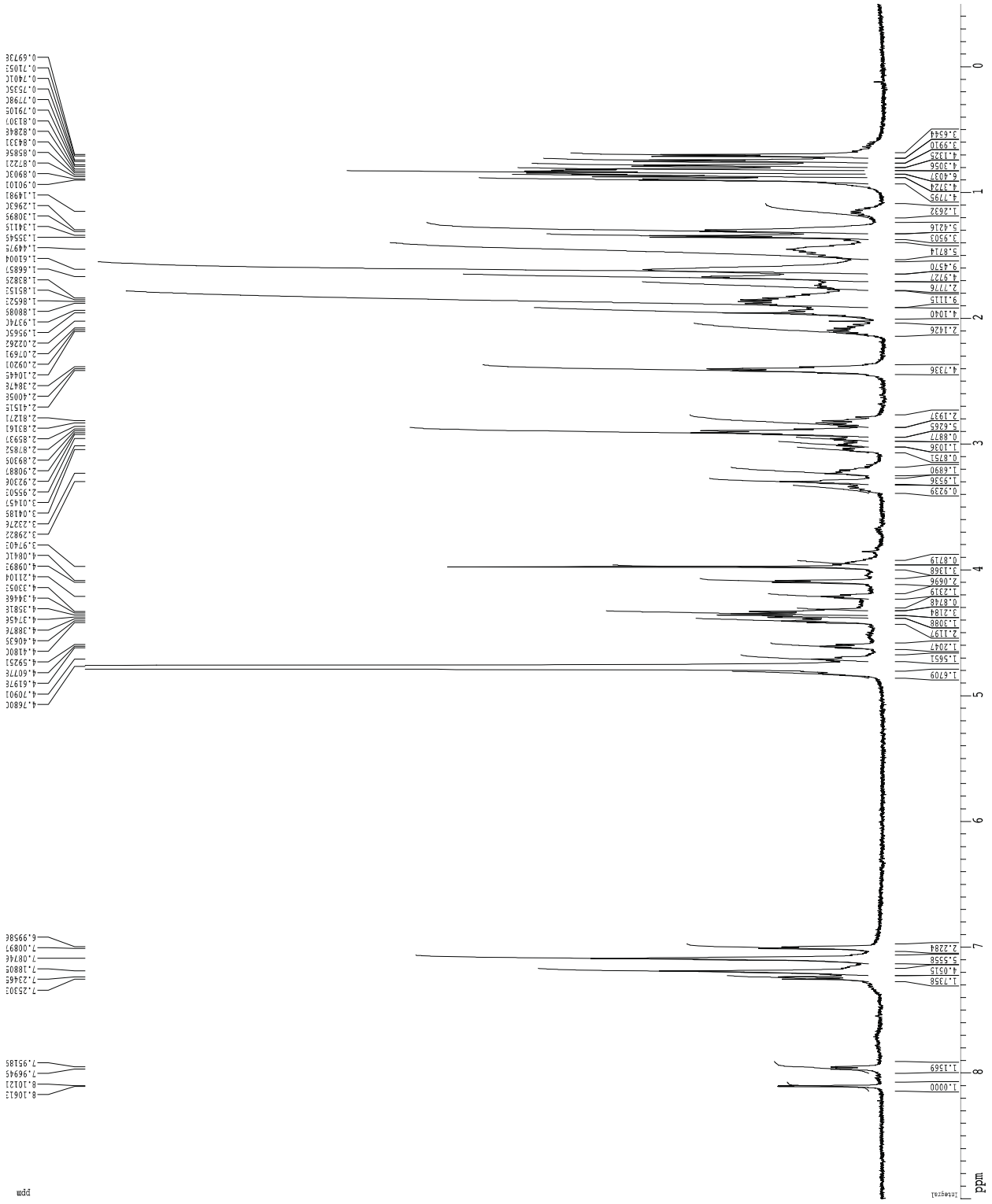

2D TOCSY spectrum of **1.2c**, 500 mHz, 1 mM in D_2O, 298 K, 150 ms spin-lock mixing time

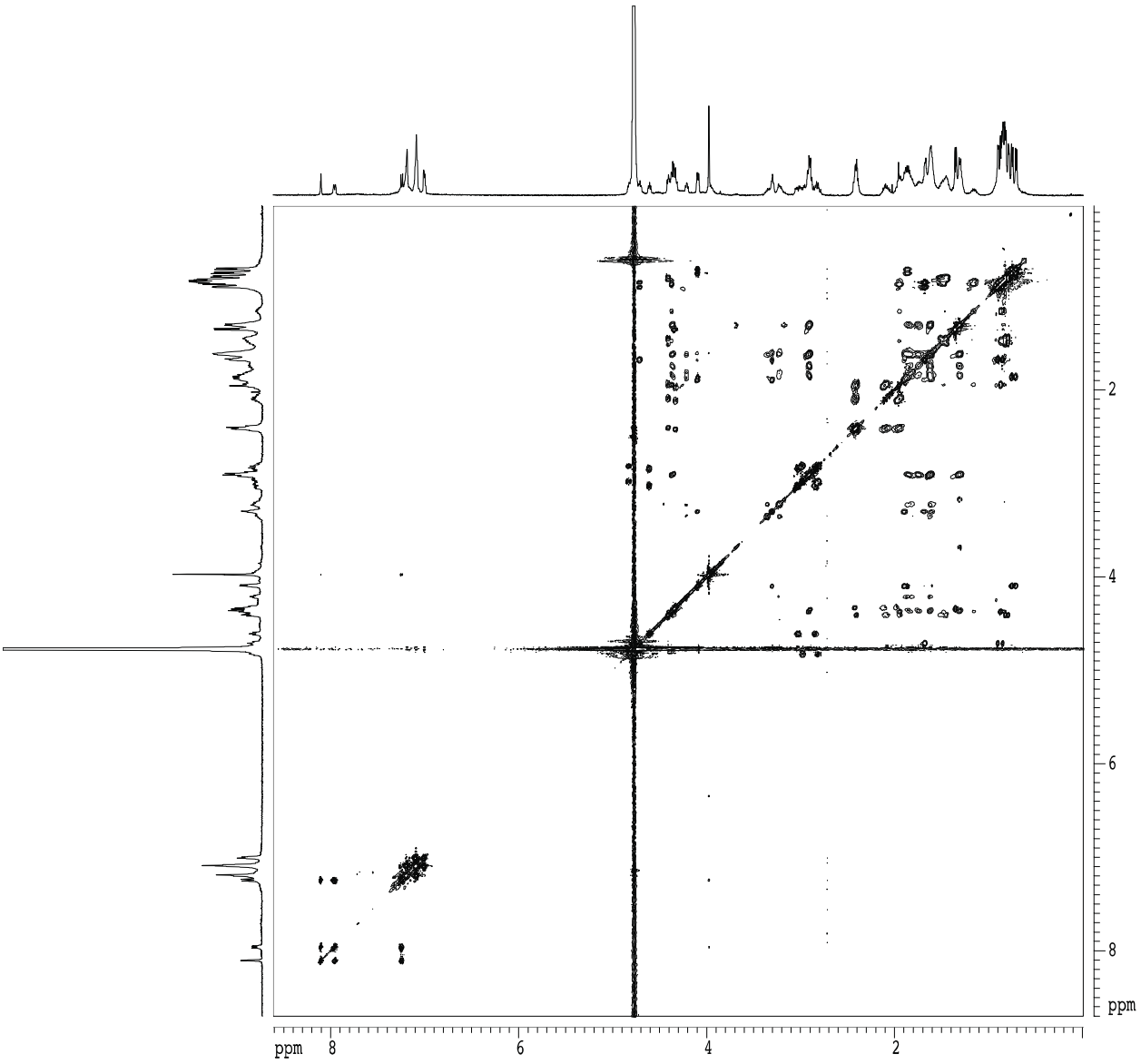

2D ROESY spectrum of **1.2c**, 500 mHz, 1 mM in D_2O, 298 K, 300 ms spin-lock mixing time

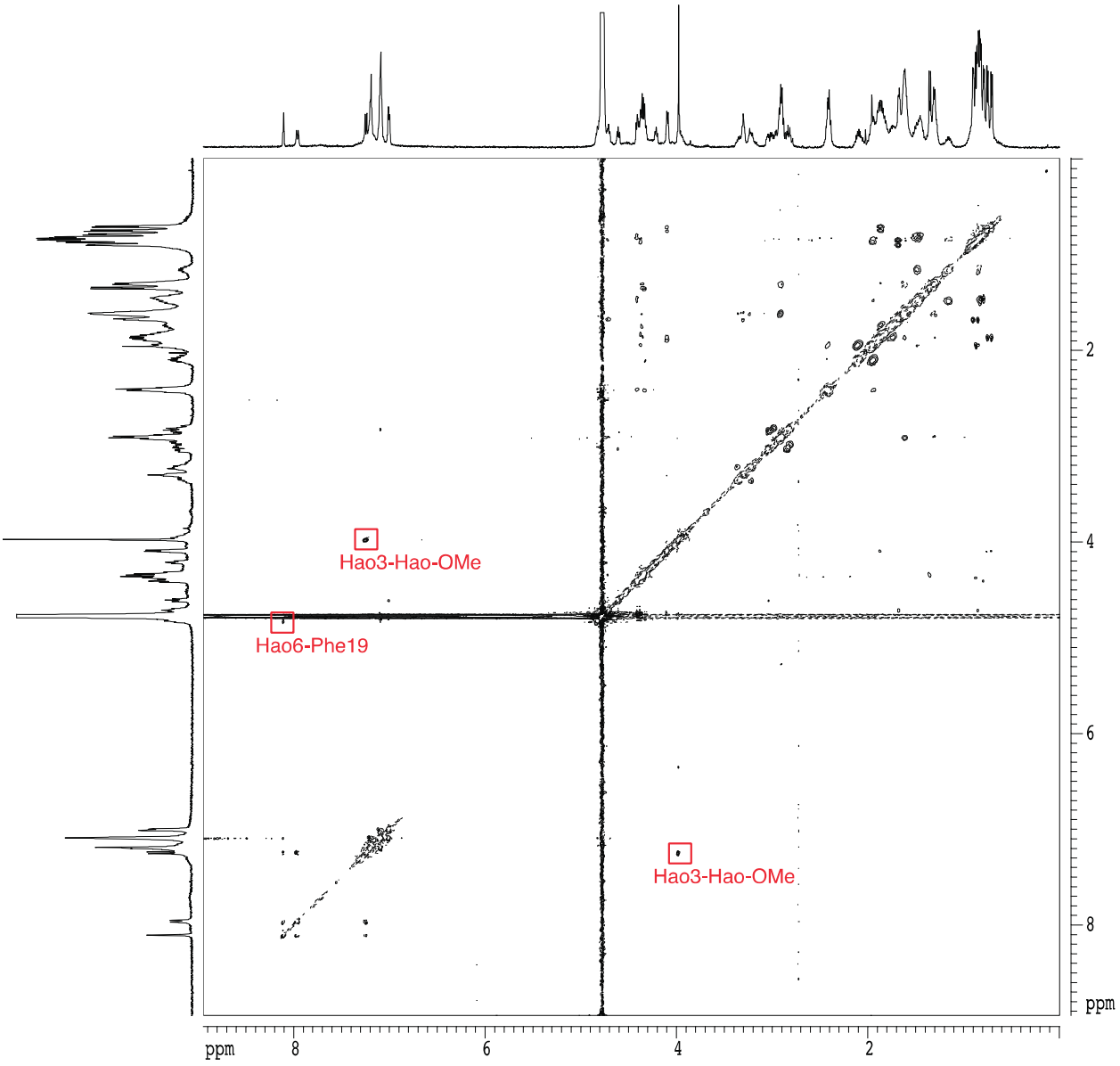

HPLC trace of **1.2d**

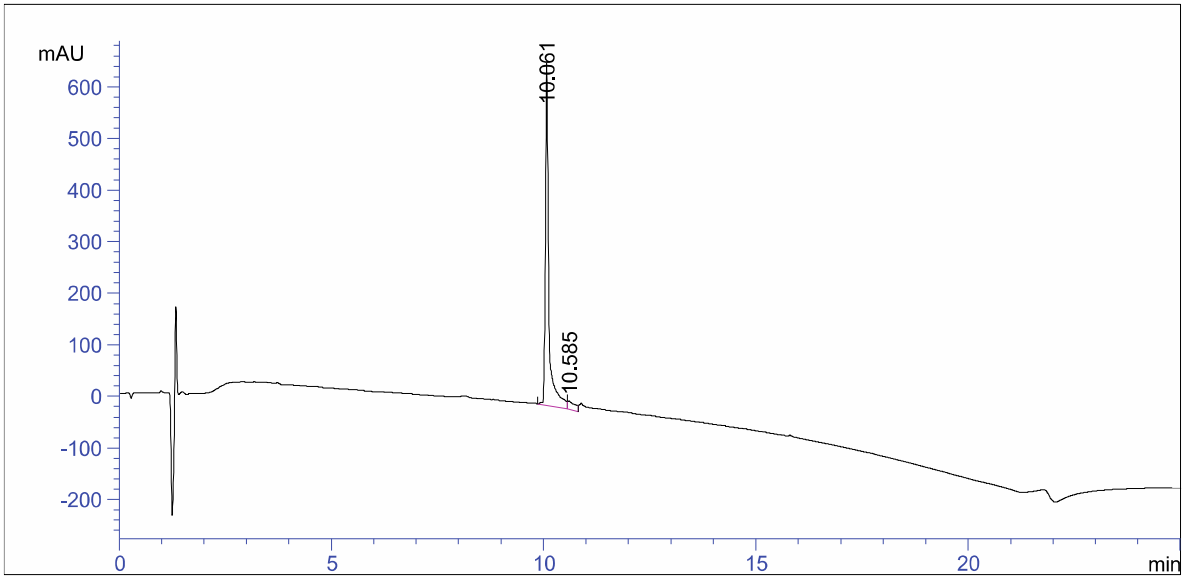

==========

Area Percent Report

==========

Signal 1: VWD1 A, Wavelength=214 nm

Peak #	RetTime [min]	Type	Width [min]	Area mAU *s	Height [mAU]	Area %
1	10.061	BV	0.0807	3680.14526	663.46790	94.5747
2	10.585	VV	0.1604	211.11090	16.88858	5.4253
Totals :				3891.25616	680.35648	

==========

ESI-MS of **1.2d**
chemical formula: $C_{86}H_{132}N_{20}O_{20}$
exact mass: 1780.9876
calculated *m/z*:
$[M+2H]^{2+}$: 891.4938
$[M+3H]^{3+}$: 594.6625

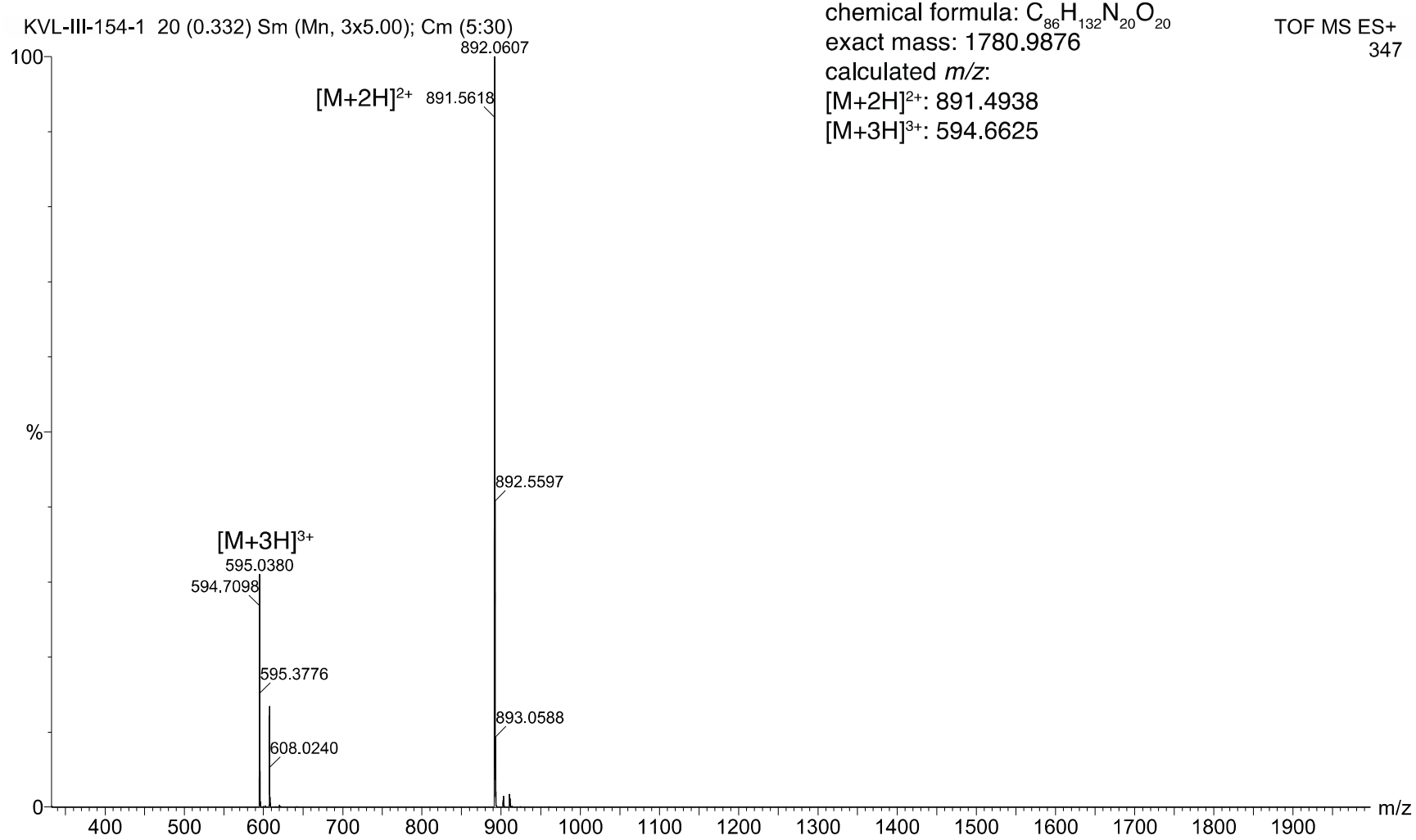

1D ^{1}H NMR spectrum of **1.2d**, 500 mHz, 1 mM in D_2O, 298 K

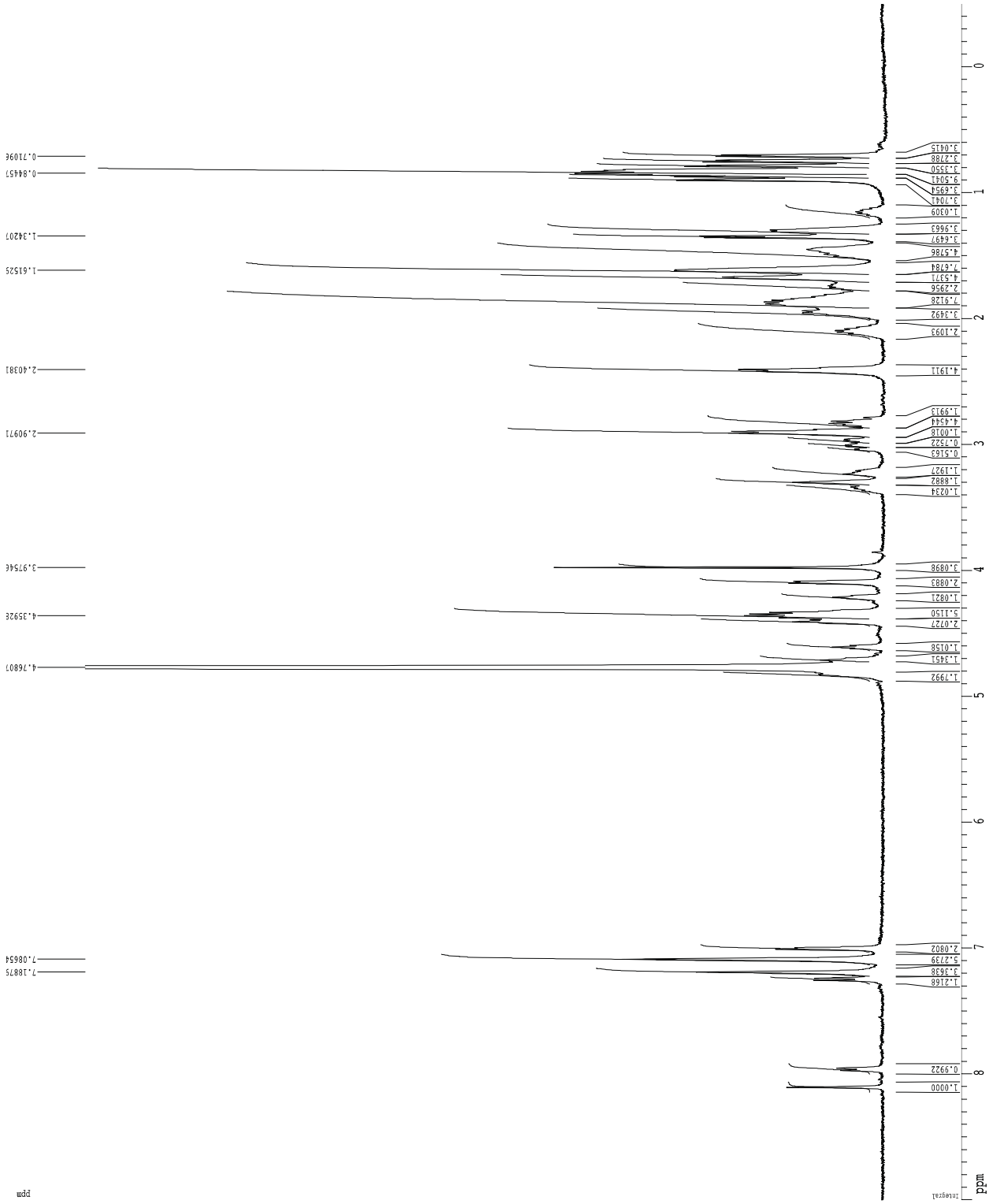

2D TOCSY spectrum of **1.2d**, 500 mHz, 1 mM in D_2O, 298 K, 150 ms spin-lock mixing time

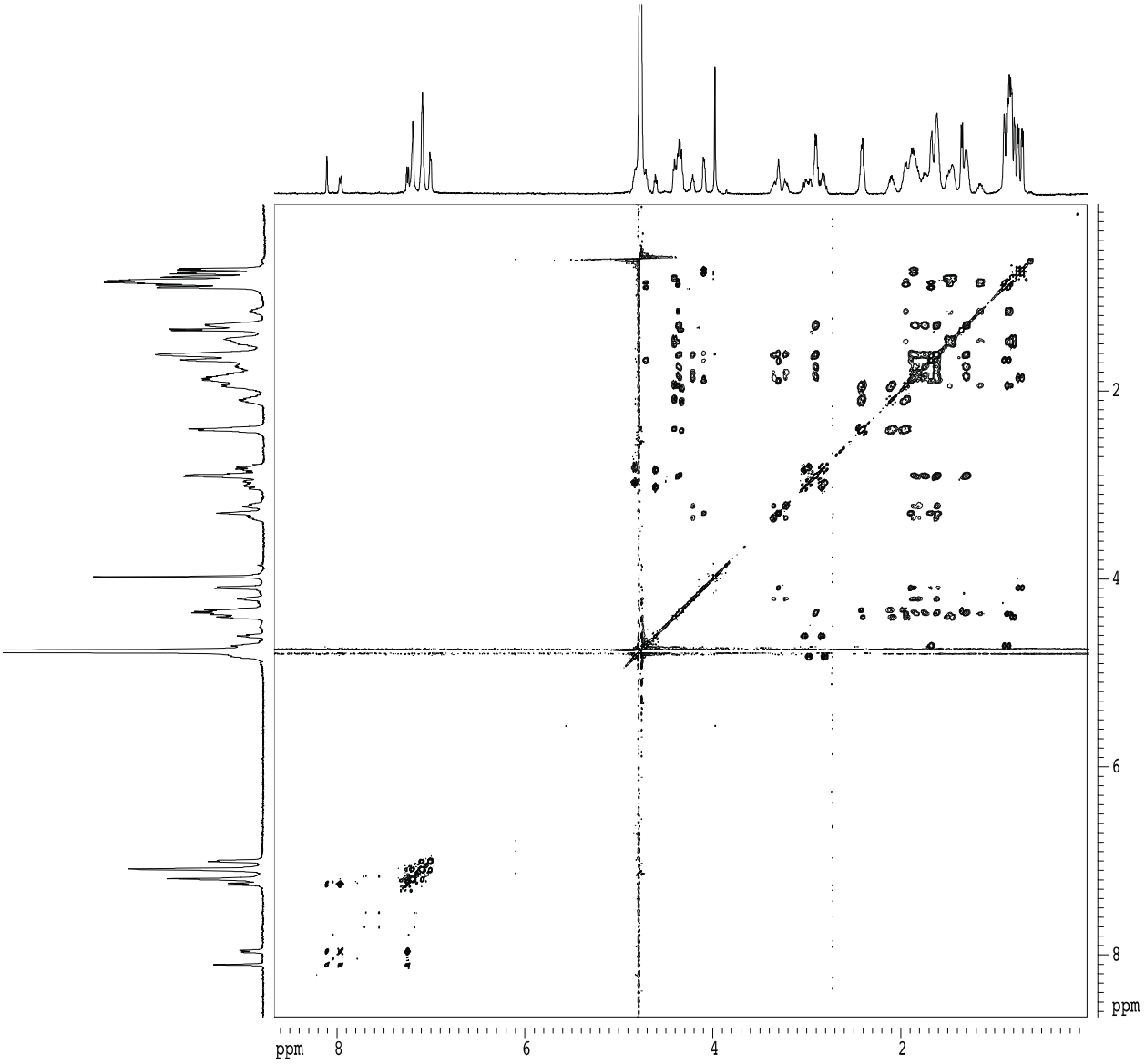

2D TOCSY spectrum of **1.2d**, 500 mHz, 1 mM in D_2O, 298 K, 150 ms spin-lock mixing time

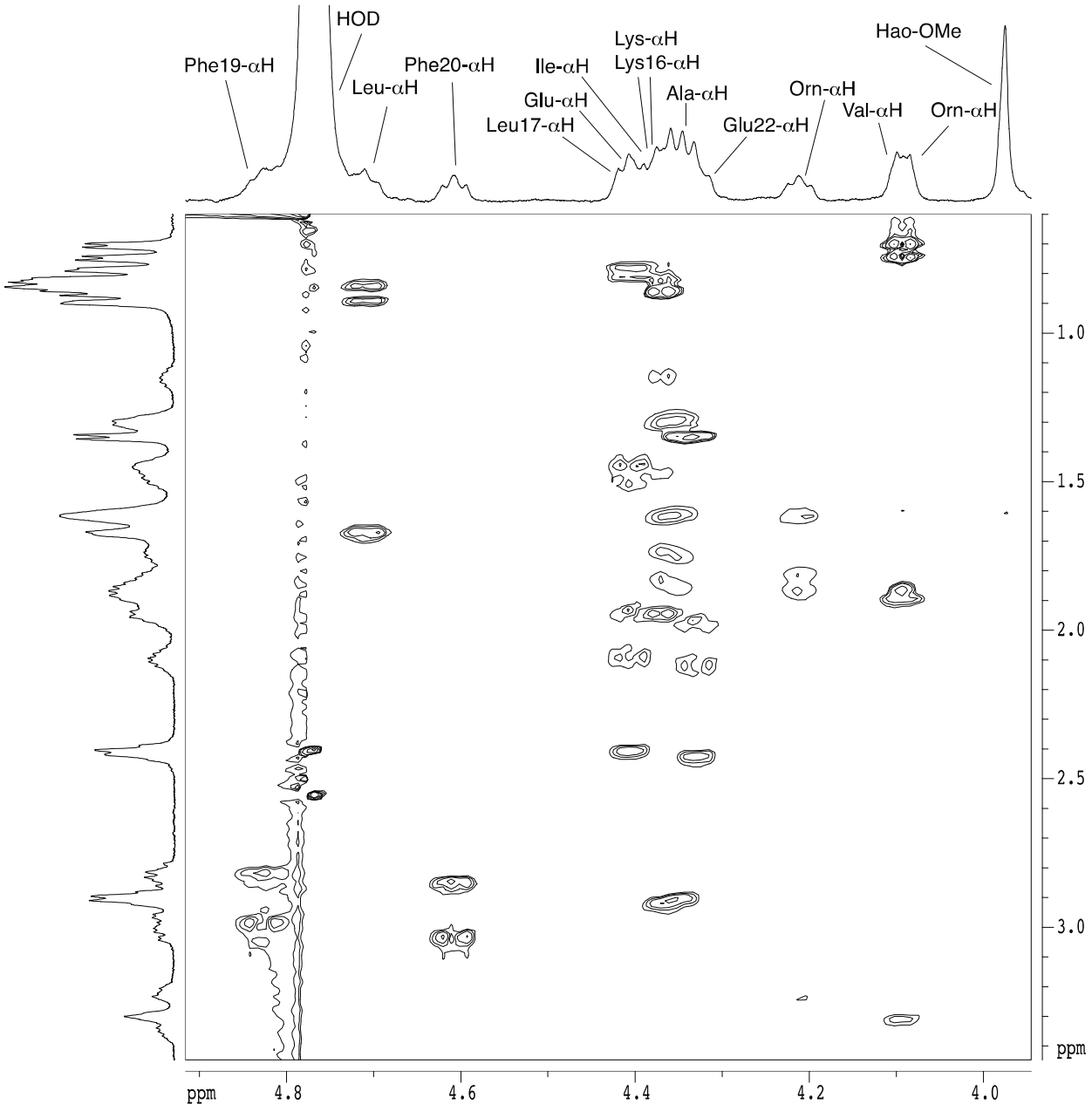

2D ROESY spectrum of **1.2d**, 500 mHz, 1 mM in D_2O, 298 K, 300 ms spin-lock mixing time

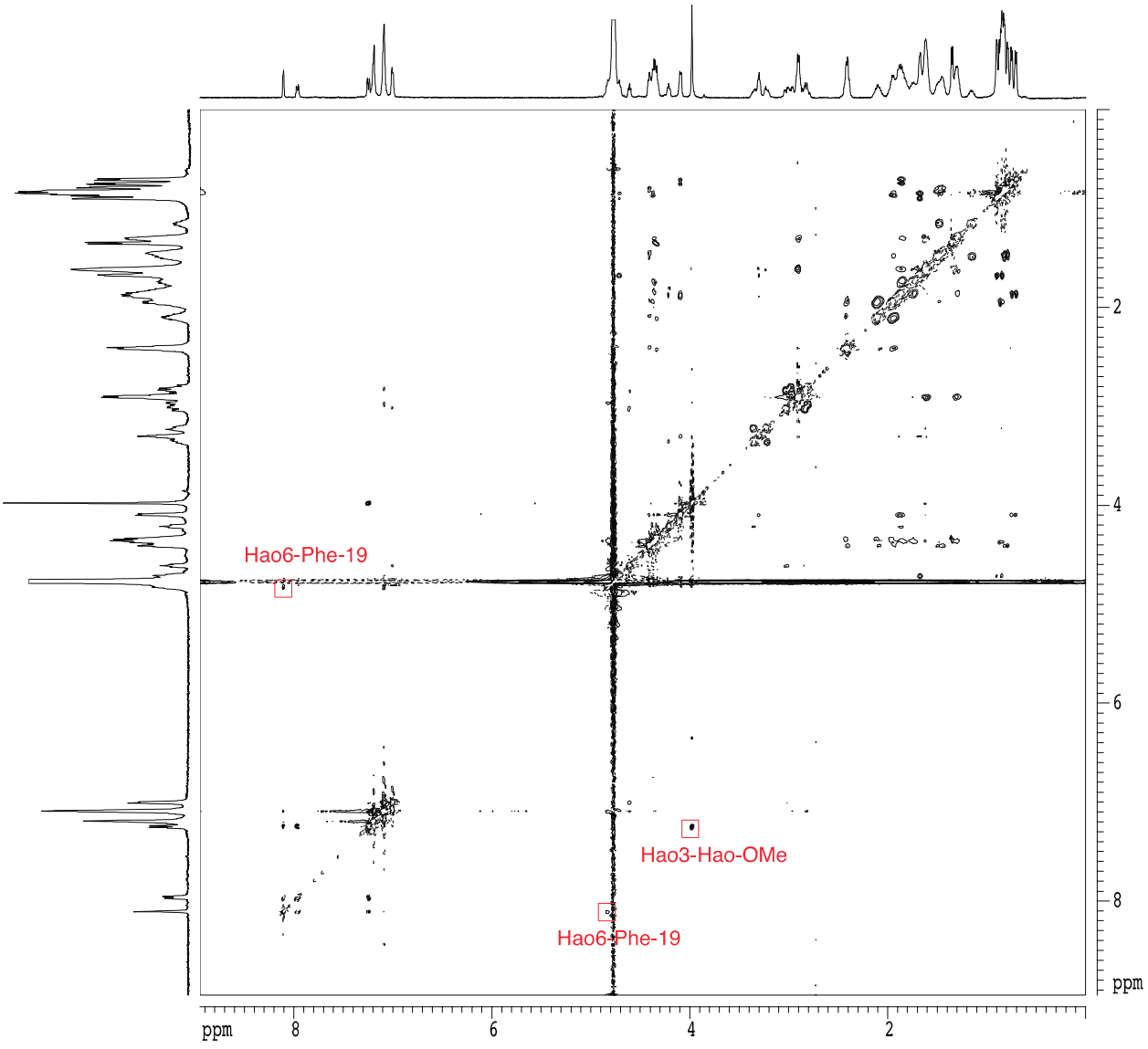

1D ^{1}H NMR spectrum of **1.2d** with solvent suppression, 600 mHz, 1.5 mM in 9:1 H_2O:D_2O, 278 K, 32 scans

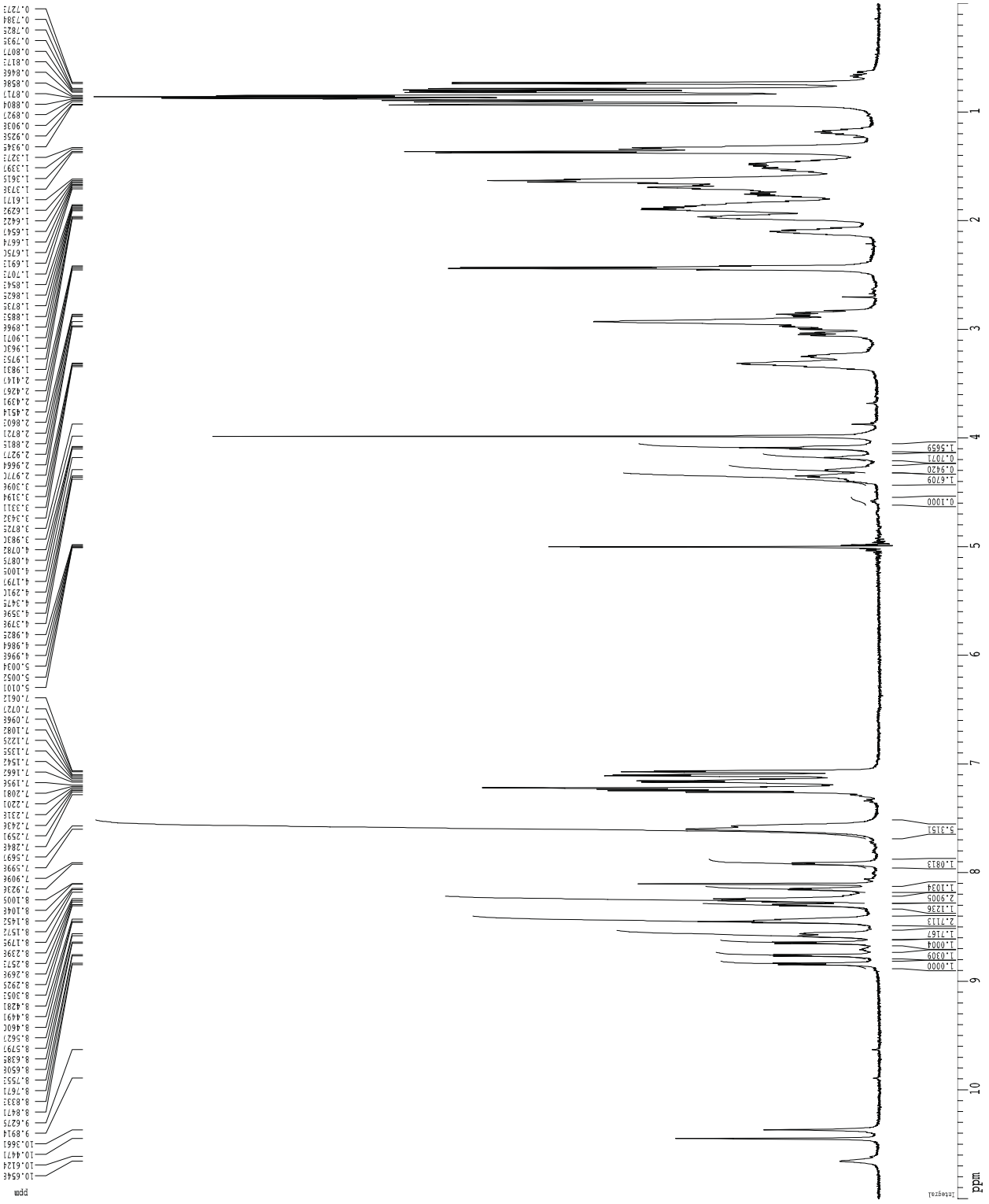

1D ^{1}H NMR spectrum of **1.2d** with solvent suppression, 600 mHz, 1.5 mM in 9:1 H_2O:D_2O, 278 K, 32 scans

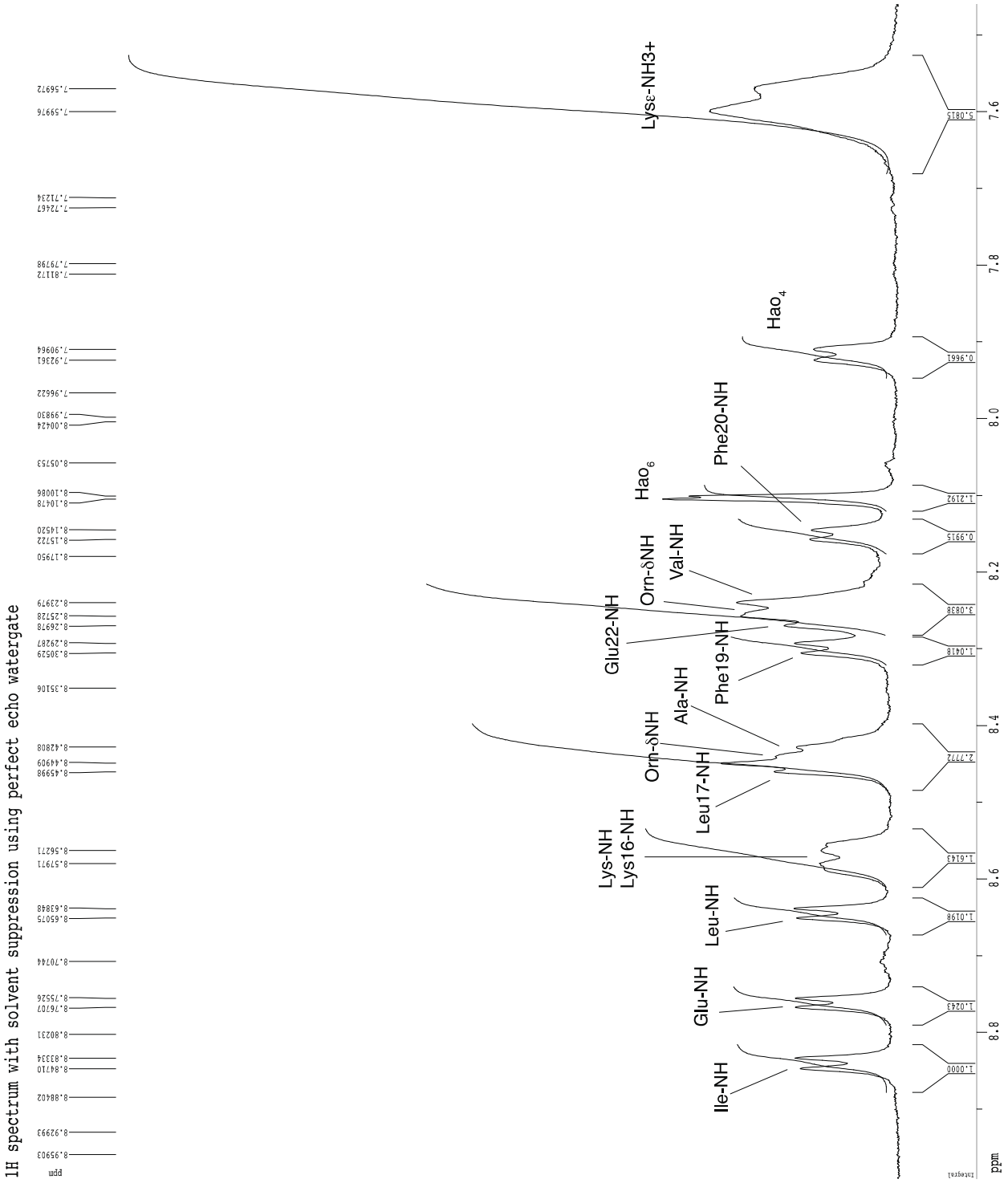

2D TOCSY spectrum of **1.2d** with solvent suppression, 600 mHz, 1.5 mM in 9:1 H_2O:D_2O, 278 K, 200 ms spin-lock mixing time

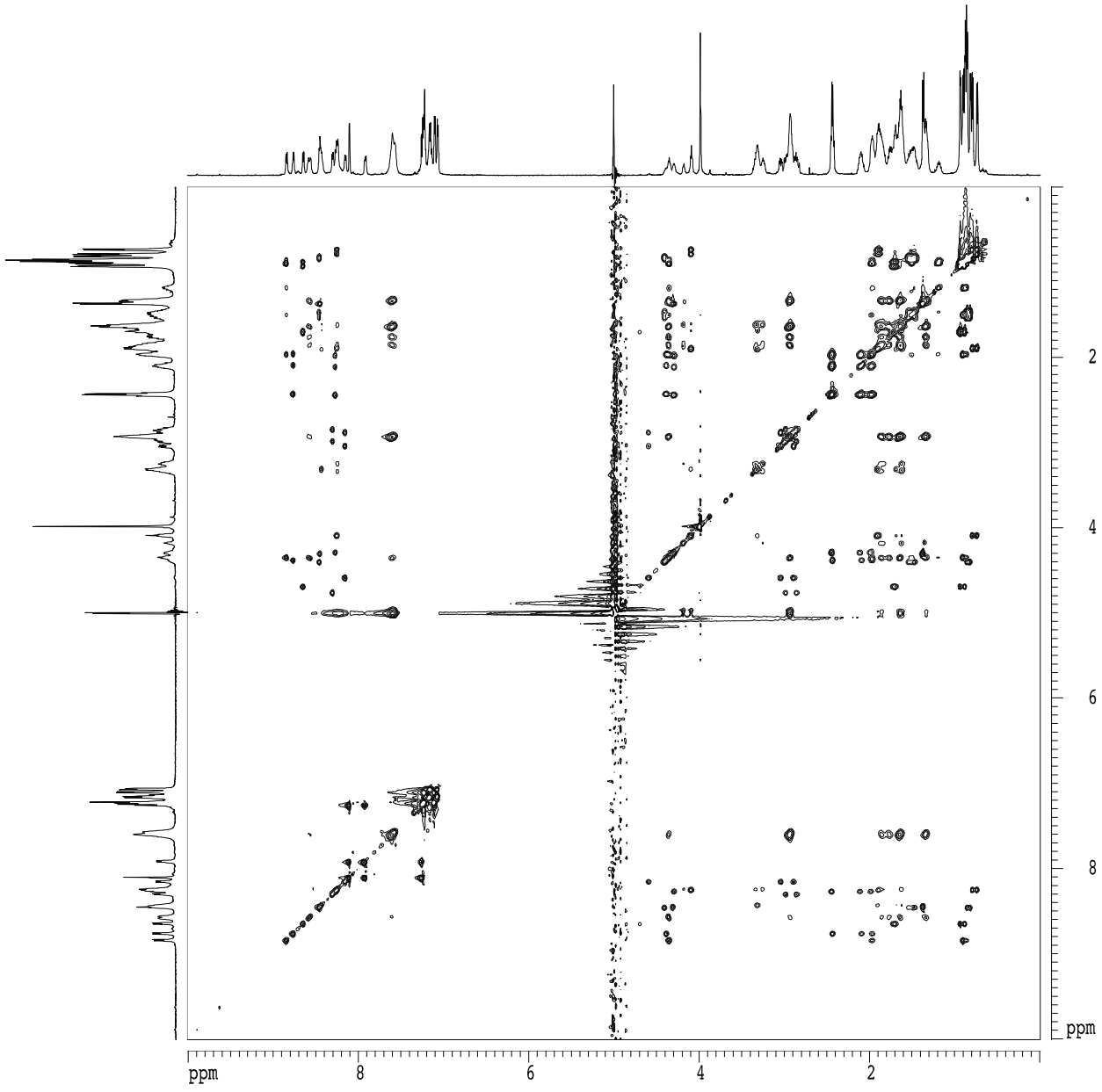

2D TOCSY spectrum of **1.2d** with solvent suppression, 600 mHz, 1.5 mM in 9:1 H_2O:D_2O, 278 K, 200 ms spin-lock mixing time

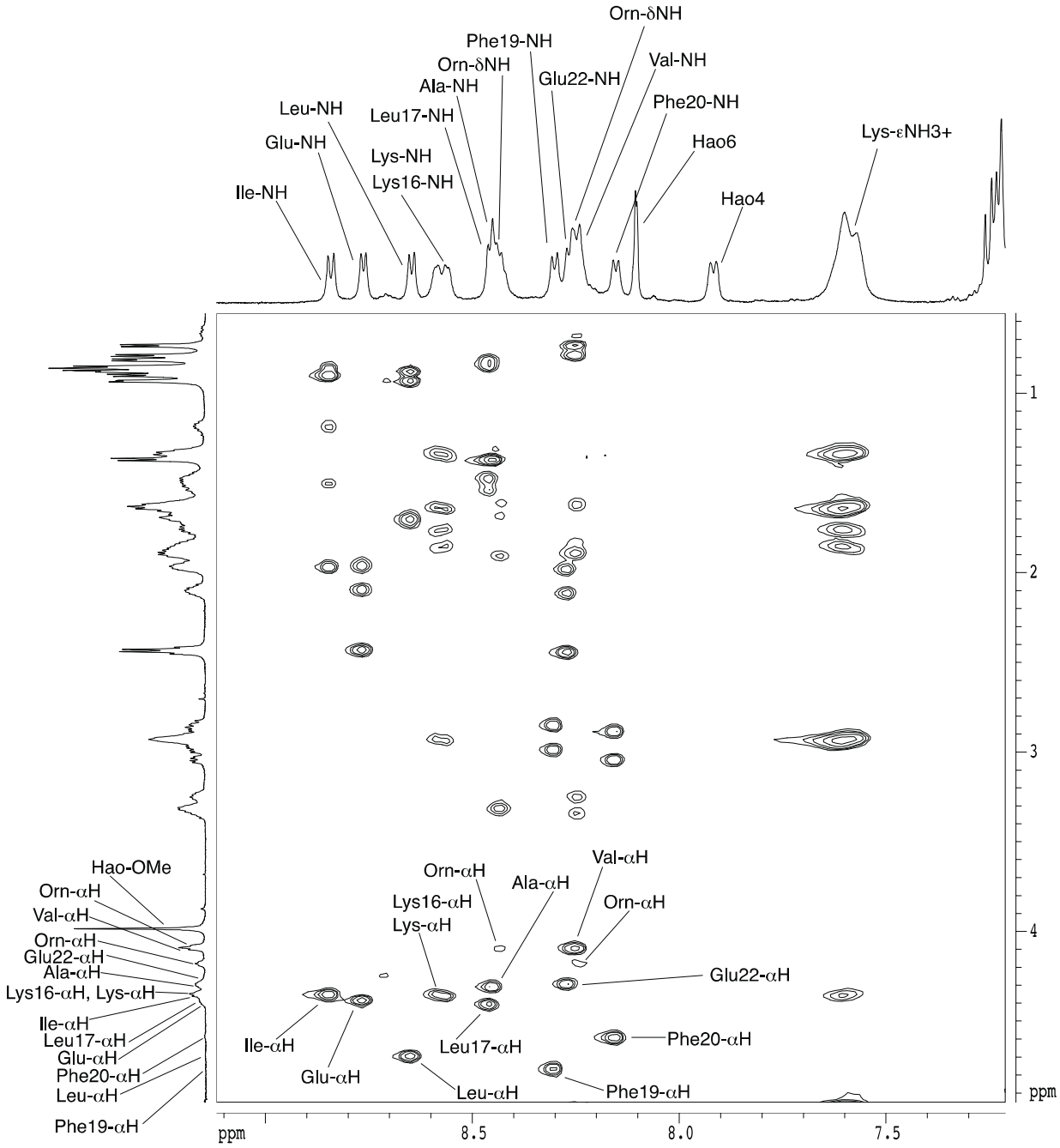

2D ROESY spectrum of **1.2d** with water suppression, 600 mHz, 9:1 H_2O:D_2O, 278 K, 100 ms spin-lock mixing time

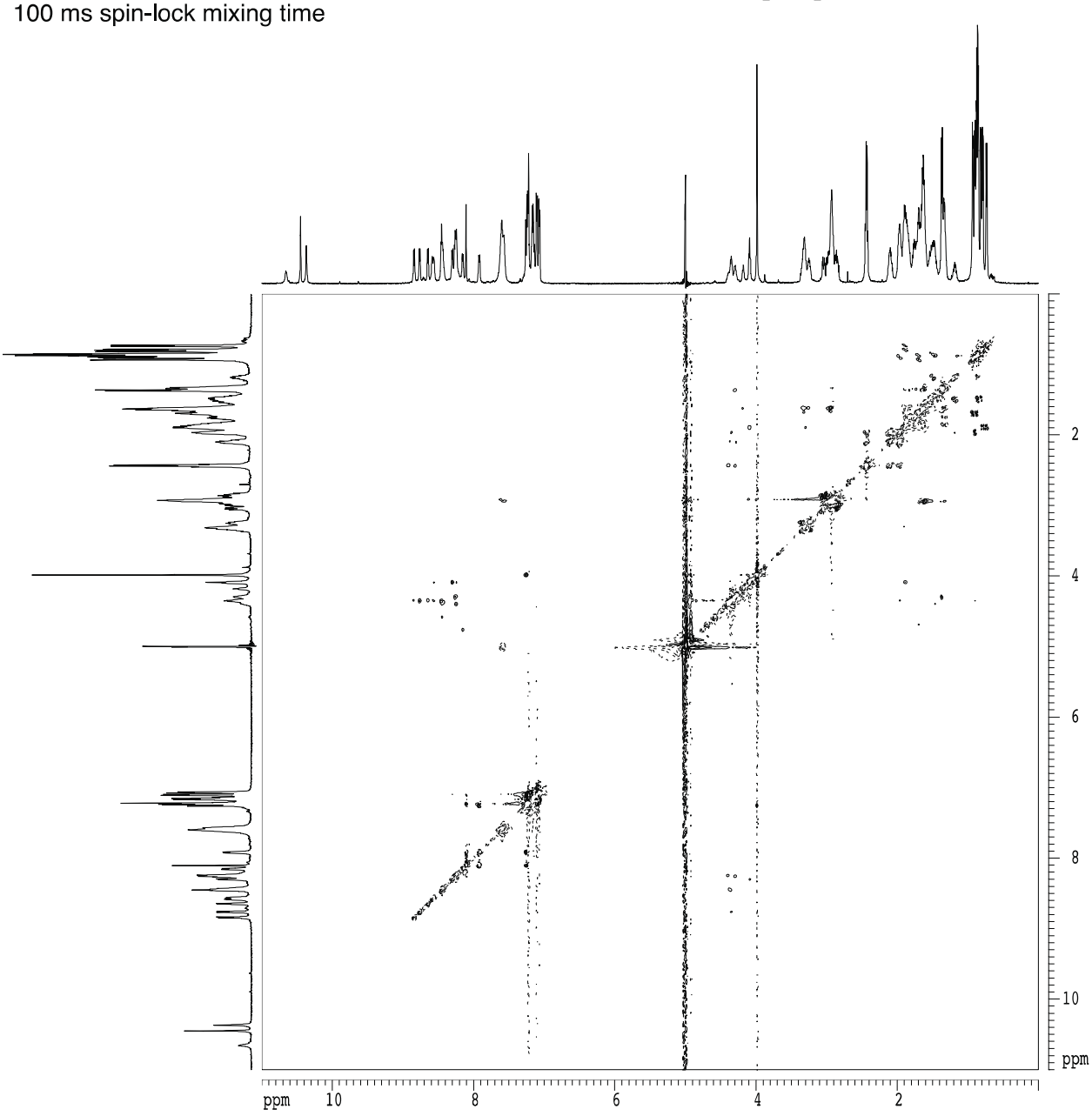

2D ROESY spectrum of **1.2d** with solvent suppression, 600 mHz, 1.5 mM in 9:1 H_2O:D_2O, 278 K, 100 ms spin-lock mixing time

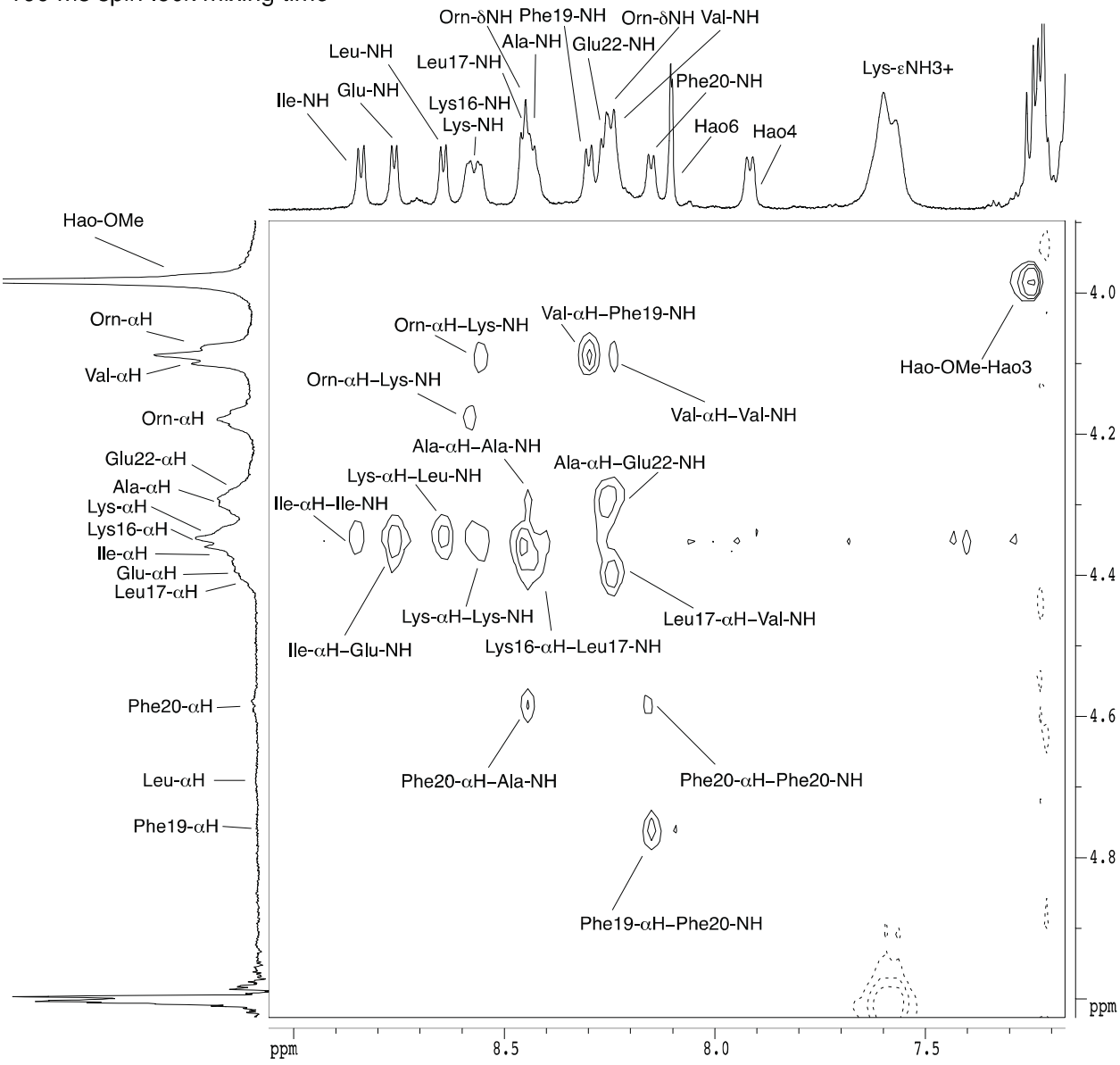

2D ROESY spectrum of **1.2d** with solvent suppression, 600 mHz, 1.5 mM in 9:1 H_2O:D_2O, 278 K, 100 ms spin-lock mixing time

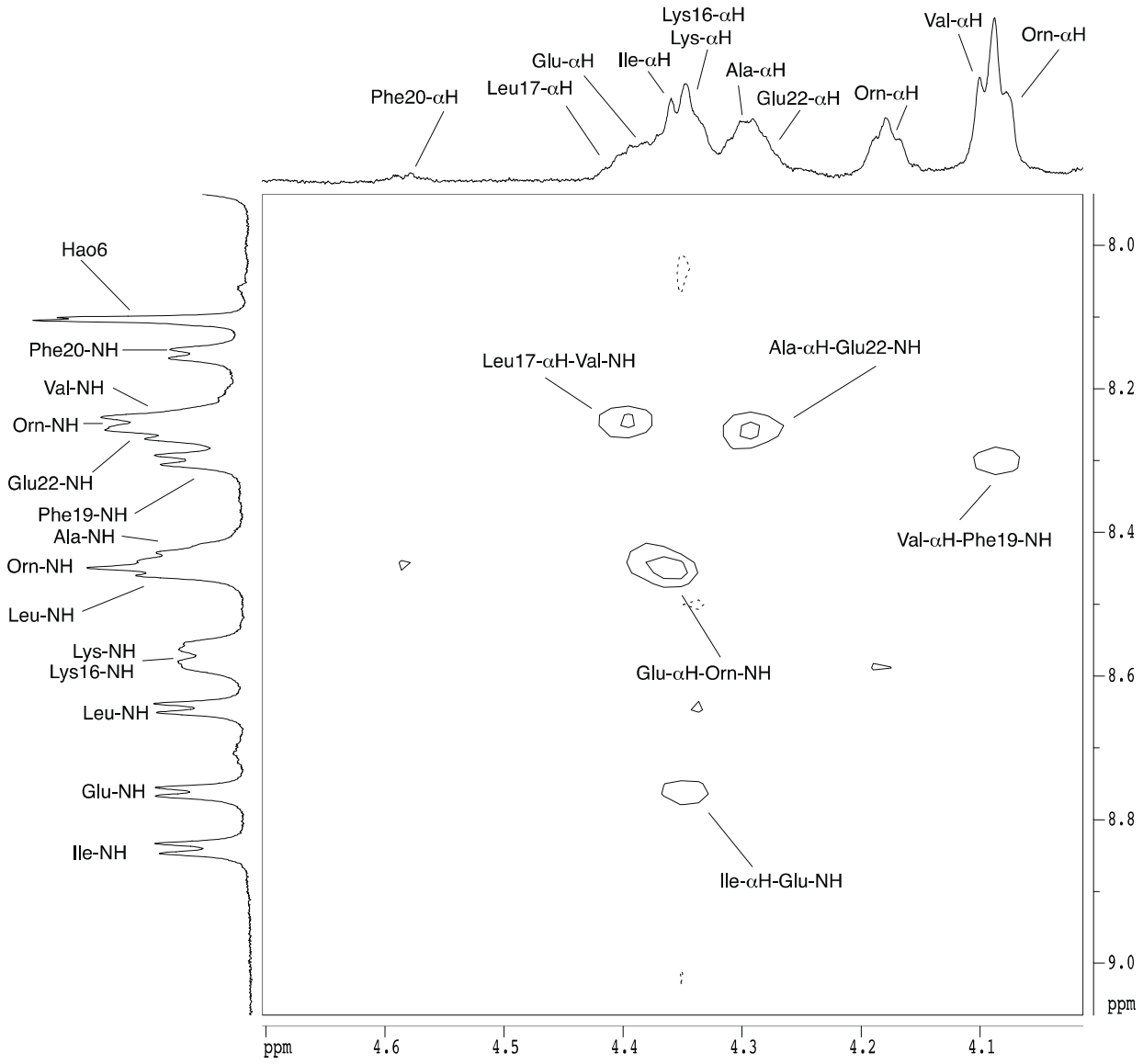

2D COSY spectrum of **1.2d** with solvent suppression, 500 mHz, 1.5 mM in 9:1 H_2O:D_2O, 278 K, 16 scans

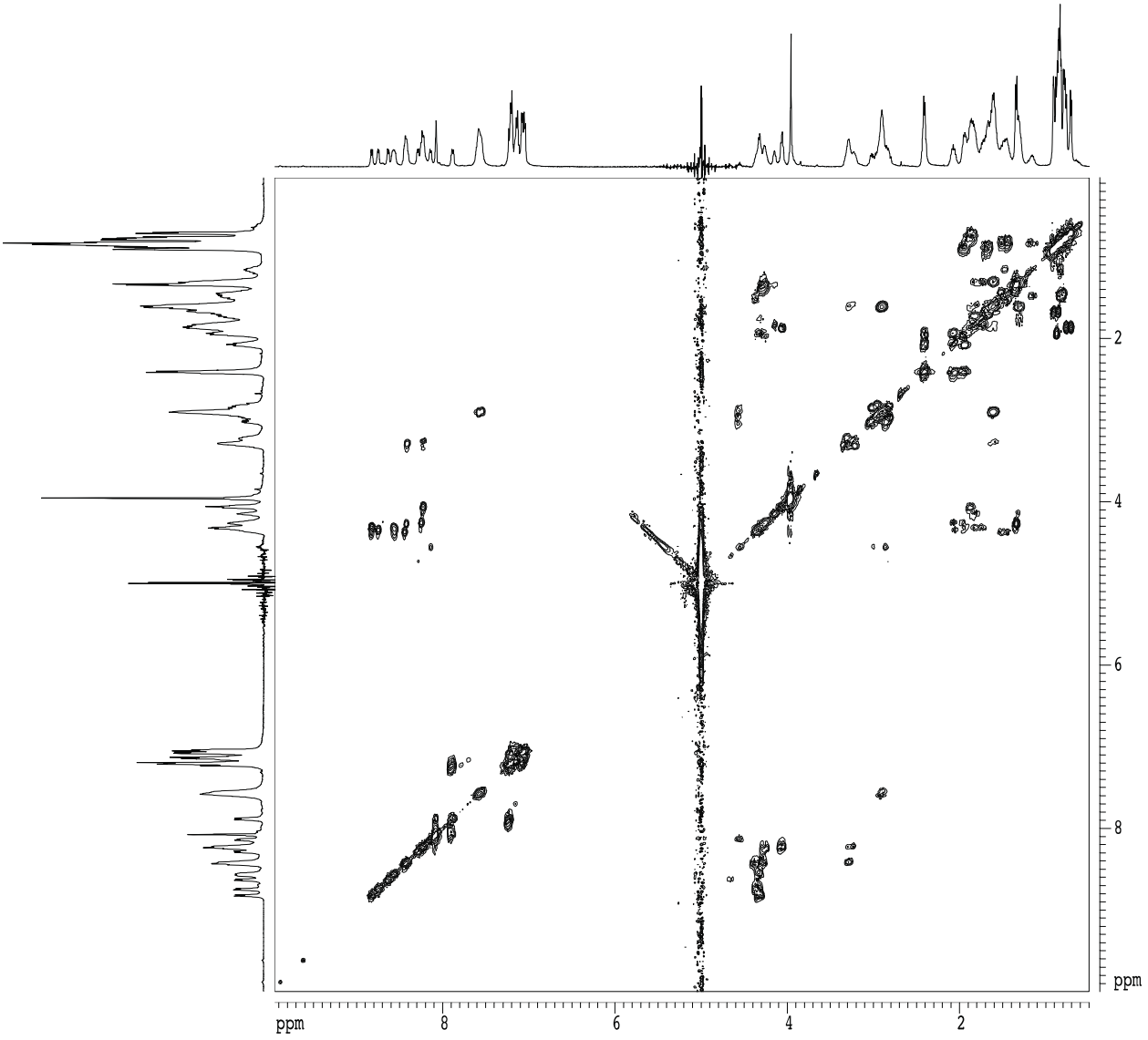

2D COSY spectrum of **1.2d** with solvent suppression, 500 mHz, 1.5 mM in 9:1 H_2O:D_2O, 278 K, 16 scans

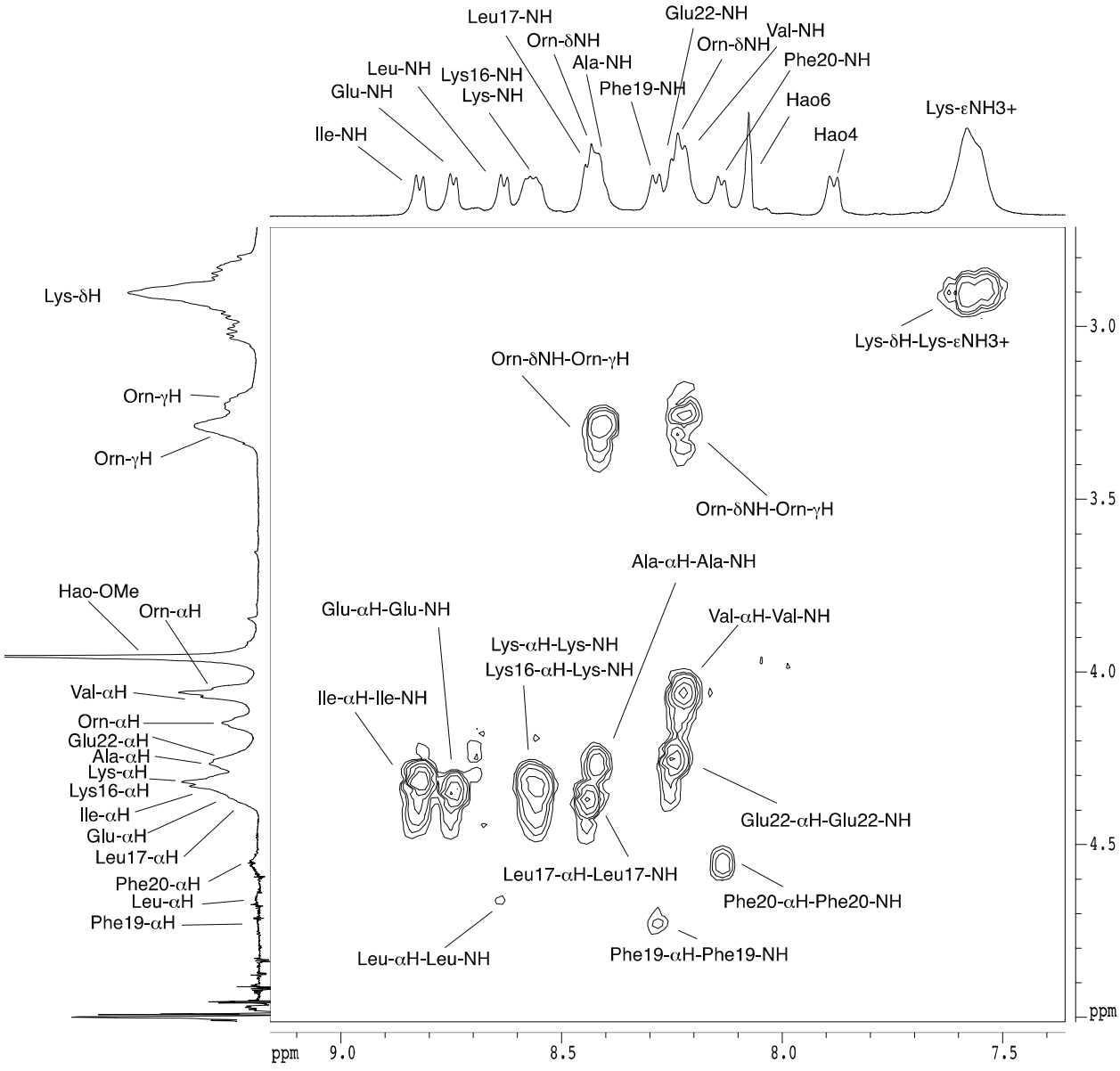

References and Notes

[1] Cheng, P.-N.; Nowick, J. S. *J. Org. Chem.* **2011,** *76*, 3166-3173.

[2] Bollhagen, R.; Schmiedberger, M.; Barlos, K.; Grell, E. *J. Chem. Soc., Chem. Commun.* **1994**, *22*, 2559-2560.

[3] Teplow, D. B. *Methods Enzymol.* **2006,** *413*, 20-33.

CHAPTER 2

Aβ-tau Macrocyclic β-Sheet Chimeras

PREFACE

Chapter 2 explores macrocyclic β-sheet chimeras incorporating residues from more than one amyloidogenic sequence. These macrocycles can modestly delay or suppress $A\beta_{40}$ aggregation and slightly delay AcPHF6 aggregation at stoichiometric concentrations. Because amyloid plaques are not homogeneous structures, and contain Aβ fibrils and neurofibrillary tangles composed of tau, potential interactions are possible between Aβ and tau. Aβ is susceptible to cross-amyloid interaction, and Aβ has been suggested to interact with IAPP[1], a-synuclein,[2] and transthyretin.[3]

These macrocyclic β-sheet chimeras highlight the sensitivity of $A\beta_{40}$ and AcPHF6 toward hybrid amyloidogenic sequences composed from $A\beta_{40}$ and tau. Chimeras **2.1b** and **2.2b** delay and suppress $A\beta_{40}$ aggregation at stoichiometric amounts, while **2.3a** effectively suppresses $A\beta_{40}$ aggregation at the tested concentrations. Targeting AcPHF6 aggregation proved challenging, as **2.1b** did not stall AcPHF6 aggregation, while **2.2b** and **2.3a** each stall AcPHF6 aggregation by 46 and 74 minutes, respectively, at stoichiometric concentrations. **2.3a** proved to be the lead macrocycle, suppressing $A\beta_{40}$ aggregation and creating the largest aggregation delay in AcPHF6 of all the macrocyclic β-sheet chimeras tested. Delayed AcPHF6 aggregation by **2.2b** and **2.3a** suggests AcPHF6 interacts and is most receptive to residues on the F_{19} face of $A\beta_{40}$.

The macrocyclic β-sheet chimera project catalyzed my transition from biological work to working at a chemistry bench. Synthesizing macrocyclic β-sheet chimeras allowed me to become familiar with peptide synthesis, NMR spectroscopy and fluorescence assays.

INTRODUCTION

Alzheimer's disease (AD) is a conformational disease afflicting over five million Americans.[4] AD is characterized by the misfolding of amyloid beta peptide (Aβ) and tau protein, forming extracellular beta (β)-sheet rich plaques of Aβ and intracellular β-sheet deposits of tau protein known as neurofibrillary tangles (NFTs) (Figure 2.1).[5] Recent evidence has shown Aβ and tau cointeract to promote neurodegeneration, illustrating the complexity of AD aetiology.[6] The Aβ-tau cointeraction begs the need for model systems to understand and develop strategies of treatment.

The cointeraction of Aβ and tau is widely documented[7,8,9], and several veins of thought are proposed through their interactions. Aβ can induce tau aggregation, creating β-sheet tangles leading to neurodegenerative failure.[10,11,12] Aβ toxicity can be driven by tau *in vitro*, as tau depleted cells are resistant to Aβ induced death.[13] Aβ and tau can also function symbiotically, forming complexes that drive onset of neuronal loss of function.[14,15] Aβ-tau cointeractions provide a starting point in developing strategies against neuronal disintegration.

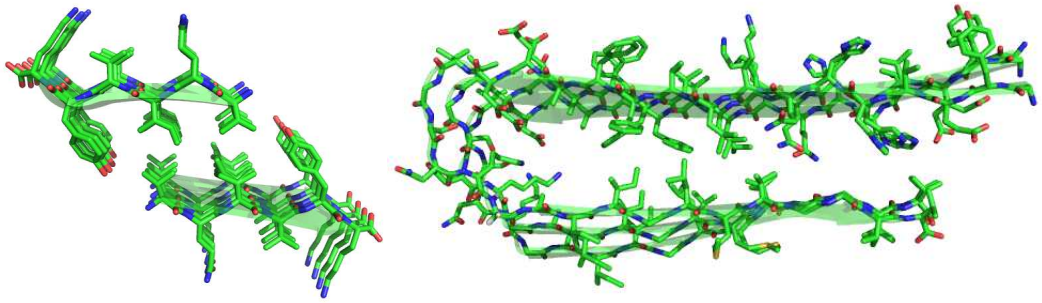

Figure 2.1. Examples of amyloid aggregation. Left: Solid state model of fibrils formed from tau ^{306}VQIVYK^{311} showing the hydrophobic contacts on the VIY face (PDB:2ON9). Right: Solution state NMR model of $A\beta_{40}$ fibrils showing the U-shaped parallel stacking of β-sheets[16].

The design of peptide β-sheet breakers provides strategies in modulating amyloid aggregation.[17] Previous work in the Nowick group focuses on the engineering of macrocyclic β-sheets to delay or inhibit onset of peptide aggregation.[18,19] These macrocyclic β-sheets contain an

amyloidogenic sequence, known as a recognition or top strand, flanked by two ornithine turns linked to a bottom strand (Figures 2.2 and 2.3). The bottom strand possesses an unnatural amino acid handle Hao, composed of hydrazide, aminoaromatic and oxalyl moieties, flanked by residues to tune macrocycle solubility under aqueous conditions and promote β-sheet folding (Figures 2.2 and 2.3). These macrocycles delay $A\beta_{40}$ aggregation and inhibit AcPHF6 aggregation. Because of the presence of the blocking strand, it is not possible to insert sequences from two different peptides onto one macrocycle. I attempt to display two peptide sequences simultaneously by creating peptide chimeras, with one face displaying residues from Aβ and the opposite face displaying residues from tau. Because a heptapeptide β-sheet possesses two faces, one face displaying three residues from the amyloidogenic sequence and another face displaying four residues from the amyloidogenic sequence keeping the *in vivo* interactions in mind between Aβ and tau, I attempt to improve the current family of macrocyclic β-sheet inhibitors with Aβ-tau chimera sequences. These β-sheet macrocyclic chimeras will display residues from the amyloidogenic regions of Aβ N-terminus and tau, each responsible for amyloid fibrillization.

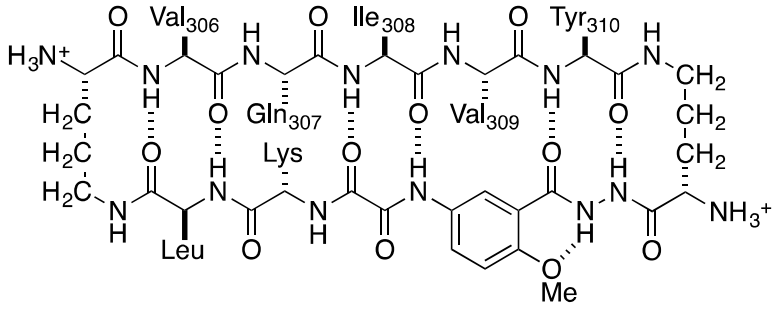

Figure 2.2. Pentapeptide VQIVY macrocyclic β-sheet containing residues from $tau_{306\text{-}310}$. The VQIVY macrocycle inhibits AcPHF6 fibrillization.

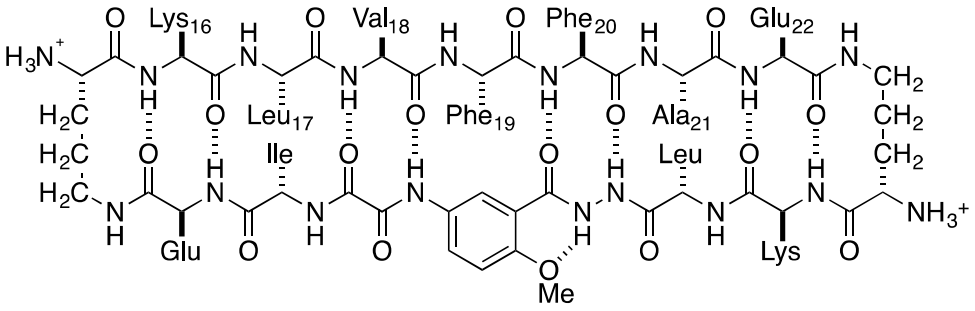

Figure 2.3. Heptapeptide KLVFFAE macrocyclic β-sheet containing residues $A\beta_{16\text{-}22}$. The KLVFFAE macrocycle delays $A\beta_{40}$ aggregation.

Design of β-sheet macrocycle chimeras. Development of peptide chimeras utilizes sequences in the N-terminus of $A\beta_{40}$ (^{15}QKLVFFAED^{23}) and the microtubule domain of tau (^{306}VQIVY^{310}), also prone to aggregation. The N-terminus of $A\beta_{40}$ is the main hydrophobic cassette responsible for aggregation, and the microtubule domain of tau is also responsible for tau aggregation. In this study, the VIY residues appear in all macrocyclic β-sheet chimeras tested, as amyloid aggregation is driven by hydrophobic collapse and $tau_{306\text{-}310}$ fibrils contain one tyrosine residue situated in the hydrophobic fibril pocket. $A\beta_{40}$ contains two phenylalanine residues on the N-terminus implicated in aggregation, F_{19} and F_{20}, therefore residues from the N-terminus will be evaluated in this study.

Thioflavin T fluorescence assays of $A\beta_{40}$ aggregation. Thioflavin T (ThT) fluorescence assays monitor $A\beta_{40}$ aggregation over time. $A\beta_{40}$ fibrillization shows three distinct phases: a lag phase consisting of mostly unstructured $A\beta_{40}$, a growth phase composed of a heterogeneous mixture of monomer and oligomeric complexes, and an equilibrium phase comprised of Aβ fibrils (Figure 2.4).

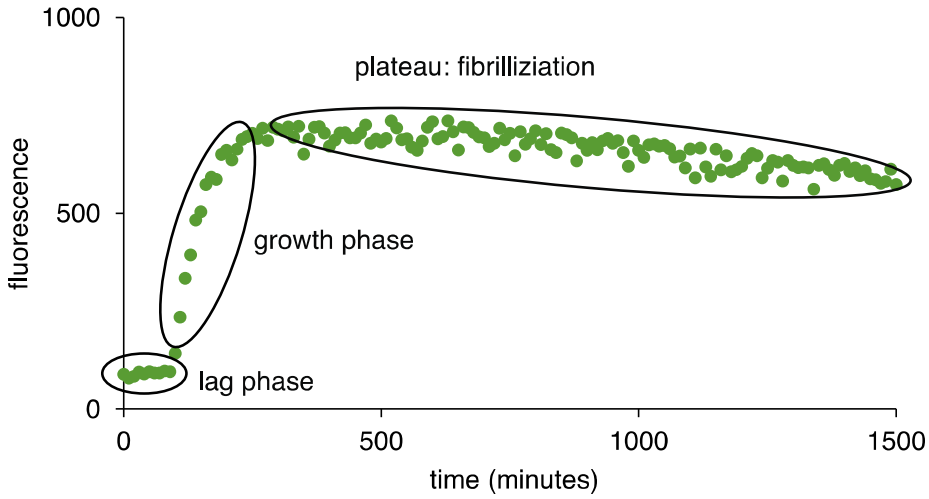

Figure 2.4. Schematic of the Thioflavin T fluorescence assay of $A\beta_{40}$ aggregation.

Thioflavin S fluorescence assays of AcPHF6 aggregation. Thioflavin S (ThS) fluorescence assays monitor AcPHF6 aggregation over time. The hexapeptide AcPHF6 is an *in vitro* platform to replicate tau aggregation. AcPHF6 contains the residues $tau_{306\text{-}311}$, corresponding to the microtubule domain of tau responsible for β-sheet aggregation. AcPHF6 fibrillization is instant, occurring within minutes. AcPHF6 fibrillization contains two phases, a growth phase indicating oligomer growth and formation and a plateau phase indicating formation of β-sheet aggregates (Figure 2.5).[20]

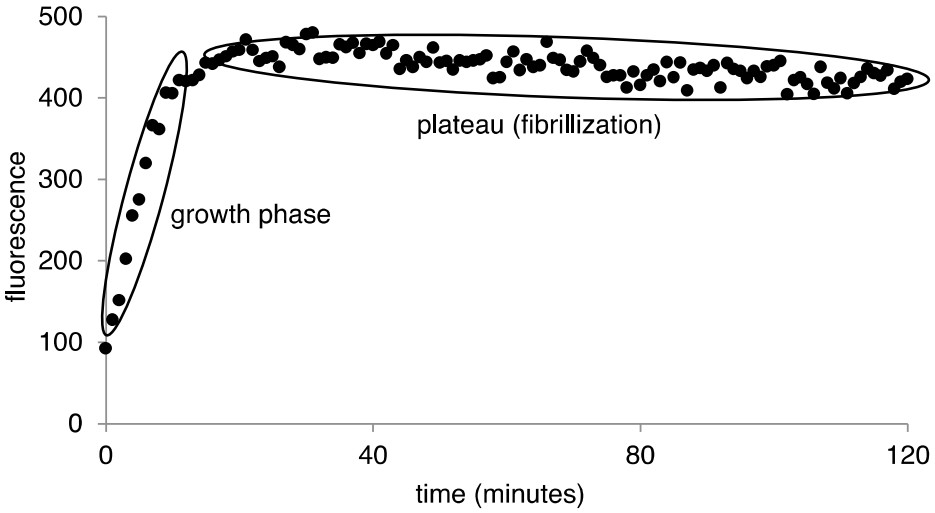

Figure 2.5. Growth curve of AcPHF6 using Thioflavin S fluorescence assay.

RESULTS AND DISCUSSION

1. Synthesis and evaluation of chimera 2.1a. The study began with the synthesis of macrocyclic β-sheet chimera **2.1a**. **2.1a** contains residues $A\beta_{16,18,20,22}$ and $tau_{306,308,310}$ to create the hybrid sequence N'-KVVIFYE-C', with residues KVFE corresponding to $A\beta_{40}$ and residues VIY corresponding to tau (Figure 2.6). Glutamate and lysine residues are added on the bottom strand match the polarity of the KVFE face, while the two leucine residues on the bottom strand were chosen to match the hydrophobicity of the VIY face and promote macrocyclic β-sheet folding. Chimera **2.1a** is soluble in D_2O.

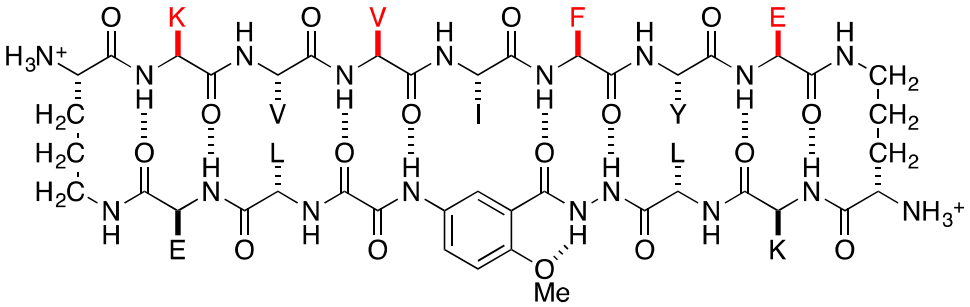

Figure 2.6. Macrocyclic β-sheet chimera **2.1a.** The KVFE residues in red correspond to the $A\beta_{40}$ N-terminus and the VIY residues in black correspond to the tau microtubule domain.

2.1a shows a high baseline fluorescence, indicating self-assembly of **2.1a** in solution. At 1, 2 and 4 equivalents of **2.1a**, no inhibition was observed (Figure 2.7). The aggregation of **2.1a** does not interfere with AcPHF6 fibrillization. At 4 equivalents, the growth curve of AcPHF6 flattens, indicating fibrillization has occurred with larger amounts of **2.1a.** The overall charge of **2.1a** is +2, created by the free amines on each ornithine turn. Initial results suggest the overall +2 charge on **2.1a** is not sufficient to create monomeric macrocycles in solution, and its self-assembly can accelerate AcPHF6 fibrillization. **2.1a** can behave as a seed to induce AcPHF6 fibrillization.

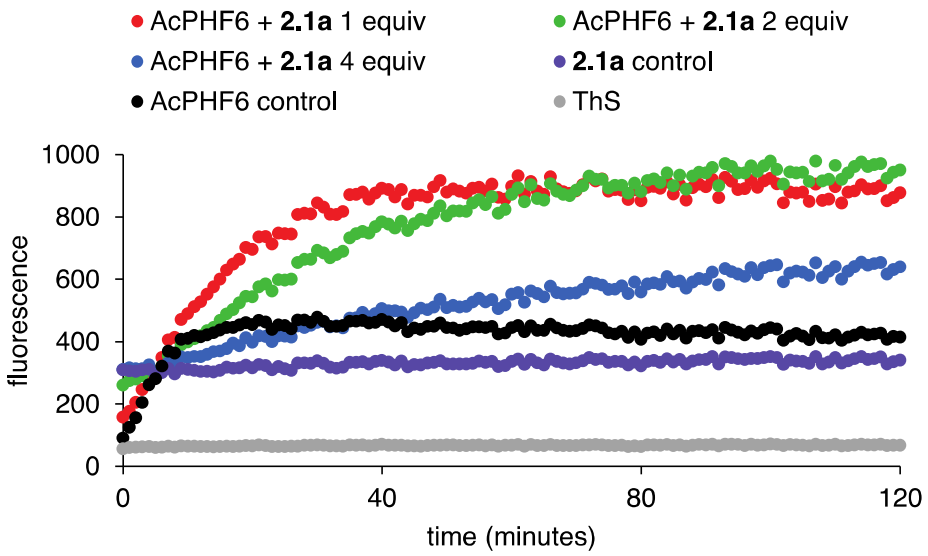

Figure 2.7. Effect of **2.1a** on AcPHF6 aggregation. At stoichiometric concentrations, **2.1a** aggregates in MOPS buffer but does not impede AcPHF6 aggregation.

2. Design and evaluation of chimera 2.1b. The glutamate residue on the bottom strand of **2.1a** was modified to a lysine residue to increase macrocycle solubility and create macrocyclic β-sheet chimera **2.1b** (Figure 2.8). The lysine substitution on the bottom left corner of the bottom strand of **2.1b** increases the overall charge of the molecule from +2 to +4. When evaluated against AcPHF6 aggregation, solubility did increase, as noted by the drop in fluorescence in **2.1b**

control wells. At 1 equivalents, **2.1b** delays AcPHF6 aggregation by 2.7 minutes and at 2 equivalents, **2.1b** delays AcPHF6 aggregation by 3.7 minutes. At 4 equivalents, **2.1b** delays AcPHF6 aggregation by 4.3 minutes. Stoichiometric amounts of **2.1b** slightly delay AcPHF6 aggregation by minutes, indicating increased solubility of the macrocycle does not significantly improve AcPHF6 inhibition (Figure 2.9). **2.1b** does not accelerate AcPHF6 aggregation, suggesting monomeric macroycles are less likely to catalyze AcPHF6 aggregation than self assembling macrocycles.

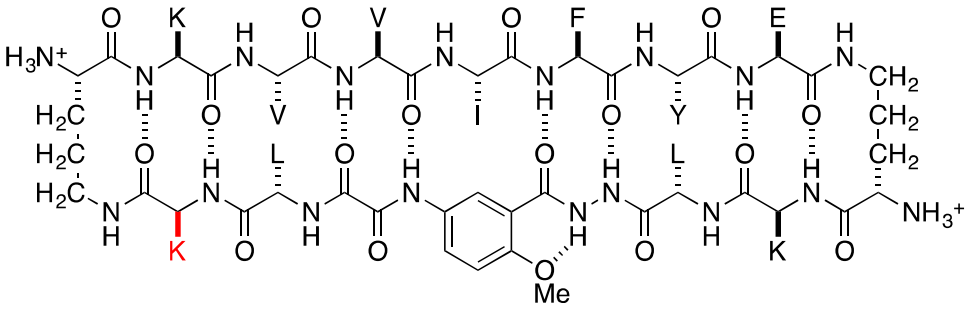

Figure 2.8. Macrocyclic β-sheet chimera **2.1b.** The glutamate to lysine mutation on the bottom strand is highlighted in red.

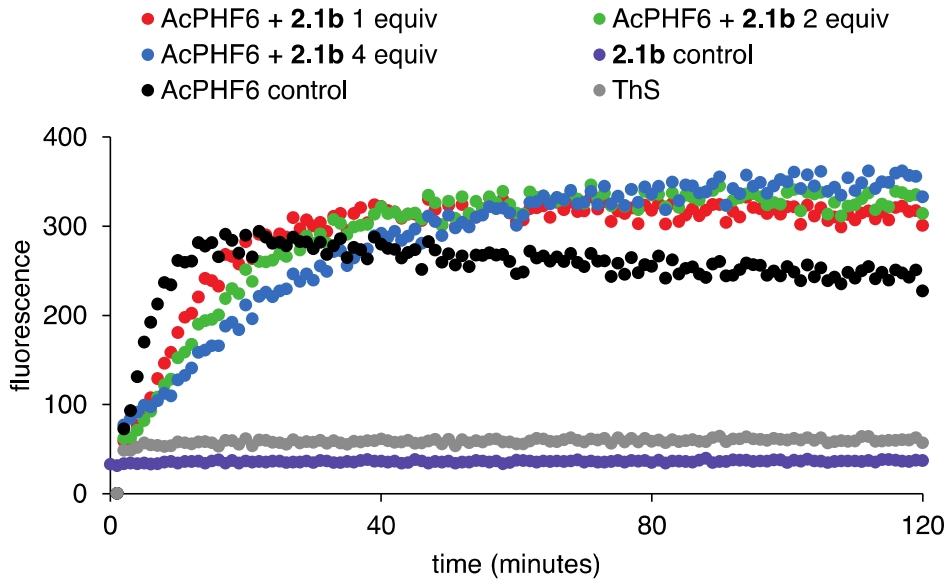

Figure 2.9. Effect of **2.1b** on AcPHF6 aggregation. Thioflavin S assay of AcPHF6 and **2.1b** at 1, 2 and 4 equivalents. **2.1b** does not self assemble in solution, and only slightly interferes with AcPHF6 aggregation.

Thioflavin T fluorescence assays show **2.1b** is soluble in MOPS buffer and is a much

better inhibitor of $A\beta_{40}$ aggregation than AcPHF6 aggregation. At 0.5 equivalents, **2.1b** delays $A\beta_{40}$ aggregation by 248 minutes, implying $A\beta_{40}$ can interact with the VIY tau face of **2.1b**. **2.1b** shows a dose dependent response; at 1 equivalents, $A\beta_{40}$ aggregation is delayed by 1225 minutes and at 1.5 equivalents of **2.1b**, $A\beta_{40}$ aggregation is suppressed for the entire experiment (Figure 2.10). In all conditions, **2.1b** interferes with $A\beta_{40}$ aggregation at stoichiometric concentrations. These results suggest $A\beta_{40}$ is responsive to chimera macrocycles, and inclusion of tau sequences can suppress $A\beta_{40}$ fibrillization. **2.1b** also suggests $A\beta_{40}$ can participate in cross interactions with tau. The VIY face of **2.1b** provides a hydrophobic strip of residues that can participate in branched or aromatic interactions with either the N- or C- terminus of $A\beta_{40}$. The Aβ-tau cointeraction is a potential strategy to develop macrocyclic β-sheet inhibitors of amyloid aggregation.

With the small delay in AcPHF6 inhibition by **2.1b**, I set out to improve macrocyclic β-sheet inhibition of AcPHF6 by increasing hydrophobicity on the tau face of the macrocycles.

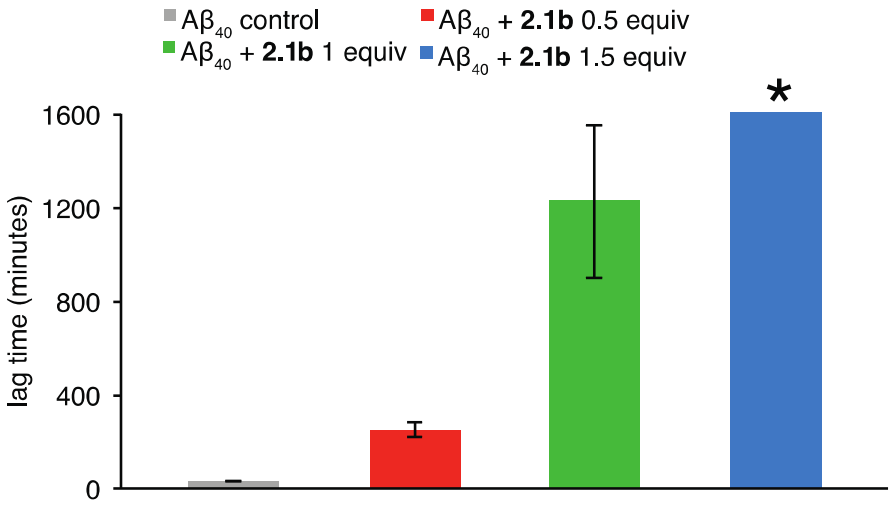

Figure 2.10. Effect of **2.1b** on $A\beta_{40}$ aggregation. $A\beta_{40}$ lag times in the presence of **2.1b**. **2.1b** delays $A\beta_{40}$ aggregation at 1.5 equivalents. The asterisk above the blue column indicates aggregation suppression throughout the entire course of the experiment.

3. Design of chimeras 2.2a and 2.2b. Prior work in the Nowick group details the

significance of the hydrophobic VIY face of AcPHF6 in modulating fibrillization. The hydrophobicity of the tau VIY face of **2.1b** can be increased by mutation of the leucine residues on the bottom strand of the β-sheet macrocycle. Two macrocycles were synthesized to increase hydrophobicity and investigate the effect of aromatic residue position on macrocycle activity. Chimera **2.2a** contains a leucine to tyrosine mutation (Figure 2.11), and chimera **2.2b** possesses a leucine to phenylalanine mutation (Figure 2.12). Adding aromatic residues can increase macrocycle interactions with AcPHF6, as aromatic π interactions play significant roles in β-sheet amyloid aggregation.[21]

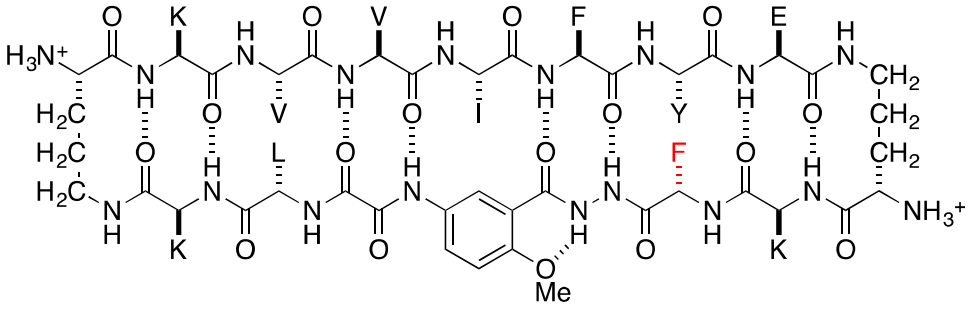

Figure 2.11. Macrocyclic β-sheet chimera **2.2a.** The leucine to phenylalanine mutation on the bottom strand is highlighted in red.

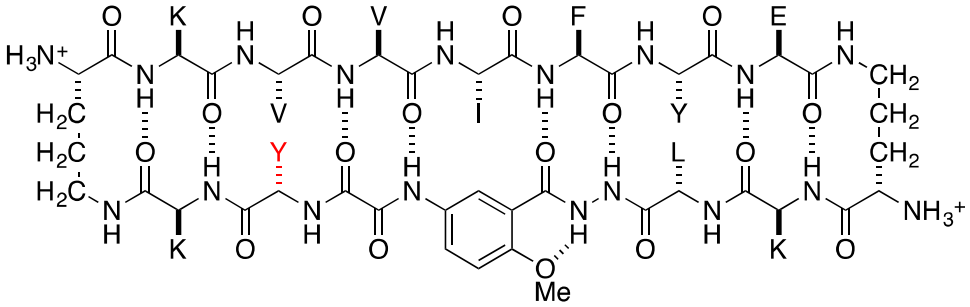

Figure 2.12. Macrocyclic β-sheet chimera **2.2b.** The leucine to tyrosine mutation on the bottom strand is highlighted in red.

4. Effect of 2.2a on amyloid aggregation. 2.2a is soluble in MOPS buffer, and modestly delays AcPHF6 aggregation. At 1 equivalents, **2.2a** delays AcPHF6 aggregation by 1.3 minutes, and at 2 equivalents, AcPHF6 aggregation is delayed by 8.3 minutes. At 4 equivalents, **2.2a** delays AcPHF6 aggregation by 15.7 minutes (Figure 2.13). Mutation of the leucine to phenylalanine in **2.2a** suggests the increased hydrophobicity of the VIY face increases **2.2a**

affinity to AcPHF6. Although lag time is only increased by a few minutes, AcPHF6 does show some flexibility in interaction with peptide sequences. AcPHF6 can interact with macrocyclic β-sheets containing the VIY face of tau, provided the macrocycle contains more than one aromatic residue on the VIY face. AcPHF6 appears to preferentially interact with the VIY face of **2.2a**, indicating it is less likely to participate in hydrophobic interactions with the KVFE face of the $A\beta_{40}$ N-terminus.

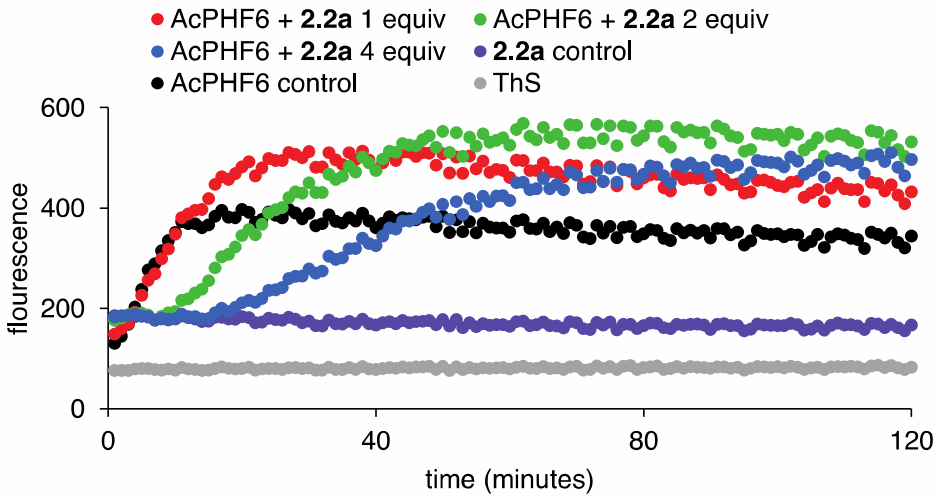

Figure 2.13. Effect of **2.2a** on AcPHF6 aggregation. Thioflavin S assay shows **2.2a** modestly inhibits AcPHF6 aggregation.

Thioflavin T fluorescence assays show **2.2a** modestly delays $A\beta_{40}$ aggregation. At 0.5 equivalents **2.2a** delays $A\beta_{40}$ aggregation by 277.5 minutes, and at 1 equivalents **2.2a** delays $A\beta_{40}$ aggregation by 445 minutes. At 4 equivalents **2.2a** delays $A\beta_{40}$ aggregation by 675 minutes, indicating **2.2a** shows a dose dependent response. **2.2a** interacts with $A\beta_{40}$ at stoichiometric amounts, suggesting multiple molecules of **2.2a** are required to delay $A\beta_{40}$ aggregation (Figure 2.14). Increasing hydrophobicity on the tau VIY face of **2.2a** does not increase **2.2a** activity against $A\beta_{40}$. These results also suggest $A\beta_{40}$ can interact the tau VIY face of **2.2a**, but the preferred hydrophobic face occurs on the $A\beta_{40}$ KVFE face. With the modest delays in $A\beta_{40}$ and

tau aggregation by **2.2a**, macrocyclic β-sheet chimera **2.2b** was prepared to investigate if positioning of aromatic residues of the macrocycle bottom strand influences amyloid aggregation.

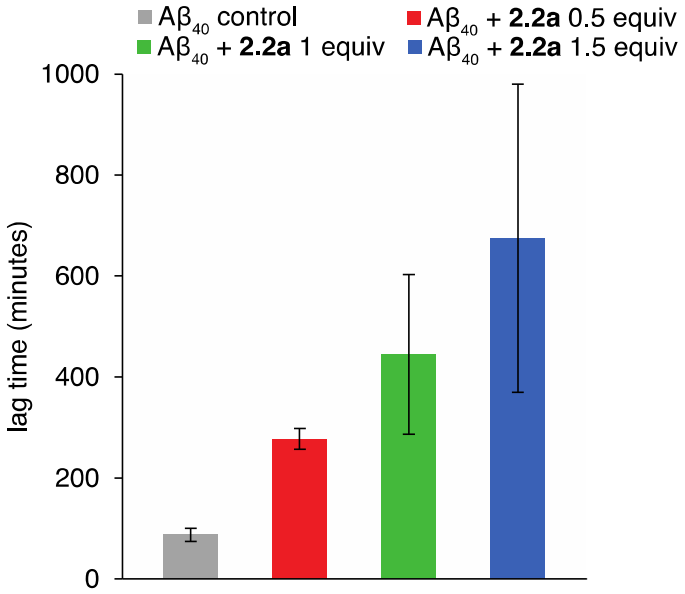

Figure 2.14. Effect of **2.2a** on $A\beta_{40}$ aggregation. **2.2a** modestly delays $A\beta_{40}$ aggregation at stoichiometric ratios.

5. Effect of 2.2b on amyloid aggregation. Synthesis of **2.2b** furnishes a water-soluble macrocycle. At 1 equivalents **2.2b** delays AcPHF6 aggregation by 3.7 minutes, and increased amounts of **2.2b** show a dose dependent response. 2 equivalents of **2.2b** increases the aggregation delay from 16.7 minutes, and at 4 equivalents, **2.2b** delays AcPHF6 aggregation by 45.7 minutes (Figure 2.15). Addition of the tyrosine residue on the bottom strand adds aromaticity to the VIY face and increases binding between **2.2b** and AcPHF6. These assays suggest AcPHF6 preferentially binds to the tau VIY face of **2.2b.** AcPHF6 is less responsive to chimera peptide inhibitors than $A\beta_{40}$, noted by the slight effects on AcPHF6 aggregation by **2.2b** and prior macrocycles. Addition of an aromatic residue increases macrocycle affinity to AcPHF6, suggesting AcPHF6 primarily interacts with **2.2a** and **2.2b** by aromatic interactions. Branched residues on the bottom strand of the macrocycle do not facilitate macrocycle

interactions with AcPHF6, as observed with **2.1a** and **2.1b**, and incorporation of just one aromatic residue on the bottom strand is sufficient to see improved macrocycle affinity to AcPHF6.

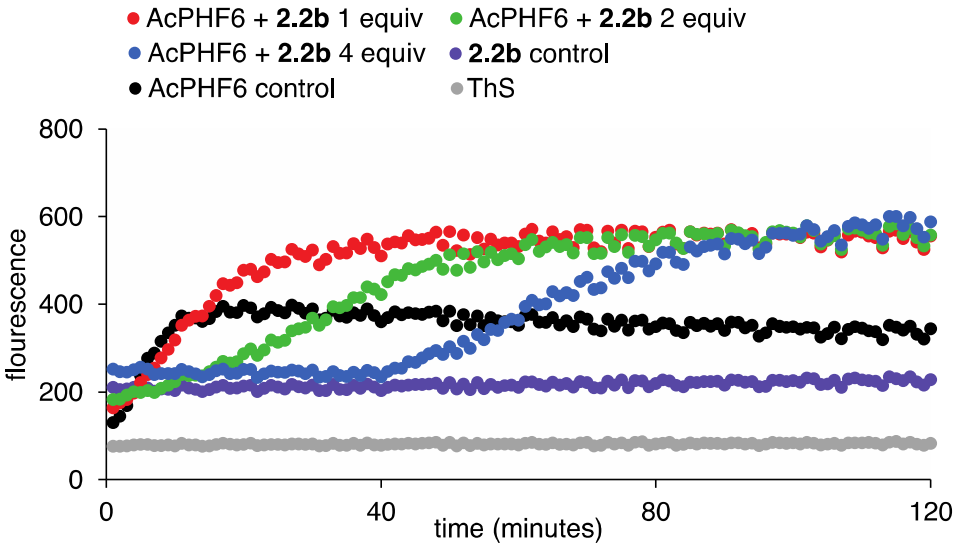

Figure 2.15. Effect of **2.2b** on AcPHF6 aggregation. **2.2b** shows a dose dependent response and modestly delays AcPHF6 aggregation.

Thioflavin T fluorescence assays show **2.2b** is a more effective inhibitor against $A\beta_{40}$ aggregation. At 0.5 equivalents, **2.2b** delays $A\beta_{40}$ aggregation by 1075 minutes and at 1.0 and 1.5 equivalents **2.2b** suppresses $A\beta_{40}$ aggregation (Figure 2.16). Addition of tyrosine of the bottom strand of **2.2b** to create an extended aromatic pocket on the tau VIY face influences $A\beta_{40}$ fibrillization, implying the hydrophobic face can recognize Aβ by aromatic interactions. Hydrophobic interactions are known to play a significant role in Aβ fibril formation, and the aromatic face presented can create a hydrophobic binding site for $A\beta_{40}$. Addition of tyrosine to the bottom strand proves to be beneficial to **2.2b** activity, as $A\beta_{40}$ aggregation is suppressed and delay of AcPHF6 aggregation is improved. To further improve macrocycle activity against AcPHF6, and to facilitate AcPHF6 interactions with residues from $A\beta_{40}$, macrocycles **2.3a** and **2.3b** were prepared with shifted $A\beta_{40}$ sequences.

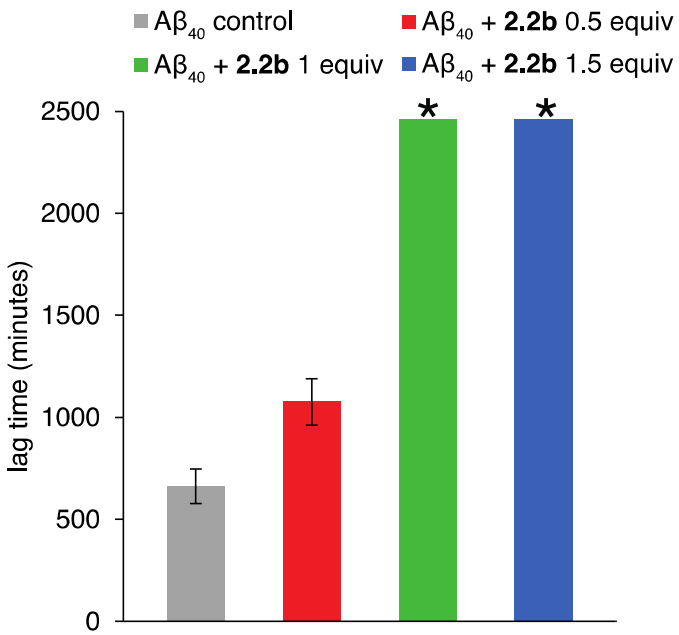

Figure 2.16. Effect of **2.2b** on $A\beta_{40}$ aggregation. The asterisk above the columns indicates $A\beta_{40}$ suppression lasted throughout the duration of the experiment.

6. Design of chimeras 2.3a and 2.3b. To complete the analysis of chimera sequences in the heptapeptide platform, residue shifts between the $A\beta_{16\text{-}23}$ region were employed to explore if AcPHF6 can interact with the $A\beta_{40}$ N-terminus. Because $A\beta_{40}$ forms beta-helical bundles composed of U-shaped superstructures containing the ^{15}QKLVFFAED^{23} region, The QLFAD face is a candidate region in development of effective macrocyclic β-sheet inhibitors.

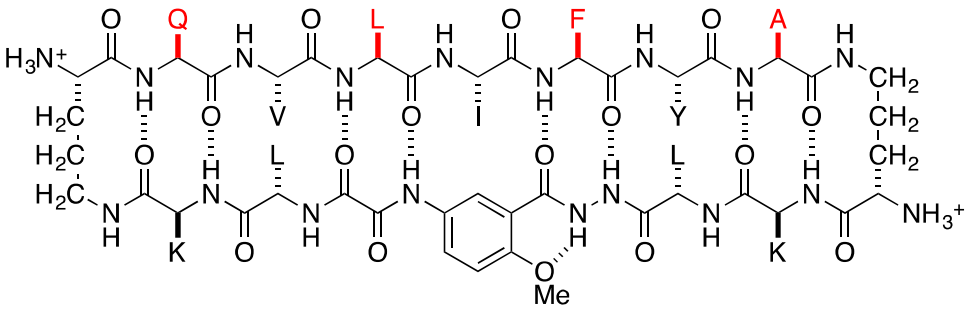

Figure 2.17. Chimera **2.3a. 2.3a** contains residues $Q_{15}L_{17}F_{19}A_{21}$ from $A\beta_{40}$ (red) and residues $V_{306}I_{308}Y_{310}$ from tau (black).

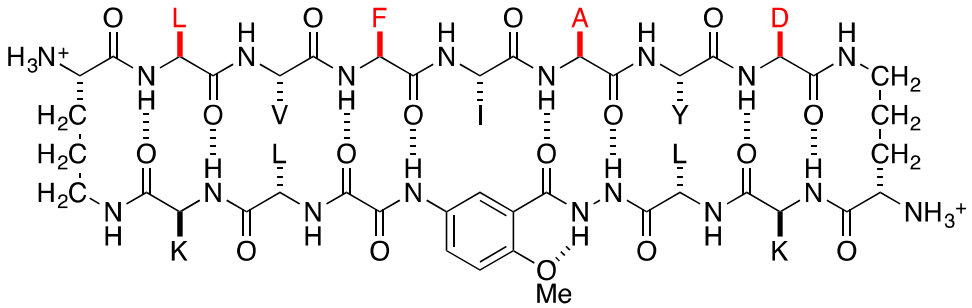

Figure 2.18. Chimera **2.3b. 2.3b** contains residues $L_{17}F_{19}A_{21}D_{23}$ (red) from $A\beta_{40}$ and residues $V_{306}I_{308}Y_{310}$ (black) from tau.

7. Effect of 2.3a on amyloid aggregation. Chimera **2.3a** presents the QLFA face, corresponding to residues $Q_{15}L_{17}F_{19}A_{21}$ of $A\beta_{40}$. Under MOPS buffer, **2.3a** shows high baseline fluorescence, indicating self-assembly recognized by Thioflavin S. At 1 equivalents of **2.3a** delays AcPHF6 aggregation by 3.4 minutes and at 2 equivalents of **2.3a** delays AcPHF6 aggregation by 74.3 minutes (Figure 2.19). At 4 equivalents of **2.3a** no AcPHF6 inhibition is observed, indicating the fluorescence signal of AcPHF6 is overshadowed by **2.3a** self assembly. **2.3a** shows AcPHF6 can participate in cross-amyloid interactions with $A\beta_{40}$, and prefers macrocycles containing the QLFA face, as **2.3a** delays AcPHF6 aggregation for over one hour. **2.3a's** increased activity against AcPHF6 aggregation can be attributed to its aromatic and aliphatic character. Unlike macrocycles in the **2.1** and **2.2** series, which contain the KVFE face from $A\beta_{40}$, two polar residues and two aliphatic residues, **2.3a** contains one polar residue and three aliphatic residues. The overall charge on both the **2.2** series and **2.3a** is +4, but in **2.3a** the majority of the polar contacts reside on the bottom strand. Thus, the increased aliphatic character of **2.3a** facilitates interactions with AcPHF6, and suggests AcPHF6 prefers polar contacts such as glutamine rather than ionized contacts such as glutmate. AcPHF6 can participate in cross amyloid interactions with the $A\beta_{40}$ N-terminus, showing a preference for the face possessing the F_{19} residue.

The aggregation encountered in **2.3a** can be attributed to the elimination of polar flanking

contacts in the recognition strand. Although the net overall charge of **2.3a** is +4, there is an unequal distribution of polar contacts within the macrocycle. Compared to more soluble macrocycles such as **2.1a**, shifting of the Aβ sequence towards the C-terminus creates a face on **2.3a** containing residues QLFA, which has only one polar glutamine residue and three aliphatic residues, compared to **2.1a** and **2.2a**, which contains two polar residues and two aliphatic residues from the KVFE face. Thus, the recognition strand of **2.3a** only possesses a +1 charge from the ornithine free amine, compared to the +3 charge offered by the blocking strand's two lysines and ornithine free amine. Unequal charge distribution causes **2.3a** to be solvated only on the bottom strand of the macrocycle, thus causing the recognition strand to self assemble in solution by hydrophobic interactions. Amidst the self-assembly, **2.3a** is the most effective β-sheet macrocyclic chimera against amyloid aggregation.

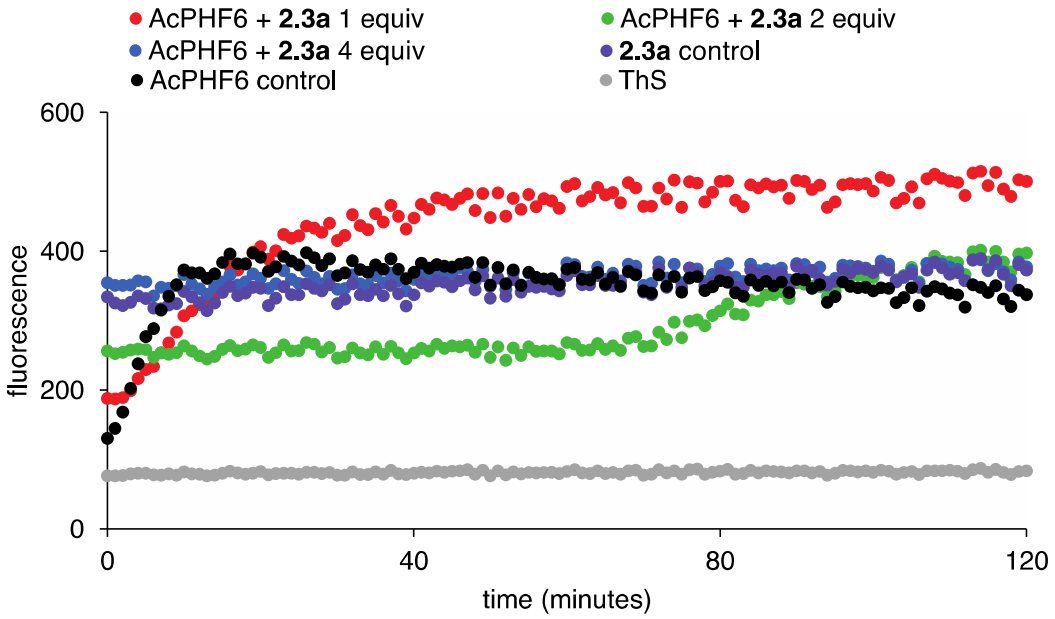

Figure 2.19. Effect of **2.3a** on AcPHF6 aggregation. **2.3a** delays AcPHF6 aggregation at stoichiometric concentrations.

When assayed against $A\beta_{40}$ aggregation, **2.3a** suppresses $A\beta_{40}$ aggregation at 0.5, 1.0 and 1.5 equivalents (Figure 2.20). $A\beta_{40}$ suppression at substoichiometric concentrations of **2.3a** indicates **2.3a** interacts with more than one molecule of $A\beta_{40}$. $A\beta_{40}$ contains two aromatic

residues, F_{19} and F_{20}, both implicated in fibril formation, and **2.2b** and **2.3a** shows $A\beta_{40}$ fibrillization can be suppressed by macrocycles possessing either the KVFE face or the QLFA face. **2.3a** suggests $A\beta_{40}$ aggregation can be suppressed using residues from either face of the N-terminus, and similar to AcPHF6, prefers the N-terminus face containing residues flanking F_{19}. $A\beta_{40}$ behaves similarly to AcPHF6 against **2.3a**, showing significant delay in AcPHF6 and suppression of $A\beta_{40}$. **2.3a's** activity towards amyloid aggregation suggests F_{19} is more critical than F_{20} in the cross-interaction of amyloidogenic sequences.

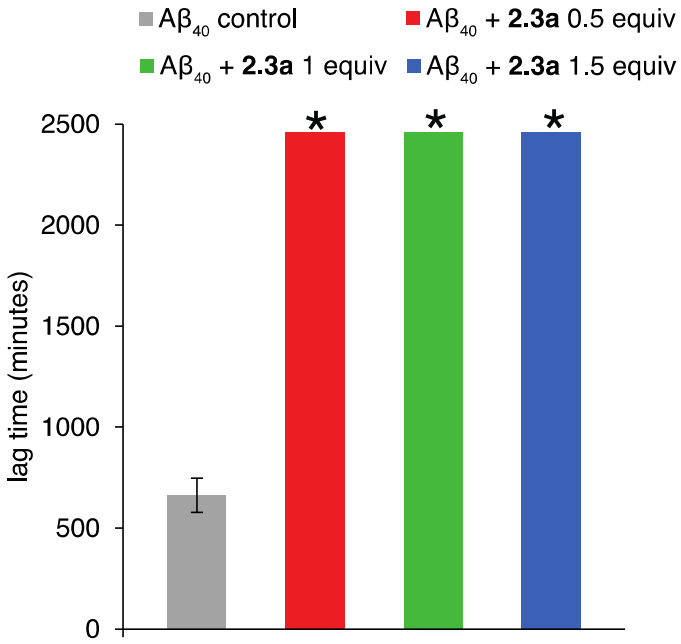

Figure 2.20. Effect of **2.3a** on $A\beta_{40}$ aggregation. **2.3a** suppresses $A\beta_{40}$ fibrillization at 0.5, 1 and 1.5 equivalents.

8. Effect of 2.3b on amyloid aggregation. Macrocyclic β-sheet **2.3b** incorporates $L_{17}F_{19}A_{21}D_{23}$, from $A\beta_{40}$ onto the heptapeptide macrocycle. The LFAD sequence creates a more hydrophobic face on the macrocycle, containing only one polar residue from D_{23}. The sequence shift towards the $A\beta_{40}$ C-terminus in **2.3b** gives **2.3b** a net overall charge of +3. **2.3b** control wells show a high baseline fluorescence, indicating self-assembly in MOPS buffer. Just like **2.3a**, **2.3b** contains two branched residues and F_{19} on the recognition strand, and has a majority

of the ionized contacts on the bottom strand of the macrocycle. However, **2.3a** possesses a glutamine residue while **2.3b** contains an aspartate residue, and this difference creates detrimental effects on **2.3b**. At 1 equivalent, **2.3b** delays AcPHF6 aggregation by 2 minutes and at 2 equivalents, AcPHF6 aggregation is delayed by 12.7 minutes (Figure 2.21). At 4 equivalents, no inhibition is observed, and the aggregation fluorescence of **2.3b** in solution interferes with the AcPHF6 fluorescence readout. Based on these results, **2.3b** slightly delays AcPHF6 aggregation, much less effectively than **2.3a**. The LFAD face of **2.3b**, although more hydrophobic than the KVFE face of $A\beta_{40}$, does not improve its activity against AcPHF6 aggregation. **2.3b** behaves more poorly than **2.3a,** highlighting the significance of the glutamine residue over the aspartate residue. At pH 7.4, the D_{23} residue is deprotonated, allowing D_{23} to only participate as a hydrogen bond acceptor, while Q_{15} can participate in hydrogen bonding donor and acceptor interactions. The self-assembly of **2.3a** in solution can prevent interaction of the recognition strand with its intended target, amyloidogenic peptides. Maintaining flanking polar residues is important in designing effective macrocyclic β-sheet inhibitors.

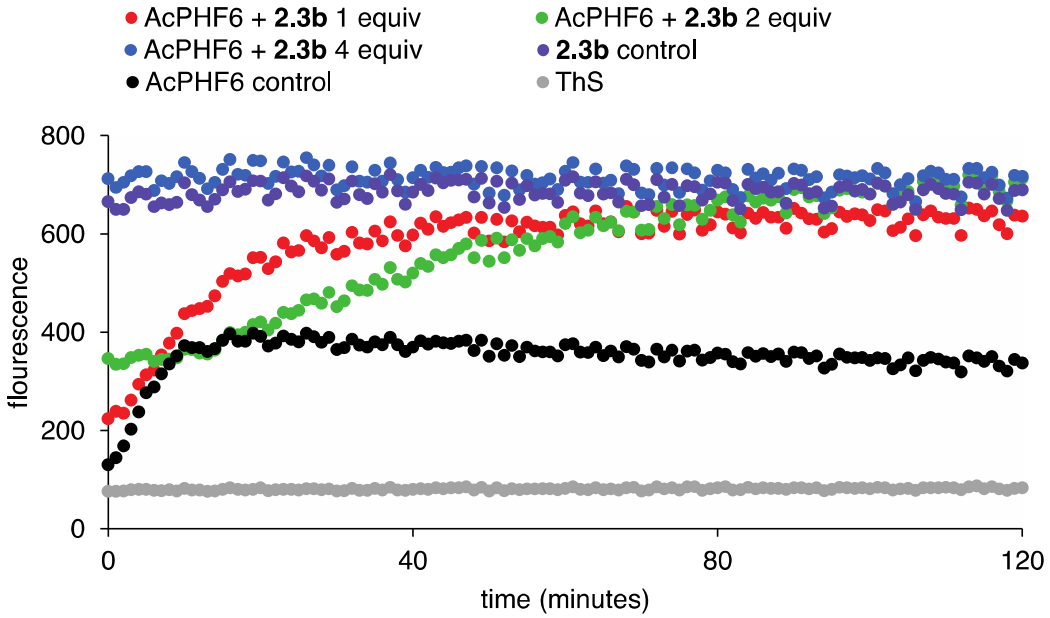

Figure 2.21. Effect of **2.3b** on AcPHF6 aggregation. **2.3b** modestly delays $A\beta_{40}$ aggregation,

and its self assembly in solution can interfere with AcPHF6 aggregation.

Fluorescence assays show **2.3b** does not inhibit $A\beta_{40}$ fibrillization. $A\beta_{40}$ responds to **2.3b** in a similar fashion as AcPHF6, showing slight delays in aggregation by **2.3b**. The suppression of $A\beta_{40}$ fibrillization initially observed in **2.3a** is destroyed in **2.3b**, suggesting D_{23} is a less effective residue at improving macrocycle activity against $A\beta_{40}$ fibrillization. At 0.5 equivalents, **2.3b** delays $A\beta_{40}$ fibrillization by 92.5 minutes, and at 1 equivalents **2.3b** delays $A\beta_{40}$ fibrillization by 105 minutes (Figure 2.22). **2.3b** behaves in a slight dose-dependent response; at 1.5 equivalents **2.3b** delays $A\beta_{40}$ fibrillization by 112.5 minutes (Figure 2.22). Although **2.3b** shows a minute amount of increase in lag time, **2.3b** does not interact strongly with $A\beta_{40}$. Although D_{23} in **2.3b** is a critical residue in $A\beta_{40}$ aggregation, as it is in the turn region of the fibril and can participate in salt bridge interactions, inclusion of D_{23} into **2.3b** decreases its inhibitory activity, presumably due to increased self-assembly.[22] These results suggest polar residues such as lysine or glutamine, along with a hydrophobic core, are essential to developing optimal $A\beta_{40}$ inhibitors. Increasing macrocycle hydrophobicity does not create improved macrocyclic β-sheet inhibitors. Taken together, unequal charge distribution and lack of flanking polar residues can create significant effects in solubility and binding affinity towards amyloidogenic sequences of interest.

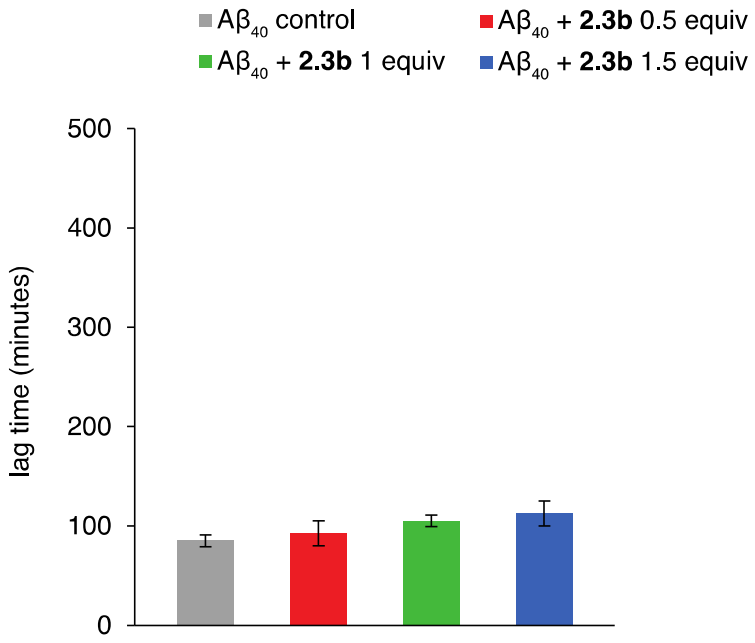

Figure 2.22. Effect of **2.3b** on $A\beta_{40}$ aggregation. **2.3b** does not impede $A\beta_{40}$ aggregation at stoichiometric concentrations.

CONCLUSION

The Aβ-tau macrocyclic β-sheet chimeras do show inhibition at stoichiometric amounts, and offer insight on the behavior of amyloid peptides towards chimera β-sheet macrocycles. **2.1a** was created containing the N-terminus of $A\beta_{40}$ displaying the F_{20} residue, and **2.1b** contains a glutamate to lysine residue on the bottom strand to probe the effect of charge on macrocycle solubility. **2.1a** self assembles in solution and catalyzes AcPHF6 fibrillization, and **2.1b** only has modest effects on AcPHF6 fibrillization, but effectively suppresses $A\beta_{40}$ aggregation at 1.5 equivalents. **2.1b** shows $A\beta_{40}$ is responsive to macrocycles possessing sequences containing the F_{20} residue, while AcPHF6 is more selective and less receptive to chimera peptides. Chimeras **2.2** were designed with the incorporation of an aromatic residue on the bottom strand to increase macrocycle affinity to AcPHF6 and to probe the effects of aromatic residue position towards amyloid aggregation. Chimera **2.2a** contains a leucine to phenylalanine mutation on the bottom strand and shows increased activity against AcPHF6 fibrillization and decreased activity against

$A\beta_{40}$ fibrillization. Chimera **2.2b** shows improved activity against AcPHF6 aggregation and suppression of $A\beta_{40}$ aggregation at stoichiometric amounts. **2.2a** and **2.2b** show AcPHF6 affinity to macrocycles can be increased by adding aromatic residues to the bottom strand, and suggests AcPHF6-macrocycle interactions are mediated by aromatic interactions. **2.3a** and **2.3b** were created to investigate facial preferences of amyloid peptides towards macrocyclic β-sheets containing the N-terminus of $A\beta_{40}$ displaying the F_{19} residue. **2.3a** is the most effective inhibitor, delaying AcPHF6 fibrillization for over one hour, and suppresses $A\beta_{40}$ aggregation at substoichiometric concentrations as low as 0.5 equivalents. **2.3a** shows AcPHF6 can respond to $A\beta_{40}$ sequences, and prefers the N-terminus of $A\beta_{40}$ displaying the F_{19} residue. **2.3b** shows significantly decreased inhibitory activity, slightly delaying AcPHF6 fibrillization by minutes and delaying $A\beta_{40}$ aggregation only by minutes. **2.3b** also self assembles in solution, potentially affecting accessibility of the **2.3b** recognition strand by amyloid peptides. Lastly, **2.3b** shows AcPHF6 and $A\beta_{40}$ are sensitive to residue positioning on the macrocycle, exhibiting decreased activity against AcPHF6 and $A\beta_{40}$. **2.1b** and **2.3a** provide circumstantial evidence of cross-amyloid interactions between $A\beta_{40}$ and tau. Chimeras **2.1a** and **2.3b**, although weak inhibitors, can be further tuned to study the self-assembly of Aβ-tau macrocycles. These chimeras can be extended into molecular recognition to understand the facial recognition between two different amyloidogenic protein sequences. Hybrid peptide sequences can be exercised to understand Aβ-tau complexes driving Alzheimer's disease[23], with the potential to determine structural information encoding facial recognition.

An issue unaddressed by macrocycles designed by the Nowick group is the structural resolution information encoded by macrocycle binding and behavior. Fluorescence assays indirectly probe inhibition by binding β-sheet rich aggregates, yet offer little information on

oligomeric structures, the proposed toxic entity in the amyloid hypothesis.[24,25,26] To better understand the nature of recognition between peptide and macrocycle, and to fine tune macrocycle activity, advanced mass spectrometric techniques including hydrogen deuterium exchange (HDX) and ion mobility spectrometry (IMS) can provide insight on comprehending amyloid mediated identification.[27,28] Other analytical techniques such as NMR and X-ray crystallography have provided meaningful understanding into residue interactions, yet they provide a fragmented picture in studying unstable oligomeric intermediates. Mass spectrometry provides an avenue to study noncovalent interactions under native conditions, offering the potential to observe the oligomeric complexes formed (dimer, trimer, tetramer) between peptide and macrocycle.

References and Notes

[1] Yan, L.-M.; Velkova, A.; Tatarek-Nossol, M.; Andreetto, E.; Kapurniotu, A. *Angew. Chem. Int. Ed. Engl.* **2007,** *46,* 1246-1252.

[2] Ono, K.; Takahashi, R.; Ikeda, T., Yamada, M. *J. Neurochem.* **2012,** *122,* 883-890.

[3] Schwarzman, A.; Gregori, L.; Vitek, M. P.; Lyubski, S.; Strittmatter, W. J.; Enghilde, J. J.; Bhasin, R.; Silverman, J.; Weisgraber, K. H.; Coyle, P. K.; Zagorski, M. G.; Talafous, J.; Eisenberg, M.; Saunders, A. M.; Roses, A. D.; Goldgaber, D. *Proc. Natl. Acad. Sci. USA* **1994,** *91,* 8368-8372.

[4] Theis, W.; Bleiler, L. *Alzheimers Dement.* **2013,** *9,* 208-245.

[5] Ittner, L. M.; Ke, Y. D.; Delerue, F.; Bi, M.; Gladbach, A.; van Eersel, J.; Wolfing, H.; Chieng, B. C.; Christie, M. D.; Napier, I. A.; Eeckert, A.; Staufenbiel, M.; Hardeman, E.; Gotz, J. *Cell* **2010,** *142,* 387-397.

[6] Busciglio, J.; Lorenzo, A.; Yeh, J.; Yankner, B. A. *Neuron* **1995,** *14,* 879-888.

[7] Ballatore, C.; Lee, V. M.-Y.; Trojanowski, J. Q. *Nat. Rev. Neurosci.* **2007,** *8,* 663-672.

[8] King, M. E., Kan, H.-O.; Baas, P. W.; Erisir, A.; Glabe, C. G.; Bloom, G. S. *J. Cell Biol.* **2006,** *175,* 541-546.

[9] Fein, J. A.; Sokolow, S.; Miller, C. A.; Vinters, H. V.; Yang, F.; Cole, G. M.; Gylys, K. H.; *Am. J. Pathol.* **2008**, *172,* 1683-1692.

[10] Gotz, J.; Chen, F.; van Dorpe, J.; Nitsch, R. M. *Science* **2001,** *293,* 1491-1495.

[11] Oddo, S.; Caccamo, A.; Tran, L.; Lambert, M.P.; Glabe, C. G.; Klein, W. L.; LaFerla, F. M. *J. Biol. Chem.* **2006,** *281,* 1599-1604.

[12] Ma, Q.-L.; Yang, F.; Rosario, E. R.; Ubeda, O. J.; Beech, W.; Gant, D. J.; Chen, P. P.; Hudspeth, B.; Chen, C.; Zhao, Y.; Vinters, H. V.; Frautschy, S. A.; Cole, G. M. *J. Neurosci.* **2009,** *29,* 9078-9089.

[13] Rapoport, M.; Dawson, H. N.; Binder, L. I.; Vitek, M. P.; Ferriera, A. *Proc. Natl. Acad. Sci. USA* **2002,** *99,* 6364-6369.

[14] Rhein, V.; Song, X.; Wiesner, A.; Ittner, L. M.;Baysang, G.; Meier, F.; Ozmen, L.; Bluethmann, H.; Drose, S.; Brandt, U.; Savaskan, E.; Czech, C.; Gotz, J.; Eckert, E. *Proc. Natl. Acad. Sci. USA* **2009,** *106,* 20057-20062.

[15] Jin, M.; Shepardson, N.; Yang, T.; Chen, G.; Walsh, D.; Selkoe, D. J. *Proc. Natl. Acad. Sci. USA* **2011,** *108,* 5819-5824.

[16] The coordinates for the solution phase NMR model of $A\beta_{40}$ fibrils were provided by Robert Tycko.

[17] Sievers, S. A.; Karanicolas, J.; Chang, H. W.; Zhao, A.; Jiang, L.; Zirafi, O.; Stevens, J. T.; Munch, J.; Baker, D.; Eisenberg, D. *Nature* **2011,** *475,* 96-100.

[18] Zheng, J.; Liu, C.; Sawaya, M. R.; Vadla, B.; Khan, S.; Woods, R. J.; Eisenberg, D.; Goux, W. J.; Nowick, J. S. *J. Am. Chem. Soc.* **2011,** *133,* 3144-3157.

[19] Cheng, P.-N.; Liu, C.; Zhao, M.; Eisenberg, D.; Nowick, J. S. *Nat. Chem.* **2012,** *4,* 927-933.

[20] Goux, W.J.; Kopplin, L.; Nguyen, A. D.; Leak, K.; Rutkofsky, M.; Shanmuganandam, V. D.; Sharma, D.; Inouye, H.; Kirschner, D. A. *J. Biol. Chem.* **2004,** *279,* 26868-26875.

[21] Gazit, E. *FASEB J.* **2002,** *16,* 77-83.

[22] Liu, R.; McAllister, C.; Lyubchenko, Y.; Sierks, M. R. *J. Neurosci. Res.* **2004,** *75,* 162–171.

[23] Guo, J.-P.; Arai, T.; Miklossy, J.; McGeer, P. L. *Proc. Natl. Acad. Sci. USA* **2006,** *103,* 1953-1958.

[24] Hardy, J. A.; Allsop, D. *Trends Pharmacol. Sci.* **1991,** *12,* 383-388.

[25] Hardy, J. A.; Higgins, G. A. *Science* **1992,** *256,* 184-185.

[26] Hardy, J. A.; Selkoe, D. J. *Science* **2002,** *297, 353-356.*

[27] Woods, L. A.; Radford, S. E.; Ashcroft, A. E. *Biochim. Biophys. Acta* **2013,** *1834,* 1257-1268.

[28] Bernstein, S. L.; Dupuis, N. F.; Lazo, N. D.; Wyttenbach, T.; Condron, M. M.; Bitan, G.; Teplow, D. B.; Shea, J.-E.; Ruotolo, B. T.; Robinson, C. V.; Bowers, M. T. *Nat. Chem.* **2009,** *1,* 326-331.

Experimental Section for Chapter 2

Peptide synthesis. Macrocycles were synthesized as previously developed[1] on 2-chlorotrityl chloride resin using fluorenylmethoxycarbonyl (Fmoc)-solid phase peptide synthesis. Briefly, the linear crude product was cleaved from the resin using an acetic acid solution, concentrated and redissolved in methylene chloride and hexanes to azeotrope the residual acid and furnish a white, flaky product. To promote intramolecular cyclization, the peptide was dissolved at low (0.5 mM) concentrations in N,N-dimethylformamide (DMF) under nitrogen using an excess of HOBt, HBTU, and N-methylmorpholine (NMM) overnight. The cyclized protected peptide was concentrated to give a yellow oil, and deprotected with trifluoroacetic acid (TFA) followed by quenching with distilled water. The solution was concentrated to afford a yellow oil, and the peptide was purified using reverse phase high performance liquid chromatography (RP-HPLC) followed by lyophilization to afford a white, fluffy solid.

NMR spectroscopy. Peptides were gravimetrically measured into a glass dram vial and dissolved in "100%" D_2O (Cambridge Isotope Laboratories, DLM-4) to a final concentration of 2 mM. Molecular weights were calculated with the free amines as a TFA salt. ^1H NMR spectra were conducted on a Bruker 500 MHz NMR spectrometer equipped with a cryoprobe at 298 K for 64 scans.

Thioflavin S (ThS) assays. ThS fluorescence assays were carried out in Corning 96-well black clear bottom plates (Corning) with shaking on a Gemini XPS fluorescence plate reader (Molecular Devices). Readings were collected at 27 °C every minute for 120 minutes, excitation 440 nm, emission 490 nm.

Preparation of ThS stock solution. Thioflavin S assays were executed as previously described.[2] 2 mgs of Thioflavin S, practical grade (Sigma-Aldrich, T1892) were dissolved in 4 mLs 18 MΩ

H_2O and filtered through 0.2 μM nylon filters. The ThS stock solution was diluted with MOPS buffer (pH 7.2) to create a working stock of 250 μM ThS in 20 mM MOPS, pH 7.2.

Preparation of inhibitor solution. Peptides were measured gravimetrically to create a 1 mM solution in 18 MΩ H_2O. The inhibitor was plated into the wells at the appropriate concentrations, followed by addition of 18 MΩ water, 140 μL 20 mM MOPS pH 7.2, and 250 μM ThT stock.

Preparation of AcPHF6 solution. AcPHF6 was dissolved in 0.2 μM filtered 18 MΩ H_2O to create a 1 mM working stock. AcPHF6 was added to reaction wells lastly, because of its immediate aggregation. The plate was sealed with sealing film and the experiment was initiated. Experiments were run in triplicate.

Table S2.1. Volumes of 96-Well ThS Reaction Plate.

Wells	ThS solution (μL)	inhibitor solution (μL)	water (μL)	AcPHF6 solution (μL)	MOPS buffer (μL)
ThS control	20	0	40	0	140
AcPHF6 control	20	0	35	5	140
AcPHF6 + 1 equiv inhibitor	20	5	30	5	140
AcPHF6 + 2 equiv inhibitor	20	10	25	5	140
AcPHF6 + 4 equiv inhibitor	20	20	15	5	140

Thioflavin T (ThT) fluorescence assays. ThT fluorescence assays were carried out in Corning 96-well black clear bottom plates with shaking on a Gemini XPS fluorescence plate reader (Molecular Devices). Readings were collected at 37 °C every 10 minutes for 41 hours at excitation 442 nm, emission 482 nm, with 5 seconds shaking before the first reading and 575 seconds shaking in between readings.

Preparation of ThT stock solution. Thioflavin T stock was freshly prepared before each assay. 2.5 mg of ThT (Sigma-Aldrich, T3516-5G) was gravimetrically measured and dissolved in 10 mLs 18 MΩ H_2O and filtered through 0.2 μM nylon filters. The Thioflavin T solution was diluted to 1/25 and was measured at 412 nm with a JASCO-V-530 UV-Vis spectrophotometer (ε_{ThT} = 36,000 $M^{-1}\cdot cm^{-1}$). The Thioflavin T solution was further diluted with 10x PBS with 0.02% NaN_3, pH 7.4 to create a working stock of 100 μM ThT in 5x PBS, pH 7.4.

Preparation of inhibitor solutions. Peptides were measured gravimetrically to create a 1 mM solution in 18 MΩ H_2O. An aliquot was diluted by 1/25 for spectrophotometric measurements using a JACSO-V-530-UV-Vis spectrophotometer (ε_{Hao} = 9850 M^{-1} cm^{-1} at 280 nm). The 1 mM solution was further diluted with 18 MΩ H_2O to create a 200 μM working stock. The inhibitor was plated into the wells at the appropriate concentrations, followed by addition of 18 MΩ water and 100 μM ThT stock.

Preparation of $A\beta_{40}$ solution. Prior to the start of the experiment three Nanosep 100 kDa centrifuge filters (Pall, OD100C34) were washed with 500 μL of 18 MΩ water, three times for 5 minutes at 10,000 rpm. Synthetic $A\beta_{40}$ was purchased from GL Biochem Shanghai. 1.5 mg $A\beta_{40}$ was measured gravimetrically in a 1.5 mL eppendorf tube and dissolved in 146 μL 100 mM NaOH (analytical grade, Fisher SS266-1) to create a 2 mM solution.[3] The $A\beta_{40}$ solution was sonicated for 30 seconds in a water bath and further diluted with 1315 μL of 18 MΩ water to create a working stock solution of 200 μM. The $A\beta_{40}$ solution was sonicated again for 30 seconds, and 500 μL aliquots were filtered through three Nanosep 100 kDa centrifuge filters for 5 minutes at 10,000 rpm. $A\beta_{40}$ was added lastly to the wells in 20 μL aliquots for a final reaction volume of 200 μL. The plate was sealed with sealing film, inserted into the plate reader, and the experiment was initiated. Experiments were run in quadruplicate.

Table S2.2. Volumes of 96-Well ThT Reaction Plate.

Wells	ThT solution (μL)	inhibitor solution (μL)	water (μL)	$A\beta_{40}$ solution (μL)
ThT control	40	0	160	0
$A\beta_{40}$ control	40	0	180	20
$A\beta_{40}$ + 0.5 equiv inhibitor	40	10	130	20
$A\beta_{40}$ + 1.0 equiv inhibitor	40	20	120	20
$A\beta_{40}$ + 1.5 equiv inhibitor	40	30	110	20

ThS assays of **2.1a**

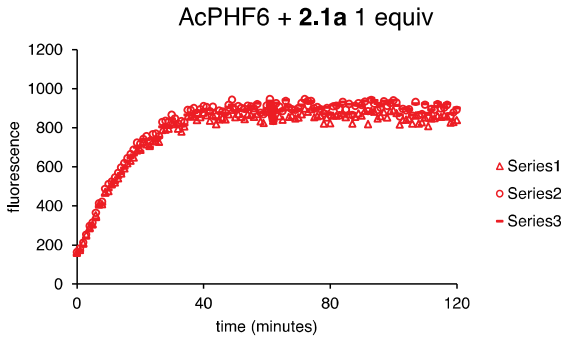

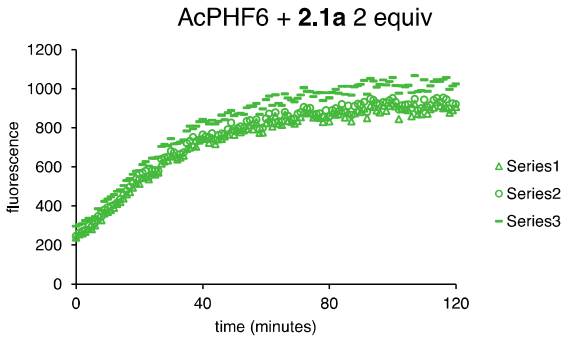

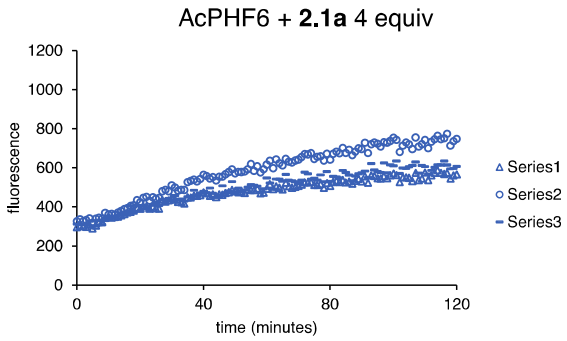

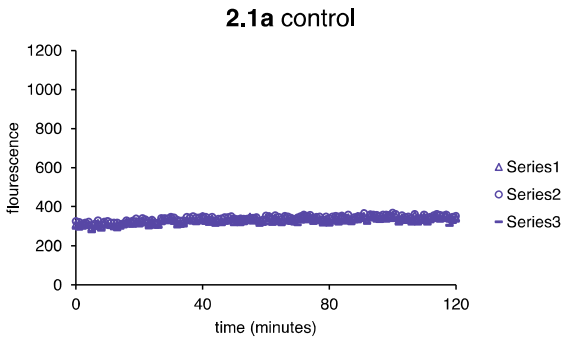

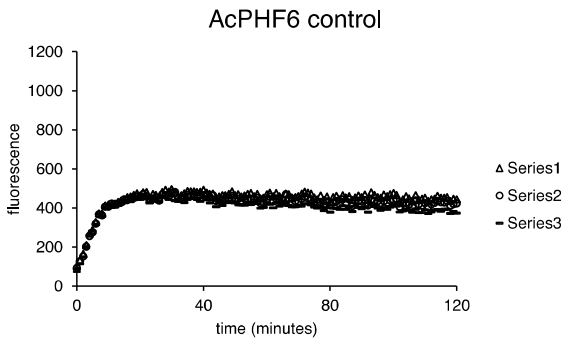

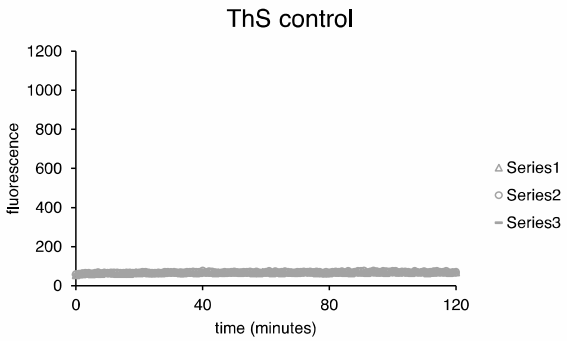

ThS assays of **2.1b**

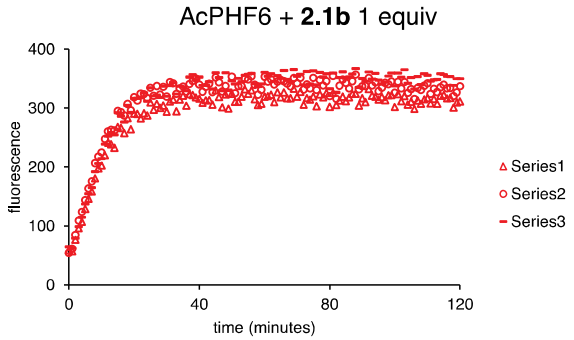

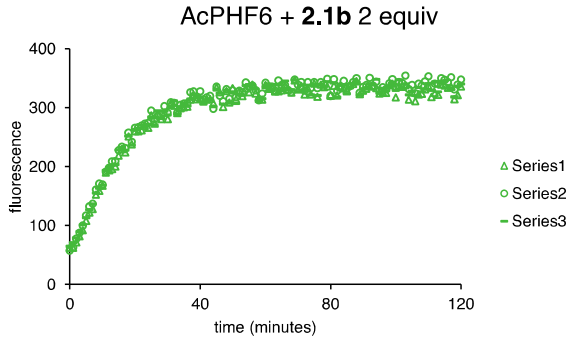

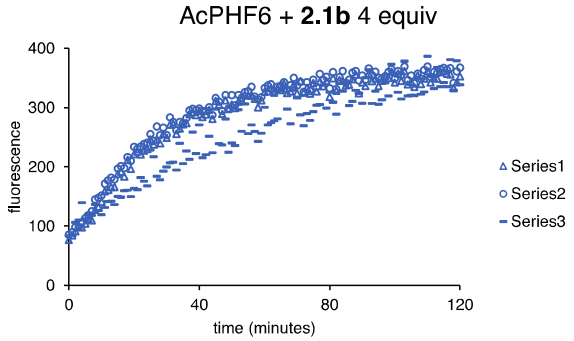

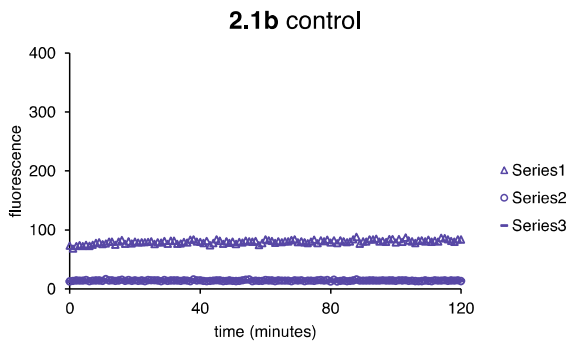

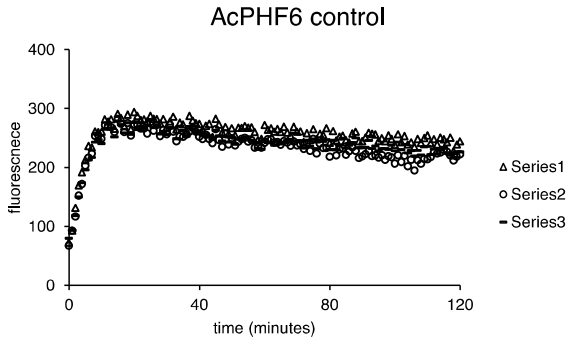

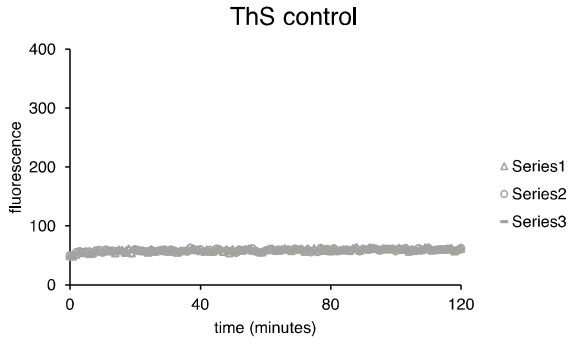

Tht assays of **2.1b**

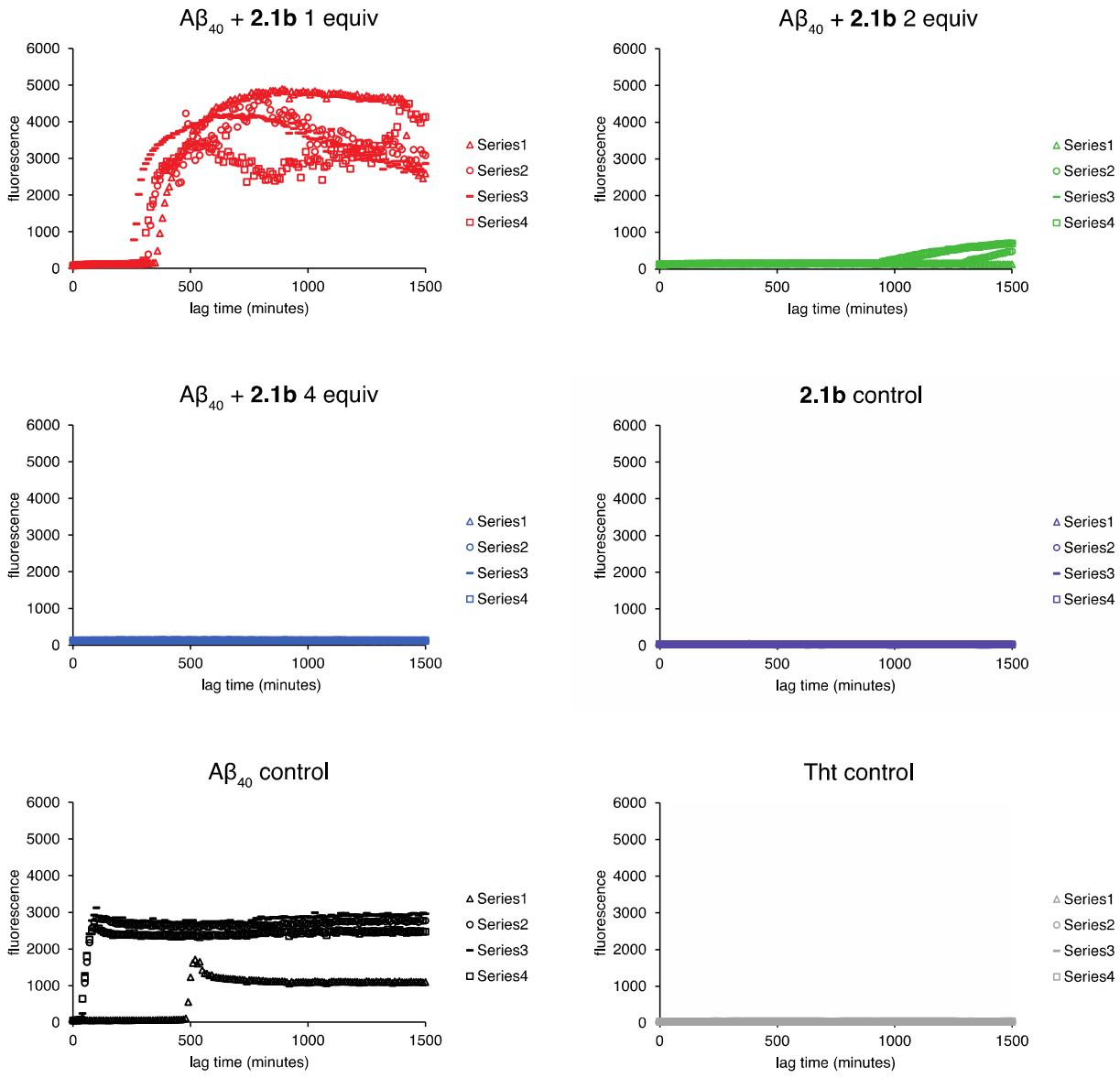

ThS assays of **2.2a**

AcPHF6 + **2.2a** 1 equiv

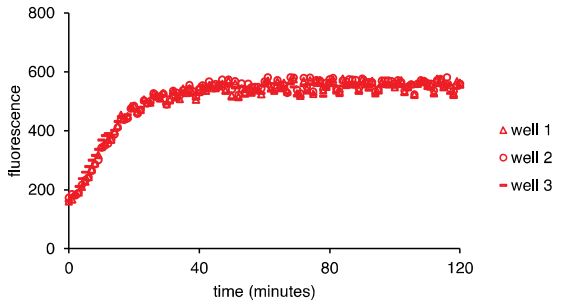

AcPHF6 + **2.2a** 2 equiv

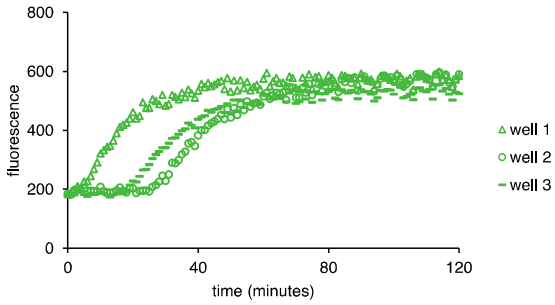

AcPHF6 + **2.2a** 4 equiv

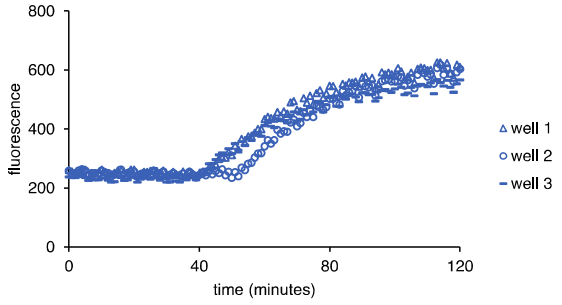

2.2a control

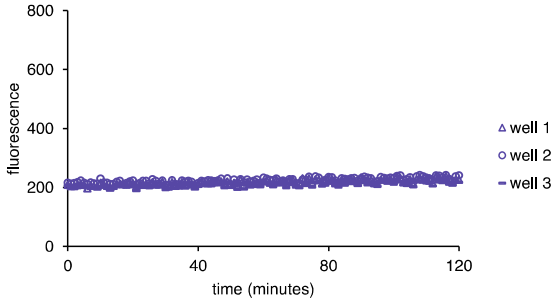

AcPHF6 control

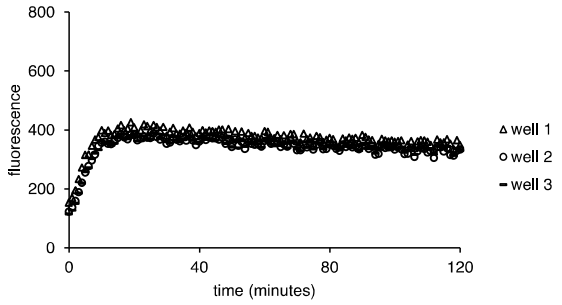

ThS control

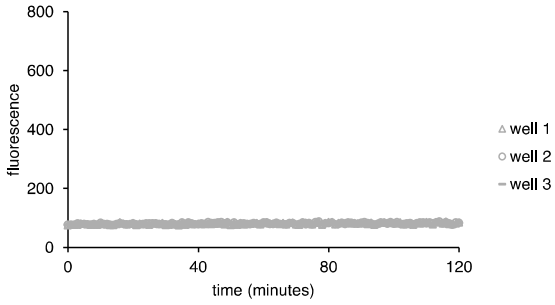

Tht assays of **2.2a**

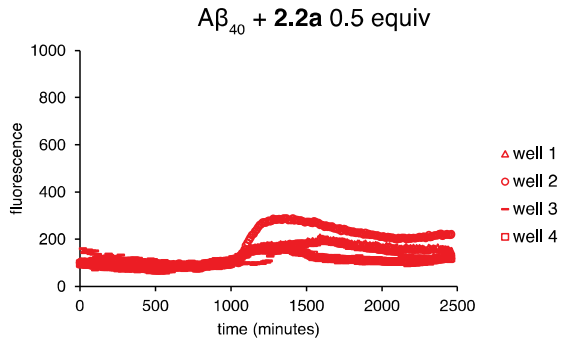

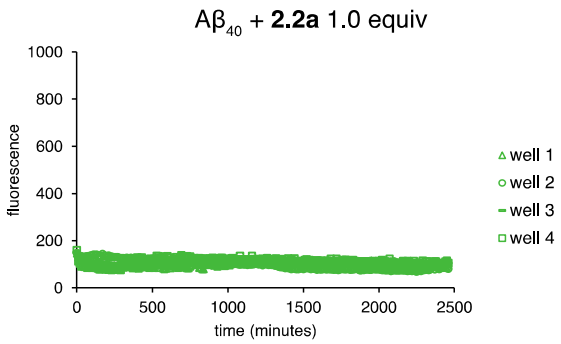

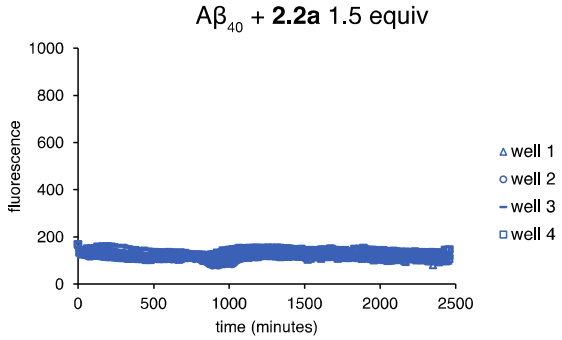

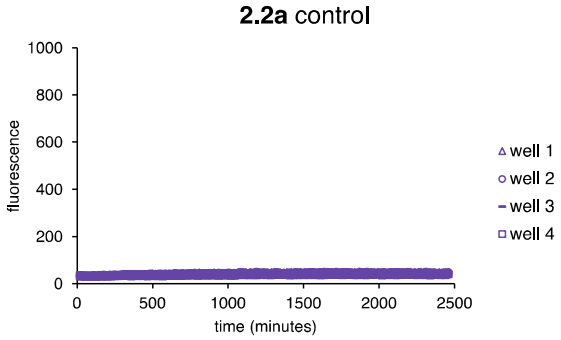

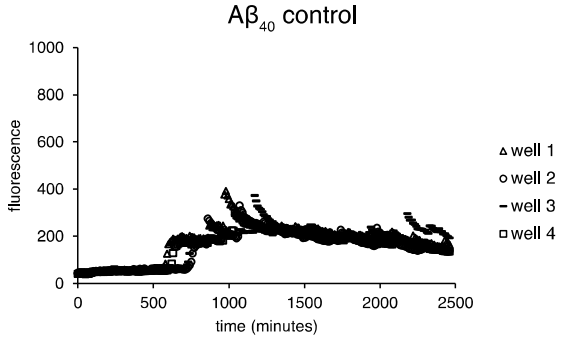

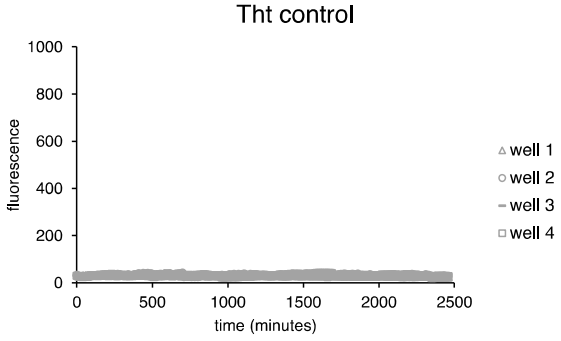

Tht assays of **2.2b**

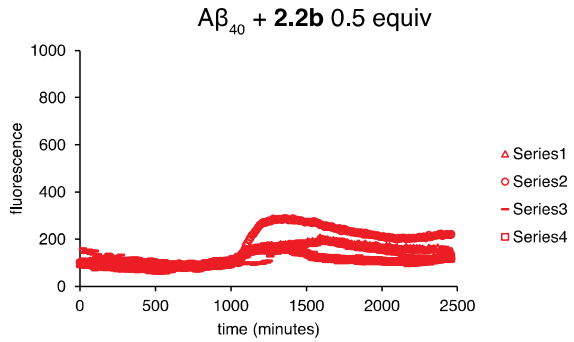

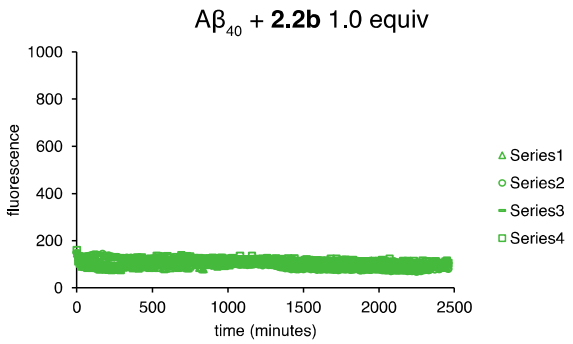

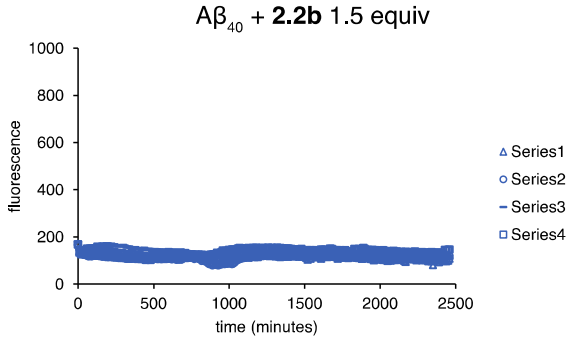

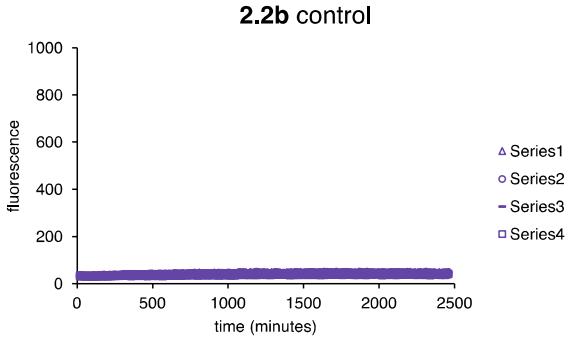

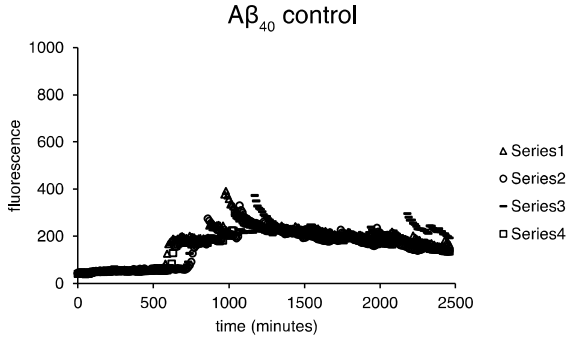

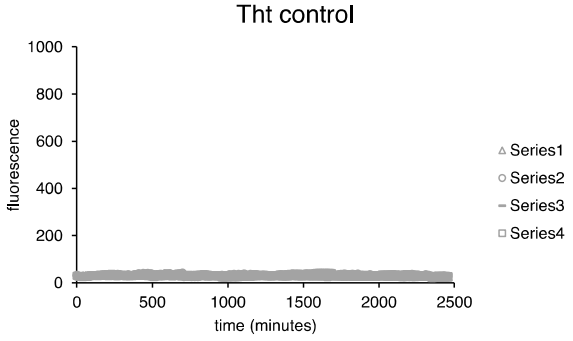

ThS assays of **2.3a**

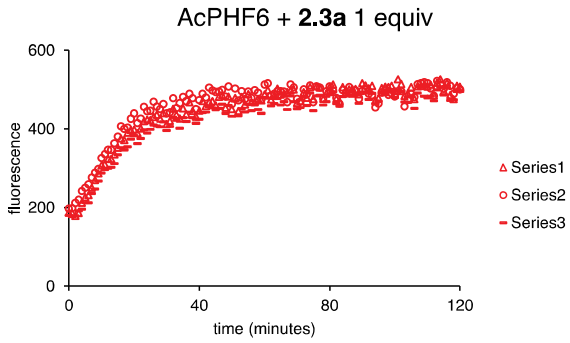

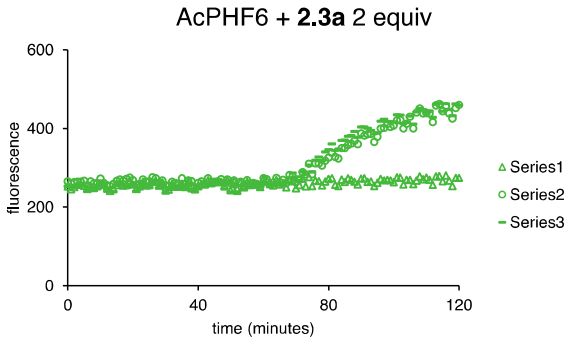

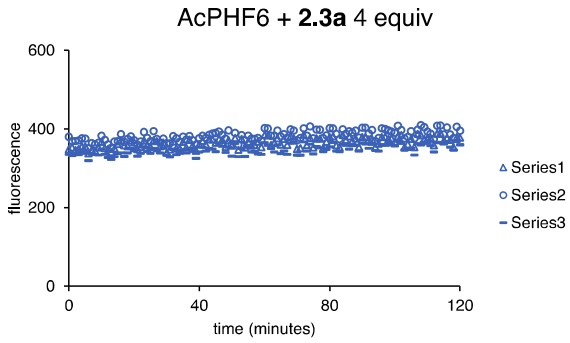

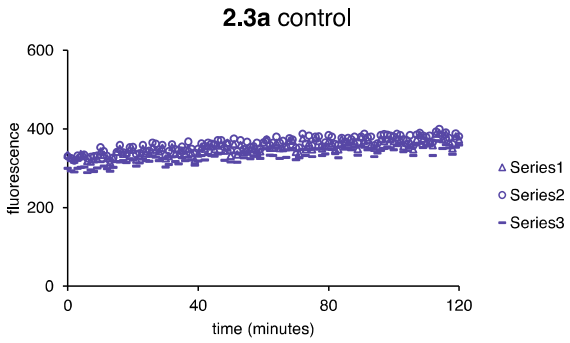

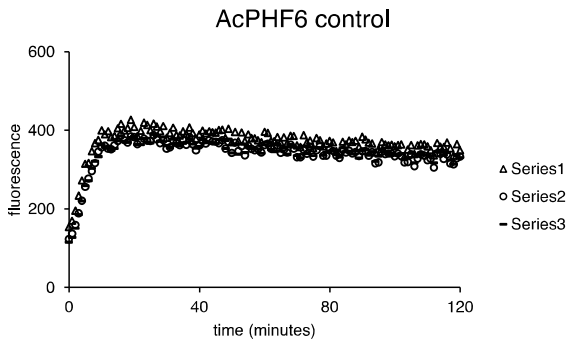

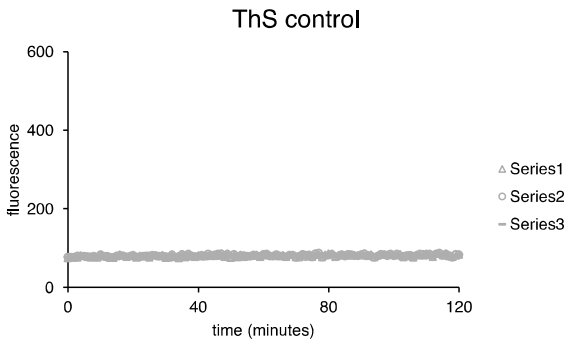

Tht assays of **2.3a**

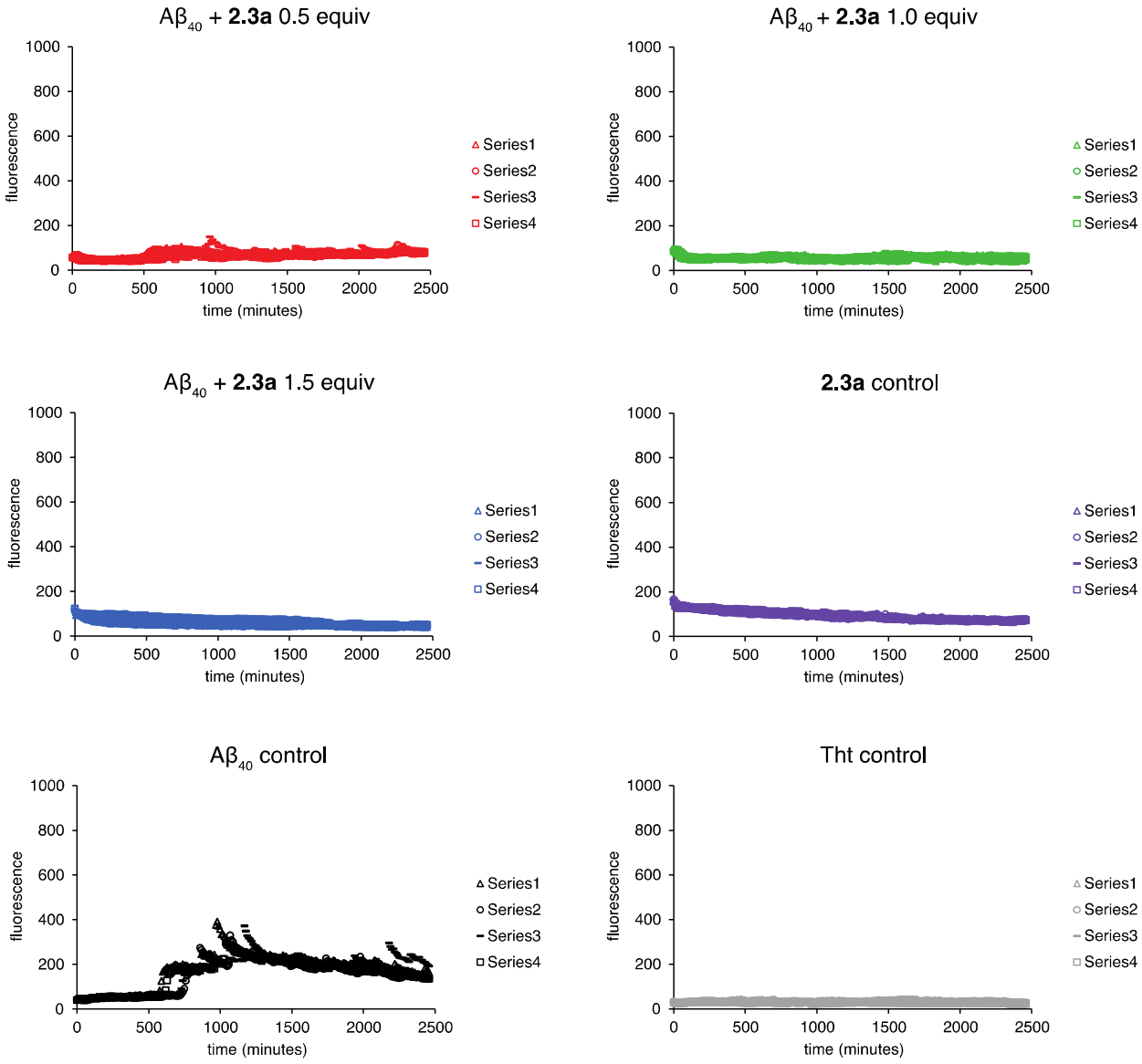

ThS assays of **2.3b**

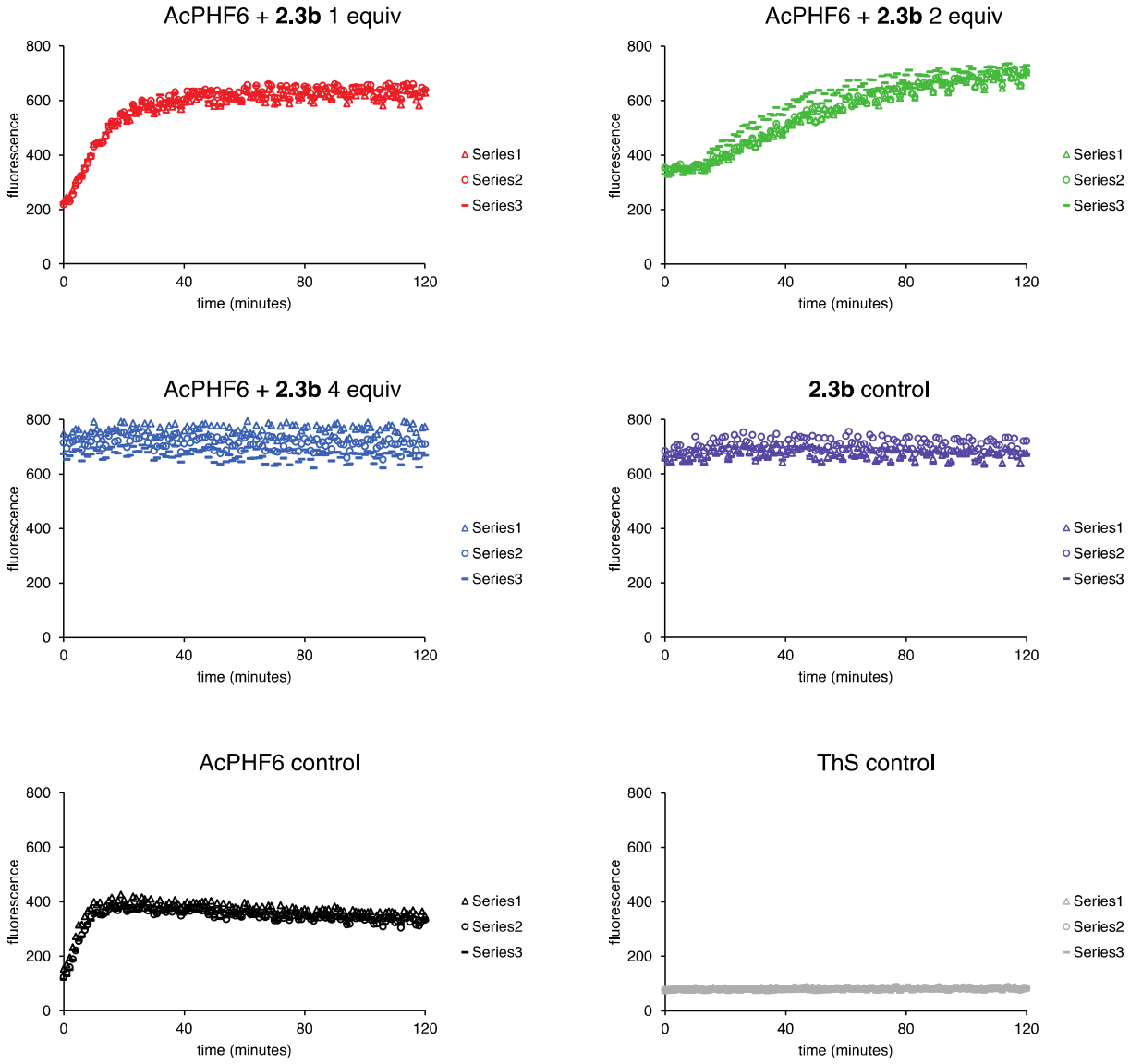

Tht assays of **2.3b**

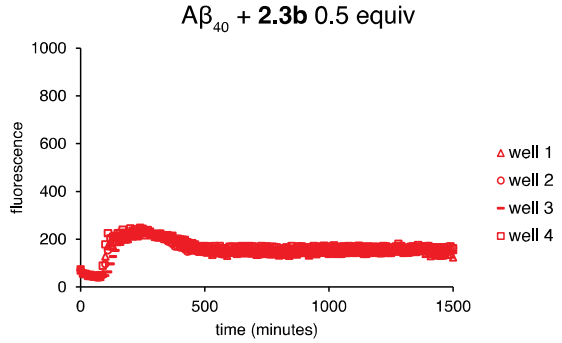

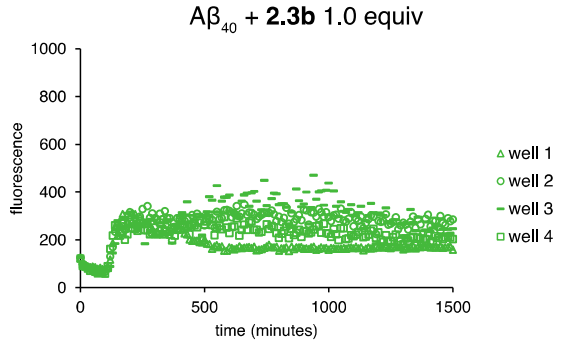

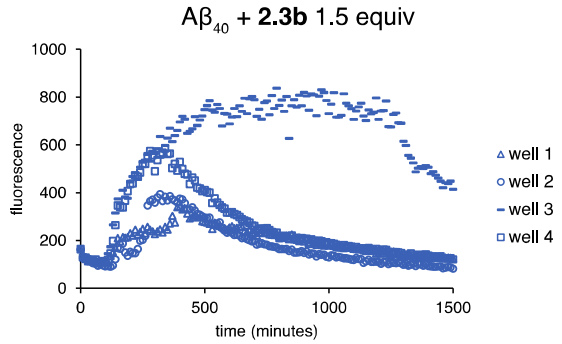

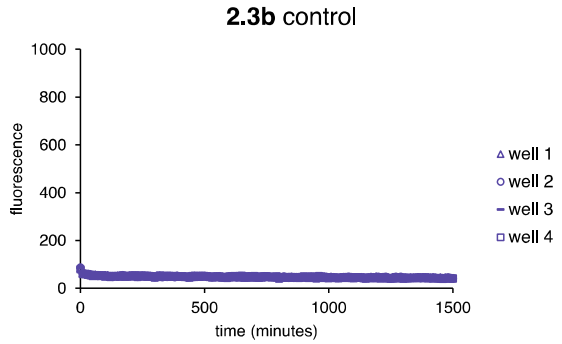

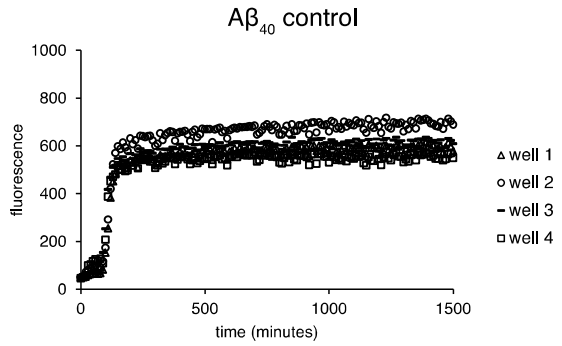

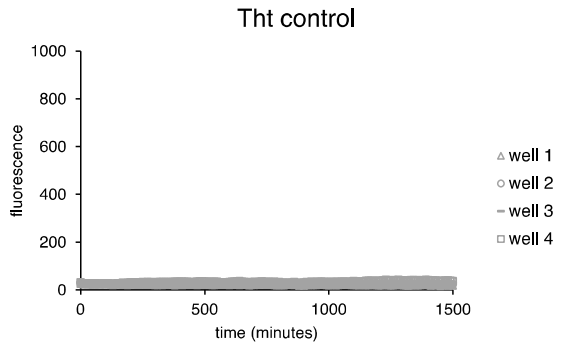

HPLC trace of **2.1a**

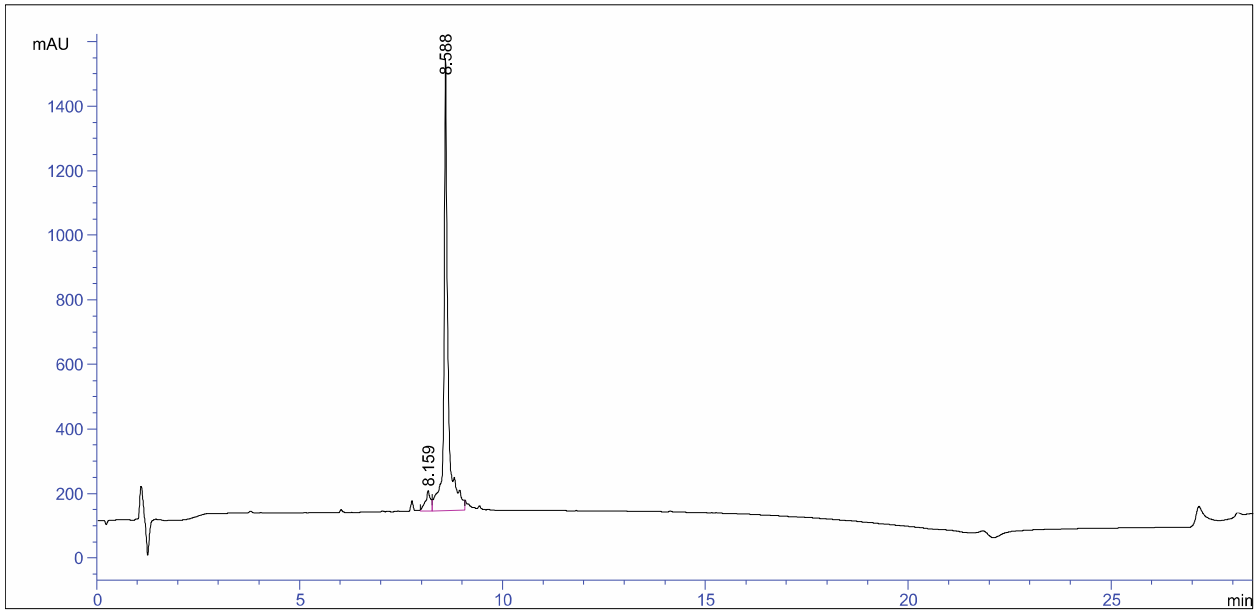


```
=====================================================================
                        Area Percent Report
=====================================================================

Sorted By             :      Signal
Multiplier:                   :      1.0000
Dilution:                     :      1.0000
Sample Amount:                :     20.00000  [ng/ul]    (not used in calc.)
Use Multiplier & Dilution Factor with ISTDs

Signal 1: VWD1 A, Wavelength=214 nm

Peak RetTime Type  Width     Area      Height     Area
  #   [min]        [min]  mAU   *s    [mAU   ]      %
----|-------|----|-------|----------|----------|--------|
   1   8.159 BV    0.1204  542.72394   61.51540   5.3419
   2   8.588 VB    0.0995 9617.00684 1367.06506  94.6581

Totals :                  1.01597e4  1428.58046

=====================================================================
                        *** End of Report ***
```

ESI-MS of **2.1a**
chemical formula: $C_{88}H_{136}N_{20}O_{22}$
exact mass: 1825.0138
calculated *m/z*:
$[M+2H]^{2+}$: 913.5069
$[M+3H]^{3+}$: 609.3379

TOF MS ES+
83.0

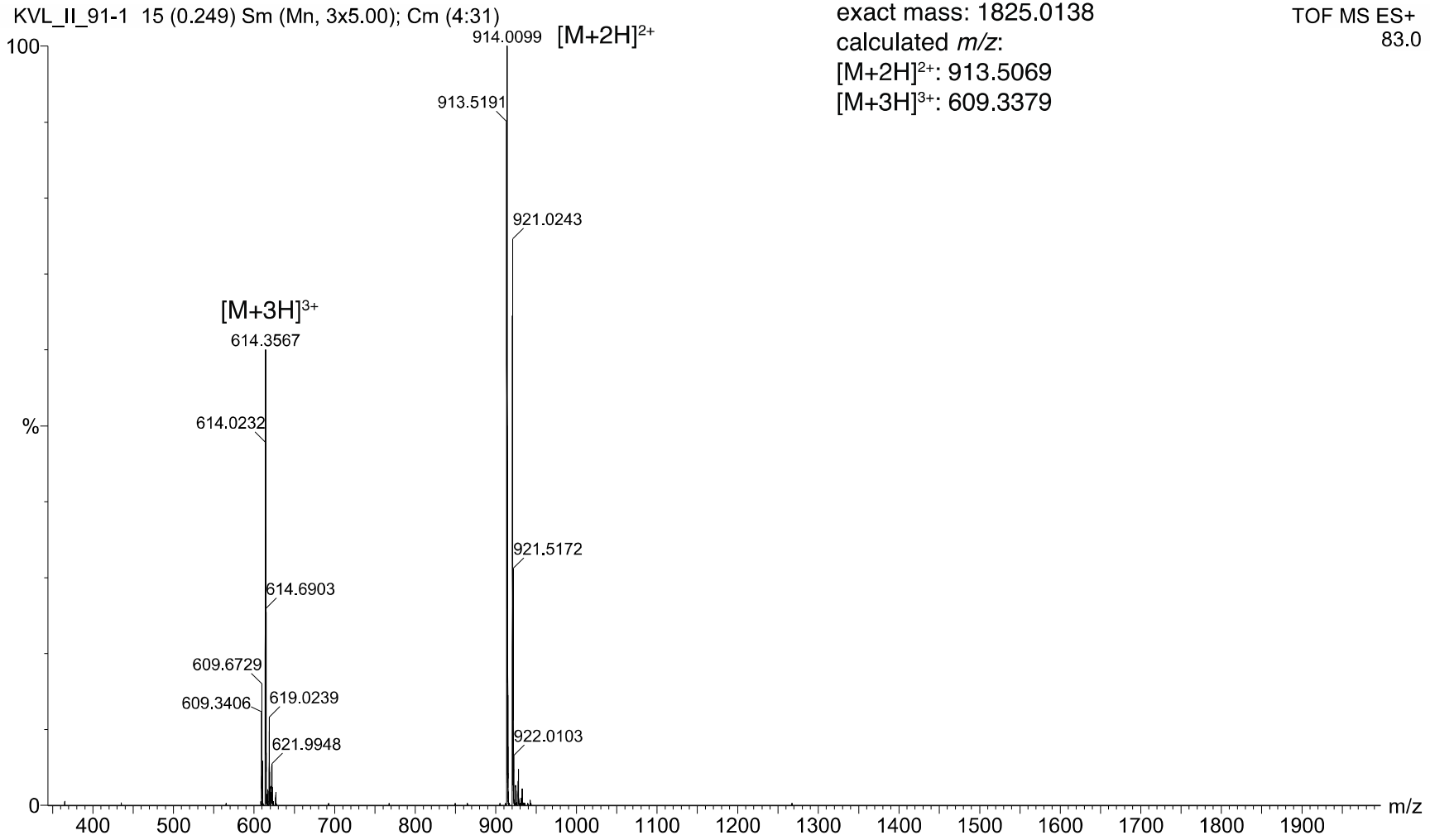

1D ^{1}H NMR spectrum of **2.1a**, 500 mHz, 1 mM in D_2O, 298 K

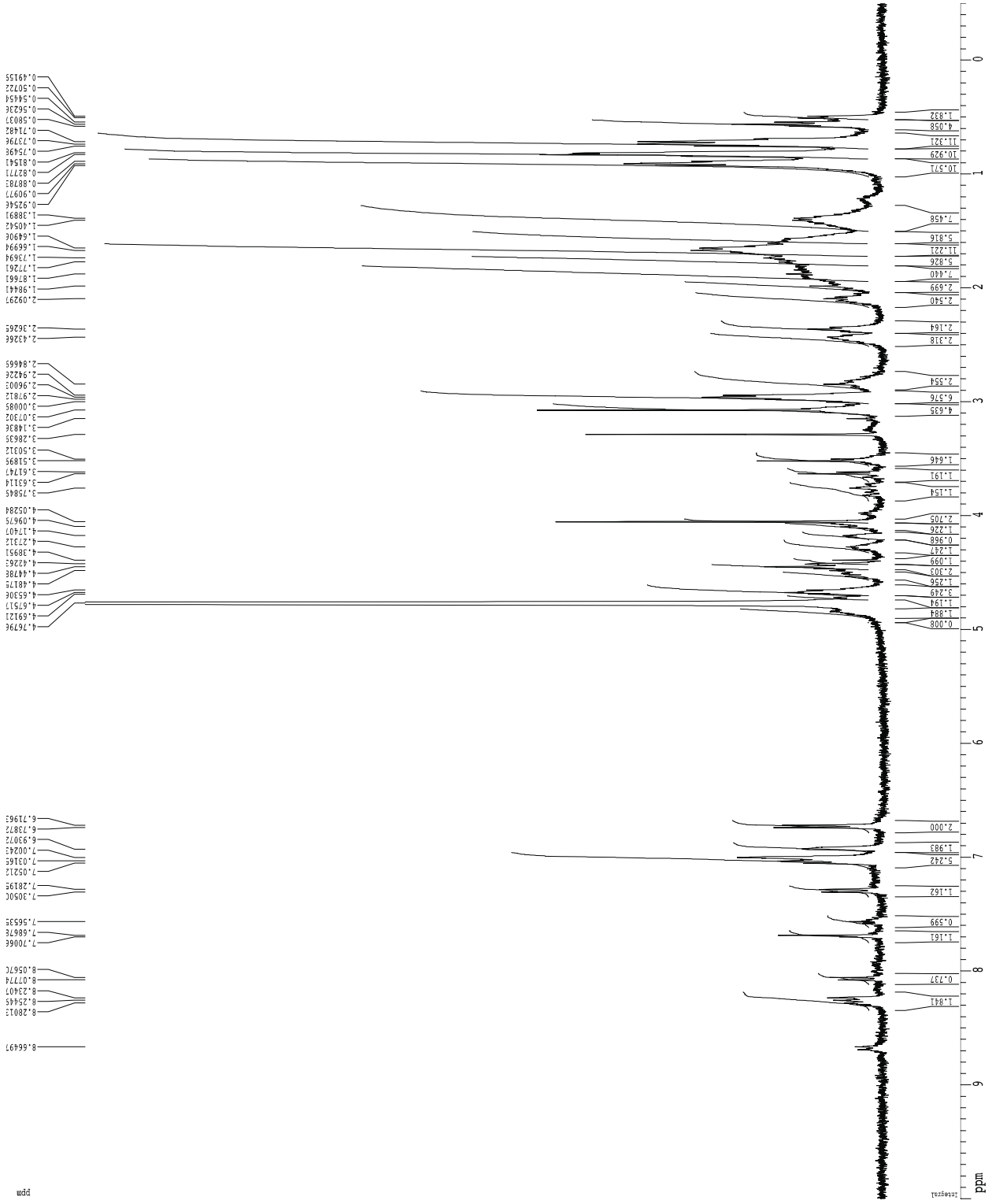

HPLC trace of **2.1b**

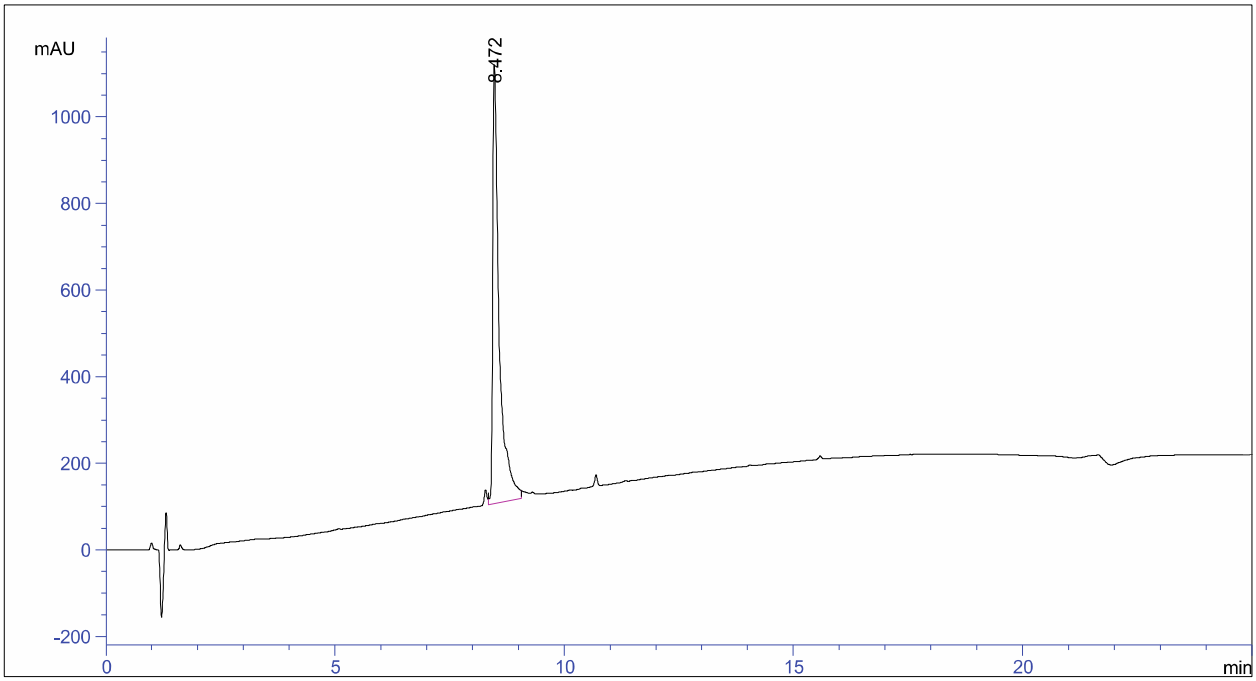


```
=====================================================================
                        Area Percent Report
=====================================================================

Sorted By             :      Signal
Multiplier:                   :      1.0000
Dilution:                     :      1.0000
Use Multiplier & Dilution Factor with ISTDs


Signal 1: VWD1 A, Wavelength=214 nm

Peak RetTime Type  Width     Area      Height     Area
  #   [min]        [min]  mAU   *s    [mAU   ]      %
----|-------|----|-------|----------|----------|--------|
   1   8.472 VB    0.1442 9905.07227 1004.02417 100.0000

Totals :                  9905.07227 1004.02417

=====================================================================
                        *** End of Report ***
```

ESI-MS of **2.1b**
chemical formula: $C_{89}H_{141}N_{21}O_{20}$
exact mass: 1824.0662
calculated *m/z*:
$[M+2H]^{2+}$: 913.0331
$[M+3H]^{3+}$: 609.0221

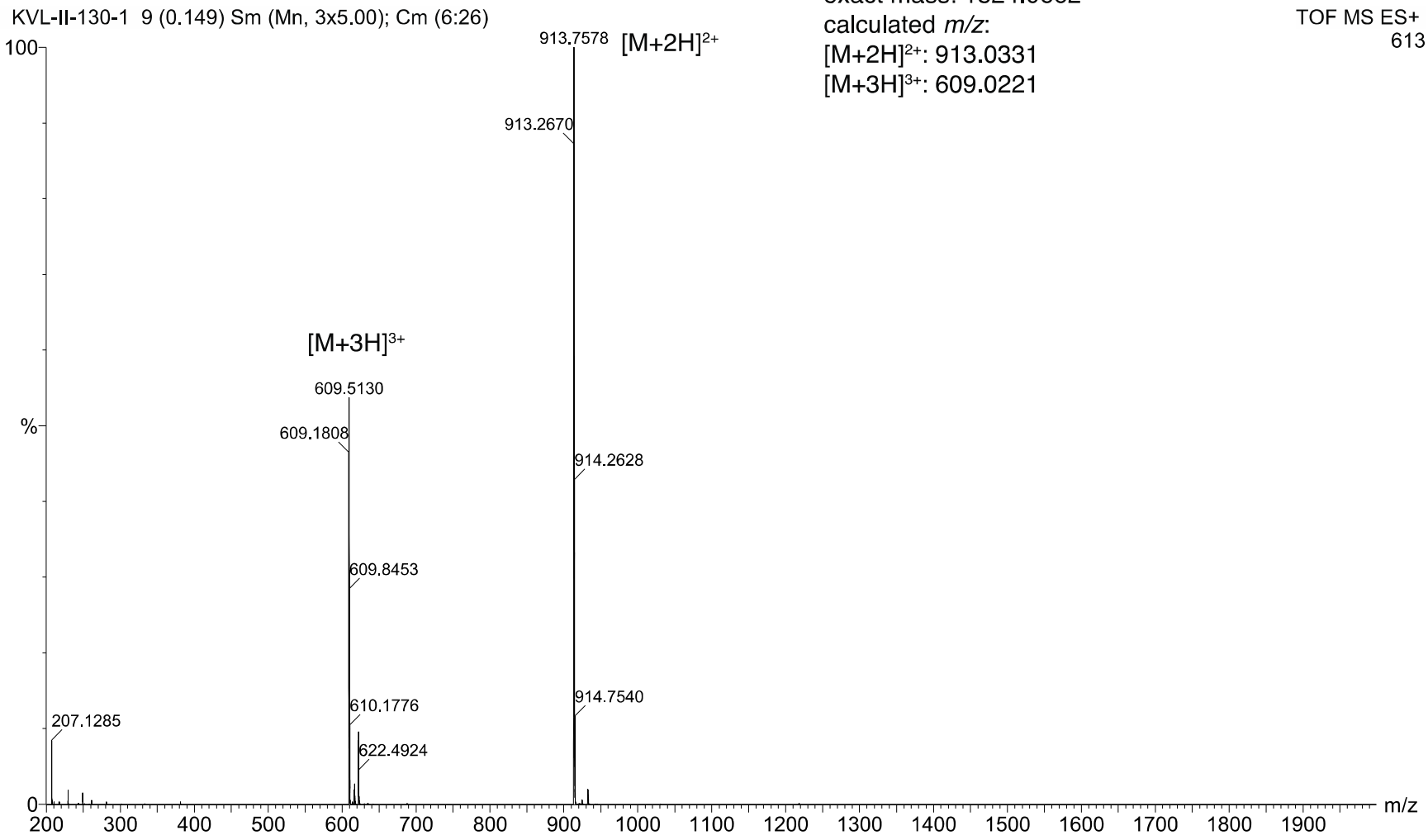

1D ^{1}H NMR spectrum of **2.1b**, 500 mHz, 1 mM in D_2O, 298 K

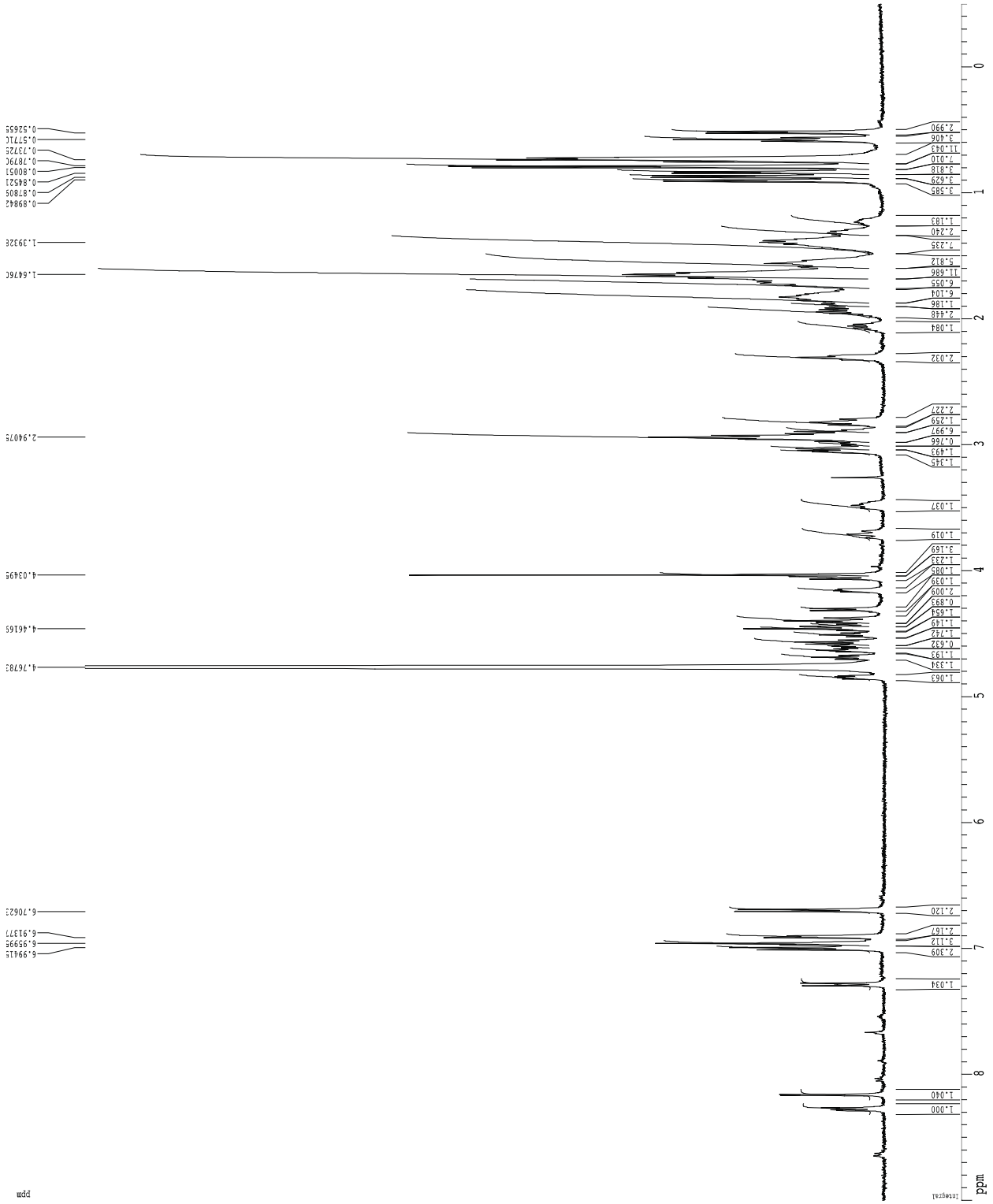

HPLC trace of **2.2a**

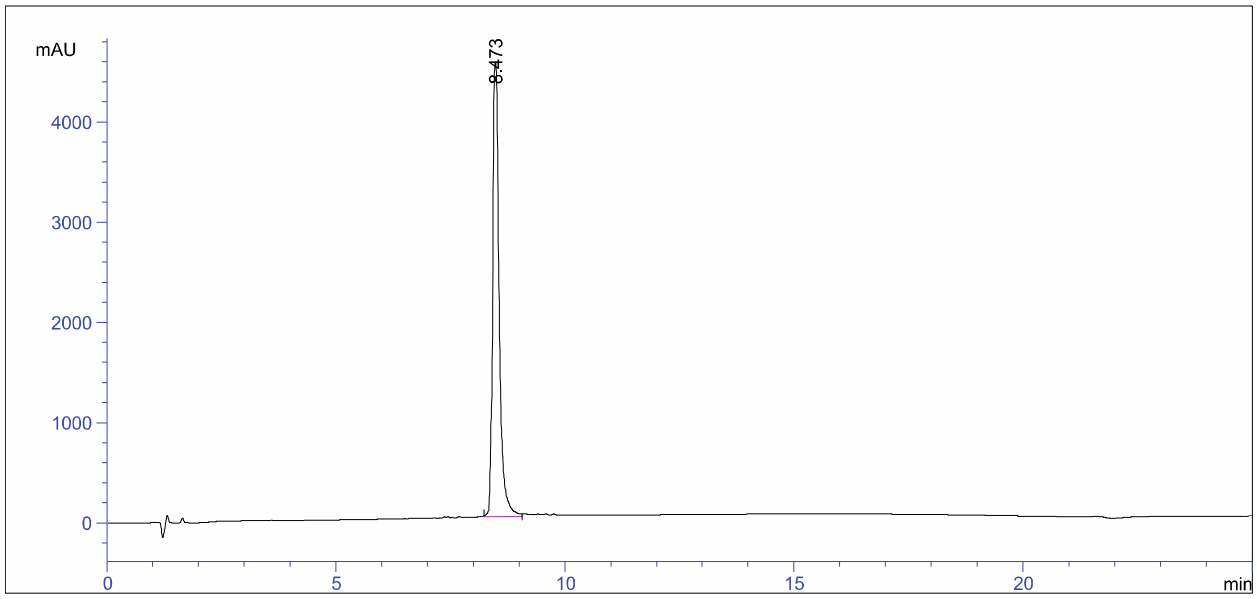


```
=====================================================================
                        Area Percent Report
=====================================================================

Sorted By             :      Signal
Multiplier:                   :      1.0000
Dilution:                     :      1.0000
Use Multiplier & Dilution Factor with ISTDs


Signal 1: VWD1 A, Wavelength=214 nm

Peak RetTime Type  Width     Area      Height     Area
  #   [min]        [min]  mAU   *s    [mAU   ]      %
----|-------|----|-------|----------|----------|--------|
   1   8.473 BB    0.1502 4.48059e4  4537.07129 100.0000

Totals :                  4.48059e4  4537.07129

=====================================================================
                        *** End of Report ***
```

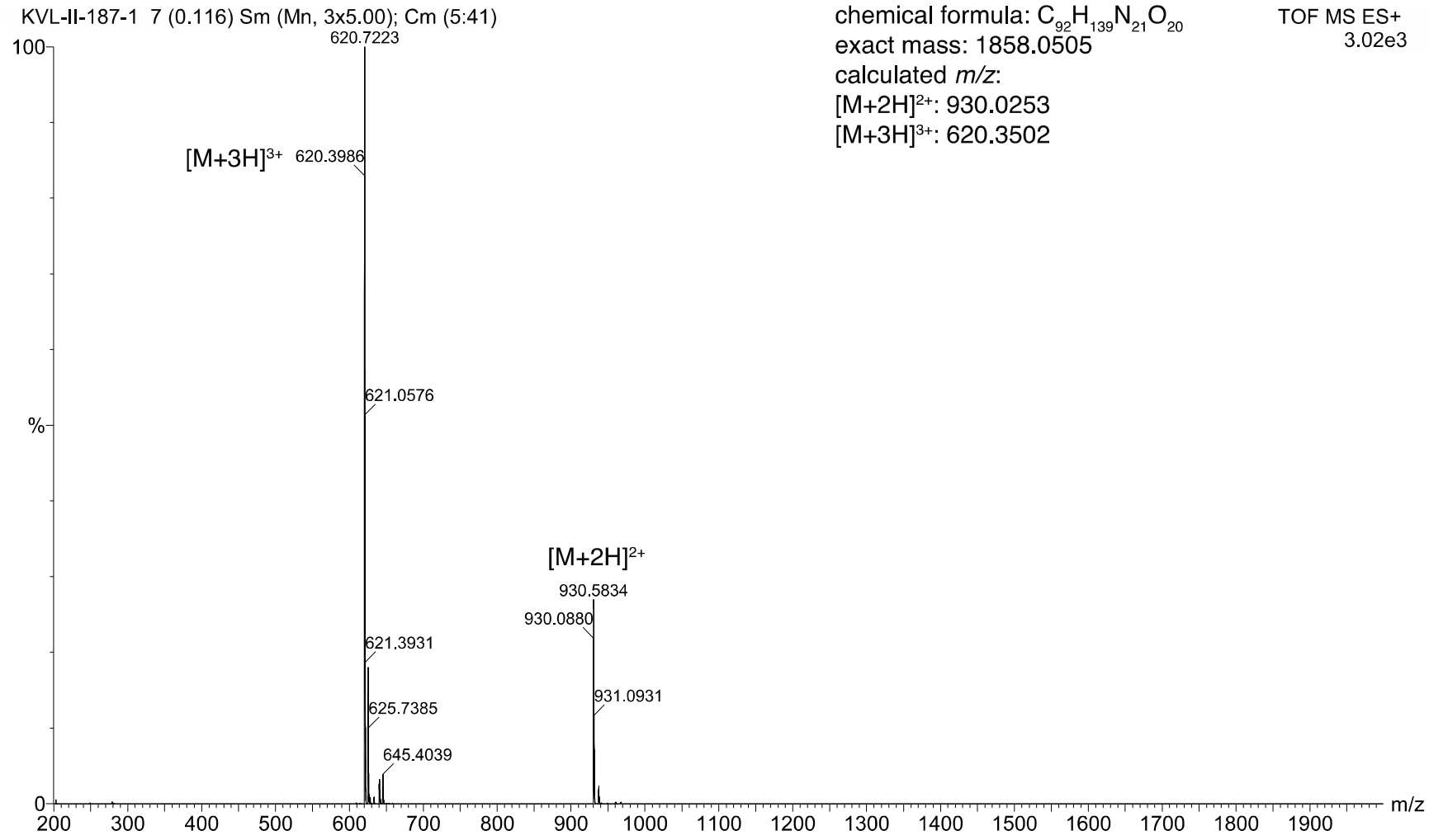
KVL-II-187-1 7 (0.116) Sm (Mn, 3x5.00); Cm (5:41)
ESI-MS of 2.2a
chemical formula: C92H139N21O20
exact mass: 1858.0505
calculated m/z:
[M+2H]2+: 930.0253
[M+3H]3+: 620.3502
TOF MS ES+
3.02e3
620.7223
[M+3H]3+ 620.3986
621.0576
621.3931
625.7385
645.4039
[M+2H]2+
930.5834
930.0880
931.0931
100
%
0
200 300 400 500 600 700 800 900 1000 1100 1200 1300 1400 1500 1600 1700 1800 1900
m/z

1D ^{1}H NMR spectrum of **2.2a**, 500 mHz, 2 mM in D_2O, 298 K

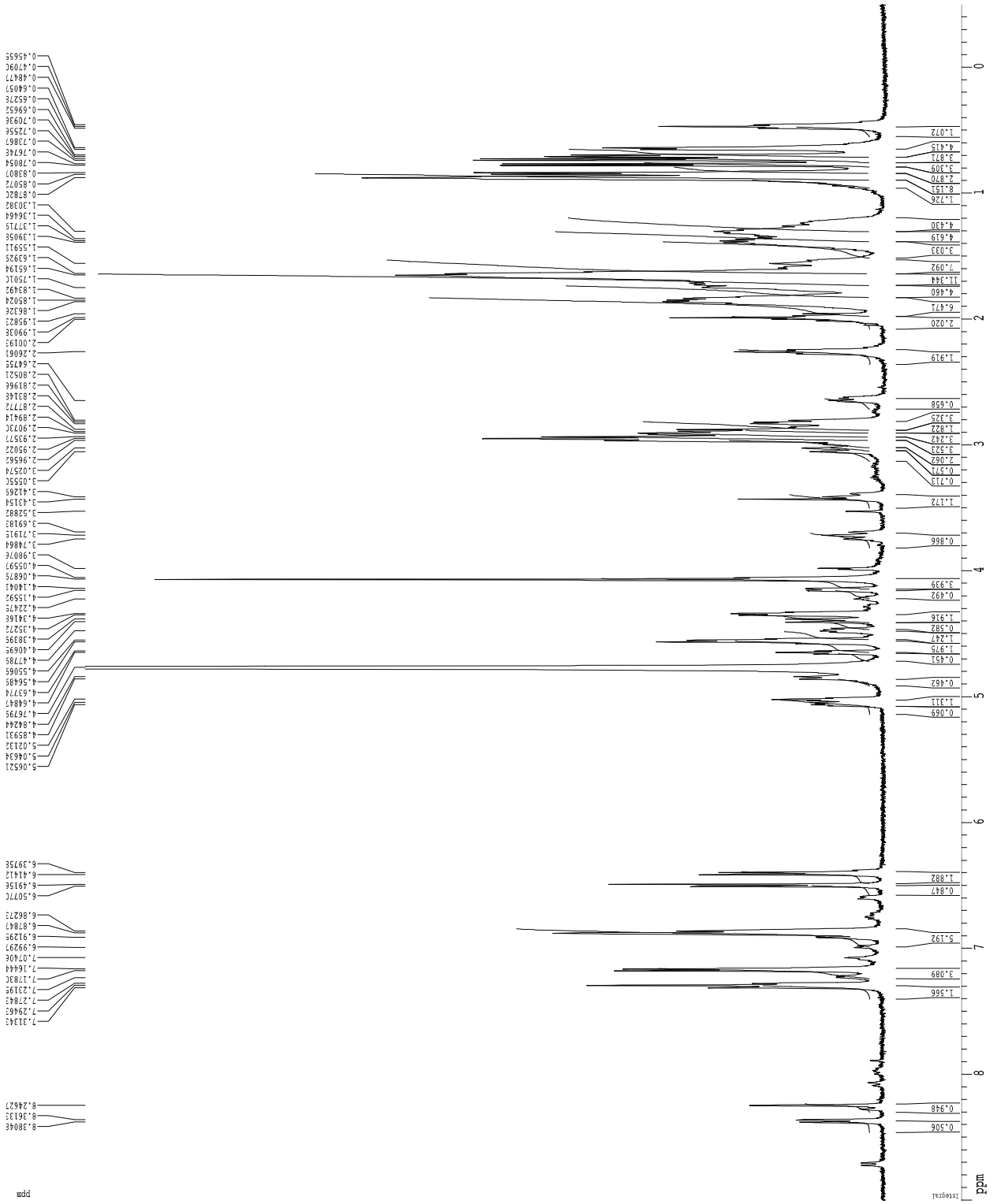

HPLC trace of **2.2b**

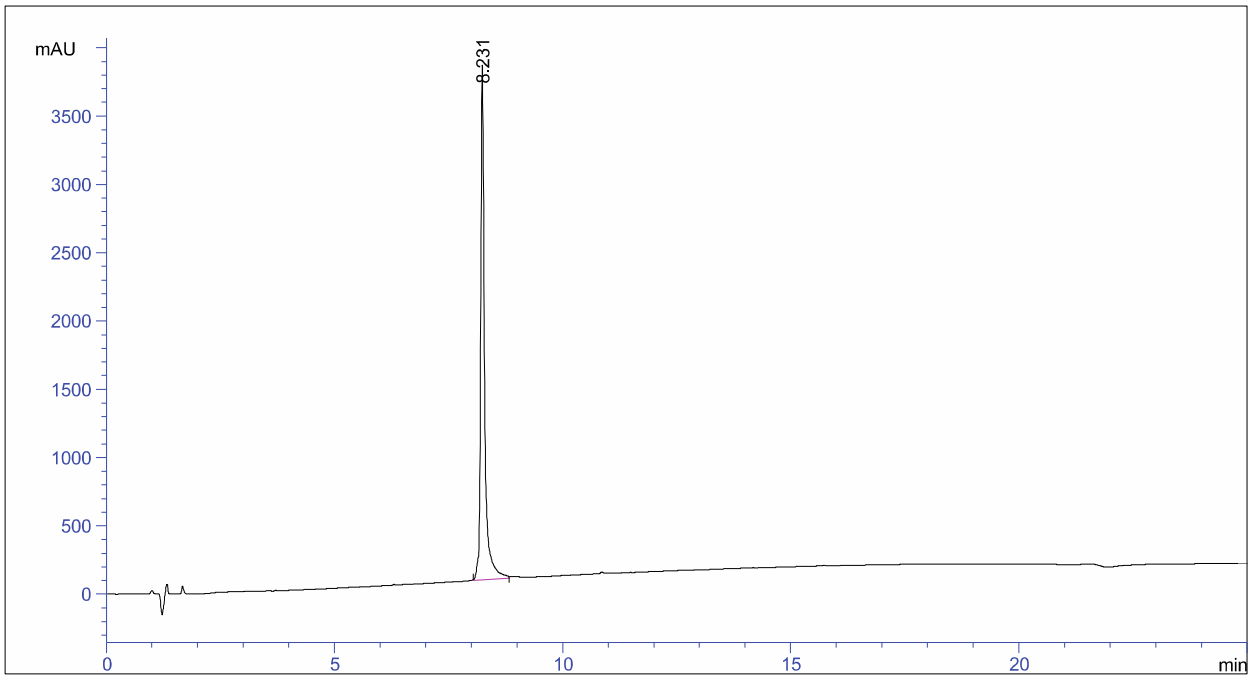


```
=====================================================================
                        Area Percent Report
=====================================================================

Sorted By             :      Signal
Multiplier:                   :      1.0000
Dilution:                     :      1.0000
Use Multiplier & Dilution Factor with ISTDs


Signal 1: VWD1 A, Wavelength=214 nm

Peak RetTime Type  Width     Area      Height     Area
  #   [min]        [min]  mAU   *s    [mAU   ]      %
----|-------|----|-------|----------|----------|--------|
   1   8.231 BB    0.0955 2.23956e4  3616.79565 100.0000

Totals :                  2.23956e4  3616.79565

=====================================================================
                        *** End of Report ***
```

ESI-MS of **2.2b**
chemical formula :$C_{92}H_{130}N_{21}O_{21}$
exact mass: 1874.0454
calculated m/z:
$[M+2H]^{2+}$: 938.0227
$[M+3H]^{3+}$: 625.6818

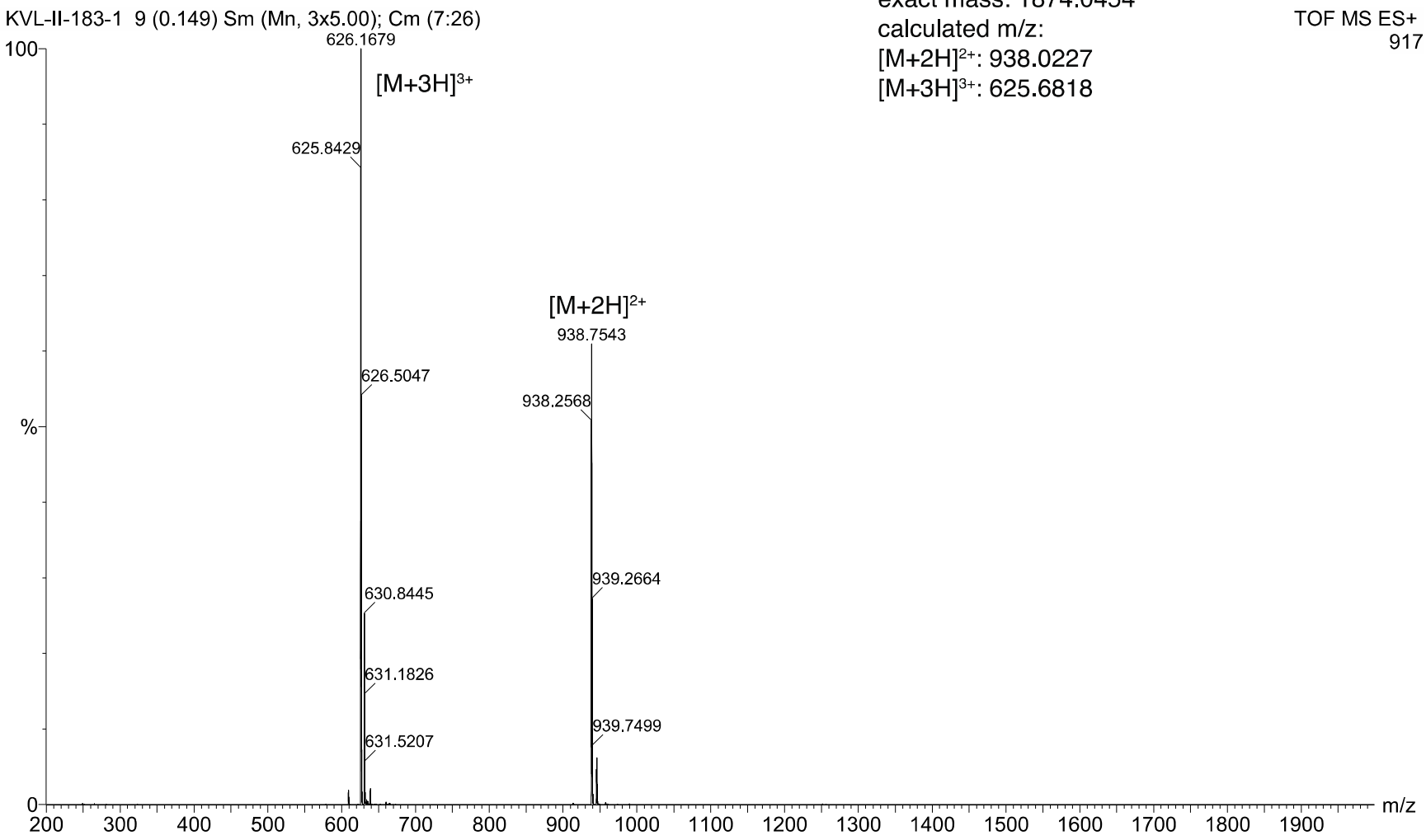

1D ^{1}H NMR spectrum of **2.2b**, 500 mHz, 2 mM in D_2O, 298 K

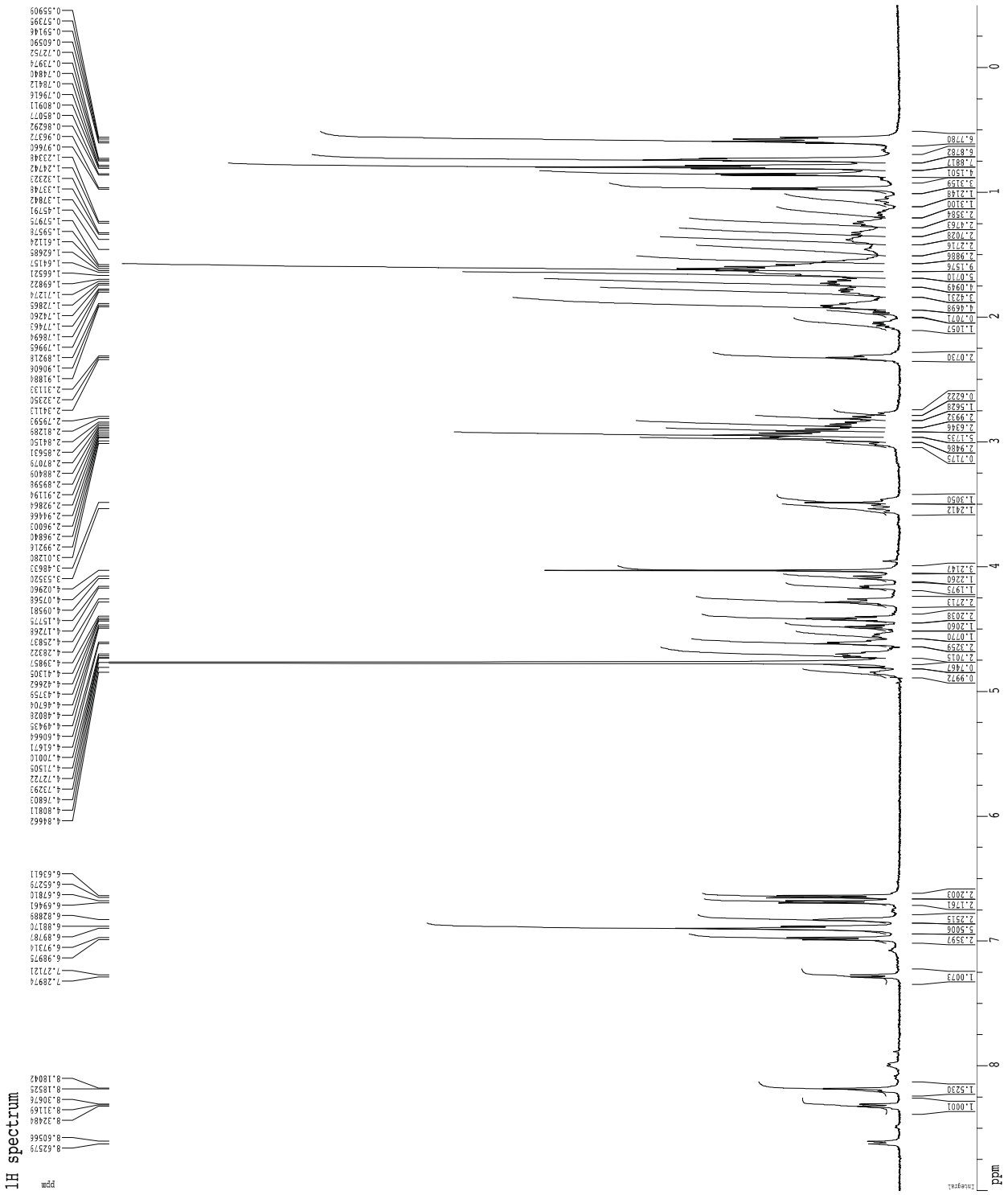

HPLC trace of **2.3a**

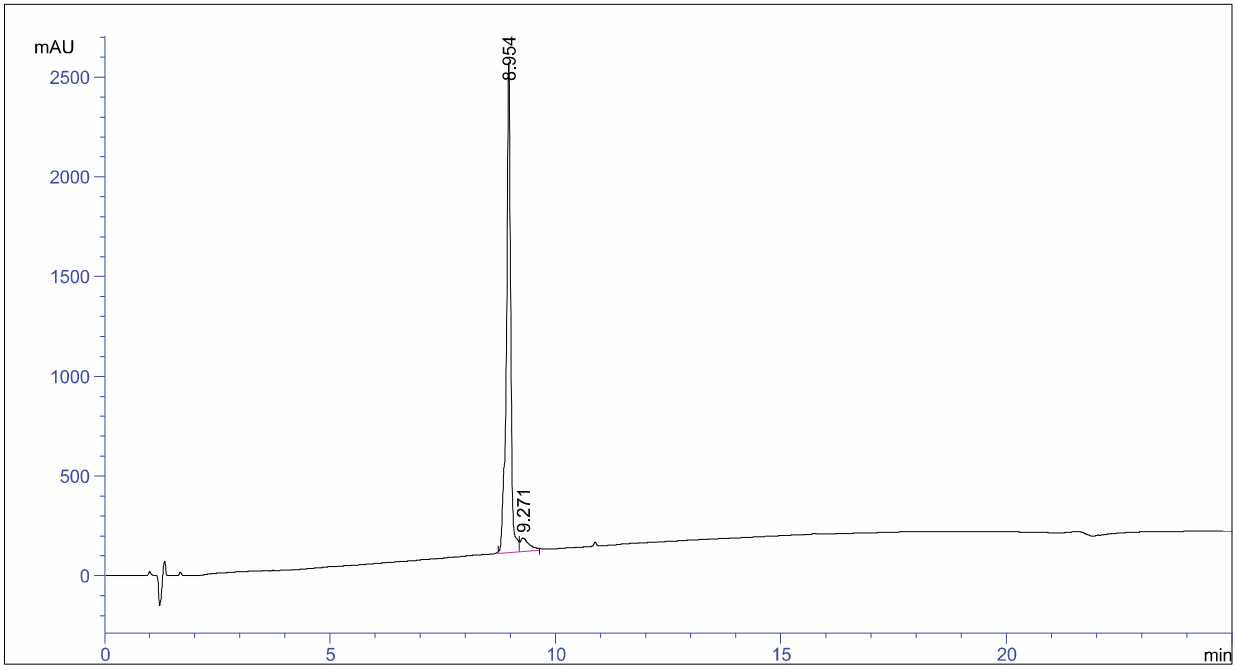


```
=====================================================================
                        Area Percent Report
=====================================================================

Sorted By             :      Signal
Multiplier:                   :      1.0000
Dilution:                     :      1.0000
Use Multiplier & Dilution Factor with ISTDs


Signal 1: VWD1 A, Wavelength=214 nm

Peak RetTime Type  Width     Area      Height     Area
  #   [min]        [min]  mAU   *s    [mAU   ]      %
----|-------|----|-------|----------|----------|--------|
   1   8.954 BV    0.1021 1.63627e4  2423.14038  94.5663
   2   9.271 VB    0.1903  940.18610   68.06148   5.4337

Totals :                  1.73029e4  2491.20186

=====================================================================
                        *** End of Report ***
```

ESI-MS of **2.3a**
chemical formula: $C_{87}H_{137}N_{21}O_{19}$
exact mass: 1780.0400
calculated *m/z*:
$[M+2H]^{2+}$: 891.0200
$[M+3H]^{3+}$: 594.3467

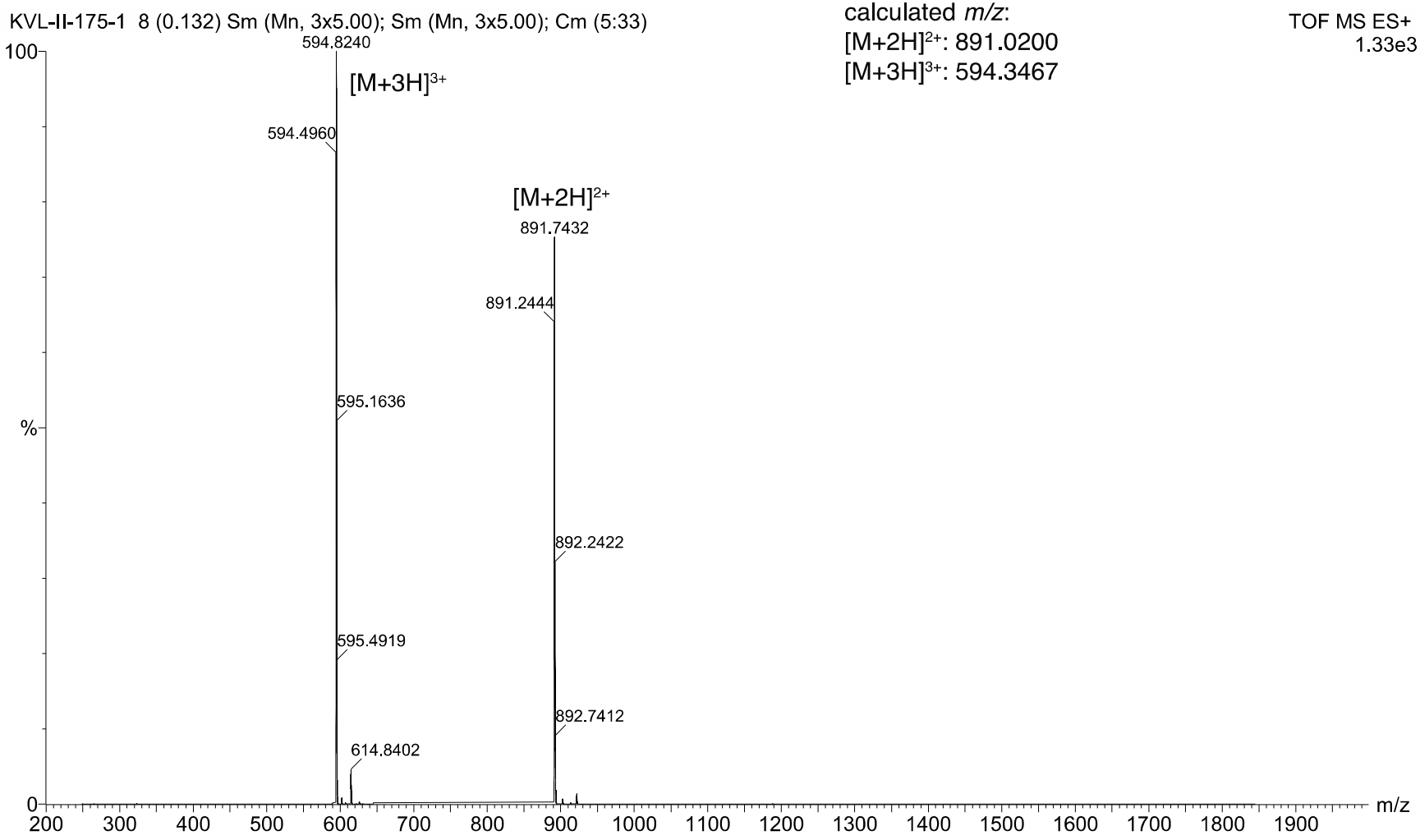

1D ^{1}H NMR spectrum of **2.3a**, 500 mHz, 2 mM in D_2O, 298 K

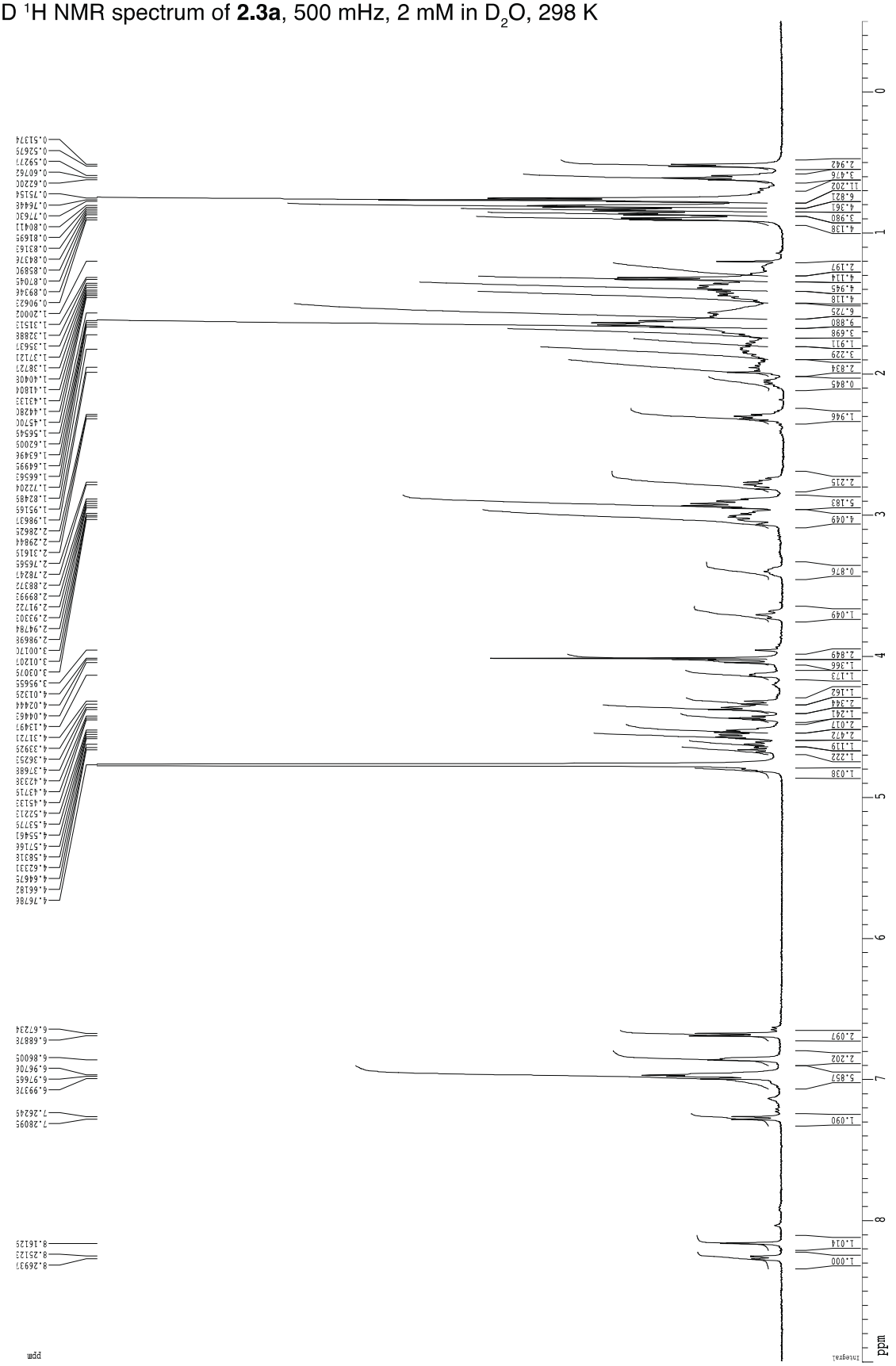

HPLC trace of **2.3b**

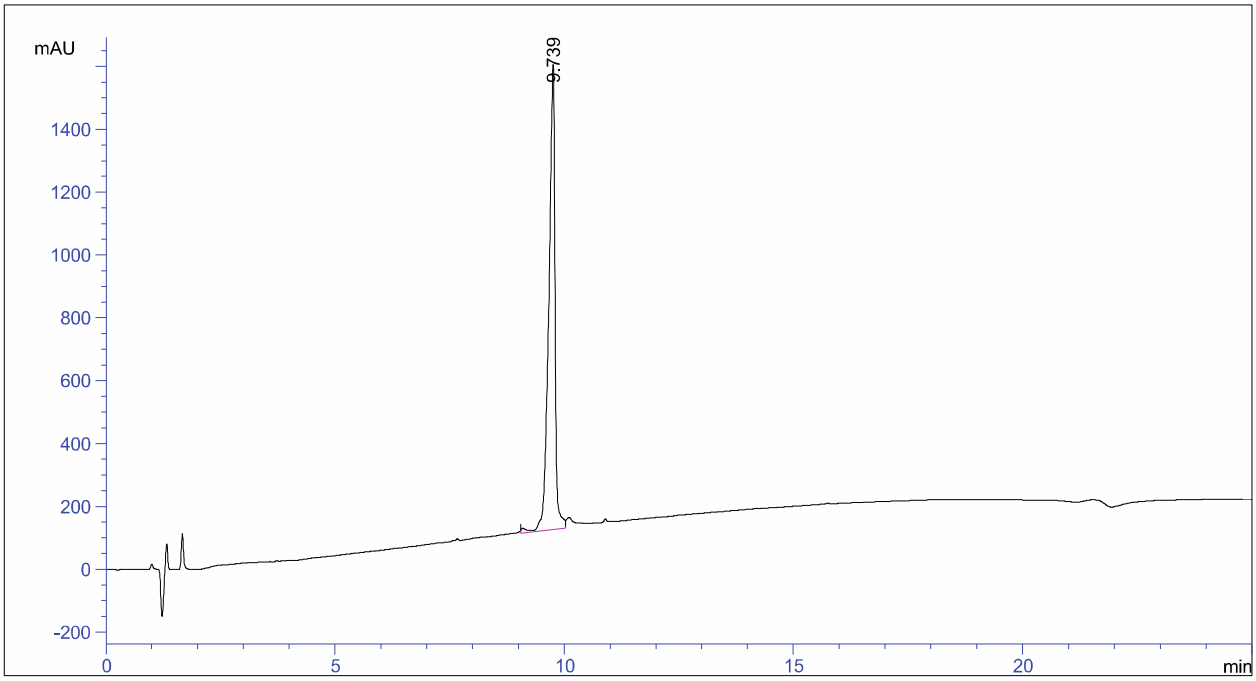


```
==========================================================================
                          Area Percent Report
==========================================================================

Sorted By             :      Signal
Multiplier:                   :      1.0000
Dilution:                     :      1.0000
Use Multiplier & Dilution Factor with ISTDs


Signal 1: VWD1 A, Wavelength=214 nm

Peak RetTime Type  Width     Area      Height     Area
  #   [min]        [min]  mAU   *s    [mAU   ]       %
----|-------|----|-------|----------|----------|--------|
   1   9.739 BV    0.1360 1.39126e4  1440.29187 100.0000

Totals :                  1.39126e4  1440.29187

==========================================================================
                          *** End of Report ***
```

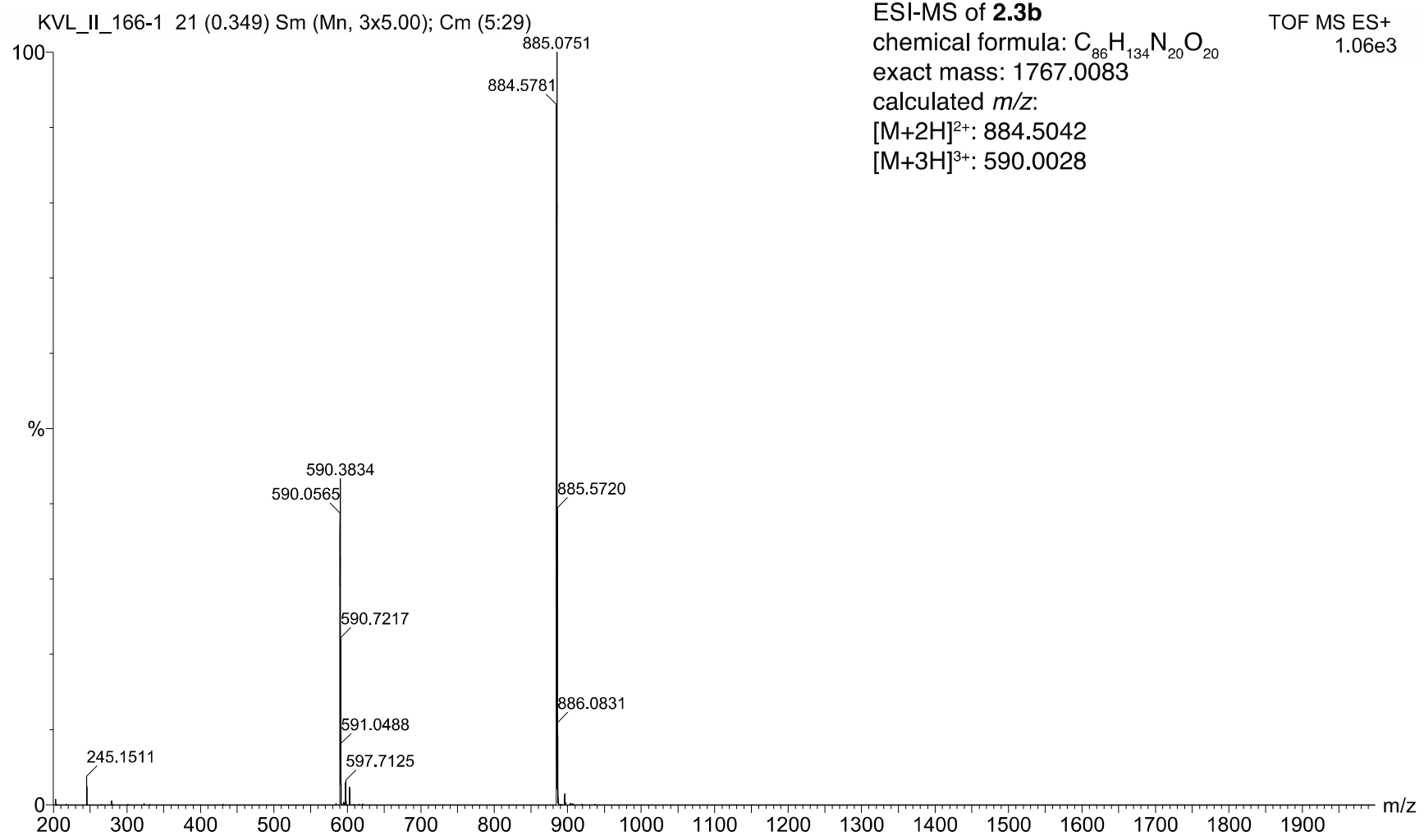
KVL_II_166-1 21 (0.349) Sm (Mn, 3x5.00); Cm (5:29)
ESI-MS of **2.3b**
chemical formula: $C_{86}H_{134}N_{20}O_{20}$
exact mass: 1767.0083
calculated *m/z*:
$[M+2H]^{2+}$: 884.5042
$[M+3H]^{3+}$: 590.0028
TOF MS ES+
1.06e3
100
%
0
885.0751
884.5781
590.3834
590.0565
885.5720
590.7217
886.0831
591.0488
245.1511
597.7125
200 300 400 500 600 700 800 900 1000 1100 1200 1300 1400 1500 1600 1700 1800 1900
m/z

1D ^{1}H NMR spectrum of **2.3b**, 500 mHz, 2 mM in D_2O, 298 K

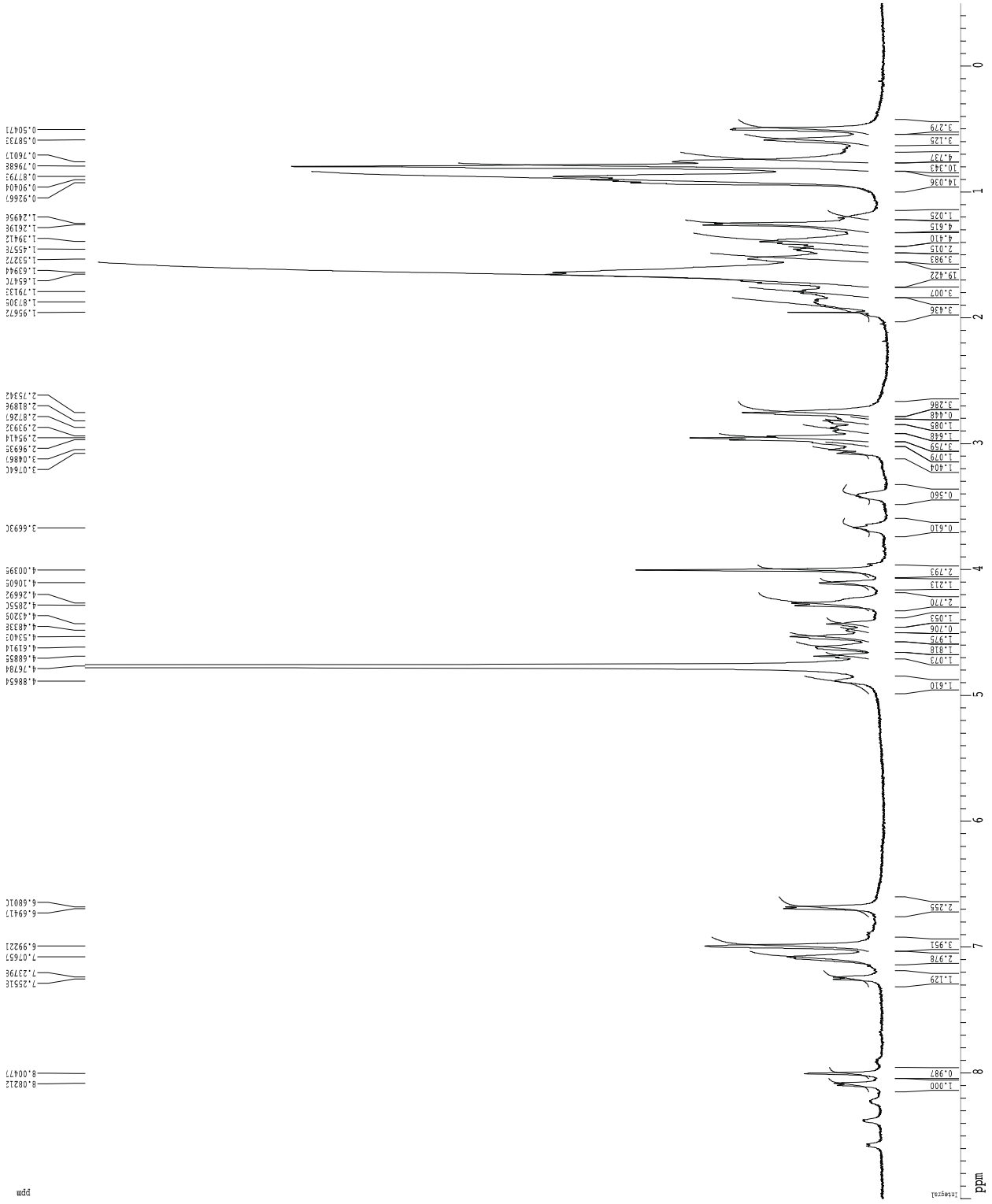

References and Notes

[1] Cheng, P.-N.; Nowick, J. S. *J. Org. Chem.* **2011,** *76,* 3166-3173.

[2] Zheng, J.; Liu, C.; Sawaya, M. R.; Vadla, B.; Khan, S.; Woods, R. J.; Eisenberg, D.; Goux, W. J.; Nowick, J. S. *J. Am. Chem. Soc.* **2011,** *133,* 3144-3157.

[3] Teplow, D. B. *Methods Enzymol.* **2006,** *413,* 20-33.